

Microbial Processes Within Bentonite Barrier Materials

A thesis submitted to the University of Manchester for the degree of Doctor of Philosophy in
the Faculty of Science and Engineering

2018

Haydn Martin Haynes

School of Earth, and Environmental Sciences

Contents

Contents	2
Figures.....	8
Tables.....	11
Abstract.....	13
Declaration.....	14
Copyright statement.....	15
Acknowledgements.....	16
The Author.....	17
Statement.....	18
1. Introduction: Bentonite Utilization in the Geological Disposal of Radioactive Waste, and the Activity/Viability of Microorganisms in such an Environment.....	20
1.1. Introduction.....	20
1.1.1. Nuclear fuel cycle	21
1.1.2. UK waste inventory	21
1.1.3. Geological disposal facility.....	23
1.1.4. Microbe interactions with GDF materials.....	26
1.2. Bentonite	27
1.2.1. Bentonite mineralogy.....	28
1.2.2. Particle size and surface area	30
1.2.3. Electric double layer theory	31
1.2.4. Cations	32
1.2.5. Swelling	33
1.2.6. Dispersion and colloids.....	34
1.3. Factors influencing bentonite structure.....	36
1.3.1. Gamma radiation and bentonite	36
1.3.2. Radiolysis and porewater chemistry	36
1.3.3. Density and swelling pressure	37
1.3.4. Temperature and evolving resaturation	37
1.4. Bentonite microbiology	38

1.5. Bentonite chemical interactions	39
1.5.1. Iron	39
1.5.2. Selenium	40
1.6. Microbial processes	40
1.6.1. Fe(III)-reducing bacteria	43
1.6.2. Sulfate-reducing bacteria	48
1.6.3. Microbial selenium reduction	50
1.6.4. Microbially-induced corrosion	50
1.6.5. Limits to microbial growth	51
1.7. Summary	56
1.8. Aims and questions:	57
1.9. References	57
2. Methodology	68
2.1. Microbiological techniques	68
2.1.1. Cell culturing	68
2.1.2. Minimal medium clay suspensions	69
2.1.3. Most probable number (MPN) enumerations	70
2.1.4. Molecular ecology	71
2.2. Mineralogical techniques	73
2.2.1. X-ray Diffraction (XRD)	73
2.2.2. Electron Paramagnetic Resonance (EPR)	74
2.2.3. Mössbauer spectroscopy	76
2.2.4. Transmission Electron Microscopy (TEM)	78
2.3. Aqueous analyses	79
2.3.1. Ion Chromatography (IC)	79
2.3.2. Inductively Coupled Plasma Atomic Emission Spectroscopy (ICP-AES)	80
2.3.3. Spectrophotometry	82
2.4. References	85
3. Response of Bentonite Microbial Communities to Stresses Relevant to Geodisposal of Radioactive Waste	88
3.1. Preface	88

3.2. Abstract.....	89
3.3. Introduction.....	90
3.4. Material and methods.....	92
3.4.1. Selection of bentonites.....	92
3.4.2. Analytical methods	93
3.4.3. Sample and media preparation.....	95
3.4.4. Microbiology methods.....	96
3.5. Results.....	98
3.5.1. Characterization of the bentonites	98
3.5.2. Most Probable Number (MPN) enumerations	99
3.5.3. Molecular ecology	102
3.6. Discussion.....	107
3.6.1. As received bentonite.....	107
3.6.2. Bentonite exposed to pressure	109
3.6.3. Bentonite exposed to heat	110
3.6.4. Bentonite exposed to gamma radiation.....	110
3.7. Conclusions.....	111
3.8. Acknowledgements.....	113
3.9. References.....	113
3.10. Supplementary	117
4. The Molecular Ecology of the FEBEX <i>in-situ</i> Project Along the Temperature/Evolving Resaturation Gradient.....	118
4.1. Preface.....	118
4.2. Abstract.....	119
4.3. Introduction.....	120
4.4. Methods.....	122
4.4.1. FEBEX core extraction and treatment	122
4.4.2. Media preparation and MPN enumeration.....	124
4.4.3. Temperature prediction.....	125
4.4.4. Molecular ecology methods.....	125
4.5. Results.....	127
4.5.1. Geophysical conditions.....	127

4.5.2. Most Probable Number (MPN) enumerations	127
4.5.3. Transect 1-3	128
4.5.4. Transect 16-18	129
4.5.5. Transect 28-30	130
4.5.6. Potential for microbially-driven processes	131
4.5.7. qPCR	132
4.6. Discussion	133
4.6.1. Most Probable Number (MPN) enumerations	133
4.6.2. Molecular ecology	134
4.7. Conclusions.....	135
4.8. Acknowledgements.....	137
4.9. References.....	137
5. Monitoring Bioreduction of Iron (III) in Bentonites Using a Magnetic Approach ...	140
5.1. Preface.....	140
5.2. Abstract.....	141
5.3. Introduction.....	142
5.4. Materials and methods	146
5.4.1. Material selection, and clay suspension preparation.....	146
5.4.2. Solution analysis	147
5.4.3. Solid phase analysis	148
5.5. Results.....	151
5.5.1. Material characterization	151
5.5.2. Microbial Fe(III)-reduction in the substrates	152
5.5.3. pH and Eh	153
5.5.4. Electron donor, and electron acceptor utilization	154
5.5.5. Changes in the cation exchange capacity of the substrates (CEC) and mineral dissolution	155
5.5.6. EPR investigation of bioreduction-induced changes in Fe(III) speciation	156
5.5.7. Iron speciation using Mössbauer spectroscopy.....	158
5.6. Discussion	160

5.7. Conclusions.....	163
5.8. Acknowledgements.....	164
5.9. References.....	164
5.10. Supplementary	167
6. Selenium Speciation in Microbially Reduced SWy-3 Montmorillonite.....	172
6.1. Preface.....	172
6.2. Graphical abstract	173
6.3. Abstract.....	173
6.4. Introduction.....	174
6.5. Materials and methods	176
6.5.1. Experiment preparation.....	176
6.5.2. Analytical Methods.....	178
6.6. Results.....	180
6.6.1. Material characterization	180
6.6.2. Selenite removal.....	181
6.6.3. Selenate removal	183
6.7. Discussion	186
6.8. Conclusions.....	187
6.9. Acknowledgements.....	188
6.10. References.....	188
6.11. Supplementary	190
7. The Viability and Activity of Fe(III)-reducing Bacteria in Response to Bentonite Density and Swelling Pressure.....	194
7.1. Preface.....	194
7.2. Abstract.....	195
7.3. Introduction.....	196
7.4. Materials and methods	198
7.4.1. Material preparation.....	198
7.4.2. Pressure vessel preparation and use	201
7.4.3. Follow up analyses.....	204
7.5. Results.....	206
7.5.1. Saturation stage.....	206
7.5.2. Experimental stage.....	208

7.5.3. Sample description and characterization	210
7.5.4. Most Probable Number (MPN) enumerations	211
7.6. Discussion	212
7.6.1. Saturation stage	212
7.6.2. Variability in experimental swelling pressures	213
7.6.3. Microbial viability and activity	214
7.7. Conclusions	216
7.8. Acknowledgements	217
7.9. References	217
8. Conclusions and Future Directions	220
8.1. Microbial viability	220
8.2. Fe(III)-reducing bacteria	221
8.3. Overarching conclusions	223
8.4. Future directions	223
8.4.1. Microbe viability	224
8.4.2. Biological Fe(III)-reduction of bentonites	224
8.5. References	225

Word count: 68,603

Figures

Figure 1.1: An overview of the nuclear fuel cycle (WNA, 2015).	21
Figure 1.2: Overview of the KBS-3 Swedish GDF concept, highlighting the waste form (fuel pellet), metal container (cladding tube), metal overpack (copper canister), buffer (bentonite), and host rock (SKB, 2006).....	24
Figure 1.3: Structural units of pyrophyllite octahedral, and tetrahedral sheets (adapted from (Wilson et al., 2011))......	29
Figure 1.4: Two parallel 2:1 layers of a smectite mineral (Wilson et al., 2011).	30
Figure 1.5: Diagrammatic representation of electric double layer theory (Moore and Reynolds Jr, 1997).	31
Figure 1.6: Exchange free energy (ΔG^0_{ex}) plotted against the equivalent anionic radius (r_a) for the exchange of several cations with Cs^+ , comparing a dry clay to one containing a 3M interlayer solution (Eberl, 1980).	33
Figure 1.7: Changes in average particle size (μm) in response to swelling pressure (kPa) (pressure occurring as the result of the absorption of water in a confined space), and relative swelling (%) (Katti and Katti, 2006).....	34
Figure 1.8: Overview of the issues that determine if colloidal transport will have a significant effect on radionuclide transport (Chapman et al., 1993).	35
Figure 1.9: The movement of water through a bentonite buffer (Wilson et al., 2011).....	38
Figure 1.10: The major TEAPs located within an aquifer (Lovley and Chapelle, 1995).	41
Figure 1.11: Redox potentials for a range of electron acceptors (Madigan, 2015).	42
Figure 1.12: Proteins responsible for electron transfer in <i>Shewanella oneidensis</i> , known paths are displayed with solid arrows, hypothetical ones are indicated with dashed arrows (Richter et al., 2012).	45
Figure 1.13: The chemical structure of two commonly used chelating agents ethylenediaminetetraacetic acid (EDTA) and nitrilotriacetic acid (NTA) (Dobbin et al., 1996).	47
Figure 1.14: Overview of sulphate reduction in the SRB <i>Desulfovibrio aespoeensis</i> (Hallbeck, 2014).	49
Figure 1.15: Summary of reactions generated by the radiolysis of water, and a summary of the key products (Daly, 2009).....	56
Figure 2.1: The energy difference (ΔE) of electron spin states as a function of magnetic field strength (B_0), with the absorption profile observed at resonance (Weber et al., 1998).	75
Figure 2.2: Conversion of an absorption spectra into the first derivative (Weber et al., 1998).	75
Figure 2.3: A basic diagram of a Mössbauer spectrometer. The velocity (v) oscillates the distance of the gamma radiation (γ) source from the absorber. The detector picks up the transmission (T) of the gamma radiation through the absorber (Gütlich, 2011).	77
Figure 2.4: Comparison of a TEM microscope (a), and a light microscope (Tanaka, 2017). ..	78
Figure 2.5: An overview of an ion chromatograph. The solvent reservoir, and pump + gradient system moves the mobile phase to the injection unit where the sample is inserted. The mobile phased then passes through the column (stationary phase), and the output recorded using a detector (Fritz, 2000).	80

Figure 2.6: Overview of an ICP-AES spectrometer. The solution is pumped into a nebulizer which sprays the sample into a stream of argon. The mist is converted into a plasma using the ICP torch, and the intensities of the species are recorded by the spectrometer (Boss and Fredeen, 2004).	81
Figure 2.7: Diagram of a spectrophotometer being used to calculate the optical density of a cell solution (Madigan, 2015).	83
Figure 2.8: Chemical structure of Ferrozine (3-(2-Pyridyl)-5,6-diphenyl-1,2,4-triazine-p,p'-disulfonic acid) (Stookey, 1970).	84
Figure 2.9: Absorption spectrum for Fe(II) complexed with Ferrozine (Stookey, 1970). Lamda max (λ_{max}) has been annotated.	84
Figure 3.1: Number of SRB in the Postgate B enrichments (MPN g ⁻¹) following no treatment (as received), pelletisation at ~74 MPa (pressure), heating at 90 °C for 24 hours (temperature), and a gamma radiation dose of 1000 Gy (irradiation).	101
Figure 3.2: Number of IRB cells (MPN g ⁻¹) in the fully defined growth medium for the as received bentonite, and for bentonite after exposure to pressure at ~74 MPa (pressure), after heating at 90 °C for 24 hours (temperature), and after a gamma radiation dose of 1000 Gy (irradiation).	102
Figure 3.3: Comparison of SRB (<i>Desulfosporosinus</i> , <i>Desulfotomaculum</i>), and other key bacteria (<i>Bacillus</i> , <i>Clostridium</i>) contained in the Postgate B MPN enrichments (first dilution in series, scored positive). (A) As received bentonite (As Received). (B) Bentonite after exposure to pressure at ~74 MPa (Pressure). (C) Bentonite after heating at 90 °C for 24 hours (Temperature). (D) Bentonite after exposure to gamma irradiation (1000 Gy) (Irradiation).	105
Figure 3.4: Bacteria affiliated with Fe(III)-reducing activity identified in the fully defined growth medium enrichments (dilution which provided the strongest result, typically first MPN dilution). (A) As received bentonite (As Received). (B) Bentonite after exposure to pressure at ~ 74 MPa (Pressure). (C) Bentonite after exposure to heat treatment at 90 °C for 24 hours (Temperature). (D) Bentonite after exposure to gamma irradiation (1000 Gy) (Irradiation).	107
Figure 4.1: Diagrammatic representation of the FEBEX <i>in-situ</i> experiment (Huertas et al., 2000).	121
Figure 4.2: Breakdown of the FEBEX-DP sections (Wersin et al., 2017). Samples used in this work were taken from section 48, which was located at the halfway point of heater 2.	123
Figure 4.3: Location of the FEBEX cores extracted from section 48 of the FEBEX-DP.	124
Figure 4.4: Breakdown of classes identified in the bentonite core transect made up of BC-48-1 (55 °C), BC-48-2 (72 °C), and BC-48-3 (83 °C), and the distance of the cores from the heater.	129
Figure 4.5: Classes present in bentonite cores BC-48-16 (55 °C), BC-48-17 (72 °C), BC-48-18 (92 °C), and the distance of the cores from the heater.	130
Figure 4.6: Overview of the classes present in the transect containing the bentonite cores BC-48-28 (55 °C), BC-48-29 (72 °C), BC-48-30-1 (92 °C), BC-48-30-2 (92 °C), and the distance of the cores from the heater.	131
Figure 4.7: The number of copies present in each DNA extract from the bentonite cores, and the distance of the cores from the heater.	133
Figure 5.1: The amount of 0.5 M hydrochloric acid extractable Fe(II) in the FEBEX bentonite, and the SWy-2 montmorillonite as determined by Ferrozine assay.	153

Figure 5.2: The change in key interlayer cations (sodium, calcium, potassium, magnesium) expressed as milliequivalents per gram in solution over the course of the experiment.....	156
Figure 5.3: EPR spectrum of the native, and reduced FEBEX bentonite, and SWy-2 montmorillonite. The spectra were normalized to a frequency of 9.8718 GHz, and instrument error was corrected by comparing to a standard (strong pitch) of known <i>g</i> value.....	158
Figure 5.4: Mössbauer spectra of the native and bio-reduced FEBEX bentonite, and SWy-2 montmorillonite, along with fitted iron species.	160
Figure 6.1: The amount of soluble selenium, and 0.5 M hydrochloric acid extractable Fe(II) present in the selenite clay suspensions.	182
Figure 6.2: TEM image of the selenium phase in the acetate, and <i>G. sulfurreducens</i> amended selenite clay suspensions, along with the EDS spectra for the associated area.	183
Figure 6.3: The concentration of soluble selenium, and 0.5 M hydrochloric acid extractable Fe(II) in the selenate clay suspensions.....	185
Figure 6.4: TEM image of the selenium product in the acetate, and <i>G. sulfurreducens</i> amended Se(VI) microcosms, as well as the EDS spectra for the associated area.	185
Figure 7.1: Schematic of the pressure vessels (image obtained from (Bengtsson et al., 2015)).	202
Figure 7.2: Changes in swelling pressure (kPa), and external temperature (°C) over the course of the saturation stage.	207
Figure 7.3: Box and whisker plots depicting the variability in the swelling pressure (kPa) once the pressure vessels had reached a steady state.	207
Figure 7.4: Mechanical pressure (kPa), and external temperature (°C) data from the experimental stage of the study.....	209
Figure 7.5: Variability in the mechanical pressure (kPa) of the pressure vessels during the experimental stage of the work.	209

Tables

Table 1.1: Breakdown of the UK's nuclear waste inventory by volume in its stored, conditioned, and treated states, as well as its radioactivity during the year 2040, and 2200 (RWM, 2016a). HLW, high level waste; ILW, intermediate level waste; LLW, low level waste; SF, spent fuel.	22
Table 1.2: Priority radionuclides with their half-lives, and specific activities (data from (Delacroix et al., 2002)).	23
Table 1.3 Example host rocks and the reasons they were chosen (Sites sourced from (RWM, 2016b)).	26
Table 1.4: Key issues relating to GDF construction and microbes (+/- indicate positive or negative impacts on a GDF).	27
Table 1.5: Mineralogical composition of bentonites, and their source (adapted from (Hicks et al., 2009)).	28
Table 1.6: Chemical formula of pyrophyllite and smectite minerals, R refers to exchangeable cations found in the interlayer region, adapted from (Moore and Reynolds Jr, 1997).	29
Table 1.7: Examples of extremophilic microorganisms	51
Table 1.8: Water activity (aw) in different scenarios, and the activity limits of microorganisms. Adapted from (Brown, 1976).	53
Table 3.1: Key chemical characteristics, including the water content, loss on ignition (LOI), pH, surface area (SA), concentration of key interlayer cations (sodium, calcium, potassium, magnesium), along with the concentration of sulphate, the redox state of 0.5 M HCl extractable iron, and the mineralogy.	99
Table 3.2: Number of IRB and SRB per gram in each of the substrates, along with the 95% confidence intervals (MPN, most probable number; CI, confidence interval; LL, lower limit; UL, upper limit).	100
Table 4.1: Approximations of the geophysical conditions encountered during the FEBEX in-situ project using data obtained from published sources: 1, (Lanyon and Gaus, 2016). 2, (Martinez et al., 2016).	127
Table 4.2: Key metabolic processes, and their temperature limits under optimum growth conditions as inferred from type strain papers of the closest relatives identified by Illumina sequencing of the bentonite core DNA extracts. x denotes the identification of a close relative carrying out a metabolic process, but no temperature constraints available.	132
Table 5.1: Chemical and physical properties of the FEBEX bentonite, and SWy-2 montmorillonite including water content, loss on ignition, pH, surface area, the key interlayer cation concentrations (sodium, calcium, potassium, magnesium), sulphate, manganese, and iron contents, as well as 0.5 M hydrochloric acid extractable iron (Fe(II) and total), and the mineralogy.	152
Table 5.2: Parameters and statistical data for the fitted Mössbauer spectra, X 2, chi-squared; CS, center shift relative to α -Fe(0); QS, quadrupole splitting.	160
Table 6.1: Physical and chemical characteristics of the SWy-3 montmorillonite including water content, loss on ignition, pH, surface area (SA), key interlayer cations (sodium, calcium, potassium, magnesium), sulphate, 0.5 M hydrochloric acid extractable Fe(II), as well as the mineralogy.	181
Table 7.1: Concentrations of compounds in the artificial groundwater (AGW) (Bengtsson and Pedersen, 2017).	199

Table 7.2: Statistical data for the swelling pressure (kPa) in the pressure vessels when they reached a steady state, and the variation in external temperature (°C) during the saturation stage of the experiment.	208
Table 7.3: Statistical data of the mechanical pressures (kPa) in the pressure vessels, as well as the external temperature (°C) during the experimental stage of the study.	210
Table 7.4: Images of the SWy-3 montmorillonite plugs after the experiment. Along with information on the plugs, and <i>Bacillus subterraneus</i> doped SWy-3 (Doped) including grain density of the bentonites (kg m^{-3}), water content (%), interlayer cation (sodium, calcium, potassium, magnesium) concentrations in solution per gram of substrate (mg g^{-1}), sulphate concentration in solution per gram of substrate (mg g^{-1}), volatile fatty acids (VFAs) in solution per gram of substrate (mg g^{-1}), the iron content of the SWy-3 montmorillonite, and the amount of Fe(II), and total Fe extracted using 0.5 M hydrochloric acid per gram of substrate (mg g^{-1}).	211
Table 7.5: The dry weight MPN g-1 values for the doped SWy-3 montmorillonite, and the pressure vessel plugs. Along with 95 % confidence interval (CI), lower limits (LL), and upper limits (UL).	212
Table 7.6: Relationships between swelling pressure (y, kPa), and temperature (x, °C) with predicted swelling pressures (including error margins) at 20 °C.....	213

Haydn Haynes

Microbial Processes Within Bentonite Barrier Materials

Doctor of Philosophy (PhD)

The University of Manchester, 2018

Bentonites are montmorillonite-based materials being considered for use as engineered barriers during the disposal of high heat generating radioactive wastes. Bentonite has several beneficial properties when it comes to the disposal of nuclear waste, including the ability to swell in the presence of water producing a low permeability, material with amphoteric ion exchange sites able to absorb radionuclides. They also offer the ability to buffer the pH, providing stable conditions for the enclosed canisters.

Microorganisms have been identified in natural bentonite horizons and may be viable and active under geological disposal conditions. Initial studies focused on the viability of sulphate-reducing bacteria (SRB) due to their role in the corrosion of canister materials. Fe(III)-reducing bacteria (IRB) were also of interest as Fe(III)-reduction in smectite minerals influences their geochemistry, and ability to swell. Indigenous microbial communities in a range of bentonites were subjected to mechanical pressure, heat, and gamma radiation treatments, and their IRB, and SRB contents counted. All the bentonites contained viable microorganisms after the treatments albeit in low numbers. Cores from a field-scale geological disposal experiment (FEBEX-DP) were also analyzed to see how the temperature gradient influenced the long-term viability of microorganisms. The FEBEX cores tested negative for culturable organisms. However, DNA was extracted, and 16S rRNA genes amplified and sequenced, suggesting an enrichment in anaerobic bacteria at the lower end of the temperature gradient (55 °C).

The reduction of Fe(III) by the subsurface bacterium *G. sulfurreducens* was quantified in SWy-2 montmorillonite and FEBEX bentonite. A significant degree of biological Fe(III)-reduction was observed in the SWy-2 montmorillonite (81 % reduced). Meanwhile, the FEBEX bentonite was largely recalcitrant to biological Fe(III)-reduction (17 % reduced). The lack of Fe(III)-reduction in the FEBEX bentonite was attributed to the presence of iron oxides coating the montmorillonite, or potentially a lower swelling ability which decreased the exposure of Fe(III) in the bentonite to *G. sulfurreducens* cells. The Fe(III)-reduction in the SWy-2 montmorillonite increased the cation exchange capacity (CEC), which could influence the swelling pressure generated by the bentonite. The role of swelling pressure in restricting microbial Fe(III)-reduction in the SWy-3 montmorillonite was also investigated, and suggested a wet density of over 1900 kg m⁻³ (1411 kg m⁻³ dry density) in SWy-3 montmorillonite would be required to halt biological Fe(III)-reduction, with considerable activity observed at 1750 kg m⁻³ (1176 kg m⁻³ dry density) and below. Fe(III)-reduction in SWy-2 montmorillonite also affected the solubility of selenium oxyanions. Selenite and selenate oxyanions were both reduced and precipitated, selenate as a result of direct biological reduction with *G. sulfurreducens* cells, and selenate via a chemical reaction with the montmorillonite.

The results of the molecular ecology on the FEBEX in-situ cores, combined with data from the IRB swelling pressure experiments suggest that microbial activity will be inhibited if a sufficient bentonite buffer density is maintained. If the bentonite density decreases, then microbial activity might be restored, most likely by spore-forming bacteria. In the case of IRB, biological Fe(III)-reduction could cause further swelling pressure decreases. However, IRB may also promote the capture of selenium oxyanions, and potentially other radionuclide species, minimizing their migration from a geodisposal barrier system.

Declaration

No portion of the work referred to in this thesis has been submitted in support of an application for another degree or qualification of this or any other university or other institute of learning.

Copyright statement

- i. The author of this thesis (including any appendices and/or schedules to this thesis) owns certain copyright or related rights in it (the “Copyright”) and s/he has given The University of Manchester certain rights to use such Copyright, including for administrative purposes.
- ii. Copies of this thesis, either in full or in extracts and whether in hard or electronic copy, may be made **only** in accordance with the Copyright, Designs, and Patents Act 1988 (as amended) and regulations issued under it or, where appropriate, in accordance with licensing agreements which the University has from time to time. This page must form part of any such copies made.
- iii. The ownership of certain Copyright, patents, designs, trademarks and other intellectual property (the “Intellectual Property”) and any reproductions of copyright works in the thesis, for example graphs and tables (“Reproductions”), which may be described in this thesis, may not be owned by the author and may be owned by third parties. Such Intellectual Property and Reproductions cannot and must not be made available for use without prior written permission of the owner(s) of the relevant Intellectual Property and/or Reproductions.
- iv. Further information on the conditions under which disclosure, publication and commercialization of this thesis, the Copyright and any Intellectual Property and/or Reproductions described in it may take place is available in the University IP Policy (see <http://documents.manchester.ac.uk/DocuInfo.aspx?DocID=24420>), in any relevant Thesis restriction declarations deposited in the University Library, The University Library’s regulations (see <http://www.library.manchester.ac.uk/about/regulations/>) and in The University’s policy on Presentation of Theses.

Acknowledgements

I would like to take the time to thank everyone who contributed their expertise and assisted with the work presented in this thesis. Firstly, I would like to thank Jon Lloyd, and Carolyn Pearce for providing engaging discussion on the topic areas, their contributions towards the development of this research, and for taking the time to review manuscripts. I would also like to thank Radioactive Waste Management (RWM) for providing the funding for this work and providing insight from a nuclear waste management organizations perspective. Guidance from Matt Bailey, and Rob Winsley was of help in understanding the role of this work, and other PhD projects in the implementation of geological waste disposal.

I would also like to thank the people whose technical support made this research possible, including Chris Boothman, Al Bewsher, Paul Lythgoe, John Waters, Heath Bagshaw, from the School of Earth, and Environmental Science, Adam Brookfield from the School of Chemistry, Ruth Edge from the Dalton Cumbrian Facility, Jon Harrington from the British Geological Survey, and Anke Neumann from Newcastle University.

The support, encouragement of the Geomicrobiology research group was also invaluable in making the last 4 years of study enjoyable. Thanks go out to the people who have showed me how to use equipment, provided a spare pair of hands when needed, and kept me amused after the 100th or so Ferrozine assay. Special thanks go out to the people who introduced me to the world of climbing, and those who have started along the way and continue to climb today.

I would like to thank old friends and new from Manchester especially Nadine and Dunny. Finally, I would like to thank family and friends from home for their support, and encouragement over the course of my study including Mom, Dad, Jack, Ash, Amber, Hannah, Harriet, Graham, Tom, and Natalie. An honorable mention goes out to “the great” uncle John who sadly is not here to see the completion of this work.

The Author

The author of this research graduated from the University of Manchester in 2014 with a MSc (Hons) in Earth Science. The author completed a research project in his 4th year of study titled “Geochemical Cycling of Uranium in Clays” in the Geomicrobiology research group in the School of Earth, and Environmental Sciences where he has continued to pursue the work detailed in this thesis under the supervision of Prof. Jon Lloyd, and Dr. Carolyn Pearce.

During his time working towards this thesis the author has published a paper titled “Response of Bentonite Microbial Communities to Stresses Relevant to Geodisposal of Radioactive Waste” and has provided his input to the MIND (Microbiology in Nuclear Waste Disposal) EU project.

Statement

The work in this thesis is presented in the Journal Format and is made up of the pieces of work described below. Due to the nature of the Journal Format a degree of repetition is observed in each of the chapters, especially the introduction, and methodology. This is to allow for the research chapters to be submitted for publication in scientific journals. At the time of preparing this thesis submission chapter 3 has been published.

Chapter 1 - Introduction: Bentonite Utilization in the Geological Disposal of Radioactive Waste, and the Activity/Viability of Microorganisms in such an Environment

H. M. Haynes – Principal author

Chapter 2 – Methodology

H. M. Haynes – Principal author

Chapter 3 – Response of Bentonite Microbial Communities to Stresses Relevant to Geodisposal of Radioactive Waste

Published in Chemical Geology <https://doi.org/10.1016/j.chemgeo.2018.10.004>

H. M. Haynes – Principal author; C. I. Pearce – Manuscript review; C. Boothman – Sequencing and bioinformatics; J. R. Lloyd – Manuscript review and principal supervisor

Chapter 4 – The Molecular Ecology of the FEBEX *in-situ* Project Along the Temperature/Evolving Resaturation Gradient

H. M. Haynes – Principal author; C. I. Pearce – Manuscript review; C. Boothman – Sequencing and bioinformatics; J. R. Lloyd – Manuscript review and principal supervisor

Chapter 5 – Monitoring Bioreduction of Iron (III) in Bentonites Using a Magnetic Approach

H. M. Haynes – Principal author; C. I. Pearce – Manuscript review; A. Neumann – Mössbauer spectroscopy; A. Brookfield – Electron paramagnetic resonance; J. R. Lloyd – Manuscript review and principal supervisor

Chapter 6 – Selenium Speciation in Microbially Reduced SWy-3 Montmorillonite

H. M. Haynes – Principal author; C. I. Pearce – Manuscript review; J. R. Lloyd – Manuscript review and principal supervisor

Chapter 7 – The Viability and Activity of Iron (III)-reducing Bacteria in Response to Bentonite Density and Swelling Pressure

H. M. Haynes – Principal author, C. I. Pearce – Manuscript review, J. Harrington – Equipment development and experimental design; J. R. Lloyd – Manuscript review and principal supervisor

Chapter 8 – Conclusions and Future Directions

H. M. Haynes – Principal author

1. Introduction: Bentonite Utilization in the Geological Disposal of Radioactive Waste, and the Activity/Viability of Microorganisms in such an Environment

1.1. Introduction

The UK has been harnessing nuclear fission since the 1950s, primarily for electricity generation, as well as for the manufacture of products related to civil defense, medical therapies, and research. Nuclear power generation is a low carbon source of electricity, and will be a crucial element of meeting climate targets set out in the Paris Agreement (UN, 2015), and Kyoto Protocol (UN, 2008). However, legacy wastes, and future wastes are costly to process, and their disposal in a safe manner is required to mitigate risks to public, and environmental health. An internationally recognized method for disposing of nuclear wastes is through a multi-barrier underground disposal system known as a geological disposal facility (GDF) (NDA, 2013). GDFs are made up of the waste form, container, a buffer, and the host rock (SKB, 2006)

Bentonite is a clay-based material being considered by Radioactive Waste Management Limited (RWM) (the organization responsible for nuclear waste disposal in the UK), and other national waste management agencies, for use as a buffer material in the disposal of high heat generating nuclear wastes (Wilson et al., 2011). Bentonite has several advantageous characteristics including the ability to swell, low permeability, radionuclide retention, and the capacity to filter colloids and microbes. Despite these properties there are still significant data gaps to be answered regarding the effects of microbes on bentonite mineralogy, and barrier performance. The consequences of microbial activity on bentonite performance are of interest to RWM and other national waste disposal agencies, as well as participants in the Microbiology in Nuclear Waste Disposal (MIND) program.

This literature review summarizes the suitability of bentonite for use as a buffer in the disposal of HLW, and the potential influences of microbial activity on the structure of bentonite, the stability of canisters intended for nuclear waste disposal, and hence engineered barrier performance within a GDF. Of relevance to this thesis is the activity of Fe(III)-reducing bacteria (IRB), and sulphate-reducing bacteria (SRB) whose physiology is described in detail, along with the mechanisms employed by microorganisms to withstand extreme stress, which will control their viability in a geological waste disposal scenario. Such work is vital to contributing to the knowledge base regarding the disposal of radioactive wastes.

1.1.1. Nuclear fuel cycle

The nuclear fuel cycle encompasses a series of processes involved in the manufacture, usage, recycling, and disposal of nuclear fuel. The nuclear fuel cycle is a complicated process, and waste products of varying hazard are produced at every step. Some of the products from the nuclear fuel cycle are also used for weapon manufacture, medical therapies, and research.

Figure 1.1 depicts a simplified version of the nuclear fuel cycle.

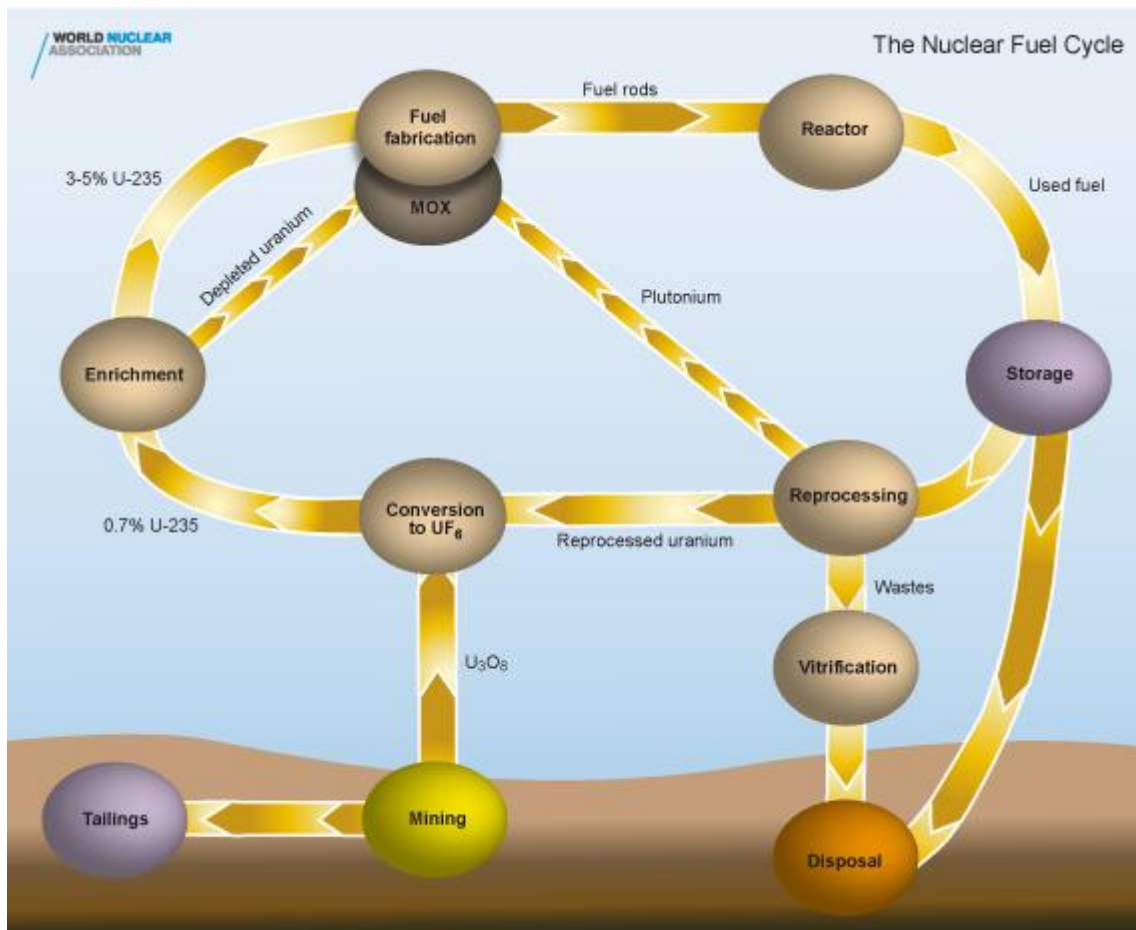


Figure 1.1: An overview of the nuclear fuel cycle (WNA, 2015).

1.1.2. UK waste inventory

The UK classifies the wastes from the nuclear fuel cycle into six categories, low level waste (LLW), intermediate level waste (ILW), high level waste (HLW), spent fuel (SF), separated plutonium and uranium (RWM, 2016a). These can be grouped into two kinds of waste, low heat generating wastes (LHGW), and high heat generating wastes (HHGW). LHGW consists of LLW which is made up of general refuse such as paper, plastic etc. that becomes contaminated during the operation of nuclear facilities, LLW is disposed of at the Low Level

Waste Repository, Cumbria (Wilkins et al., 2010). ILW is also LHGW, and is generated during SF reprocessing, as well as being made up of contaminated building materials, and the graphite from reactor cores, ILW will eventually be disposed of in a geological disposal facility (GDF). HHGW is mostly made up of SF the term given to reactor fuel which is no longer usable and is normally stored for future disposal. Reprocessed SF generates uranium, and plutonium products, along with HLW. HLW is vitrified into glass and will be disposed of in a future GDF. The volumes and radioactivity of the mentioned wastes are described in Table 1.1:

Table 1.1: Breakdown of the UK's nuclear waste inventory by volume in its stored, conditioned, and treated states, as well as its radioactivity during the year 2040, and 2200 (RWM, 2016a). HLW, high level waste; ILW, intermediate level waste; LLW, low level waste; SF, spent fuel.

Waste category	Stored volume (m ³)	Conditioned volume (m ³)	Packaged volume (m ³)	Activity (TBq)	
				2040	2200
HLW	1,410	1,410	9,290	3.5×10^7	1.1×10^6
ILW	2.7×10^5	3.5×10^5	4.6×10^5	1.9×10^6	1.2×10^6
LLW	9,330	1.1×10^4	1.2×10^4	0.908	2.48
Pu	0.567	174	620	6.2×10^4	4.4×10^4
SF	9,850	9,850	6.6×10^4	1.9×10^8	2.5×10^7
U	1.1×10^5	1.6×10^5	2.2×10^5	8,430	8,430
Total	4.0×10^5	5.4×10^5	7.6×10^5	2.3×10^8	2.7×10^7

The table shows that the volume of HHGW is much lower than LLGW, however both are comparable when the packaged volume is taken into consideration. This is because of the extra shielding required for HHGW to protect workers, and equipment from the heat, and radioactivity. HHGW accounts for 99.2 % of the radioactivity in the year 2040, and 95.8 % in the year 2200. Listed in Table 1.2 are a series of radionuclides that RWM consider to be the highest priority when it comes to geological disposal (RWM, 2016a).

Table 1.2: Priority radionuclides with their half-lives, and specific activities (data from (Delacroix et al., 2002)).

Radioisotope	Half-life (years)	Specific activity (Bq g ⁻¹)
C-14	5.73×10^3	1.65×10^{11}
Cl-36	3.00×10^5	1.23×10^9
Co-60	5.27	4.18×10^{13}
Se-79	6.50×10^4	2.59×10^9
Kr-85	10.7	1.45×10^{13}
Tc-99	2.11×10^5	6.36×10^8
I-129	1.57×10^7	6.53×10^6
Cs-135	2.30×10^6	4.44×10^7
Cs-137	30.2	3.20×10^{12}
U-233	1.59×10^5	3.57×10^8
U-235	7.04×10^8	8.00×10^4
U-238	4.47×10^9	1.24×10^4
Np-237	2.14×10^6	2.64×10^7

The half-life refers to the time it takes for half the quantity of a radionuclide to decay to its daughter products, specific activity is the radioactivity per quantity of the radionuclide (often expressed as Becquerels per gram (Bq g⁻¹). As can be inferred from Table 1.2 a lot of these radionuclides exhibit high activity and will remain in significant quantities for hundreds of thousands of years, many of these radionuclides are also of toxicological concern. The design of a GDF must take these factors into account and provide stable conditions for many thousands of years.

1.1.3. Geological disposal facility

The term geological disposal facility (GDF) is used to describe a waste repository situated under several hundred meters of host rock, and is the preferred option for 25 nuclear waste generating nations (NDA, 2013). GDFs implement a multi-barrier system which utilizes engineering, and the properties of the host rock to isolate the waste from its wider surroundings. The multi-barrier system is formed of several components: the waste form, a container, in some instances a metal overpack, the host rock, and a buffer material that fills the gap between the container and the host rock; a representation of this system is described in Figure 1.2 (SKB, 2006).

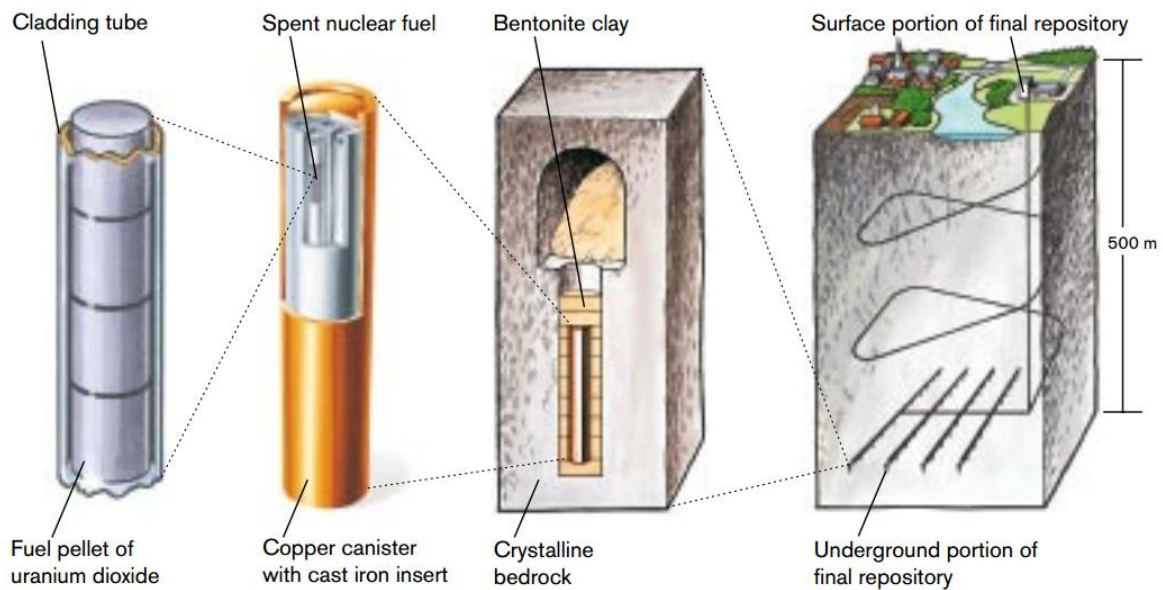


Figure 1.2: Overview of the KBS-3 Swedish GDF concept, highlighting the waste form (fuel pellet), metal container (cladding tube), metal overpack (copper canister), buffer (bentonite), and host rock (SKB, 2006).

1.1.3.1. Waste forms

Vitrified HLW is formed when highly active liquor is heated in the presence of glass-forming additives at high temperatures, the molten glass is poured into stainless steel containers (Harrison, 2014). Spent fuel is currently stored in cooling ponds where it is expected to remain for up to 140 years; this will allow for it to cool to a temperature safe for disposal (NDA, 2014). Once cooled the SF will be transferred into cast iron inserts, or carbon steel baskets depending on the waste canister chosen (Hicks et al., 2018). Both the HLW, and SF waste forms are recalcitrant to leaching, however some components of SF are expected to leach if they come into contact with groundwater (Bauhn et al., 2018). The containers, inserts, and baskets housing the waste are purely for handling purposes and are not expected to serve a long-term function.

1.1.3.2. Container (overpack)

In the case of the KBS-3 Swedish GDF concept, overpacks have several safety functions including protecting the waste from physical disturbances, isolation from groundwaters, partial protection from groundwater following canister breach, controlling redox conditions

around the waste during corrosion, and allowing the movement of gas away from the waste (Harvey et al., 2012). Overpacks typically house several smaller containers, and depending on host rock, and desired lifetime are made from corrosion-resistant materials such as carbon steel, or copper (Hicks et al., 2018).

1.1.3.3. Buffer material

Buffers are designed to fill in the space between the host rock and the overpack. Some of the functions of the buffer are similar to the overpack including protecting the waste from rock movements, restricting groundwater flow to the container and maintaining stable chemical conditions. The buffer provides additional radionuclide retardation by providing sorption sites, and also prevents the accumulation of gases (Bailey, 2015). Crushed salt, cement-based materials, and clays are typical choices for buffers, the geological environment ultimately dictates which is the most suitable (Baldwin et al., 2008). Clays have a low permeability, surface sites for adsorption of radionuclides, pH buffering properties, and small pore spaces; bentonite is the preferred clay as it swells in contact with water, further reducing the permeability and pore sizes (Wilson et al., 2011). Cementitious materials generate alkaline conditions which inhibit corrosion and decrease the solubility of some radionuclides (RWM, 2016b). However cementitious material usage in conjunction with HLW is limited, due to challenges associated with thermal stability (Holton et al., 2012). Crushed salt is being considered for use in conjunction with a salt host rock (Table 1.3), as host rock creep will compact the salt producing an impermeable barrier (RWM, 2016b). This project is focused on bentonite buffers and further discussion of them can be found in later sections.

1.1.3.4. Host rock

There are several properties relating to the host rock and its influence on the engineered components that dictate whether the geological environment is suitable or not. These properties include its ability to conduct heat, its hydrogeological characteristics, chemistry, and the mechanical behavior of the host rock (Baldwin et al., 2008). Suitable host rocks may be considered as falling into one of three categories, higher strength rocks, lower strength sedimentary rocks, and evaporites (Table 1.3) (RWM, 2016b).

Table 1.3 Example host rocks and the reasons they were chosen (Sites sourced from (RWM, 2016b)).

Host Rock	Example	Advantages
Higher Strength Rocks (SKB, 2006)	Forsmark Site, Sweden (granite)	<ul style="list-style-type: none"> - High quartz content (permits thermal conductivity) - High average uniaxial compressive strength (UCS) values of 225 MPa - Geologically ancient deformation zones - Limited groundwater flow
Lower Strength Sedimentary Rocks (Nagra, 2002)	Opalinus Clay, Switzerland	<ul style="list-style-type: none"> - Simple geological structure permitting long-term predictions - Homogenous lithology with poor permeability - Low-permeability formations above and below
Evaporites (BMW, 2008)	Gorleben Salt Dome, Germany	<ul style="list-style-type: none"> - Germany has a long history of salt formation mining - Rock creep causes formations to seal under mechanical load - Poor permeability - High thermal conductivity

1.1.4. Microbe interactions with GDF materials

Very few near-surface environments can be considered sterile, and therefore microbes may impart an influence during the construction, and operation of a GDF, listed below (Table 1.4) is some of the key issues being discussed when it comes to microbes, and their potential impact.

Table 1.4: Key issues relating to GDF construction and microbes (+/- indicate positive or negative impacts on a GDF).

Process	Impact	Reference
Gas metabolism		
Hydrogen consumption	+ Hydrogen produced by abiotic reactions is consumed by microbes, reducing gas pressure, and explosion risk.	(Bachofen, 1991)
Methane production	- Methanogens generate methane from carbon dioxide, and organic matter, increasing gas pressure, and explosion risk.	(Askarieh et al., 2000)
Methane consumption	+ Methane consumed as an electron donor by a variety of organisms including SRB, aerobic methanotrophs, and denitrifying bacteria.	(Meulepas et al., 2010)
Cellulose		
Incomplete microbial degradation	- Depending on the microbial community anaerobic microbial degradation of cellulose produces methane, carbon dioxide, hydrogen, acetate, and hydrogen sulfide.	(Beguin and Aubert, 1994)
ISA degradation	+ Microbes degrade ISA (a strong complexant formed by chemical alkali hydrolysis of cellulose), preventing the production of soluble radionuclide complexes.	(Bassil et al., 2015)
Radionuclides		
Adsorption and uptake	- Radionuclides become associated with cells and potentially transported.	(Newsome et al., 2014)
Biom mineralization	+ Precipitation of insoluble radionuclides.	(Newsome et al., 2014)
Material interactions		
Corrosion	-/+ Hydrogen sulphide produced by SRB will cause corrosion of steel canisters but may also precipitate a protective film.	(El Mendili et al., 2013)
Clay alteration	- Fe(III) reduction by Fe(III)-reducing bacteria may cause smectite dissolution.	(Kim et al., 2004)

1.2. Bentonite

Bentonite is being considered as a buffer material for geological disposal as it has several advantageous properties including a low permeability, the ability to self-seal following gas migration, resistance to mechanical forces, retention of radionuclides and colloids, and swelling in the presence of water (Hicks et al., 2009). The definition of a bentonite has changed several times over the past century, but in the geological disposal community is used to describe a clay rich in smectite material (Wilson et al., 2011). Bentonite is formed from the hydrothermal alteration of a variety of rocks including tuffs and lavas at low temperatures, and contains other clay minerals such as illite, as well as accessory minerals like feldspar, quartz, and plagioclase (Hicks et al., 2009). Several types of smectite exist including beidellite, nontronite, saponite, and hectorite, however sodium-enriched montmorillonite is preferred for use as a buffer, as it has a greater swelling ability (Hicks et al., 2009).

1.2.1. Bentonite mineralogy

The mineralogical composition of bentonites varies greatly between deposits, Table 1.5 provides an overview of some common bentonites. It is worth noting that the chemical composition of bentonites does vary, even between samples extracted from the same quarry, so the below values should only be used as a guide (Karnland, 2010).

Table 1.5: Mineralogical composition of bentonites, and their source (adapted from (Hicks et al., 2009).

	MX-80	Avonseal	Kunipia F	Montigel	FEBEX
Source	Wyoming, USA	Canada	Japan	Germany	Almeria, Spain
Montmorillonite (wt %)	87	79	98-99	66	89-95
Quartz/Chalcedony (wt %)	3	5	<1	8.3	1-3
Cristobalite (wt %)	2	-	-	-	1-3
Feldspar (wt %)	3	1.5	-	2-4	1-3
Calcite/Siderite (wt %)	-	-	<1	-	0.6
Pyrite (wt %)	0.25	-	-	-	0.02
Mica (wt %)	4	-	-	12-15	-
Illite (wt %)	1	9.5	-	2	-
Gypsum (wt %)	0.7	2	-	1.8	0.14
Rutile/Anatase (wt %)	0.2	-	-	-	-
Organic Matter (wt %)	0.2	0.3	-	0.03	0.3
Other (wt %)	-	-	-	2-3	0.8

As can be observed from Table 1.5 montmorillonite is the main component and is responsible for the properties alluded to previously. Montmorillonite and the other smectite minerals are made up of a 2:1 layer structure, consisting of an octahedral sheet sandwiched between two tetrahedral sheets (Moore and Reynolds Jr, 1997). Pyrophyllite is a 2:1 clay mineral with no layer charge and is a precursor to smectite minerals. Pyrophyllite has the formula $\text{Al}_2\text{Si}_4\text{O}_{10}(\text{OH})_2$ with the octahedral sheet formed of Al^{3+} ions surrounded by three unit oxygens, and the tetrahedral sheets formed of Si^{4+} ions surrounded by 2 unit oxygens (Wilson et al., 2011). Models of the octahedral and tetrahedral sheets of pyrophyllite are shown in Figure 1.3.

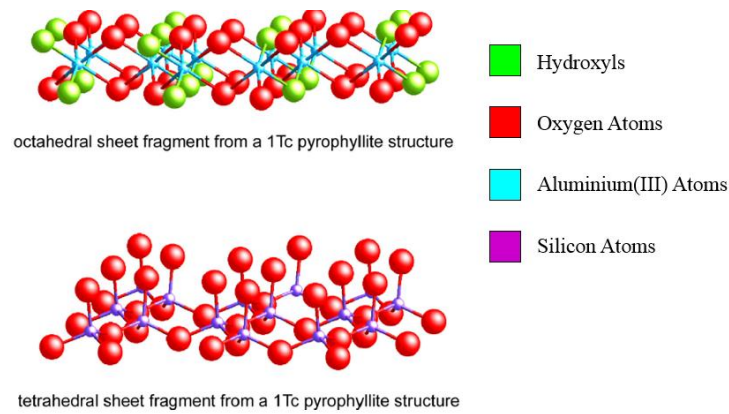


Figure 1.3: Structural units of pyrophyllite octahedral, and tetrahedral sheets (adapted from (Wilson et al., 2011)).

Smectites are formed by substitution of the Al^{3+} ions for Fe^{2+} and Mg^{2+} in the octahedral layer and substitution of the Si^{4+} ions for Fe^{3+} and Al^{3+} in the tetrahedral layer, this leads to the development of a negative layer charge (Moore and Reynolds Jr, 1997). The formula of pyrophyllite and a variety of smectite minerals are compared in Table 1.6.

Table 1.6: Chemical formula of pyrophyllite and smectite minerals, R refers to exchangeable cations found in the interlayer region, adapted from (Moore and Reynolds Jr, 1997).

Mineral	Formula	Octahedral Charge	Tetrahedral Charge
Pyrophyllite	$\text{Al}_2\text{Si}_4\text{O}_{10}(\text{OH})_2$	0	0
Montmorillonite	$\text{R}_{0.33}^+(\text{Al}_{1.67}\text{Mg}_{0.33})\text{Si}_4\text{O}_{10}(\text{OH})_2$	- 0.33	0
Beidellite	$\text{R}_{0.33}^+\text{Al}_2(\text{Si}_{3.67}\text{Al}_{0.33})\text{O}_{10}(\text{OH})_2$	0	- 0.33
Nontronite	$\text{R}_{0.33}^+\text{Fe}^{3+}_2(\text{Si}_{3.67}\text{Al}_{0.33})\text{O}_{10}(\text{OH})_2$	0	- 0.33
Hectorite	$\text{R}_{0.33}^+(\text{Mg}_{2.67}\text{Li}_{0.33})\text{Si}_4\text{O}_{10}(\text{OH})_2$	- 0.33	0
Saponite	$\text{R}_{0.33}^+(\text{Mg}_{2.67}\text{R}_{0.33}^{3+})(\text{Si}_{3.34}\text{Al}_{0.66})\text{O}_{10}(\text{OH})_2$	+ 0.33	- 0.66

The 2:1 layers of smectite minerals are stacked on top of each other in a parallel fashion (Wilson et al., 2011), shown in Figure 1.4.

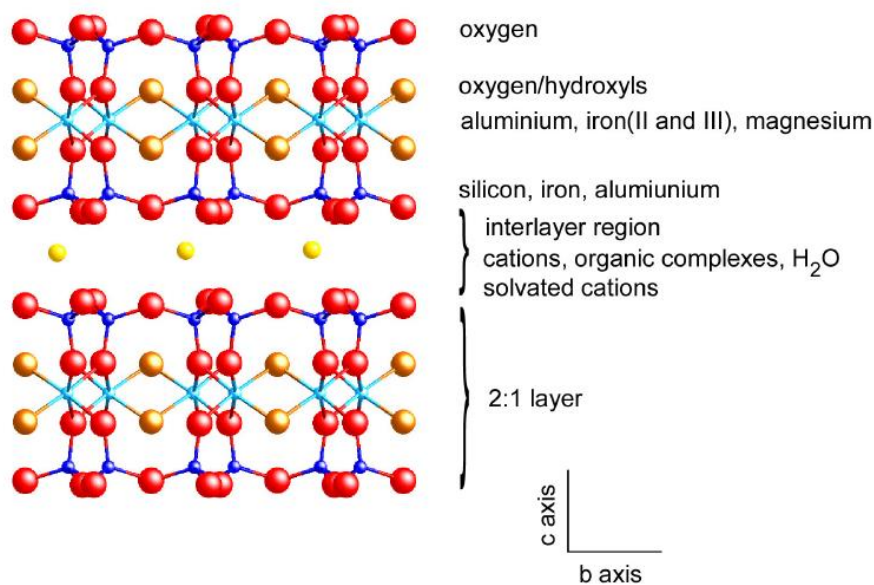


Figure 1.4: Two parallel 2:1 layers of a smectite mineral (Wilson et al., 2011).

1.2.2. Particle size and surface area

Montmorillonite is typically made up of laminar aggregates, with a poorly defined form, and a large variety in size, and thickness (Güven, 1988). These aggregated particles are commonly referred to as primary particles, and have a width of approximately one to two μm . When soaked in a solution these particles break into smaller free particles, with a width of less than 0.2 μm (Wilson, 2013). Free particles can consist of a single layer, up to twenty layers corresponding to thicknesses between 10 Å and 200 Å, with morphologies ranging from ribbon-like units, to subhedral with irregular outlines, and euhedral with hexagonal or rhombic forms (Güven, 1988). As a result in this change of form between a dry and wet state the surface area of montmorillonite can vary greatly depending on the humidity, and is also known to change depending on the technique used for measurement (Wilson, 2013). A typical technique used in mineralogy for surface area measurement is nitrogen adsorption using Brunauer-Emmett-Teller (BET) theory (Brunauer et al., 1938). BET is conducted on a dry sample, and under these conditions the nitrogen is unable to penetrate the interlayers of the montmorillonite, and therefore only the external surfaces are measured. An alternative to BET is methylene blue absorption which allows measurement of the mineral in a hydrated state; chemisorption of the methylene blue molecule can occur on all of the clay surfaces (including the interlayer), however the stacking of particles, and competing ions may

interfere with the result (Santamarina et al., 2002). Kinter and Diamond (1956) used a combination of nitrogen adsorption, and glycerol retention to determine the free particle surface area of five sodium-montmorillonites, they found the external surface areas were between $16\text{-}35\text{ m}^2\text{ g}^{-1}$, and the internal surface areas $583\text{-}714\text{ m}^2\text{ g}^{-1}$, they also discovered that the exchangeable cation has an influence with K^+ and NH_4^+ giving low internal surface areas, and Na^+ high internal surface areas. The internal surface area of pure montmorillonite was theoretically determined to be between $760\text{ and }810\text{ m}^2\text{ g}^{-1}$ (Kinter and Diamond, 1956), much higher than the experimental values, however more recent studies have come closer to these values with transmission electron microscopy (TEM) measurements recording $669\text{ m}^2\text{ g}^{-1}$ (Nadeau, 1985), and atomic force microscopy (AFM) achieving $780\text{ m}^2\text{ g}^{-1}$ (Tournassat et al., 2003).

1.2.3. Electric double layer theory

To balance the net negative charge on individual 2:1 layers, cations and accompanying polar fluids (such as water) are drawn into the space between layers, expanding the interlayer region (Moore and Reynolds Jr, 1997). The interaction of the interlayer region and associated cations can be explained by the electric double layer theory. The negatively charged (001) surface draws in a layer of water known as the immobile liquid layer, the associated cations are concentrated at the mineral surface (Moore and Reynolds Jr, 1997). This concentrated cation layer attracts loosely bound anions making up the diffuse layer, and subsequent diffuse layers are made of alternating cations and anions, until the charge is neutralized. A diagram of the electric double layer theory is presented in Figure 1.5.

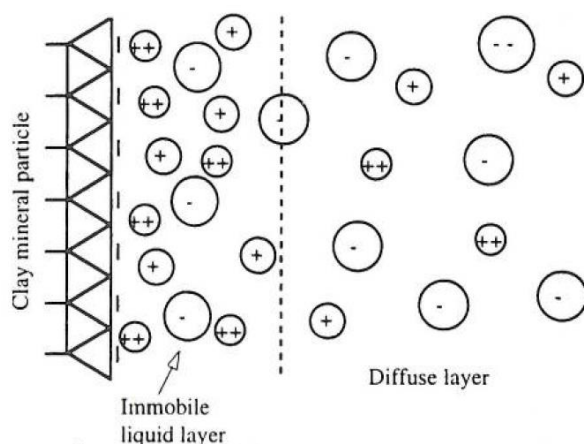
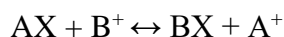


Figure 1.5: Diagrammatic representation of electric double layer theory (Moore and Reynolds Jr, 1997).

The thickness of the immobile liquid layer decreases with increasing cation charge, as fewer cations are required to neutralize the (001) surface, if the immobile liquid layer is thin enough van der Waals forces between clay particles bind them together and cause flocculation (Moore and Reynolds Jr, 1997).

1.2.4. Cations

As opposed to a uniform negative charge across the clay surface, the charge deficit is localized to the defects arising from substitution and the subsequent effect the loss of a proton has on the location of electrons next to the defect (Bleam, 1990). It is these regions that the cations are drawn to. The amount of cations a clay can hold is referred to as the cation exchange capacity (CEC), and is of interest due to its effects on the electric double layer, as well as the physical and chemical properties of the clay (Moore and Reynolds Jr, 1997). The exchanging of cations in the interlayer region for other cations can be approximated by the law of mass action, which states that the rate of a chemical reaction is proportional to the concentration of the reactants as stated below (Eberl, 1980):



A and B refer to the available cations and X the clay surface. Law of mass action is applicable for highly concentrated single-cation solutions, however predictability with low concentration and multi-cation solutions is poor, with the effects of pH, heterogeneity of the layer charge, cation concentration, temperature, as well as the size and charge of individual cations all playing a role in cation exchange (Moore and Reynolds Jr, 1997). Figure 1.6 plots the exchange free energy (ΔG^0_{ex}) of several cations against the equivalent anionic radius (r_a) relative to Cs^+ in a dry montmorillonite, and one with a 3M interlayer solution. The lowest curve for a given (r_a) is the most preferred cation to exchange with, and the distance between curves shows how much the cation is preferred (Eberl, 1980).

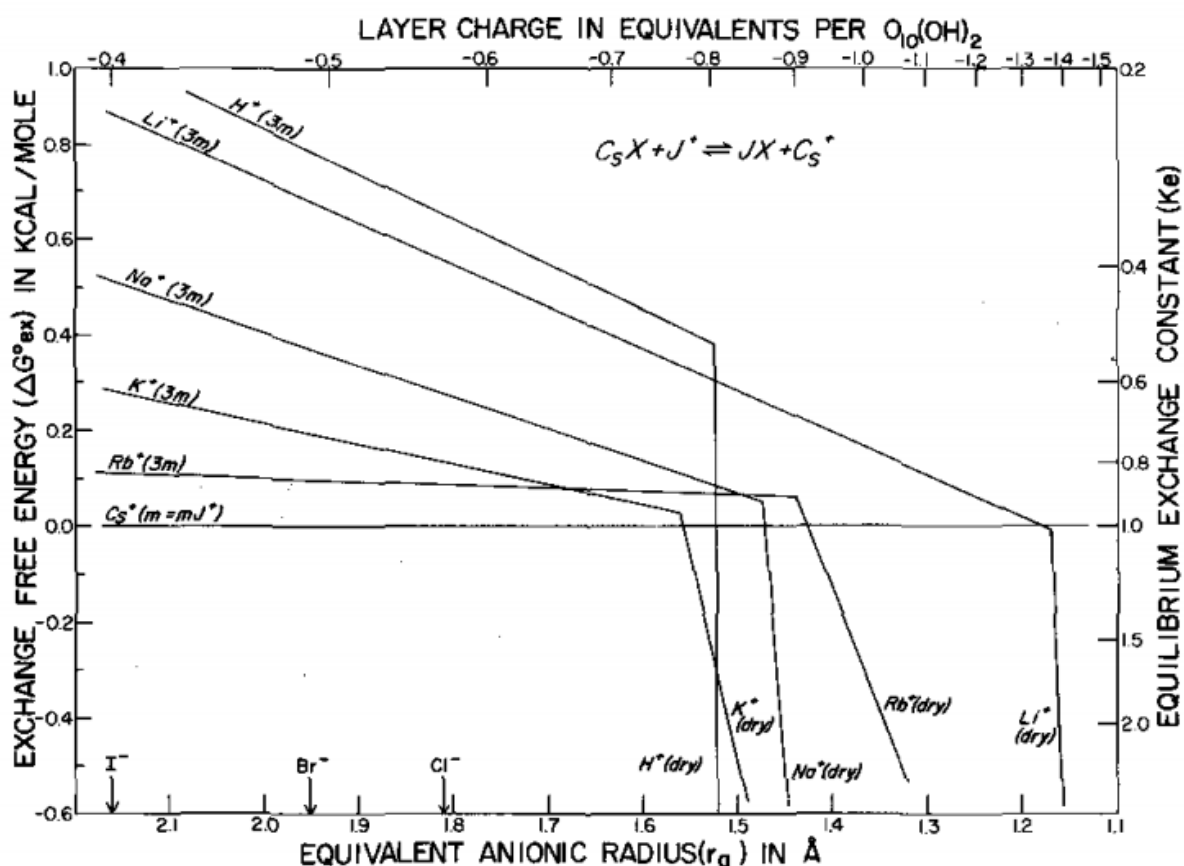


Figure 1.6: Exchange free energy (ΔG°_{ex}) plotted against the equivalent anionic radius (r_a) for the exchange of several cations with Cs^+ , comparing a dry clay to one containing a 3M interlayer solution (Eberl, 1980).

1.2.5. Swelling

The extent of montmorillonite swelling following the adsorption of water is strongly dependent on the solute concentration of the surrounding solution, as well as the species of cation involved (Wilson, 2013). Following the adsorption of monovalent cations such as Na^+ delamination may occur, causing the separation of silicate sheets by over 100 Å, a process known as osmotic swelling (Norrish, 1954). Cations bearing a stronger positive charge limit swelling to approximately four layers of water, equivalent to 10 Å (Wilson, 2013). This phenomenon is not observed in all montmorillonites, especially those bearing divalent counterions, where swelling cannot exceed 19 Å (Norrish, 1954). This unusual behavior in divalent counterion-bearing montmorillonites occurs as a result of the balancing of the van der Waals forces between interlayers, and the electrostatic attraction between the clay surface, and interlayer cations (Helmy, 1998). Variations in swelling have also been observed in montmorillonites from different sites, Wyoming montmorillonite consisting of 2000-5000 Å sized particles exhibits osmotic swelling at 60% relative humidity, while Camp Bertaux

montmorillonite formed from 100 Å particles does not osmotically swell until a relative humidity of 90% (Mering and Oberlin, 1971). Montmorillonite also undergoes transformation following swelling, with the mean particle size of Wyoming montmorillonite decreasing (Figure 1.7), and a change from an ordered distribution of particles to a randomized distribution (Katti and Katti, 2006).

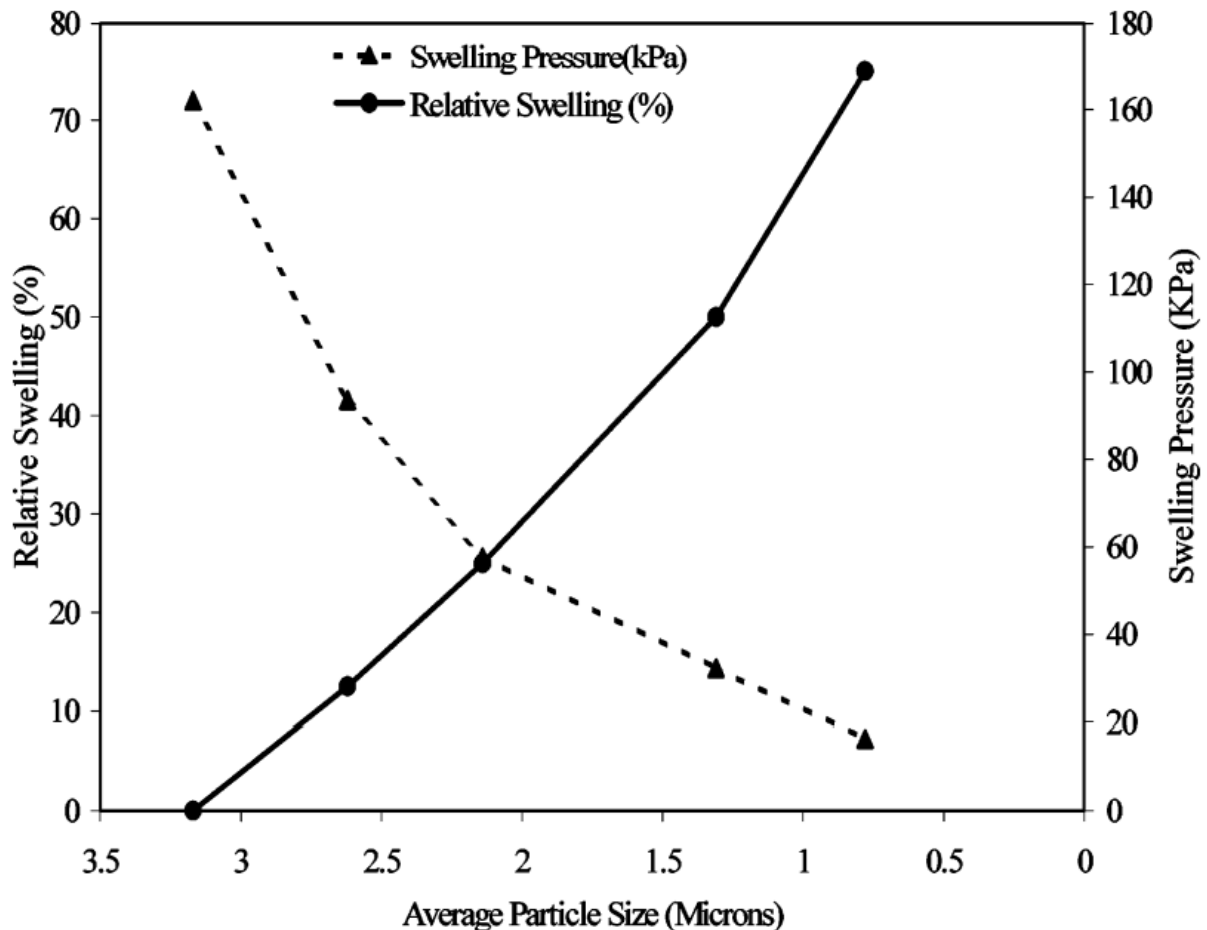


Figure 1.7: Changes in average particle size (μm) in response to swelling pressure (kPa) (pressure occurring as the result of the absorption of water in a confined space), and relative swelling (%) (Katti and Katti, 2006).

1.2.6. Dispersion and colloids

The above responses to the adsorption of water also influence the behavior of colloids in a dilute montmorillonite suspension. Monovalent cation-bearing montmorillonites disperse into single sheets, compared to divalent cation-bearing montmorillonites which form stacks of four to seven sheets referred to as tactoids (Schramm and Kwak, 1982). The behavior of

sodium-saturated bentonites in solution can cause erosion, to the detriment of engineered barriers (Wilson, 2013). Once again the particle size plays a large role in determining dispersity with the small particles of Camp Berteaux montmorillonite being much more recalcitrant to dispersal, compared to the large particles of Wyoming montmorillonite (Mering and Oberlin, 1971). Dispersal of montmorillonite is more prevalent in alkaline conditions, particularly when the concentration of solutes is low, flocculation of montmorillonite particles occurs under acidic conditions (Wilson, 2013). The presence of organic compounds also augments dispersal, with low concentrations of humic acids having a particularly strong influence (Tarchitzky and Chen, 2002). The sorption of radionuclides to colloids is a concern, as the mobility of colloids may promote radionuclide transport into the host rock, whilst decreasing the sorption capacity of the buffer material (Alexander and Neall, 2011). Whether the presence of colloids will impact radionuclide transport or not is dependent on several factors described in Figure 1.8.

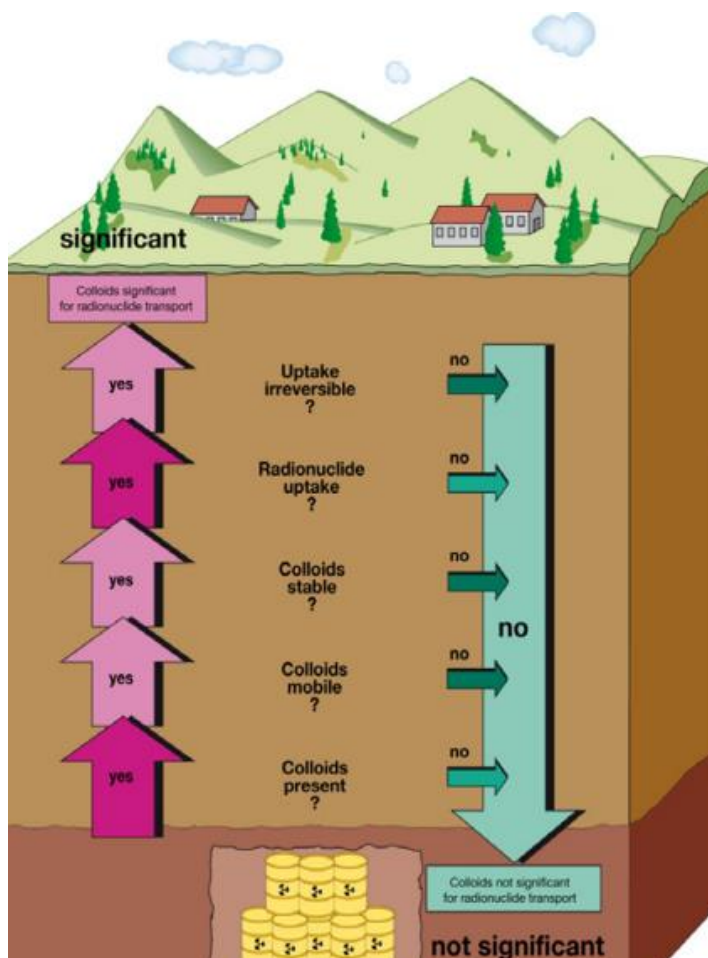


Figure 1.8: Overview of the issues that determine if colloidal transport will have a significant effect on radionuclide transport (Chapman et al., 1993).

1.3. Factors influencing bentonite structure

As well as the chemical factors described above a number of physical, and biological factors relevant to geological disposal need to be taken into account when considering the behavior of bentonite in a repository. These include gamma irradiation, swelling pressure needed to produce a functional barrier, resaturation of the barrier during its lifetime, and the impact of microbiological activity on barrier performance.

1.3.1. Gamma radiation and bentonite

Despite the crystal structure of many clay minerals being disrupted by gamma radiation, smectite minerals are remarkably recalcitrant to gamma-induced defects (Allard et al., 2012). Electron paramagnetic resonance spectroscopy (EPR) conducted on Slovak bentonites subjected to 10 kGy detected no structural changes (Galambos et al., 2012). A similar conclusion was reached with infrared (IR) spectroscopy and ^{27}Al and ^{29}Si nuclear magnetic resonance (NMR) probing of SWy-1 bentonite exposed to 2 MGy of gamma radiation, although minor disparities in the water content were noted (Negron et al., 2002). Small changes in the interactions of gamma irradiated bentonites with other particles have been detected, for example MX-80 bentonite irradiated with 80 kGy shows enhanced surface complexation of Co^{2+} (Holmboe et al., 2011). The stability of MX-80 bentonite colloids has also been shown to increase as a result of an increase in surface potential, following a dose of 53.2 kGy (Holmboe et al., 2009). An increase in the Fe(II)/Fe(total) ratio of Swy-2 montmorillonite from 3 % to 30% was observed following a daily dose rate of 13 kGy, as a result of the reductants, and oxidants formed during water radiolysis; the newly formed Fe(II) was found to decompose the radiolysis product H_2O_2 via the Fenton reaction (Holmboe et al., 2012).

1.3.2. Radiolysis and porewater chemistry

Radiolysis is the process by which molecules dissociate as a result of ionizing radiation, as a result of the breaking of one or more chemical bonds, products formed by the radiolysis of water include hydroxyl radicals ($\bullet\text{OH}$), hydrogen peroxide (H_2O_2), hydronium (H_3O^+), and molecular hydrogen (H_2) (Holmboe et al., 2012). An important consequence of H_2O_2 production is its decomposition via the autocatalytic Fenton reaction described in the equations below (Vasquez-Medrano et al., 2018):



The compounds produced by H_2O_2 decomposition are termed highly reactive oxygen species (ROS), and as observed in the equations above can be generated via reactions with iron in both of its oxidation states. In the unlikely event of radionuclide release, the radiolysis of water via radionuclides in the pore water, and subsequent ROS generation could potentially cause oxidation of the bentonite buffer (Liu and Neretnieks, 2003). Gas generation via radiolysis may also reduce thermal conductivity (Wilson et al., 2011), although gases have been shown to migrate through bentonite when a sufficient gas pressure is generated (Rocco et al., 2017).

1.3.3. Density and swelling pressure

Two of the main roles of bentonite in behaving as a buffer material are to restrict hydraulic permeability so diffusion is the dominant transport mechanism, and for it to self-seal so gaps within the buffer and excavation-damaged zone (EDZ) are closed (Sellin and Leupin, 2013). As mentioned previously, montmorillonite the key constituent of bentonite has a negatively charged surface that attracts cations and the water molecules associated with them, this causes the clay to expand (Moore and Reynolds Jr, 1997). As the bentonite swells the buffer mass is balanced and a swelling pressure is developed, for the safety requirements to be fulfilled a swelling pressure of between 0.1 and 1.0 MPa is required (Sellin and Leupin, 2013). For a swelling pressure to develop, the bentonite needs to be contained in a volume smaller than its maximum swelling volume, under these conditions the swelling pressure is related to the mass of water and clay in the system (m_w/m_s), which is dependent on the density of the clay-water system (ρ_m) (Karnland, 1998). Water saturated MX-80 bentonite at densities of 1.5, 1.8, and 2.0 g cm⁻³ has roughly equivalent swelling pressures of 0.1, 1.5, and 7.8 MPa (Masurat et al., 2010b).

1.3.4. Temperature and evolving resaturation

HLW and SF generate substantial amounts of heat, and most disposal agencies place a temperature limit of 100 °C at the canister surface, as high temperatures can have a detrimental effect on bentonite performance (Hicks et al., 2009). Fully saturated bentonite is

roughly 33 % water by mass, which means evolving resaturation and the chemistry of the occupying fluid have a substantial effect on the thermal properties of bentonite (Wilson et al., 2011). It is believed that groundwater circulating through the host rock will be drawn into the bentonite buffer, due to its affinity for cations, and subsequent osmotic effects (SKB, 2006). The predicted time it would take for the buffer to become fully resaturated varies with the permeability of the host rock, it is predicted to take decades in highly permeable host rocks, whereas in low permeability rocks such as clays resaturation could take millennia (Rutqvist and Tsang, 2008). The combination of water infiltration at the host rock contact, and evaporation at the canister surface may generate a circulation system, leading to the uneven distribution of water through the buffer (Figure 1.9) (Wilson et al., 2011). If water ingress is insufficient this may lead to desiccation at the canister, a decrease in thermal conductivity, a loss in swelling pressure, and the concentration of corrosion products at the canister surface.

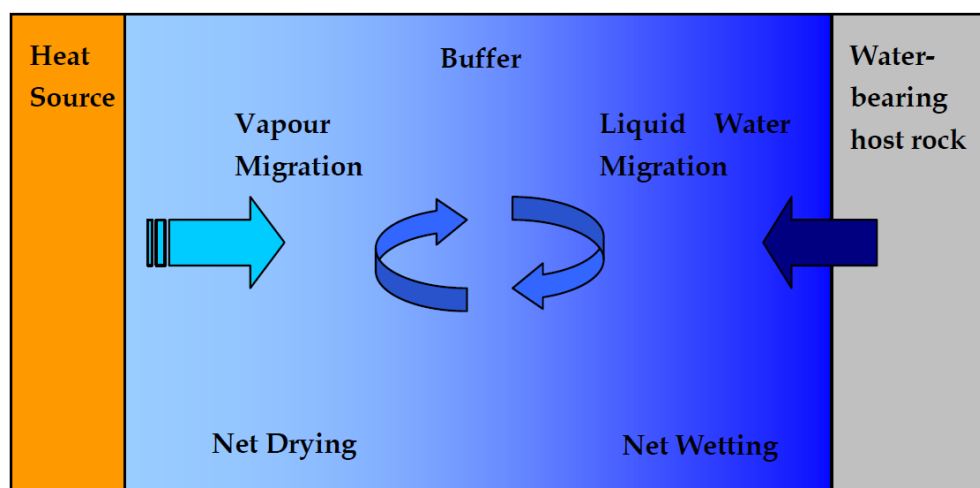


Figure 1.9: The movement of water through a bentonite buffer (Wilson et al., 2011).

1.4. Bentonite microbiology

Bentonites and other clays have a naturally occurring microbial community (Lopez-Fernandez et al., 2015). Some of these microbes display a remarkable tolerance to environmental stresses, and are capable of withstanding simulated repository conditions (Pedersen, 2010), such as radiation fluxes, elevated temperatures, swelling pressure, reduced pore size, decreased water activity, and a lack of nutrients (Mulligan et al., 2009). Such conditions are likely to eradicate non-spore-forming bacteria, but it is thought that spore-

forming bacteria could survive for extended periods of time (Pedersen et al., 2000b). Microbes influence their surroundings, causing the precipitation of solutes, excretion of complexing agents, contaminant sorption, pore obstruction changing local flow conditions, breakdown of organics, and gas generation (Mulligan et al., 2009). A lot of microbial processes generate gases, typically in the form of hydrogen and carbon dioxide; gases reduce thermal conductivity, and could disrupt the macro-structure of the buffer (Pedersen, 2000). Such disruption may form new pore spaces, as well as widening present pores, leading to an increase in permeability (Mulligan et al., 2009). Microbial processes have the potential for a direct impact on the bentonite, such as Fe(III)-reducing bacteria which may reduce structural Fe(III) to Fe(II), leading to the dissolution of the smectite (Kim et al., 2004). Microbes can also preferentially adsorb radionuclides (Ohnuki et al., 2010), leading to either biomineralisation and immobilization, or transport via adsorption to microbes (Newsome et al., 2014). Microbes in a bentonite backfill may also be detrimental to an engineered barrier system (EBS) by enhancing canister corrosion (Wilson et al., 2011).

1.5. Bentonite chemical interactions

An important consideration when it comes to the use of bentonite as a buffer material is its interactions with radionuclides. Iron is the most abundant redox-active element in montmorillonite, and therefore will play a role in the speciation of redox-active radionuclides. Selenium was chosen due to its interactions with the Fe(III)-reducing bacterium *Geobacter sulfurreducens* (Pearce et al., 2009).

1.5.1. Iron

Iron accounts for around 20 % of the elemental composition of nontronites and 2 % of montmorillonites (Gorski et al., 2013). Iron commonly exists in two oxidation states; Fe(II) typically under reducing conditions, and Fe(III) under oxidizing conditions. The abundance of iron in montmorillonite, and other smectite minerals means its oxidation state can have an impact on the mineralogy, and geochemical characteristics (Gorski et al., 2012). In terms of geological disposal this could potentially lead to illitisation, and smectite interlayer collapse (Kim et al., 2004), although the extent of this is debated (Dong, 2012). Iron reduction in bentonites is typically investigated using reducing agents such as dithionite (Komadel et al., 1990), however a range of IRB are also capable of reducing structural iron in bentonites

(Kostka et al., 1999). The extent of microbial Fe(III)-reduction is typically less than that achieved using reducing agents (Ribeiro et al., 2009), which is likely due to biologically reduced Fe(II) blocking absorption sites, and unfavorable energetics (Liu et al., 2017).

1.5.2. Selenium

A few selenium isotopes are generated during nuclear fission including the unstable ^{79}Se a beta-emitter with a half-life of 3.27×10^5 years. Under oxidizing conditions selenium commonly exists as the highly soluble, and toxic selenate (SeO_4^{2-}), and selenite (SeO_3^{2-}) oxyanions. Several less toxic and insoluble forms exist as well including elemental selenium, selenium disulfide (S_2Se) and iron selenide (FeSe) which occur following reduction of the oxyanion forms (Orucoglu and Hacıyakupoglu, 2015). Bentonites selectivity for positively charged ions as a result of its negative interlayer charge means it has little capacity for the adsorption of negatively charged selenium oxyanions (Kim et al., 2012). Interactions of selenium with bentonite typically consist of surface complexes in the form of selenious acid (H_2SeO_3) between pH 5 and 7, as well as ternary surface complexes with Ca^{2+} and Mg^{2+} at pH 7 and above (Montavon et al., 2009). Modification of bentonites using zero valent iron (Li et al., 2015), and aluminium (Wang et al., 2015) have been shown to improve the adsorption of selenium oxyanions, however such modifications would be impractical to implement in a geological disposal scenario.

1.6. Microbial processes

Microorganisms are abundant in the subsurface, they are able to achieve growth by coupling the oxidation of organic matter to the reduction of a wide variety of electron acceptors (Lovley and Chapelle, 1995). Oxygen, nitrate, manganese(IV), iron(III), and sulfate are common electron acceptors implicated in organic matter oxidation, and their usage is separated into distinct zones in the subsurface (Reeburgh, 1983). These distinct zones exist because of competition between microorganisms for electron donors, and physiological constraints on metabolism (Lovley and Chapelle, 1995). Figure 1.10 highlights the major terminal electron-accepting processes (TEAP) located in a deep aquifer, oxygen is consumed first, followed by nitrate and manganese(IV), iron(III) is next, and then sulfate, carbon dioxide is converted to methane in the final TEAP (Lovley and Chapelle, 1995).

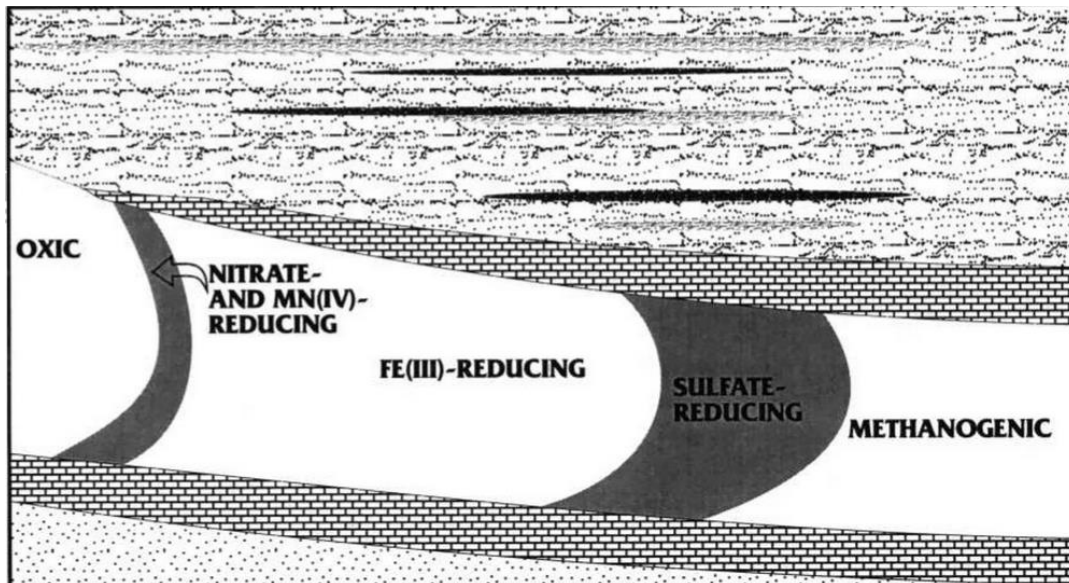


Figure 1.10: The major TEAPs located within an aquifer (Lovley and Chapelle, 1995).

The energetics behind the system can be explained by the redox tower (Figure 1.11), which is made up of a series of electron acceptors. Electrons are donated by an electron donor, and captured by an electron acceptor (Madigan, 2015).

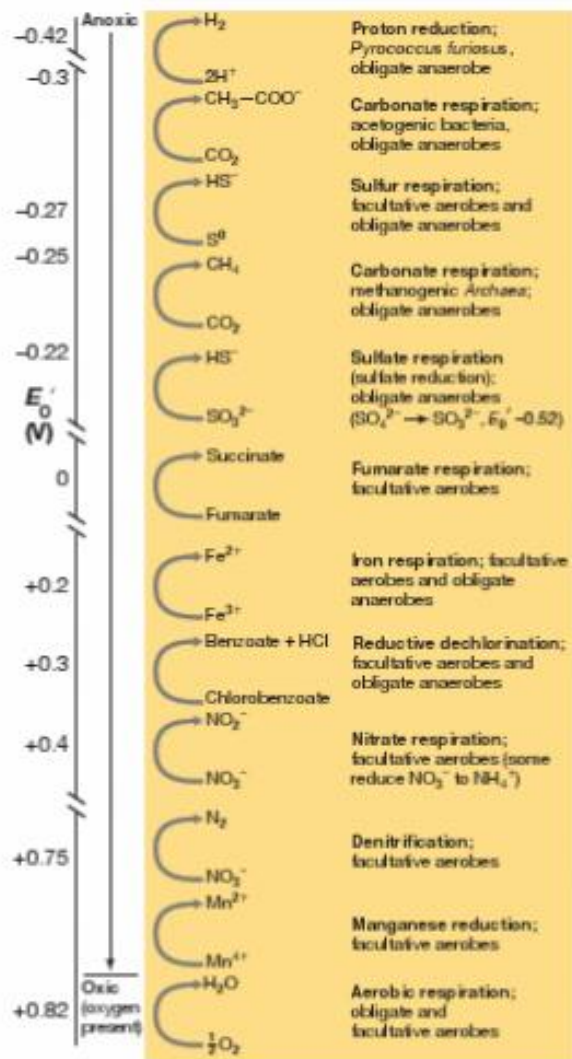


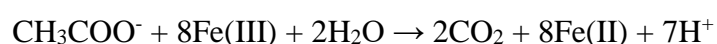
Figure 1.11: Redox potentials for a range of electron acceptors (Madigan, 2015).

Aside from reaction kinetics oxygen is the first terminal electron acceptor because most anaerobic microorganisms are inactive in the presence of oxygen, nitrate-reducers are capable of aerobic respiration, but are unable to reduce nitrate until oxygen is depleted (Tiedje, 1988). The location of the remaining TEAPs can be correlated with the concentration of the electron donor hydrogen in the environment. The concentration of hydrogen increases down the zones, with the nitrate reduction zone having the lowest concentration, and the methanogenesis zone the highest (Lovley and Chapelle, 1995). The energy yield from hydrogen oxidation coupled to an electron acceptor decreases from nitrate reduction down to methanogenesis, therefore the organisms with the greatest tolerance to hydrogen depletion proliferate, until their growth is limited by electron acceptor availability, once the previous

terminal electron acceptor is depleted the next TEAP can begin, as long as the hydrogen concentration is sufficient (Lovley and Goodwin, 1988). This trend is influenced by other factors, for example whilst Fe(III)-reducers can concurrently reduce Fe(III) and Mn(IV), the reduced Fe(III) is chemically reoxidized by Mn(IV), and therefore overall Fe(III) removal is not achieved until Mn(IV) becomes depleted (Lovley, 1991). Fe(III) reduction is also carried out by a select few sulfate-reducers, who appear to utilize Fe(III) before sulfate (Coleman et al., 1993). As well as certain bacteria and archaea utilizing multiple electron acceptors, changes in environmental conditions can permit multiple TEAPs in the same area, such behavior will continue until a group of microorganisms begins to outcompete the others (Lovley and Chapelle, 1995). In terms of considering the TEAPs most relevant to bentonite in an engineered barrier system, and to explore in detail the key groups, attention has been focused on Fe(III)-reducers due to their implication in smectite dissolution (Kim et al., 2004), as well as sulfate-reducers because of their association with canister corrosion (Masurat et al., 2010a).

1.6.1. Fe(III)-reducing bacteria

Under anaerobic conditions Fe(III)-reducing bacteria couple the oxidation of organic matter to the reduction of Fe(III), a process called dissimilatory iron reduction (Lovley et al., 1987). Fe(III)-reduction occurs in a number of key biological reactions such as the Fenton reaction (Imlay, 2003), however Fe(III)-reducing bacteria are unique in their utilization of Fe(III)-reduction for growth (Lovley, 1991). Dissimilatory iron reduction can be summarized by the following equation (in this case acetate is the organic substrate) (Lovley and Phillips, 1988):



Fe(III)-reducing bacteria can oxidize a wide variety of organic substrates, including aromatic compounds (Lovley et al., 1989a) and short-chain fatty acids (Lovley et al., 1989b).

Alteromonas putrefaciens MR-1 (later reclassified as *Shewanella oneidensis* MR-1 (Venkateswaran et al., 1999)) has been shown to utilize hydrogen as an electron donor, as well as the organic substrates commonly used by other Fe(III)-reducing bacteria (Lovley et al., 1989b). In some circumstances organic substrates are responsible for the nonenzymatic reduction of Fe(III) (Hem, 1972), however at circumneutral pH the enzymatic reduction of Fe(III) is the dominant process in non-sulfidogenic anoxic environments (Lovley et al., 1991). Fe(III) reduction is enzymatically mediated via proteins of varying specificity

(Mazoch et al., 2004). In the case of *Geobacter sulfurreducens*, and *S. oneidensis* MR-1 Fe(III)-reduction is carried out by a collection of proteins known as *c*-type cytochromes (Aklujkar et al., 2013).

1.6.1.1. *c*-type cytochromes

c-type cytochromes are a redox active heme-containing proteins that transfer electrons between the internal cytoplasm and the cell surface of Gram-negative iron-reducing bacteria (Aklujkar et al., 2013). Found in a variety of microbes including the iron-reducers *Geobacter* sp. and *Shewanella* sp. *c*-type cytochromes are mostly non-specific and can reduce a variety of electron acceptors, including Fe(III), Cr(VI) and U(VI) (Richter et al., 2012). In the case of *S. oneidensis* MR-1 the transfer of electrons involves over 40 biomolecules including *c*-type cytochromes, quinones, dehydrogenase enzymes and Fe-S proteins (Esther et al., 2015) (Figure 1.12). The cytoplasmic membrane protein A (CymA) is a tetraheme *c*-type cytochrome, which serves as a quinol dehydrogenase transporting electrons from the menaquinol pool into the periplasm (Figure 1.12) (Richter et al., 2012). Multiple routes are available for the electrons after CymA, including transfer to the fumarate reductase FccA which reduces fumarate (Figure 1.12). FccA also acts as an electron store, allowing the cell to continue organic matter oxidation in the absence of an electron acceptor (Schuetz et al., 2009). Electrons from CymA and FccS are transferred to the metal-reducing protein A (MtrA), a *c*-type cytochrome located in the periplasm (Figure 1.12) (Esther et al., 2015). MtrA serves two functions, including the transfer of electrons, as well as forming a complex at the outer membrane with metal-reducing protein B (MtrB) and either metal-reducing protein C (MtrC) or outer membrane cytochrome A (OmcA) (Figure 1.12) (Richter et al., 2012). MtrB is a porin protein which allows the transfer of electrons from MtrA in the periplasm across the outer membrane to the terminal reductases MtrC and OmcA (Figure 1.12), mutants deficient in MtrA are unable to form stable complexes and are incapable of transferring electrons across the outer membrane (Schicklberger et al., 2011). MtrC and OmcA are the terminal reductases expressed under Fe(III)-reducing conditions (Figure 1.12), mutants deficient in MtrC display reduced growth with Fe(III) as the terminal electron acceptor, meanwhile OmcA deficient mutants are affected under Mn(IV)-reducing conditions (Richter et al., 2012).

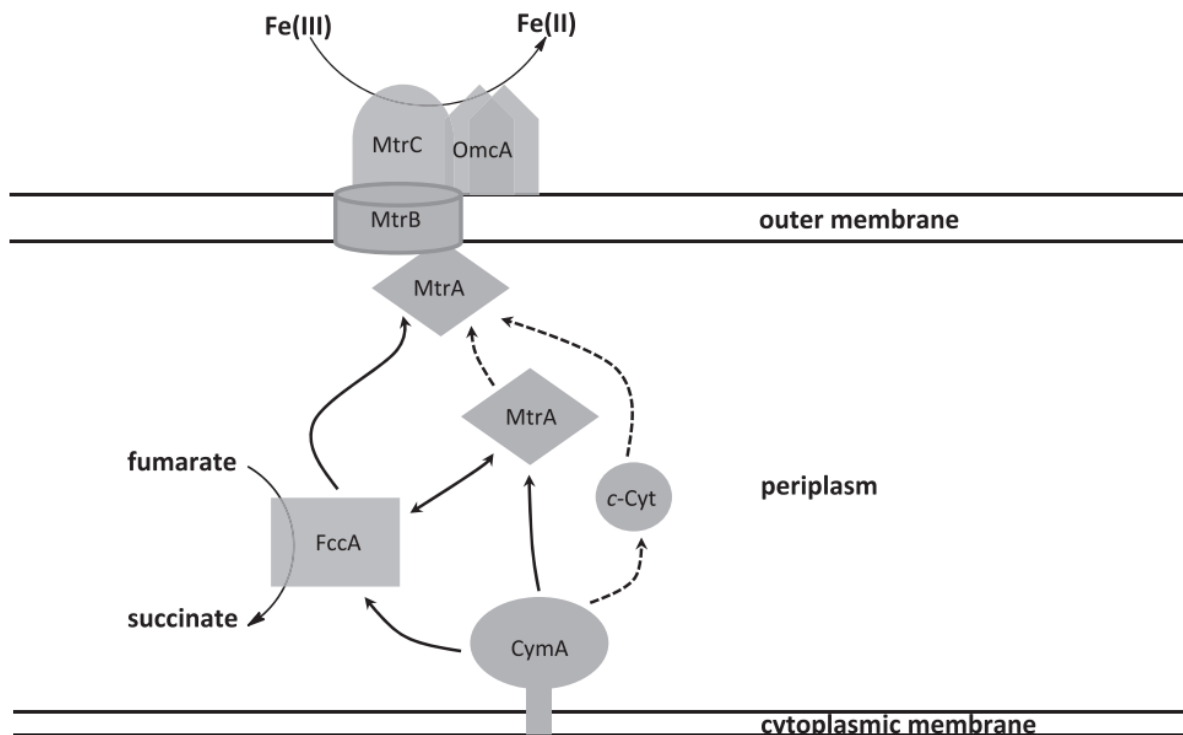


Figure 1.12: Proteins responsible for electron transfer in *Shewanella oneidensis*, known paths are displayed with solid arrows, hypothetical ones are indicated with dashed arrows (Richter et al., 2012).

G. sulfurreducens is believed to have 111 genes that code for *c*-type cytochromes, 30 of which are believed to be responsible for cytochromes on the outer membrane (Esther et al., 2015). The transfer of electrons from the periplasm to the outer membrane is poorly understood, although periplasmic *c*-type cytochrome A (PpcA) appears to be an electron transfer intermediate (Morgado et al., 2010). Four outer membrane cytochromes (Omc) are known to play a role in Fe(III) reduction, OmcB is a crucial protein involved in insoluble Fe(III) and Fe(III) citrate reduction, OmcE and OmcS are involved in direct electron transfer to the Fe(III), meanwhile OmcZ is responsible for electron transfer in biofilms (Esther et al., 2015).

1.6.1.2. Fe(III) scavenging mechanisms

Fe(III) is typically insoluble which means that the Fe(III)-reducing cells need additional means of accessing the Fe(III) with their outer membrane *c*-type cytochromes. Several mechanisms are employed by Fe(III)-reducing bacteria including direct contact with the

substrate (Childers et al., 2002), chelating agents (Lovley and Woodward, 1996), electron shuttling compounds (Lovley et al., 1996a), and extracellular nanowires (Gorby et al., 2006).

1.6.1.3. Direct contact and nanowires

In the presence of soluble Fe(III), the Fe(III)-reducing bacterium *Geobacter metallireducens* appears to be nonmotile (Lovley et al., 1993). However, in the absence of soluble electron acceptors *G. metallireducens* exhibits chemotaxis, and develops flagella, to move to insoluble electron acceptors such as Fe(III) oxides and oxyhydroxides (Childers et al., 2002).

Geobacter sp. also develop pilli on one side of the cell. Pilli are used by a broad range of microorganisms to attach to surfaces (Nassif et al., 1997). Pilli deficient *G. sulfurreducens* mutants can attach to Fe(III) oxides, but were unable to reduce the Fe(III) (Reguera et al., 2005). The pilli of *G. sulfurreducens* (often referred to as microbial nanowires) are electrically conductive and play a role in the transfer of electrons from the cell surface to the substrate (Malvankar et al., 2011). Whilst the nanowires conduct electrons, *G. sulfurreducens* mutants lacking the c-type cytochrome OmcS are incapable of reducing Fe(III) oxides (Mehta et al., 2005). OmcS is located on the pilli of *G. sulfurreducens* (Leang et al., 2010), and is responsible for the final step in the transfer of the electrons to the Fe(III) oxides (Qian et al., 2011). *Shewanella* sp. are also able to mediate iron reduction via nanowires, but are also able to utilize a number of indirect strategies (Esther et al., 2015).

1.6.1.4. Electron shuttling compounds

Electron shuttling compounds are redox-active compounds that can transport electrons from the cell surface to the Fe(III) substrate (Brutinel and Gralnick, 2012). Electron shuttling compounds can be derived from the environment such as humic substances, soluble quinones and some compounds containing sulphur, as well as being generated by microorganisms (Stams et al., 2006). In the case of humic substances, the microbes donate electrons to quinone structures within the humic substances reducing them to their hydroquinone form, the hydroquinones then donate the electrons to the Fe(III) returning the humic substances to their original state (Lovley et al., 1999). *Geobacter* sp. and *Shewanella* sp. are both capable of reducing humic substances, however *Shewanella* is also capable of producing endogenous electron shuttling compounds in the form of flavin mononucleotide (FMN) and riboflavin (von Canstein et al., 2008). Of 24 *Shewanella* species sequenced, 23 possessed the genes

required for flavin biosynthesis, *Shewanella denitrificans* is the exception but also lacks the aforementioned proteins responsible for metal oxide reduction (Brutinel and Gralnick, 2012). FMN is produced in the periplasm by the hydrolysis of flavin adenine dinucleotide (FAD) by the protein UshA, FMN is then subsequently incorporated into FccA or diffuses via outer membrane porins for use as an electron shuttle (Covington et al., 2010).

1.6.1.5. Chelating agents

Chelating agents are organic ligands that bind to iron oxides, greatly increasing their bioavailability (Lovley et al., 1994). Such organic ligands include ethylenediaminetetraacetic acid (EDTA), *N*-methyliminodiacetic acid, nitrilotriacetic acid (NTA) (Figure 1.13), ethanol diglycine, as well as sodium hexametaphosphate (Lovley et al., 1996b). Chelators have been shown to solubilize a wide variety of iron oxide forms, including goethite and hematite which are highly crystalline forms that are typically recalcitrant to reduction (Lovley and Woodward, 1996). Chelated Fe(III) may be reduced at the cell surface utilizing the same proteins involved in insoluble Fe(III) reduction (Haas and Dichristina, 2002), or there is a possibility that the chelated Fe(III) is reduced in the periplasm via a mechanism unrelated to the aforementioned pathways (Dobbin et al., 1996). *Shewanella* sp. are able to produce their own chelators as opposed to *Geobacter* sp., however the presence of such compounds in the environment will solubilize Fe(III) and therefore enhance Fe(III) reduction in all Fe(III)-reducing bacteria (Esther et al., 2015).

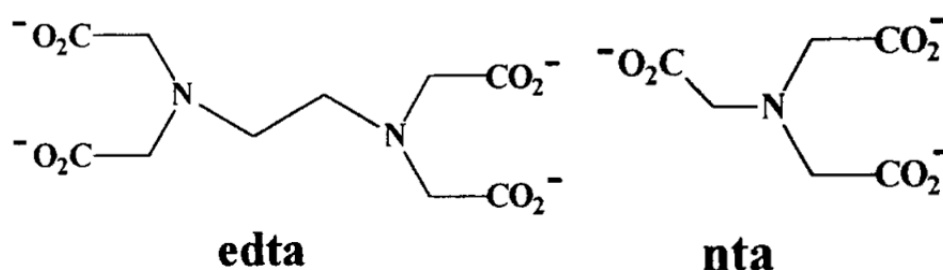


Figure 1.13: The chemical structure of two commonly used chelating agents ethylenediaminetetraacetic acid (EDTA) and nitrilotriacetic acid (NTA) (Dobbin et al., 1996).

1.6.2. Sulfate-reducing bacteria

The anaerobic sulfate-reducing bacteria (SRB) are a mixture of heterotrophs, and mixotrophs, classified by their ability to carry out dissimilatory sulfate reduction (Little et al., 2000).

Dissimilatory sulfate reduction is the process by which sulfate (SO_4^{2-}) is reduced to sulfide (S^{2-}), utilizing an electron donor (Postgate, 1979). Dissimilatory sulfate reduction is summarized below, with acetate being utilized as the electron donor in this case (Postgate, 1979):



Early research identified two groups of SRB, which carried out the incomplete oxidation of organic acids and alcohols to acetate (Gibson, 1990). The identified groups included *Desulfotomaculum*, spore-formers with a straight or curved rod shape (Campbell and Postgate, 1965), and *Desulfovibrio*, motile non-spore-formers with a vibrio shape (Postgate and Campbell, 1966). The genus *Desulfobacter* was later used to classify non-spore-forming SRB that could utilize fatty acids (Widdel and Pfennig, 1981), and aromatic compounds (Bak and Widdel, 1986a) (Bak and Widdel, 1986b). Reduction of the SO_4^{2-} and oxidation of the electron are two distinct reactions that occur in different locations of the cell, hydrogen is oxidized by hydrogenase enzymes located in the periplasm or on the cell membrane (Aubert et al., 2000). Electrons from the hydrogen oxidation are transported by several enzymes into the cytoplasm, this process is coupled to the proton gradient driving adenosine tri-phosphate (ATP) production (Hallbeck, 2014). The first step in SO_4^{2-} reduction is described below:



The adenylyl group belonging to the ATP is transferred to the SO_4^{2-} to produce adenosine 5'-phosphosulfate (APS), as well as pyrophosphate; this reaction is catalyzed by the enzyme ATP sulfurylase (ATPS) (Taguchi et al., 2004). APS is converted into SO_3^{2-} by adenosine-5'-phosphosulfate reductase (Apr), a set of enzymes that are highly conserved in SRB and sulfur-oxidizing bacteria (SOB) (Meyer and Kuever, 2007). SO_3^{2-} is subsequently converted into H_2S by dissimilatory sulfite-reductase enzymes (Dsr), coded for by another set of highly conserved genes within SRB and SOB (Biswas et al., 2014).

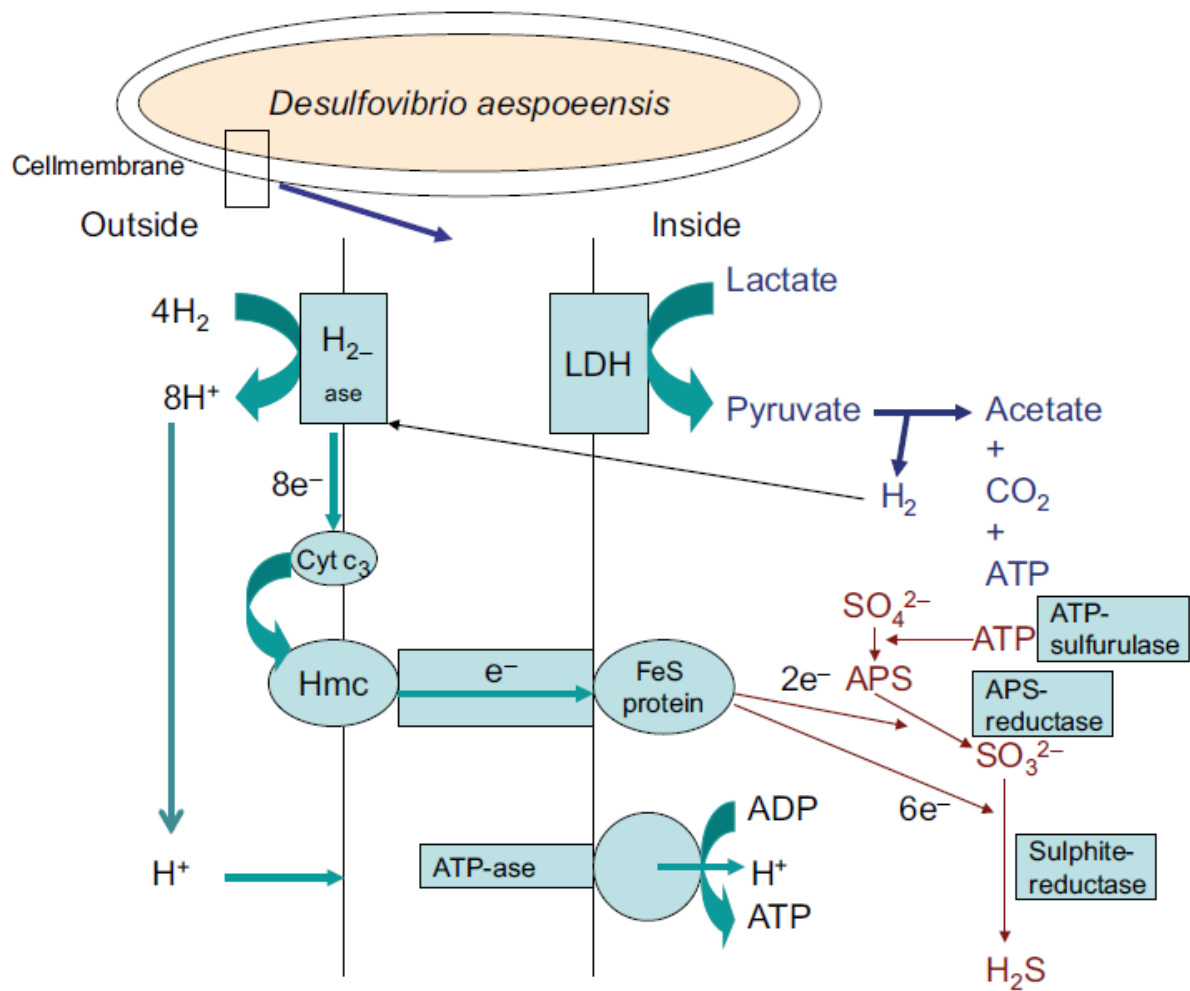


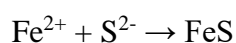
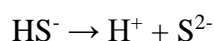
Figure 1.14: Overview of sulphate reduction in the SRB *Desulfovibrio aespoeensis* (Hallbeck, 2014).

1.6.3. Microbial selenium reduction

Several pathways exist for the reduction of selenate, and selenite oxyanions including methylation, and dissimilatory reduction (Eswayah et al., 2016). Bacteria have been primarily shown to reduce selenium oxyanions as a means of detoxification reducing soluble, and toxic selenium oxyanions to insoluble, and less toxic elemental selenium (Kessi et al., 1999). Few bacterial species have been documented with the ability to reduce selenate to selenite, but include *Thauera selenatis* (Macy et al., 1993), and *Enterobacter cloacae* (Yee et al., 2007). Membrane-bound nitrate reductase (Nap) has been implicated in selenate reduction (Macy et al., 1993), along with specific enzymes such as selenate reductase (Ser) (Yee et al., 2007). Selenite reduction is more commonly observed compared to selenate due to the thermodynamics being more favorable. Several enzymes have been implicated in selenite reduction including nitrite (Demoldecker and Macy, 1993) and sulfite reductase (Harrison et al., 1984). Fe(III)-reducing bacteria such as *Geobacter sulfurreducens*, and *Shewanella oneidensis* have also been shown to reduce selenite to elemental selenium using *c*-type cytochromes, with the potential to form selenides in the presence of an electron shuttle (Pearce et al., 2009). Typical products of microbial selenite reduction are red elemental selenium nanoparticles which form monoclinic crystalline structures (Oremland et al., 2004).

1.6.4. Microbially-induced corrosion

Microbially-induced corrosion could affect metallic waste containers as a result of microbial interactions with material surfaces, or due to the alteration of chemical conditions as metabolites are excreted (Humphreys et al., 2010). The corrosion of metal surfaces occurs because of changes to electrochemical conditions. The development of biofilms influences the local electrochemical conditions, and may enhance or reduce corrosion (Videla and Herrera, 2005). The distribution of biofilms across a surface is uneven, this leads to anodic reactions such as metal dissolution beneath the biofilm, and cathodic reactions including oxygen reduction on exposed surfaces (Little and Wagner, 1996). The biofilms inhibit oxygen diffusion to the cathodes producing a differential aeration cell, and as the biofilm turns anaerobic, the reduction of a variety of molecules including hydrogen sulfide occurs. Elemental iron reacts with oxidizing agents to produce Fe^{2+} , the hydrogen sulfide produced by SRB metabolism reacts with these Fe^{2+} ions in a series of reactions, as described below (El Mendili et al., 2013):



Whilst potentially contributing to the corrosion of waste canisters, the iron sulfide may precipitate as a protective coating, preventing further corrosion, depending on the density of the formed precipitate (El Mendili et al., 2013).

1.6.5. Limits to microbial growth

As mentioned in the previous chapter microbes can be remarkably tolerant to the stresses present under simulated repository conditions (Mulligan et al., 2009). Microbes can survive in a variety of extreme conditions (Table 1.7), some of these microbes are novel and occupy small niches, whilst others are found distributed in a broad range of environments.

Table 1.7: Examples of extremophilic microorganisms

Condition	Example of organism	Limit of growth	Reference
Low temperature	<i>Psychromonas ingrahamii</i>	- 12 °C	(Riley et al., 2008)
High temperature	Strain 121	121 °C	(Kashefi and Lovley, 2003)
High pH	<i>Bacillus firmus</i>	11.4	(Sturr et al., 1994)
Low pH	<i>Picrophilus oshimae</i>	0	(Schleper et al., 1995)
High salinity	<i>Halobacterium litoreum</i>	4.8 M NaCl	(Lu et al., 2017)
High pressure	<i>Colwellia marinimaniae</i>	140 MPa	(Kusube et al., 2017)
Radiation	<i>Deinococcus radiodurans</i>	50 Gy h ⁻¹	(Daly et al., 2004)

Each of the microbes mentioned have developed mechanisms to cope with these individual conditions, understanding how these mechanisms operate may provide solutions to controlling the microbial population of a bentonite buffer.

1.6.5.1. High temperature

Hyperthermophiles grow optimally between 80 and 106 °C, they are typically encountered in the vicinity of hydrothermal vents, where the elevated pressure prevents water from boiling (Huber and Stetter, 2001). Strain 121 a close relative of *Pyrodictium occultum* displays

resistance to autoclaving with 121 °C causing a doubling in cell numbers over 24 hours, and also remains viable following a 2 hour treatment at 130 °C (Kashefi and Lovley, 2003). High temperatures lead to the instability of a wide variety of biological molecules, methods of overcoming this issue include fast turnover of sensitive molecules, direct transfer of molecules between enzymes, as well as the production of high-temperature resistant proteins (Daniel and Cowan, 2000).

1.6.5.2. Low temperature

As temperature decreases the rate at which reactions occur slows significantly. This makes the task of identifying the lower temperature limit of life challenging, for example the doubling of permafrost bacteria at a temperature of -10 °C can take 39 days (Bakermans et al., 2003). Bacterial reproduction has been observed at -12 °C, while metabolic activity has been seen at temperatures as low as -20 °C (Rivkina et al., 2000). Some psychrophilic bacteria can also maintain low-level metabolic activity for up to 500,000 years in permafrost (Johnson et al., 2007). Low temperatures increase the rigidity of a number of structures including membranes and enzymes; membrane rigidity is of particular importance as it reduces permeability, and therefore the transport of molecules in and out of the cell (D'Amico et al., 2006). In the case of membranes, flexibility is returned by introducing short, branched, and unsaturated fatty acids (Chintalapati et al., 2004). Enhancements in enzyme flexibility are also observed, typically in areas involved with catalysis, or to the structure as a whole, and occur as a result of a decrease in certain chemical interactions including hydrogen bonding, ion pairing, and hydrophobic interactions (D'Amico et al., 2006).

1.6.5.3. Hydrostatic pressure

Hydrostatic pressure refers to the pressure generated in a fluid because of gravity, with greater pressure exerted as depth increases. Bacteria belonging to the genera *Moritella*, and *Shewanella* have been isolated from sediment extracted from the Mariana Trench (10898 m), a region where pressure exceeds 100 MPa (Kato et al., 1998). During incubation under such intense pressures, microbes have been shown to express specific genes that are more typically expressed in response to cold and heat shock (Bartlett et al., 1995). Such behavior is exhibited because high pressures destabilize tertiary and quaternary protein structures, a

consequence observed with heating; as well as impacting protein production and membrane stability, effects that typically occur in response to cooling (Bartlett, 2002).

1.6.5.4. Swelling pressure

Along with the increase in pressure that occurs as a bentonite swells, several other stresses are imparted, as porosity, and permeability decrease. Porosity dictates the size of cells that can be present, with permeability controlling nutrient transport (Sellin and Leupin, 2013). Typical bacteria can be captured on a 0.2 μm filter, however “ultra-small” bacteria can pass through these filters, with little known about their metabolic functions (Luef et al., 2015). The limit of microbial processes in regards to the swelling pressure of a bentonite have been investigated (Bengtsson and Pedersen, 2017), but swelling pressure is controlled by the density, and montmorillonite content of the bentonite, making an exact figure difficult to establish. An alternative way to describe the limits of proliferation of microbes in a compacted bentonite is with water activity (Stroes-Gascoyne et al., 2010).

1.6.5.5. Water activity

Water activity (a_w) is the vapor pressure of water within a substance divided by the vapor pressure of pure water at equal temperature, and pressure. The a_w of a substance can be used to determine if microbial activity is possible, and the types of reactions that can be expected (Brown, 1976). The optimal a_w for microbial life is 0.98, and as the vapor pressure of water decreases in a system, the fewer the types of organisms that can proliferate, Table 1.8 shows the limits of a_w that can sustain microbial life.

Table 1.8: Water activity (a_w) in different scenarios, and the activity limits of microorganisms. Adapted from (Brown, 1976).

Water Activity (a_w)	Conditions	Microorganisms
1	Pure water	<i>Caulobacter spirillum</i>
0.98	-	Optimum for most bacteria
0.96	Sea water	-
0.91	-	<i>Bacillus</i>
0.75	Salt lake	<i>Halobacterium</i>
0.6	-	<i>Xeromyces bisporus</i> (Fungi)
0.55	DNA disordered	-

The a_w in a system decreases in response to several factors including increased salinity, drying, and freezing (Cockell and Nixon, 2013). Water activity in bentonites decreases as the density increases in response to interactions with solutes, and adsorption of water to mineral surfaces (Stroes-Gascoyne et al., 2010). An a_w of less than 0.96 should minimize microbial activity in a bentonite (Pedersen et al., 2000a), adaptations to increased salinity, and desiccation are described below.

1.6.5.6. Salinity

Microbial communities are capable of reproduction in the saturated NaCl brines often found in evaporite deposits across the Earth, where a_w is typically 0.75 (Grant, 2004). Despite the requirement of a high external NaCl concentration to stabilize their membranes, these organisms need to exclude Na^+ ions from the cytoplasm to prevent enzyme inhibition, this is achieved through the accumulation of compatible solutes intracellularly to equal the external water activity, these solutes include a number of sugars, amino acids, as well as KCl (Cockell and Nixon, 2013).

1.6.5.7. Desiccation

In a typical non-aqueous microbial environment water exists on surfaces, whether they be soil particles, foodstuffs, etc. Desiccation causes the films of water on these surfaces to diminish in area, restricting microbe mobility, and the availability of solutes, leading to starvation at water activities as high as 0.86 (Cockell and Nixon, 2013). Other problems associated with desiccation include the removal of water from the structures of proteins, and DNA (Dose et al., 1992), as well as an increase in free radicals, leading to lipid peroxidation (Crowe and Crowe, 1992). The removal of water from DNA leads to lesions in the structure known as single-strand breaks (ssb), which can develop into double-strand breaks (dsb) (Dose et al., 1992). Ssb and dsb are also associated with free radical interactions, all organisms require preservation of their genetic code, as critical cell functions can be compromised (Daly, 2009). Resistance to desiccation is achieved through the scavenging of free radicals via the manganese redox cycle (Daly et al., 2007), having multiple copies of genes (Hansen, 1978), and by the proficient repair of DNA (Minton, 1994).

1.6.5.8. Radiation

The emittance of radiation from the Earth is much lower than the tolerance of radiation-resistance organisms, some researchers believe that organisms have retained their resistance from when radiation fluxes were higher (Karam and Leslie, 1999). However, these organisms are often isolated from dry environments, such as desert soils, dried food, and sawdust, with a more plausible explanation being that desiccation imparts similar stresses to radiation (Rainey et al., 2005). In fact 80% of the damage caused to DNA by radiation is imparted by reactions with free radicals, the other 20% from direct ionization (Ghosal et al., 2005). Ionizing radiation generates free radicals, and other potent oxidizing agents, via the radiolysis of water (Figure 1.15), of biggest concern is the role of superoxide radicals ($O_2^{\bullet-}$), hydrogen peroxide (H_2O_2), and hydroxyl radicals ($\bullet OH$) (Daly, 2009). Superoxide radicals behave as oxidizing and reducing agents, and are involved in lipid peroxidation, as well as protein inactivation (Regelsberger et al., 2002). Superoxide is scavenged by superoxide dismutase (SOD), with the consequence of increasing intracellular hydrogen peroxide levels (Fridovich, 1997). Hydrogen peroxide is responsible for protein damage, via the oxidation of sulphur-bearing molecules, and also produces hydroxyl radicals through the Fenton reaction (Imlay, 2003). Hydroxyl radicals will react with nearly all biomolecules at rates limited only by diffusion, their high reactivity permits only localized damage, close to where they formed (Farr and Kogoma, 1991). The extremophile *Deinococcus radiodurans* is considered a model organism when it comes to radiation tolerance, with 10% survival reported following a dose of 16 kGy (Daly et al., 2004). The adaptations that convey resistance to desiccation are believed to be responsible, with protection from free radicals through the redox cycling of manganese (Daly et al., 2007), as well as multiple copies of genes (Hansen, 1978), and the ability to repair them effectively (Minton, 1994). In regards to dissimilatory Fe(III) reduction subtle changes to Fe(III) mineral morphology can enhance microbial Fe(III)-reduction, especially in the presence of an electron shuttle (Cutting et al., 2009). The bioavailability of hematite following gamma irradiation is enhanced remarkably in the presence of an electron shuttle (Brown et al., 2014). *Geothrix fermentans* and *Geobacter* sp. incubated in natural sediments, have been shown to be viable following a dose rate of 30 Gy h^{-1} , suggesting that their role in the iron cycle is not restricted, and could possibly be enhanced (Brown et al., 2015).

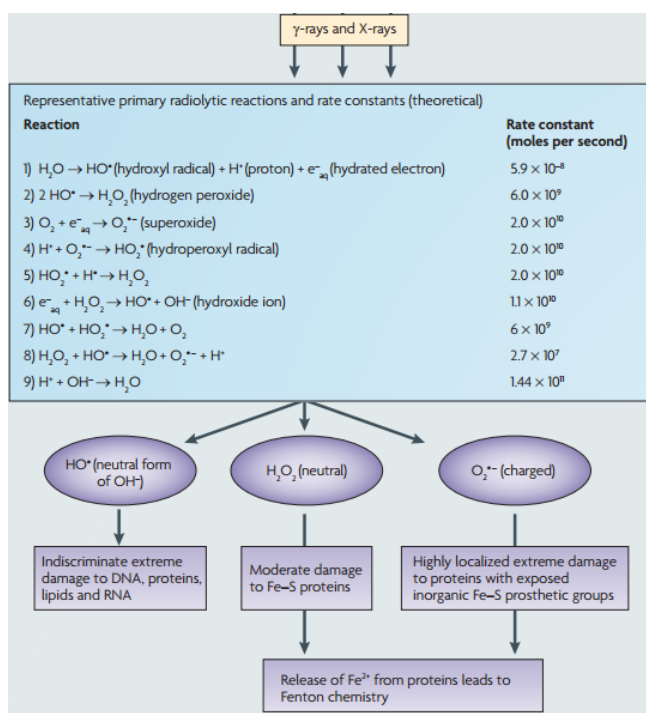


Figure 1.15: Summary of reactions generated by the radiolysis of water, and a summary of the key products (Daly, 2009).

1.7. Summary

This literature review highlights the suitability of bentonite for use as a buffer for the disposal of HHGW. Current research suggests that the impact of microbial activity on such a buffer should be minimal, however there are knowledge gaps where our understanding could be improved. At the forefront of this issue is the limited information on the microbial communities present in bentonites, and how they will respond to the stresses present in a geological disposal scenario. The extraction of DNA from bentonites has produced poor total yields (Direito et al., 2012), however recent advancements in sequencing technology give us the opportunity to explore this issue in detail.

One of the areas that has received a lot of attention in recent years is the role of swelling pressure in limiting microbial activity (Sellin and Leupin, 2013). Most of the work involving swelling pressure has focused on the role of SRB, with the aim of finding suitable bentonite density thresholds to prevent their activity (Bengtsson and Pedersen, 2017). Less attention has been given to IRB, and while there is some literature on their behavior (Ribeiro et al., 2009), we believe more work is required to understand their impact on bentonite mineralogy,

their role in radionuclide speciation, and the sort of density thresholds required to halt their activity.

1.8. Aims and questions:

The overarching aim of this thesis were to investigate microbial processes within bentonite barrier materials, with a focus on the potential impact of swelling pressure, and gamma radiation on microbial viability and diversity, as well as investigating the impact of temperature, and evolving saturation on the microbial ecology of the FEBEX *in-situ* test facility in Grimsel, Switzerland. Additional input from the literature review focused this aim into 6 key questions.

1. Will the impact of stresses encountered during geological disposal on IRB, and SRB communities, influence cell numbers, and diversity?
2. Using samples from the FEBEX *in-situ* test can we identify microbial communities in a bentonite buffer, and infer the effects of temperature, and evolving resaturation on the microbial communities?
3. Can IRB using *Geobacter sulfurreducens* as a model organism cause mineralogical transformations in bentonite materials?
4. If *Geobacter sulfurreducens* can cause mineralogical transformations in bentonite materials do these transformations influence the speciation of priority radionuclides (selenium)?
5. Can IRB activity in bentonite materials be restricted by a sufficient bentonite density?
6. Using data from the above tested hypotheses, and other published sources, can we determine the impact of microbial metabolism (especially Fe(III)-reduction) on bentonite characteristics and barrier performance? How does this information contribute to microbial control strategies?

1.9. References

- Aklujkar, M., Coppi M.V., Leang, C., Kim, B.C., Chavan, M.A., Perpetua, L.A., Giloteaux, L., Liu, A., Holmes, D.C., 2013. Proteins involved in electron transfer to Fe(III) and Mn(IV) oxides by *Geobacter sulfurreducens* and *Geobacter uraniireducens*. Microbiology-SGM, 159: 515-535.
- Alexander, W.R., Neall, F.B., 2011. NDA RWMD Colloid Strategy Review, NDA, Harwell.

- Allard, T., Balan, E., Calas, G., Fourdrin, C., Morichon, E., Sorieul, S., 2012. Radiation-induced defects in clay minerals: a review. *Nuclear Instruments & Methods in Physics Research Section B-Beam Interactions with Materials and Atoms*, 277: 112-120.
- Askarieh, M.M., Chambers, A.V., Daniel, F.B.D., Fitzgerald, P.L., Holtom, G.J., Pilkington, N.J., Rees, J.H., 2000. The chemical and microbial degradation of cellulose in the near field of a repository for radioactive wastes. *Waste Management*, 20(1): 93-106.
- Aubert, C., Brugna, M., Dolla, A., Bruschi, M., Giudici-Orticoni, M.T., 2000. A sequential electron transfer from hydrogenases to cytochromes in sulfate-reducing bacteria. *Biochimica Et Biophysica Acta-Protein Structure and Molecular Enzymology*, 1476(1): 85-92.
- Bachofen, R., 1991. Gas metabolism of microorganisms. *Experientia*, 47(6): 508-514.
- Bailey, L., 2015. Development of a generic safety narrative for a UK geological disposal facility. *Mineralogical Magazine*, 79(6): 1633-1640.
- Bak, F., Widdel, F., 1986a. Anaerobic degradation of indolic compounds by sulfate-reducing enrichment cultures, and description of *Desulfobacterium indolicum* gen-nov, sp-nov. *Archives of Microbiology*, 146(2): 170-176.
- Bak, F., Widdel, F., 1986b. Anaerobic degradation of phenol and phenol derivatives by *Desulfobacterium phenolicum* sp-nov. *Archives of Microbiology*, 146(2): 177-180.
- Bakermans, C., Tsapin, A.I., Souza-Egipsy, V., Gilichinsky, D.A., Nealson, K.H., 2003. Reproduction and metabolism at -10 degrees °C of bacteria isolated from Siberian permafrost. *Environmental Microbiology*, 5(4): 321-326.
- Baldwin, T., Chapman, N., 2008. Geological disposal options for high-level waste and spent fuel, NDA, Cumbria.
- Bartlett, D.H., 2002. Pressure effects on *in-vivo* microbial processes. *Biochimica Et Biophysica Acta-Protein Structure and Molecular Enzymology*, 1595(1-2): 367-381.
- Bartlett, D.H., Kato, C., Horikoshi, K., 1995. High-pressure influences on gene and protein expression. *Research in Microbiology*, 146(8): 697-706.
- Bassil, N.M., Bryan, N., Lloyd, J.R., 2015. Microbial degradation of isosaccharinic acid at high pH. *ISME Journal*, 9(2): 310-320.
- Bauhn, L., Hansson, N., Ekberg, C., Fors, P., Delville, R., Spahiu, K., 2018. The interaction of molecular hydrogen with alpha-radiolytic oxidants on a (U,Pu)O₂ surface. *Journal of Nuclear Materials*, 505: 54-61.
- Beguin, P., Aubert, J.P., 1994. The biological degradation of cellulose. *FEMS Microbiology Reviews*, 13(1): 25-58.
- Bengtsson, A., Pedersen, K., 2017. Microbial sulphide-producing activity in water saturated Wyoming MX-80, Asha and Calcigel bentonites at wet densities from 1500 to 2000 kg m⁻³. *Applied Clay Science*, 137: 203-212.
- Biswas, K., Taylor, M.W., Turner, S.J., 2014. dsrAB-based analysis of sulphate-reducing bacteria in moving bed biofilm reactor (MBBR) wastewater treatment plants. *Applied Microbiology and Biotechnology*, 98(16): 7211-7222.
- Bleam, W.F., 1990. The nature of cation-substitution sites in phyllosilicates. *Clays and Clay Minerals*, 38(5): 527-536.
- Brown, A.D., 1976. Microbial water stress. *Bacteriological Reviews*, 40(4): 803-846.
- Brown, A.R., Boothman, C., Pimblott, S.M., Lloyd, J.R., 2015. The impact of gamma radiation on sediment microbial processes. *Applied and Environmental Microbiology*, 81(12): 4014-4025.
- Brown, A.R., Wincott, P.L., Laverne, J.A., Small, J.S., Vaughan, D.J., Pimblott, S.M., Lloyd, J.R., 2014. The impact of gamma radiation on the bioavailability of Fe(III) minerals for microbial respiration. *Environmental Science & Technology*, 48(18): 10672-10680.

- Brunauer, S., Emmett, P.H., Teller, E., 1938. Adsorption of gases in multimolecular layers. *Journal of the American Chemical Society*, 60: 309-319.
- Brutinel, E.D., Gralnick, J.A., 2012. Shuttling happens: soluble flavin mediators of extracellular electron transfer in *Shewanella*. *Applied Microbiology and Biotechnology*, 93(1): 41-48.
- Campbell, L.L., Postgate, J.R., 1965. Classification of spore-forming sulfated-reducing bacteria. *Bacteriological Reviews*, 29(3): 359-363.
- Chapman, N.A., McKinley, I.G., Shea, M.E., Smellie, J.A.T., 1993. The poços de caldas project: natural analogues of processes in a radioactive waste repository. Elsevier, Amsterdam.
- Childers, S.E., Ciufo, S., Lovley, D.R., 2002. *Geobacter metallireducens* accesses insoluble Fe(III) oxide by chemotaxis. *Nature*, 416(6882): 767-769.
- Chintalapati, S., Kiran, M.D., Shivaji, S., 2004. Role of membrane lipid fatty acids in cold adaptation. *Cellular and Molecular Biology*, 50(5): 631-642.
- Cockell, C.S., Nixon, S., 2013. The boundaries of life. In: Smith, I.W.M., et al. (Eds.), *Astrochemistry and Astrobiology*, Springer-Verlag, Berlin, pp. 211-241.
- Coleman, M.L., Hedrick, D.B., Lovley, D.R., White, D.C., Pye, K., 1993. Reduction of Fe(III) in sediments by sulfate-reducing bacteria. *Nature*, 361(6411): 436-438.
- Covington, E.D., Gelbmann, C.B., Kotloski, N.J., Gralnick, J.A., 2010. An essential role for UshA in processing of extracellular flavin electron shuttles by *Shewanella oneidensis*. *Molecular Microbiology*, 78(2): 519-532.
- Crowe, L.M., Crowe, J.H., 1992. Anhydrobiosis - a strategy for survival. *life sciences and space research Xxiv (3) : planetary biology and origins of life*, 12: 239-247.
- Cutting, R.S., Coker, V.S., Fellowes, J.W., Lloyd, J.R., Vaughan, D.J., 2009. Mineralogical and morphological constraints on the reduction of Fe(III) minerals by *Geobacter sulfurreducens*. *Geochimica Et Cosmochimica Acta*, 73(14): 4004-4022.
- D'Amico, S., Collins, T., Marx, J.C., Feller, G., Gerday, C., 2006. Psychrophilic microorganisms: challenges for life. *EMBO Reports*, 7(4): 385-389.
- Daly, M.J., 2009. Opinion a new perspective on radiation resistance based on *Deinococcus radiodurans*. *Nature Reviews Microbiology*, 7(3): 237-245.
- Daly, M.J., Gaidamakova, E.K., Matrosova, V.Y., Vasilenko, A., Zhai, M., Leapman, R.D., Lai, B., Ravel, B., Li, S.-M.W., Kemner, K.M., Fredrickson, J.K., 2007. Protein oxidation implicated as the primary determinant of bacterial radioresistance. *PLOS Biology*, 5(4): 769-779.
- Daly, M.J., Gaidamakova, E.K., Matrosova, V.Y., Vasilenko, A., Zhai, M., Venkateswaran, A., Hess, M., Omelchenko, M.V., Kostandarithes, H.M., Makarova, K.S., Wackett, L.P., Fredrickson, J.K., Ghosal, D., 2004. Accumulation of Mn(II) in, *Deinococcus radiodurans* facilitates gamma-radiation resistance. *Science*, 306(5698): 1025-1028.
- Daniel, R.M., Cowan, D.A., 2000. Biomolecular stability and life at high temperatures. *Cellular and Molecular Life Sciences*, 57(2): 250-264.
- Delacroix, D., Guerre, J.P., Leblanc, P., Hickman, C., 2002. Radionuclide and radiation protection data handbook 2nd edition (2002). *Radiation Protection Dosimetry*, 98(1): 9-168.
- Demolldecker, H., Macy, J.M., 1993. The periplasmic nitrite reductase of *Thauera selenatis* may catalyze the reduction of selenite to elemental selenium. *Archives of Microbiology*, 160(3): 241-247.
- Direito, S.O.L., Marees, A., Roling, W.F.M., 2012. Sensitive life detection strategies for low-biomass environments: optimizing extraction of nucleic acids adsorbing to terrestrial and Mars analogue minerals. *FEMS Microbiology Ecology*, 81(1): 111-123.

- Dobbin, P.S. Burmeister, L.M.R., Heath, S.L., Powell, A.K., McEwan, A.G., Richardson, D.J., 1996. The influence of chelating agents upon the dissimilatory reduction of Fe(III) by *Shewanella putrefaciens*. 2. oxo- and hydroxo-bridged polynuclear Fe(III) complexes. *Biometals*, 9(3): 291-301.
- Dong, H.L., 2012. Clay-microbe interactions and implications for environmental mitigation. *Elements*, 8(2): 113-118.
- Dose, K., Biegerdose, A., Labusch, M., Gill, M., 1992. Survival in extreme dryness and DNA-single-strand breaks. *life sciences and space research Xxiv (3) : planetary biology and origins of life*, 12: 221-229.
- Eberl, D.D., 1980. Alkali cation selectivity and fixation by clay-minerals. *Clays and Clay Minerals*, 28(3): 161-172.
- El Mendili, Y., Abdelouas, A., Labusch, M., Gill, M., 2013. Insight into the mechanism of carbon steel corrosion under aerobic and anaerobic conditions. *Physical Chemistry Chemical Physics*, 15(23): 9197-9204.
- Esther, J., Sukla, L.B., Pradhan, N., Panda, S., 2015. Fe (III) reduction strategies of dissimilatory iron reducing bacteria. *Korean Journal of Chemical Engineering*, 32(1): 1-14.
- Eswayah, A.S., Smith, T.J., Gardiner, P.H.E., 2016. Microbial transformations of selenium species of relevance to bioremediation. *Applied and Environmental Microbiology*, 82(16): 4848-4859.
- Farr, S.B., Kogoma, T., 1991. Oxidative stress responses in *Eschericia coli* and *Salmonella typhimurium*. *Microbiological Reviews*, 55(4): 561-585.
- Fridovich, I., 1997. Superoxide anion radical (O⁻² radical anion), superoxide dismutases, and related matters. *Journal of Biological Chemistry*, 272(30): 18515-18517.
- Galambos, M., Dano, M., Rosskopfova, O., Sersen, F., Kufcakova, J., Adamcova, R., Rajec, P., 2012. Effect of gamma-irradiation on adsorption properties of Slovak bentonites. *Journal of Radioanalytical and Nuclear Chemistry*, 292(2): 481-492.
- Ghosal, D., Omelchenko, M.V., Gaidamakova, E.K., Matrosova, V.Y., Vasilenko, A., Venkateswaran, A., Zhai, M., Kostandarithes, H.M., Brim, H., Makarova, K.S., Wackett, L.P., Fredrickson, J.K., Daly, M.J., 2005. How radiation kills cells: survival of *Deinococcus radiodurans* and *Shewanella oneidensis* under oxidative stress. *FEMS Microbiology Reviews*, 29(2): 361-375.
- Gibson, G.R., 1990. Physiology and ecology of the sulfate-reducing bacteria. *Journal of Applied Bacteriology*, 69(6): 769-797.
- Gorby, Y.A., Yanina, S., McLean, J.S., Rosso, K.M., Moyses, D., Dohnalkova, A., Beveridge, T.J., Chang, I.S., Kim, B.H., Kim, K.S., Culley, D.E., Reed, S.B., Romine, M.F., Saffarini, D.A., Hill, E.A., Shi, L., Elias, D.A., Kennedy, D.W., Pinchuk, G., Watanabe, K., Ishii, S.I., Logan, B., Nealson, K.H., Fredrickson, J.K., 2006. Electrically conductive bacterial nanowires produced by *Shewanella oneidensis* strain MR-1 and other microorganisms. *Proceedings of the National Academy of Sciences of the United States of America*, 103(30): 11358-11363.
- Gorski, C.A., Aeschbacher, M., Soltermann, D., Vogelín, A., Baeyens, B., Fernandes, M.M., Hofstetter, T.B., Sander, M., 2012. Redox properties of structural Fe in clay minerals. 1. electrochemical quantification of electron-donating and -accepting capacities of smectites. *Environmental Science & Technology*, 46(17): 9360-9368.
- Gorski, C.A., Kluepfel, L.E., Voegelin, A.M., Sander, M., Hofstetter, T.B., 2013. Redox properties of structural Fe in clay minerals: 3. relationships between smectite redox and structural properties. *Environmental Science and Technology*, 47: 13477-85.
- Grant, W.D., 2004. Life at low water activity. *Philosophical Transactions of the Royal Society of London Series B-Biological Sciences*, 359(1448): 1249-1266.

- Guven, N., 1988. Smectites. *Reviews in Mineralogy*, 19: 497-559.
- Haas, J.R., Dichristina, T.J., 2002. Effects of Fe(III) chemical speciation on dissimilatory Fe(III) reduction by *Shewanella putrefaciens*. *Environmental Science & Technology*, 36(3): 373-380.
- Hallbeck, L., 2014. Determination of sulphide production rates in laboratory cultures of the sulphate reducing bacterium *Desulfovibrio aespoeensis* with lactate and H₂ as energy sources, SKB, Stockholm.
- Hansen, M.T., 1978. Multiplicity of genome equivalents in radiation-resistant bacterium *Micrococcus radiodurans*. *Journal of Bacteriology*, 134(1): 71-75.
- Harrison, G., Curle, C., Laishley, E.J., 1984. Purification and characterization of an inducible dissimilatory type sulfite reductase from *Clostridium pasteurianum*. *Archives of Microbiology*, 138(1): 72-78.
- Harrison, M.T., 2014. Vitrification of high level waste in the UK. 2nd International Summer School on Nuclear Glass Wasteform: Structure, Properties and Long-Term Behavior (Sumglass 2013), 7: 10-15.
- Harvey, E.J., White, M.J., Mackenzie, J., McKinley, I., Watson, S.P., 2012. Geological disposal concept options for vitrified HLW, Galson Sciences Ltd, Oakham.
- Helmy, A.K., 1998. The limited swelling of montmorillonite. *Journal of Colloid and Interface Science*, 207(1): 128-129.
- Hem, J.D., 1972. Chemical factors that influence availability of iron and manganese in aqueous systems. *Geological Society of America Bulletin*, 83(2): 443-450.
- Hicks, T., W., Doudou, S., Walters, W.S., 2018. Demonstrating the criticality safety of spent fuel disposal, RWM, Didcot.
- Hicks, T.W., White, M.J., Hooker, P.J., 2009. Role of bentonite in determination of thermal limits on geological disposal facility design, RWM, Didcot.
- Holmboe, M., Jonsson, M., Wold, S., 2012. Influence of gamma-radiation on the reactivity of montmorillonite towards H₂O₂. *Radiation Physics and Chemistry*, 81(2): 190-194.
- Holmboe, M., Norrfors, K.K., Jonsson, M., Wold, S., 2011. Effect of gamma-radiation on radionuclide retention in compacted bentonite. *Radiation Physics and Chemistry*, 80(12): 1371-1377.
- Holmboe, M., Wold, S., Jonsson, M., Garcia-Garcia, S., 2009. Effects of gamma-irradiation on the stability of colloidal Na⁺-montmorillonite dispersions. *Applied Clay Science*, 43(1): 86-90.
- Holton, D., Dickinson, M., Hoch, A., Cowper, M., Thetford, R., Allinson, H., Crockett, G., Cairns, M., Roberts, D., Padovani, C., Johnson, M., Carr, N., Jowett, J., Finch, C., Walsh, C., Southgate, B., Wood, P., Young, A., 2012. Project ankhiale: disposability and full life cycle implications of high-heat generating UK wastes, NDA, Cumbria.
- Huber, R., Stetter, K.O., 2001. Discovery of hyperthermophilic microorganisms. *Hyperthermophilic Enzymes*, Pt A, 330: 11-24.
- Humphreys, P., West, J., R., M., 2010. Microbial effects on repository performance, NDA, Cumbria.
- Imlay, J.A., 2003. Pathways of oxidative damage. *Annual Review of Microbiology*, 57: 395-418.
- Johnson, S.S., Hebsgaard, M.B., Christensen, T.R., Mastepanov, M., Nielsen, R., Munch, K., Brand, T., Thomas, M., Gilbert, P., Zuber, M.T., Bunce, M., Ronin, R., Gilchinsky, D., Froese, D., Willerslev, E., 2007. Ancient bacteria show evidence of DNA repair. *Proceedings of the National Academy of Sciences of the United States of America*, 104(36): 14401-14405.
- Karam, P.A., Leslie, S.A., 1999. Calculations of background beta-gamma radiation dose through geologic time. *Health Physics*, 77(6): 662-667.

- Karnland, O., 1998. Bentonite swelling pressure in strong NaCl solutions: correlation of model calculations to experimentally determined data, Clay Technology, Lund.
- Karnland, O., 2010. Chemical and mineralogical characterization of the bentonite buffer for the acceptance control procedure in a KBS-3 repository, Stockholm.
- Kashefi, K., Lovley, D.R., 2003. Extending the upper temperature limit for life. Science, 301(5635): 934-934.
- Kato, C., Li, L., Nogi, Y., Nakamura, Y., Tamaoka, J., Horikoshi, K., 1998. Extremely barophilic bacteria isolated from the Mariana Trench, Challenger Deep, at a depth of 11,000 meters. Applied and Environmental Microbiology, 64(4): 1510-1513.
- Katti, K.S., Katti, D.R., 2006. Relationship of swelling and swelling pressure on silica-water interactions in montmorillonite. Langmuir, 22(2): 532-537.
- Kessi, J., Ramuz, M., Wehrli, E., Spycher, M., Bachofen, R., 1999. Reduction of selenite and detoxification of elemental selenium by the phototrophic bacterium *Rhodospirillum rubrum*. Applied and Environmental Microbiology, 65(11): 4734-4740.
- Kim, J., Dong, H.L., Seabaugh, J., Newell, S.W., Eberl, D.D., 2004. Role of microbes in the smectite-to-illite reaction. Science, 303(5659): 830-832.
- Kim, S.S., Min, J.H., Baik, M.H., Kim, G.N., Choi, J.W., 2012. Estimation of the behaviors of selenium in the near field of a repository. Nuclear Engineering and Technology, 44(8): 945-952.
- Kinter, E.B., Diamond, S., 1956. Gravimetric determination of monolayer glycerol complexes of clay minerals. Clays and Clay Minerals, 5: 318-333.
- Komadel, P., Lear, P.R., Stucki, J.W., 1990. Reduction and reoxidation of nontronite - extent of reduction and reaction-rates. Clays and Clay Minerals, 38(2): 203-208.
- Kostka, J.E., Wu, J., Nealson, K.H., Stucki, J.W., 1999. The impact of structural Fe(III) reduction by bacteria on the surface chemistry of smectite clay minerals. Geochimica Et Cosmochimica Acta, 63(22): 3705-3713.
- Kusube, M., Kyaw, T.S., Tanikawa, K., Chastain, R.A., Hardy, K.M., Cameron, J., Bartlett, D.H., 2017. *Colwellia marinimaniae* sp nov., a hyperpiezophilic species isolated from an amphipod within the Challenger Deep, Mariana Trench. International Journal of Systematic and Evolutionary Microbiology, 67(4): 824-831.
- Ladriere, J., 1998. Irradiation effects detected by Mössbauer spectroscopy in iron complexes. Hyperfine Interactions, 113(1-4): 411-418.
- Leang, C., Qian, X., Mester, T., Lovley, D.R., 2010. Alignment of the *c*-type cytochrome OmcS along pili of *Geobacter sulfurreducens*. Applied and Environmental Microbiology, 76(12): 4080-4084.
- Li, Y.M., Cheng, W., Sheng, G.D., Li, J.F., Dong, H.P., Chen, Y., Zhu, L.Z., 2015. Synergetic effect of a pillared bentonite support on Se(VI) removal by nanoscale zero valent iron. Applied Catalysis B-Environmental, 174: 329-335.
- Little, B., Wagner, P., 1996. An overview of microbiologically influenced corrosion of metals and alloys used in the storage of nuclear wastes. Canadian Journal of Microbiology, 42(4): 367-374.
- Little, B.J., Ray, R.I., Pope, R.K., 2000. Relationship between corrosion and the biological sulfur cycle: a review. Corrosion, 56(4): 433-443.
- Liu, G.F., Qiu, S., Liu, B.Q., Pu, Y.Y., Gao, Z.M., Wang, J., Jin, R.F., Zhou, J.T., 2017. Microbial reduction of Fe(III)-bearing clay minerals in the presence of humic acids. Scientific Reports, 7.
- Liu, J.S., Neretnieks, I., 2003. Study of the consequences of secondary water radiolysis surrounding a defective canister. Nuclear Technology, 142(3): 294-305.
- Lopez-Fernandez, M., Cherkouk, A., Vilchez-Vargas, R., Jauregui, R., Pieper, D., Boon, N., Sanchez-Castro, I., Merroun, M.L., 2015. Bacterial diversity in bentonites, engineered

- barrier for deep geological disposal of radioactive wastes. *Microbial Ecology*, 70(4): 922-935.
- Lovley, D.R., 1991. Dissimilatory Fe(III) and Mn(IV) reduction. *Microbiological Reviews*, 55(2): 259-287.
- Lovley, D.R., Baedecker, M.J., Lonergan, D.J., Cozzarelli, I.M., Phillips, E.J.P., Sigel, D.I., 1989a. Oxidation of aromatic contaminants coupled to microbial iron reduction. *Nature*, 339(6222): 297-300.
- Lovley, D.R., Chapelle, F.H., 1995. Deep subsurface microbial processes. *Reviews of Geophysics*, 33(3): 365-381.
- Lovley, D.R., Coates, J.D., Bluntharris, E.L., Phillips, E.J.P., Woodward, J.C., 1996a. Humic substances as electron acceptors for microbial respiration. *Nature*, 382(6590): 445-448.
- Lovley, D.R., Fraga, J.L., Coates, J.D., Blunt-Harris, E.L., 1999. Humics as an electron donor for anaerobic respiration. *Environmental Microbiology*, 1(1): 89-98.
- Lovley, D.R., Giovannoni, S.J., White, D.C., Champine, J.E., Phillips, E.J.P., Gorby, Y.A., Goodwin, S. 1993. *Geobacter metallireducens* gen-nov sp-nov, a microorganism capable of coupling the complete oxidation of organic-compounds to the reduction of iron and other metals. *Archives of Microbiology*, 159(4): 336-344.
- Lovley, D.R., Goodwin, S., 1988. Hydrogen concentrations as an indicator of the predominant terminal electron-accepting reactions in aquatic sediments. *Geochimica Et Cosmochimica Acta*, 52(12): 2993-3003.
- Lovley, D.R., Phillips, E.J.P., 1988. Novel mode of microbial energy-metabolism - organic-carbon oxidation coupled to dissimilatory reduction of iron or manganese. *Applied and Environmental Microbiology*, 54(6): 1472-1480.
- Lovley, D.R., Phillips, E.J.P., Lonergan, D.J., 1989b. Hydrogen and formate oxidation coupled to dissimilatory reduction of iron or manganese by *Alteromonas purefaciens*. *Applied and Environmental Microbiology*, 55(3): 700-706.
- Lovley, D.R., Phillips, E.J.P., Lonergan, D.J., 1991. Enzymatic versus nonenzymatic mechanisms for Fe(III) reduction in aquatic sediments. *Environmental Science & Technology*, 25(6): 1062-1067.
- Lovley, D.R., Stolz, J.F., Nord, G.L., Phillips, E.J.P., 1987. Anaerobic production of magnetite by a dissimilatory iron-reducing microorganism. *Nature*, 330(6145): 252-254.
- Lovley, D.R., Woodward, J.C., 1996. Mechanisms for chelator stimulation of microbial Fe(III)-oxide reduction. *Chemical Geology*, 132(1-4): 19-24.
- Lovley, D.R., Woodward, J.C., Chapelle, F.H., 1994. Stimulated anoxic biodegradation of aromatic-hydrocarbons using Fe(III) ligands. *Nature*, 370(6485): 128-131.
- Lovley, D.R., Woodward, J.C., Chapelle, F.H., 1996b. Rapid anaerobic benzene oxidation with a variety of chelated Fe(III) forms. *Applied and Environmental Microbiology*, 62(1): 288-291.
- Lu, Z.Z., Li, Y., Zhou, Y., Cui, H.L., Li, Z.R., 2017. *Halobacterium litoreum* sp-nov., isolated from a marine solar saltern. *International Journal of Systematic and Evolutionary Microbiology*, 67(10): 4095-4099.
- Luef, B., Frischkorn, K.R., Wrighton, K.C., Holman, H.Y.N., Birarda, G., Thomas, B.C., Singh, A., Williams, K.H., Siegerist, C.E., Tringe, S.G., Downing, K.H., Comolli, L.R., Banfield, J.F., 2015. Diverse uncultivated ultra-small bacterial cells in groundwater. *Nature Communications*, 6.
- Macy, J.M., Lawson, S., Demoldecker, H., 1993. Bioremediation of selenium oxyanions in San-Joaquin drainage water using *Thauera selenatis* in a biological reactor system. *Applied Microbiology and Biotechnology*, 40(4): 588-594.

- Madigan, M.T., 2015. Brock biology of microorganisms. Pearson, Boston.
- Malvankar, N.S., Vargas, M., Nevin, K.P., Franks, A.E., Leang, C., Kim, B.-C., Inoue, K., Mester, T., Covalla, S.F., Johnson, J.P., Rotello, V.M., Tuominen, M.T., Lovley, D.R., 2011. Tunable metallic-like conductivity in microbial nanowire networks. *Nature Nanotechnology*, 6(9): 573-579.
- Masurat, P., Eriksson, S., Pedersen, K., 2010a. Evidence of indigenous sulphate-reducing bacteria in commercial Wyoming bentonite MX-80. *Applied Clay Science*, 47(1-2): 51-57.
- Masurat, P., Eriksson, S., Pedersen, K., 2010b. Microbial sulphide production in compacted Wyoming bentonite MX-80 under in situ conditions relevant to a repository for high-level radioactive waste. *Applied Clay Science*, 47(1-2): 58-64.
- Mazoch, J., Tesarik, R., Sedlacek, V., Kucera, I., Turanek, J., 2004. Isolation and biochemical characterization of two soluble iron(III) reductases from *Paracoccus denitrificans*. *European Journal of Biochemistry*, 271(3): 553-562.
- Mehta, T., Coppi, M.V., Childers, S.E., Lovley, D.R., 2005. Outer membrane *c*-type cytochromes required for Fe(III) and Mn(IV) oxide reduction in *Geobacter sulfurreducens*. *Applied and Environmental Microbiology*, 71(12): 8634-8641.
- Mering, J., Oberlin, A., 1971. The smectites. In: Gard, J.A. (Ed.), *The electron optical investigation of clays*. Mineralogical Society, London, pp. 231-254.
- Meulepas, R.J.W., Stams, A.J.M., Lens, P.N.L., 2010. Biotechnological aspects of sulfate reduction with methane as electron donor. *Reviews in Environmental Science and Bio-Technology*, 9(1): 59-78.
- Meyer, B., Kuever, J., 2007. Molecular analysis of the diversity of sulfate-reducing and sulfur-oxidizing prokaryotes in the environment, using *aprA* as functional marker gene. *Applied and Environmental Microbiology*, 73(23): 7664-7679.
- Minton, K.W., 1994. DNA-repair in the extremely radioresistant bacterium *Deinococcus radiodurans*. *Molecular Microbiology*, 13(1): 9-15.
- Montavon, G., Guo, Z., Lutzenkirchen, J., Alhajji, E., Kedziorek, M.A.M., Bourg, A.C.M., Grambow, B., 2009. Interaction of selenite with MX-80 bentonite: effect of minor phases, pH, selenite loading, solution composition and compaction. *Colloids and Surfaces a-Physicochemical and Engineering Aspects*, 332(2-3): 71-77.
- Moore, D.M., Reynolds Jr, R.C., 1997. *X-Ray diffraction and the identification and analysis of clay minerals*. Oxford University Press, Oxford.
- Morgado, L., Bruix, M., Pessanha, M., Londer, Y.Y., Salgueiro, C.A., 2010. Thermodynamic characterization of a triheme cytochrome family from *Geobacter sulfurreducens* reveals mechanistic and functional diversity. *Biophysical Journal*, 99(1): 293-301.
- Mulligan, C.N., Yong, R.N., Fukue, M., 2009. Some effects of microbial activity on the evolution of clay-based buffer properties in underground repositories. *Applied Clay Science*, 42(3-4): 331-335.
- Nadeau, P.H., 1985. The physical dimensions of fundamental clay particles. *Clay Minerals*, 20(4): 499-514.
- Nassif, X., Marceau, M., Pujol, C., Pron, B., Beretti, J.L., Taha, M.K., 1997. Type-4 pili and meningococcal adhesiveness. *Gene*, 192(1): 149-153.
- NDA, 2013. Geological disposal. how the world is dealing with its radioactive wastes, NDA, Harwell.
- NDA, 2014. Geological disposal: feasibility studies exploring options for storage, transport and disposal of spent fuel from potential new nuclear power stations, NDA, Harwell.
- Negron, A., Ramos, S., Blumenfeld, A.L., Pacheco, G., Fripiat, J.J., 2002. On the structural stability of montmorillonite submitted to heavy gamma-irradiation. *Clays and Clay Minerals*, 50(1): 35-37.

- Newsome, L., Morris, K., Lloyd, J.R., 2014. The biogeochemistry and bioremediation of uranium and other priority radionuclides. *Chemical Geology*, 363: 164-184.
- Norrish, K., 1954. The swelling of montmorillonite. *Discussions of the Faraday Society*(18): 120-134.
- Ohnuki, T., Kozai, N., Sakamoto, F., Ozaki, T., Nankawa, T., Suzuki, Y., Francis, A.J., 2010. Association of actinides with microorganisms and clay: implications for radionuclide migration from waste-repository sites. *Geomicrobiology Journal*, 27(3): 225-230.
- Oremland, R.S., Herbel, M.J., Blum, J.S., Langley, S., Beveridge, T.J., Ajayan, P.M., Sutto, T., Ellis, A.V., Curran, S., 2004. Structural and spectral features of selenium nanospheres produced by Se-respiring bacteria. *Applied and Environmental Microbiology*, 70(1): 52-60.
- Orucoglu, E., Hacıyakupoglu, S., 2015. Bentonite modification with hexadecylpyridinium and aluminum polyoxy cations and its effectiveness in Se(IV) removal. *Journal of Environmental Management*, 160: 30-38.
- Pearce, C.I., Pattrick, R.A.D., Law, N., Charnock, J.M., Coker, V.S., Fellowes, J.W., Oremland, R.S., Lloyd, J.R., 2009. Investigating different mechanisms for biogenic selenite transformations: *Geobacter sulfurreducens*, *Shewanella oneidensis* and *Veillonella atypica*. *Environmental Technology*, 30(12): 1313-1326.
- Pedersen, K., 2000. Microbial Processes in Radioactive Waste Disposal, SKB, Stockholm.
- Pedersen, K., 2010. Analysis of copper corrosion in compacted bentonite clay as a function of clay density and growth conditions for sulfate-reducing bacteria. *Journal of Applied Microbiology*, 108(3): 1094-1104.
- Pedersen, K., Motamedi, M., Karnland, O., Sanden, T., 2000a. Cultivability of microorganisms introduced into a compacted bentonite clay buffer under high-level radioactive waste repository conditions. *Engineering Geology*, 58(2): 149-161.
- Pedersen, K., Motamedi, M., Karnland, O., Sanden, T., 2000b. Mixing and sulphate-reducing activity of bacteria in swelling, compacted bentonite clay under high-level radioactive waste repository conditions. *Journal of Applied Microbiology*, 89(6): 1038-1047.
- Postgate, J.R., 1979. The sulfate reducing bacteria. Postgate, J. R, Cambridge University Press, Cambridge.
- Postgate, J.R., Campbell, L.L., 1966. Classification of *Desulfovibrio* species nonsporulating sulfate-reducing bacteria. *Bacteriological Reviews*, 30(4): 732-&.
- Qian, X., Mester, T., Morgado, L., Arakawa, T., Sharma, M.L., Inoue, K., Joseph, C., Salgueiro, C.A., Maroney, M.J., Lovley, D.R., 2011. Biochemical characterization of purified OmcS, a *c*-type cytochrome required for insoluble Fe(III) reduction in *Geobacter sulfurreducens*. *Biochimica Et Biophysica Acta-Bioenergetics*, 1807(4): 404-412.
- Rainey, F.A., Ray, K., Ferreira, M., Gatz, B.Z., Nobre, M.F., Bagaley, D., Rash, B.A., Park, M.J., Earl, A.M., Shank, N.C., Small, A.M., Henk, M.C., Battista, J.R., Kampfer, P., Da Costa, M.S., 2005. Extensive diversity of ionizing-radiation-resistant bacteria recovered from Sonoran Desert soil and description of nine new species of the genus *Deinococcus* obtained from a single soil sample. *Applied and Environmental Microbiology*, 71(9): 5225-5235.
- Reeburgh, W.S., 1983. Rates of biogeochemical processes in anoxic sediments. *Annual Review of Earth and Planetary Sciences*, 11: 269-298.
- Regelsberger, G., Atzenhofer, W., Ruker, F., Peschek, G.A., Jakopitsch, C., Paumann, M., Furtmüller, P.G., Obinger, C., 2002. Biochemical characterization of a membrane-bound manganese-containing superoxide dismutase from the cyanobacterium *Anabaena* PCC 7120. *Journal of Biological Chemistry*, 277(46): 43615-43622.

- Reguera, G., McCarthy, K.D., Mehta, T., Nicoll, J.S., Tuominen, M.T., Lovley, D.R., 2005. Extracellular electron transfer via microbial nanowires. *Nature*, 435(7045): 1098-1101.
- Ribeiro, F.R., Fabris, J.D., Kostka, J.E., Komadel, P., Stucki, J.W., 2009. Comparisons of structural iron reduction in smectites by bacteria and dithionite: II. A variable-temperature Mössbauer spectroscopic study of Garfield nontronite. *Pure and Applied Chemistry*, 81(8): 1499-1509.
- Richter, K., Schicklberger, M., Gescher, J., 2012. Dissimilatory reduction of extracellular electron acceptors in anaerobic respiration. *Applied and Environmental Microbiology*, 78(4): 913-921.
- Riley, M., Staley, J.T., Danchin, A., Wang, T.Z., Brettin, T.S., Hauser, L.J., Land, M.L., Thompson, L.S., 2008. Genomics of an extreme psychrophile, *Psychromonas ingrahamii*. *BMC Genomics*, 9.
- Rivkina, E.M., Friedmann, E.I., McKay, C.P., Gilichinsky, D.A., 2000. Metabolic activity of permafrost bacteria below the freezing point. *Applied and Environmental Microbiology*, 66(8): 3230-3233.
- Rocco, S., Woods, A.W., Harrington, J., Norris, S., 2017. An experimental model of episodic gas release through fracture of fluid confined within a pressurized elastic reservoir. *Geophysical Research Letters*, 44(2): 751-759.
- Rutqvist, J., Tsang, C., 2008. Review of SKB's work on coupled THM processes within SR-Can: external review contribution in support of SKI's and SSI's review of SR-Can.
- RWM, 2016a. Geological disposal derived inventory report, RWM, Didcot.
- RWM, 2016b. Geological disposal: engineered barrier system status report, RWM, Didcot.
- Santamarina, J.C., Klein, K.A., Wang, Y.H., Prencke, E., 2002. Specific surface: determination and relevance. *Canadian Geotechnical Journal*, 39(1): 233-241.
- Schicklberger, M., Buecking, C., Schuetz, B., Heide, H., Gescher, J., 2011. Involvement of the *Shewanella oneidensis* decaheme cytochrome MtrA in the periplasmic stability of the beta-barrel protein MtrB. *Applied and Environmental Microbiology*, 77(4): 1520-1523.
- Schleper, C., Puehler, G., Holz, I., Gambacorta, A., Janekovic, D., Santarius, U., Klenk, H.P., Zillig, W., 1995. *Picrophilus* gen-nov, fam-nov - a novel aerobic, heterotrophic, thermoacidophilic genus and family comprising archaea capable of growth around pH 0. *Journal of Bacteriology*, 177(24): 7050-7059.
- Schramm, L.L., Kwak, J.C.T., 1982. Influence of exchangeable cation composition on the size and shape of montmorillonite particles in dilute suspension. *Clays and Clay Minerals*, 30(1): 40-48.
- Schuetz, B., Schicklberger, M., Kuermann, J., Spormann, A.M., Gescher, J., 2009. Periplasmic electron transfer via the *c*-type cytochromes MtrA and FccA of *Shewanella oneidensis* MR-1. *Applied and Environmental Microbiology*, 75(24): 7789-7796.
- Sellin, P., Leupin, O.X., 2013. The use of clay as an engineered barrier in radioactive-waste management - a review. *Clays and Clay Minerals*, 61(6): 477-498.
- SKB, 2006. Long-term safety for KBS-3 repositories at Forsmark and Laxemar - a first evaluation, SKB, Stockholm.
- Stams, A.J.M., De Bok, F.A.M., Plugge, C.M., Van Eekert, M.H.A., Dolfing, J., Schraa, G., 2006. Exocellular electron transfer in anaerobic microbial communities. *Environmental Microbiology*, 8(3): 371-382.
- Stroes-Gascoyne, S., Hamon, C.J., Maak, P., Russell, S., 2010. The effects of the physical properties of highly compacted smectitic clay (bentonite) on the culturability of indigenous microorganisms. *Applied Clay Science*, 47(1-2): 155-162.

- Sturr, M.G., Guffanti, A.A., Krulwich, T.A., 1994. Growth and bioenergetics of alkaliphilic *Bacillus firmus* OF4 in continuous-culture at high pH. *Journal of Bacteriology*, 176(11): 3111-3116.
- Taguchi, Y., Sugishima, M., Fukuyama, K., 2004. Crystal structure of a novel zinc-binding ATP sulfurylase from *Thermus thermophilus* HB8. *Biochemistry*, 43(14): 4111-4118.
- Tarchitzky, J., Chen, Y., 2002. Rheology of sodium-montmorillonite suspensions: effects of humic substances and pH. *Soil Science Society of America Journal*, 66(2): 406-412.
- Tiedje, J.M., 1988. *Biology of anaerobic microorganisms*, John Wiley, New York.
- Tournassat, C., Neaman, A., Villieras, F., Bosbach, D., Chartlet, L., 2003. Nanomorphology of montmorillonite particles: estimation of the clay edge sorption site density by low-pressure gas adsorption and AFM observations. *American Mineralogist*, 88(11-12): 1989-1995.
- UN, 2008. *Kyoto Protocol Reference Manual*, United Nations, New York.
- UN, 2015. *Paris Agreement*, United Nations, New York.
- Vasquez-Medrano, R., Prato-Garcia, D., Vedrenne, M., Ameta, S.C., Ameta, R., 2018. Chapter 4-Ferrioxalate-Mediated Processes, *Advanced Oxidation Processes for Waste Water Treatment*. Academic Press, Cambridge.
- Venkateswaran, K., Moser, D.P., Dollhopf, M.E., Lie, D.P., Saffarini, D.A., Macgregor, B.J., Ringelberg, D.B., White, D.C., Nishijima, M., Sano, H., Burghardt, J., Stackebrandt, E., Nealson, K.H., 1999. Polyphasic taxonomy of the genus *Shewanella* and description of *Shewanella oneidensis* sp. nov. *International Journal of Systematic Bacteriology*, 49: 705-724.
- Videla, H.A., Herrera, L.K., 2005. Microbiologically influenced corrosion: looking to the future. *International Microbiology*, 8(3): 169-180.
- von Canstein, H., Ogawa, J., Shimizu, S., Lloyd, J.R., 2008. Secretion of flavins by *Shewanella* species and their role in extracellular electron transfer. *Applied and Environmental Microbiology*, 74(3): 615-623.
- Wang, H., Wu, T., Chen, J., Zheng, Q., He, C.H., Zhao, Y., 2015. Sorption of Se(IV) on Fe- and Al-modified bentonite. *Journal of Radioanalytical and Nuclear Chemistry*, 303(1): 107-113.
- Widdel, F., Pfennig, N., 1981. Studies on dissimilatory sulfate-reducing bacteria that decompose fatty-acids .1. isolation of new sulfate-reducing bacteria enriched with acetate from saline environments - description of *Desulfobacter postgatei* gen-nov, sp-nov. *Archives of Microbiology*, 129(5): 395-400.
- Wilkins, M.J., Livens, F.R., Vaughan, D.J., Lloyd, J.R., Beadle, I., Small, J.S., 2010. Fe(III) reduction in the subsurface at a low-level radioactive Waste disposal site. *Geomicrobiology Journal*, 27(3): 231-239.
- Wilson, J., Savage, D., Bond, A., Watson, S., Pusch, R., Bennett, D., 2011. Bentonite: a review of key properties, processes and issues for consideration in the UK context, NDA, Harwell.
- Wilson, M.J., 2013. Sheet silicates. In: Deer, W.A., et al. (Eds.), *The rock forming minerals*. The Geological Society, London, pp. 724.
- WNA, 2015. *The nuclear fuel cycle*. World Nuclear Association, London. Available at <http://www.world-nuclear.org/information-library/nuclear-fuel-cycle/introduction/nuclear-fuel-cycle-overview.aspx> (08/12/18).
- Yee, N., Ma, J., Dalia, A., Boonfueng, T., Kobayashi, D.Y., 2007. Se(VI) reduction and the precipitation of Se(0) by the facultative bacterium *Enterobacter cloacae* SLD1a-1 are regulated by FNR. *Applied and Environmental Microbiology*, 73(6): 1914-1920.

2. Methodology

2.1. Microbiological techniques

A combination of microbiological techniques provided the framework for the research undertaken in this thesis. All the experimental chapters in this thesis used a variety of media, and vessels to culture bacteria. In some cases, the communities in the montmorillonite-based materials were investigated further using molecular ecology techniques. The culturing methodologies describe ways to grow specific pure strains, as well as bacteria carrying out specific functions (Fe(III)-reduction etc.). The MPN enumeration section describes a simple method for counting cells using serial dilutions, and the molecular ecology methodologies explain how DNA can be extracted from communities and used to identify the bacteria present.

2.1.1. Cell culturing

Pure bacterial cultures were employed to alter the geochemistry of the montmorillonite-based materials.

2.1.1.1. *Geobacter sulfurreducens*

Geobacter sulfurreducens is an obligate anaerobe with the ability to reduce Fe(III) (Lovley et al., 2004), and Se(IV) (Pearce et al., 2009) when supplied with an appropriate electron donor such as acetate. To begin with 10 ml of stationary phase *Geobacter sulfurreducens* cells were transferred to 90 ml of NBAF, a modified fresh water medium which contained 20 mM of sodium acetate acting as the sole electron donor, along with 40 mM of fumarate acting as the sole electron acceptor. Prior to use, the NBAF medium was adjusted to pH 7, and purged with pure nitrogen, and autoclaved (126 °C, 20 mins) before use (Cutting et al., 2012). This ensured that the medium was sterile, and the conditions were suitable for *Geobacter sulfurreducens* growth. Following incubation in the dark for 48 hours at 30 °C, the *Geobacter sulfurreducens* cells were transferred to a sterile 900 ml batch of NBAF medium under a nitrogen atmosphere, and allowed to grow to late exponential/early stationary phase for another 48 hours at 30 °C. The *Geobacter sulfurreducens* cells were subsequently placed in nitrogen gassed centrifuge tubes, and centrifuged for 20 minutes (4920 g, 4 °C) before removal of the supernatant, and resuspension of the *Geobacter sulfurreducens* cells in sterile

30 mM MOPS solution. This process was repeated twice before the cells were concentrated in 50 ml of the MOPS solution. The optical density (OD₆₀₀), and therefore the *Geobacter sulfurreducens* density was determined using a spectrophotometer (Jenway (Stone, UK)).

2.1.1.2. *Bacillus subterraneus*

Bacillus subterraneus is a facultative anaerobe which is able to reduce Fe(III) under anaerobic conditions, when provided with yeast extract, and a suitable electron donor such as lactate (Kanso et al., 2002). *Bacillus subterraneus* cells were prepared aerobically by adding 100 ml of stationary phase *Bacillus subterraneus* cells to 1 l of sterile TSB medium in a conical flask, before placement on an orbital shaker at 40 °C for 12 hours. The *Bacillus subterraneus* containing TSB medium was centrifuged (4920 g, 10 °C) before the supernatant was disposed of, and the cells resuspended in artificial groundwater (AGW) (Bengtsson and Pedersen, 2017). The *Bacillus subterraneus* cells were centrifuged a further two times before suspension in 10 ml of AGW.

2.1.2. Minimal medium clay suspensions

Minimal medium clay suspensions were used to assess the ability of *Geobacter sulfurreducens* to reduce structural Fe(III) in FEBEX bentonite, and SWy-2 montmorillonite, and to investigate the fate of radionuclides in SWy-3 under biological Fe(III)-reducing conditions. Microcosms typically consisted of 30 mM MOPS (a buffering agent) and were further amended depending on the purpose. Sodium acetate (10 mM) was used as an electron donor in some treatments to enable the *Geobacter sulfurreducens* cells to utilize Fe(III) as an electron acceptor (Lovley et al., 2004). Meanwhile, 10 µM of 9, 10-Anthraquinone-2, 6-disulfonic acid (AQDS) was used as an electron shuttle to accelerate Fe(III)-reduction, and to see if it increased the extent of Fe(III)-reduction (Lovley et al., 1999). All media were corrected to pH 7 using 10 M NaOH before being purged of air with a N₂:CO₂ gas mixture, and autoclaved (126 °C, 20 mins). Serum bottles were supplemented with FEBEX bentonite, or SWy-2/3 montmorillonite (20 or 40 g l⁻¹) in an anaerobic chamber (Coylab, Grass Lake, MI, USA).

2.1.3. Most probable number (MPN) enumerations

Most probable number (MPN) enumerations were used to count the number of Fe(III)-reducing (IRB), and sulfate-reducing (SRB) bacteria present in the bentonites. MPN enumerations assess the ability for bacterial cells to grow in increasingly diluted (typically 2 or 10 fold dilutions) slurries in a series of tests (typically triplicates) over a period of time before identifying the highest dilution showing bacterial growth, and then applying a statistical test to estimate the number of viable bacterial cells present in the sample (de Man, 1983). The format for this statistical test involves inputting values into two equations. The terms for these equations are a_i which is the weight of sample per serum bottle at a certain dilution, n_i the number of serum bottles at a certain dilution, q_i the number of serum bottles at that dilution, and x is an estimated value of the MPN (Gonzalez, 1996). To solve these equations the user must keep estimating the value of x , until S_1 minus S_2 is equal to 0.

$$S_1 = \Sigma[a_i n_i]$$

$$S_2 = \Sigma[a_i \frac{q_i}{1 - e^{-aix}}]$$

The issue with such calculations is that they rely on trial and error and are therefore time consuming. Attempts to solve this issue traditionally relied on formulating MPN tables for specific experimental regimes (de Man, 1983). However, these tables are specific to the dilution steps used, and the number of samples used at a specific dilution. Unless you followed a previously reported MPN table this would require you to formulate your own MPN table. More recently computing has allowed the development of MPN calculators (Gonzalez, 1996), that are designed to process the iterations until the correct value is derived.

IRB numbers were determined using an anaerobic fully defined growth medium (Lovley and Phillips, 1986) which contained 4 mM ferrihydrite as the sole electron acceptor, along with 3.9 mM of nitrilotriacetic acid (NTA) to increase the bioavailability of the ferrihydrite, along with 2 mM of sodium acetate, and sodium lactate which acted as electron donors. The amount of viable SRB cells in bentonite samples were also counted with Postgate B medium (Postgate, 1979) made to its original specification. *Bacillus subterraneus* cells were grown in metal-reducing (MR) medium (Kanso et al., 2002). In all cases 0.45 g of sample was inoculated into 9 ml of medium in triplicate in an anaerobic chamber (Coylab, Grass Lake, MI, USA). Serial dilutions down to a factor of 10^{-5} were achieved, and the cultures were left to grow depending on the medium for between 14 and 70 days. Positive results in the SRB

samples were determined by the formation of a black precipitate (iron sulfide) as determined by eye, meanwhile positive results in the Fe(III)-containing media were assessed by an enrichment in the 0.5 M extractable Fe(II)/Fe(total) ratio using Ferrozine assay (Lovley and Phillips, 1987).

2.1.4. Molecular ecology

Molecular ecology refers to a series of techniques that investigate the diversity of microbes in samples, and the functionality of genes via the extraction, and analysis of DNA. This thesis used molecular ecology techniques to investigate how bacterial communities responded to stresses relevant to the geological disposal of radioactive waste, as well as examining bacterial communities present in a long-term, field-scale geological disposal experiment.

2.1.4.1. DNA extraction

The extraction of DNA from environmental samples is achieved using specialized DNA extraction kits, which are designed to separate DNA from environmental, and cellular detritus providing a pure DNA product. In the case of environmental slurries, a 200 µl sample was treated using a PowerSoil DNA Isolation Kit (MO BIO Laboratories INC, Carlsbad, CA, USA). Amplification of the 16S rDNA gene was amplified using PCR (polymerase chain reaction), before staining and separation using electrophoresis to confirm the presence of a usable DNA product. The DNA product was treated to a sequencing process described below.

2.1.4.1.1 DNA extraction modified for powdered bentonites

The extraction of DNA from solid bentonite samples provides extra challenges due to the combination of low biomass, and the sorption of phosphorous groups in the DNA to montmorillonite particles (Novinscak and Filion, 2011). The sorption of the DNA to the montmorillonite was counteracted by saturating the solution with phosphate (Direito et al., 2012). DNA was extracted from the FEBEX cores investigated in chapter # by treating 4 0.25 g samples with the FastDNATM Spin Kit (MP Biomedicals, Santa Ana, CA, USA), which was altered to use a DNA-free 1 M sodium phosphate buffer instead of the phosphate buffer included in the extraction kit. Confirmation of a usable DNA product was achieved using the

technique above, and the extraction methodology was also carried out on the 1 M sodium phosphate buffer to confirm it was DNA free.

2.1.4.2. Sequencing

Sequencing was used to determine the order of nucleotides the 16S rRNA gene, which was then subsequently interpreted using bioinformatics to determine the bacterial communities present in the bentonite samples. A second PCR was carried out targeting the V4 hyper variable region (515F, 5'-GTGYCAGCMGCCGCGGTAA-3'; 806R, GGACTACHVGGGTWTCTAAT-3') a region of the 16S rRNA gene where a large amount of diversity is observed, allowing DNA products from individual bacterial species to be distinguished from each other. The PCR was conducted on the Roche FastStart High Fidelity PCR System (Roche Diagnostics Ltd, Basel, SUI) which ran a program consisting of an initial denaturation step (95 °C, 2 mins), followed by 36 temperature cycles (95 °C, 30 s; 55 °C, 30 s; 72 °C, 1 min), and a final extension step (72 °C, 5 mins). PCR products obtained were then purified, and standardized to 20 ng (SequalPrep Normalization Kit, Fisher Scientific, Loughborough, UK). The PCR products were then pooled in equimolar proportions before sequencing on the Illumina MiSeq platform (Illumina, San Diego, CA, USA). The run was completed with a 4 pM sample library, spiked with 4 pM of PhiX producing a final PhiX concentration of 10 % v/v (Kozich et al., 2013).

2.1.4.3. Bioinformatics

Bioinformatics encompasses a range of software-based techniques used to interpret biological data, and in this case to determine the closest bacterial relatives to the organisms detected by sequencing DNA extracted from the bentonites. DNA (16S rRNA gene sequences) identified by the Illumina sequencing run were assigned barcodes allowing for a single mismatch. Cutadapt (Martin, 2011), FastQC (Andrews, 2016), and Sickle (Joshi and Fass, 2011) programmes were used to trim the data, and to check the quality of the data obtained. Errors produced during the sequencing run were identified using SPADes (Nurk et al., 2013), and complete sequences were generated by merging the forward, and reverse reads using Pandaseq (Masella et al., 2012). Chimeras generated during the sequencing run were removed using ChimeraSlayer (Haas et al., 2011), and operation taxonomic units (OTUs) were assigned using UPARSE (Edgar, 2013). Usearch (Edgar, 2010) was used to remove

singletons from the data, and the OTUs were matched to close relatives with a similarity of 97 % or greater. RDP classifier (Wang et al., 2007) was used to taxonomically classify the OTUs, and rarefaction curves were produced using Qiime (Caporaso et al., 2010).

2.2. Mineralogical techniques

2.2.1. X-ray Diffraction (XRD)

X-ray diffraction (XRD) is used to identify crystalline phases in powdered samples. The technique uses X-rays generated by a Cu K_{α} source which subsequently diffract off the atomic planes in a crystalline sample towards a detector. As the X-rays hit an atomic plane a series of reflected X-rays are produced. In most cases these reflected X-rays are out of alignment, and destructive interference leads to little, or no X-rays being detected. However, if Braggs law is satisfied the atomic planes are aligned, and a strong reflection is picked up by the detector (Chatterjee, 2001). Braggs law is shown below with d referring to the distance between atomic planes, θ the angle of incidence, n any numerical value, and λ the wavelength of the X-rays. In a practical scenario this is achieved by rotating the X-ray source, and detector around the sample covering a range of angle of incidences (5° to 70°), whilst the sample is rotated in a horizontal plane. This ensures that the conditions for the crystallites being probed are met, and accounts for variations in crystallite orientation because of sample preparation.

$$2d\sin\theta = n\lambda$$

Sample preparation consisted of grinding approximately 0.1 g of a sample using a mortar, and pestle before mixing with a small amount of amyl acetate and spreading evenly on a low background slide. The amyl acetate was left to evaporate before the samples were inserted into a Bruker (Billerica, MA, USA) D8 Advance diffractometer. Having been analyzed a series of peaks were identified at different angles of incidence each produced by an atomic plane. Due to the 3D nature of crystallites several peaks are generated for individual species referring to the different lattice planes present. These lattice planes have specific d-spacings which are assigned to Miller indices ($h\ k\ l$) which describe the orientation of the planes (Hammond, 2015). The Miller indices are compared to a database of known mineral standards such as the ICDD (International Centre for Diffraction Data) database.

XRD has limitations when it comes to investigating clay minerals as their platy structure produces a preferred orientation when mounted, and therefore one of the planes is much more pronounced compared to the other two planes (Moore and Reynolds Jr, 1997). Whilst this is not normally an issue when it comes to identifying clay minerals it does make quantifying the relative proportions of the minerals difficult, and therefore treatments such as ethylene glycol solvation (Mosser-Ruck et al., 2005), and alternative techniques are used to assist in this endeavor.

2.2.2. Electron Paramagnetic Resonance (EPR)

Electron paramagnetic resonance (EPR) is used to study atoms that contain unpaired electrons, often referred to as paramagnetic species. The interaction of these unpaired electrons with neighboring atoms allows us to infer information about their local chemical environment. This thesis used EPR to identify the Fe(III) species present in the montmorillonite-based materials, and to understand how they responded to biological Fe(III)-reduction. The basic principle of EPR is that electrons exist in a high and low spin state as shown in Figure 2.1 (Weber et al., 1998). When there is no magnetic field (B_0) present there is no measurable energy difference (ΔE). However, as the magnetic field is increased in the presence of electromagnetic radiation the energy of the spin states diverges in a linear fashion (Figure 2.1). At a specific magnetic field strength, the energy difference matches the electromagnetic radiation, and the unpaired electrons flip between spin states (resonate) producing an absorption peak (Figure 2.1).

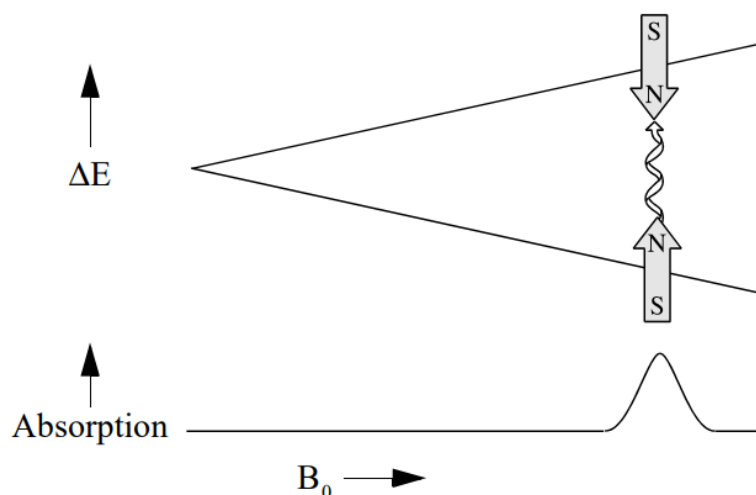


Figure 2.1: The energy difference (ΔE) of electron spin states as a function of magnetic field strength (B_0), with the absorption profile observed at resonance (Weber et al., 1998).

During analysis the EPR sample is housed in a chamber which converts the absorption signal into the first derivative (sine wave) (Figure 2.2) which is the common format to report EPR spectra in (Weber et al., 1998).

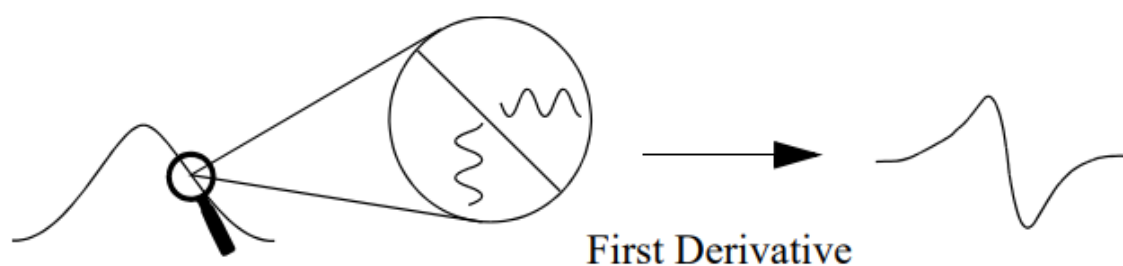


Figure 2.2: Conversion of an absorption spectra into the first derivative (Weber et al., 1998).

EPR spectra typically display intensity as a function of magnetic field (Gauss (G)). However, the location of the peaks in relation to magnetic field varies with the microwave frequency. This is a problem as the microwave source does not emit a fixed frequency causing drift between individual measurements, and a range of microwave frequencies are used for EPR depending on the species being investigated. To overcome this issue the position of peaks in an EPR spectrum are described in terms of the g value. The g value (dimensionless) is a measurement of a particle's magnetic moment, and angular momentum, and is calculated

using the equation below where h is Planck's constant (6.6×10^{-34} J s), ν is the frequency (GHz), μ_B is the Bohr magneton (9.3×10^{-28} J G⁻¹), and B_0 is the magnetic field (G) (Weber et al., 1998).

$$g = \frac{h\nu}{\mu_B B_0}$$

This can be simplified by dividing Planck's constant by the Bohr magneton.

$$g = 714.477 \times \frac{\nu}{B_0}$$

Errors associated with the instrumentation mean the recorded field (and therefore g value) are not the true values. The instrument error is calculated by measuring a standard of known g value. In this thesis strong pitch (0.11 % pitch (long-chain hydrocarbons) in potassium chloride) was used as a standard (Weber et al., 1998). Strong pitch produces a characteristic peak at $g = 2.0028$. The g value measured by the instrument was divided into the true value to derive the error, which was then corrected by multiplying the g values of the spectrum by the error.

Clay suspensions were prepared for EPR by placing 2 ml of sample in a weigh boat and allowing it to dry. The samples were then disaggregated using a pestle and mortar, and a 0.05 g aliquot was placed in an acetone washed capillary tube. Capillary tubes were measured empty before use to confirm the absence of paramagnetic species that could interfere with the measurements. In the case of anaerobic samples, the samples were dried, and prepared in an anaerobic chamber (Coylab, Grass Lake, MI, USA). The anaerobic samples were dispensed in capillary tubes equipped with a J Young tap fitting (GPE Scientific (Leighton Buzzard, UK)) that seals the tube from the external atmosphere. The samples were then transferred to a Bruker (Billerica, MA, USA) EMX Micro X-band (~ 9.9 GHz) spectrometer for analysis.

2.2.3. Mössbauer spectroscopy

Mössbauer spectroscopy exploits the Mössbauer effect to gather isotope specific chemical information about a sample including the oxidation state, and the chemical environment of the isotope being probed. In the case of geochemistry Mössbauer spectroscopy is typically used to probe ⁵⁷Fe which makes up 2.12 % of naturally occurring iron. The Mössbauer effect is the recoilless absorption and emission of gamma radiation by atoms contained in a crystal

lattice, when these conditions are satisfied the absorption of the gamma radiation can be measured with changes in this absorption being governed by the chemical environment of the atom (Gütlich, 2011). In the case of atoms not bound in a crystal lattice the recoil from the gamma radiation being absorbed, and emitted is much greater than the absorption, and no data can be collected.

The Mössbauer effect is achieved and recorded by mounting the solid sample between a gamma radiation source, and a gamma radiation detector that records the signal after it has been absorbed and emitted by the sample (Figure 2.3). To discern information about the chemical environment of the nuclei the source must decay to the isotope being studied, in the case of ^{57}Fe a ^{57}Co source is used. The absorbance of the gamma radiation by the ^{57}Fe nuclei is dependent on the velocity of the gamma radiation, with changes in the chemical environment altering the velocity required for absorbance to be observed. The velocity of the gamma radiation is varied by using a linear motor to achieve the Doppler effect, the data is then plotted as absorbance as a function of velocity (Figure 2.3).

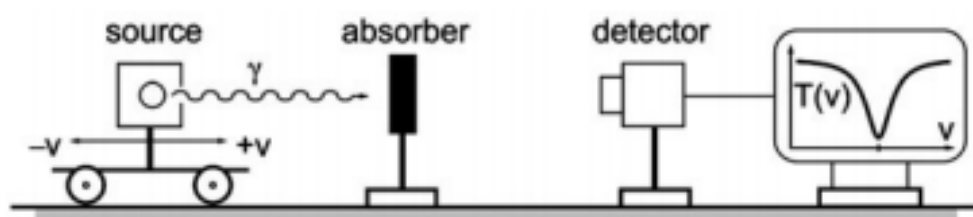


Figure 2.3: A basic diagram of a Mössbauer spectrometer. The velocity (v) oscillates the distance of the gamma radiation (γ) source from the absorber. The detector picks up the transmission (T) of the gamma radiation through the absorber (Gütlich, 2011).

Samples were prepared by passing 5 ml of bentonite slurry through a filter and discarding the supernatant. The resulting solid was mounted onto a holder and sealed with Kapton tape. Mössbauer spectra were collected using a MS4 Mössbauer spectrometer (SEE, Wilmington, MA, USA). Spectra were collected in transition mode at 13 K with the temperature maintained by a closed-cycle cryostat (SHI-850, Janis Research, Wilmington, MA, USA). The spectrometer was calibrated using 7 μm Fe(0)-foil, and spectra were fitted using a Voigt-based fitting routine using Recoil software (Rancourt and Ping, 1991).

2.2.4. Transmission Electron Microscopy (TEM)

Transmission electron microscopy (TEM) is an imaging technique that provides the magnification required to observe nanometer scale objects such as biologically-produced nanoparticles. The principle of TEM is not too dissimilar to optical microscopy, with the components of the two systems roughly laid out in a similar fashion. Light (optical) or electron waves (TEM) are generated and transmitted through a condenser lens which focuses the waves on the intended sample (Tanaka, 2017) (Figure 2.4). While optical lenses are made of glass, lenses intended for the manipulation of electron waves utilize magnetic fields to alter the path of the electrons. The objective lens magnifies the “image”, while the intermediate lens changes the imaging mode (for diffraction and other purposes), and finally the projector lens increases the size of the “image” so that it can be viewed (Tanaka, 2017) (Figure 2.4).

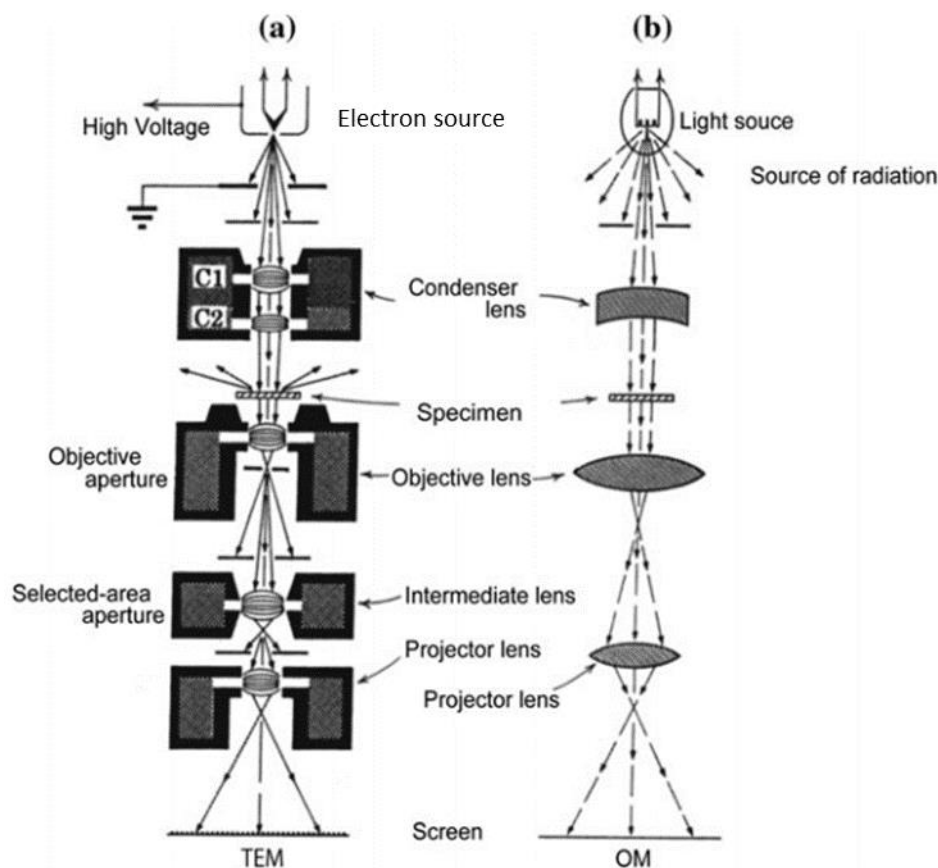


Figure 2.4: Comparison of a TEM microscope (a), and a light microscope (Tanaka, 2017).

The TEM microscope used in this research was a FEI (Hillsboro, OR, USA) TF30 Field Emission Gun (FEG) TEM operating at 300 kV. Samples were prepared by centrifuging a 1

ml aliquot of bentonite slurry (16,162 g, 5 mins) before discarding the supernatant, and redispersion of the pellet in 800 μ l of deionized water (18.2 M Ω) before diluting the solution again in deionized water by a factor of 10. A 1.3 μ l sample was placed on a carbon coated copper TEM grid (Agar Scientific (Stansted, UK)) using a pipette, and left to dry before use.

2.2.4.1. Electron Dispersive X-ray Spectroscopy (EDS)

One result of electrons being used to probe TEM samples is the emission of characteristic X-rays from the sample which are detected using the technique Electron Dispersive X-ray Spectroscopy (EDS) (Shindo and Oikawa, 2002). The emission of X-rays from the sample occurs because the electrons generated by the microscope excite electrons present in the electron shells of nuclei. Electrons from the inner shells of nuclei are ejected leaving behind an electron hole. An electron from an outer shell fills the hole releasing an X-ray equivalent to the difference in energy between the two shells. The difference between the energy of two shells is characteristic of the element the electrons belong to. Therefore, the X-rays can be used to characterize the elemental composition of a sample. EDS spectra were collected from the TEM using an Oxford (Abingdon, UK) XMax EDS detector, and analyzed using Oxford (Abingdon, UK) INCA software.

2.3. Aqueous analyses

2.3.1. Ion Chromatography (IC)

Ion chromatography (IC) is a method of separating and detecting charged particles from a solution to determine their concentration. This research used IC to quantify the concentrations of key anions in solution. The sample was mixed with a suitable buffer (mobile phase) of known volume and passed through an ion exchange column (stationary phase) consisting (in the case of anion exchange chromatography) of immobile cation species that bind to the anions in solution (Fritz, 2000) (Figure 2.5). The anions introduced with the mobile phase remain bound to the stationary phase until competing anions replace them. To identify and quantify the concentrations of the anions in solution the salinity of the mobile phase is gradually increased, and the retention of the anion species on the column recorded, by monitoring the conductivity of the solution. The retention times of the analytes are

observed as a series of peaks, which are then compared to a series of known standards of the anions in question.

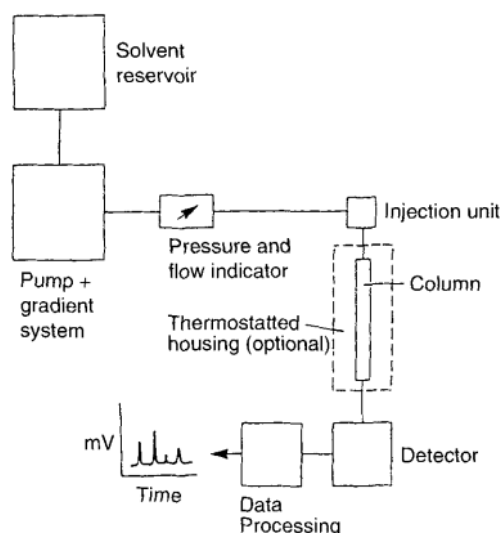


Figure 2.5: An overview of an ion chromatograph. The solvent reservoir, and pump + gradient system moves the mobile phase to the injection unit where the sample is inserted. The mobile phase then passes through the column (stationary phase), and the output recorded using a detector (Fritz, 2000).

Bentonite slurries were prepared for IC by centrifugation (14,800 rpm, 10 mins) to separate the bentonite from the aqueous solution. The solution was then diluted by a factor of 20 in deionized water. Once prepared the samples were loaded onto a Dionex (Sunnyvale, CA, USA) ICS5000 containing a Dionex Capillary AS11-HC 4 μ column. An aliquot of the samples (0.4 μ l) were introduced into the mobile phase which consisted of potassium hydroxide. The mobile phase was introduced into the column at a rate of 0.015 ml min⁻¹ with a gradient of 1 mM – 36 mM potassium hydroxide over the space of 40 minutes.

2.3.2. Inductively Coupled Plasma Atomic Emission Spectroscopy (ICP-AES)

Inductively coupled plasma atomic emission spectroscopy (ICP-AES) is a technique used to quantify chemical elements present in an aqueous sample. ICP-AES was used to establish if key montmorillonite components (iron, aluminium, silicon), along with key interlayer cations (sodium, potassium, calcium, magnesium) were being leached into solution, as well as monitoring selenium removal from solution.

The technique works by introducing the aqueous sample into a spray chamber where it is made into a mist using a nebulizer (Boss and Fredeen, 2004) (Figure 2.6). The mist is mixed with argon gas, and an ICP torch forms an argon plasma flame (Figure 2.6). The species in the sample mist lose electrons in the flame, and form charged ions that emit electromagnetic radiation of wavelengths relevant to the element excited. The wavelengths of electromagnetic radiation generated, and their relative intensities are recorded (Figure 2.6). The wavelengths and intensities are compared to standards of a known concentration.

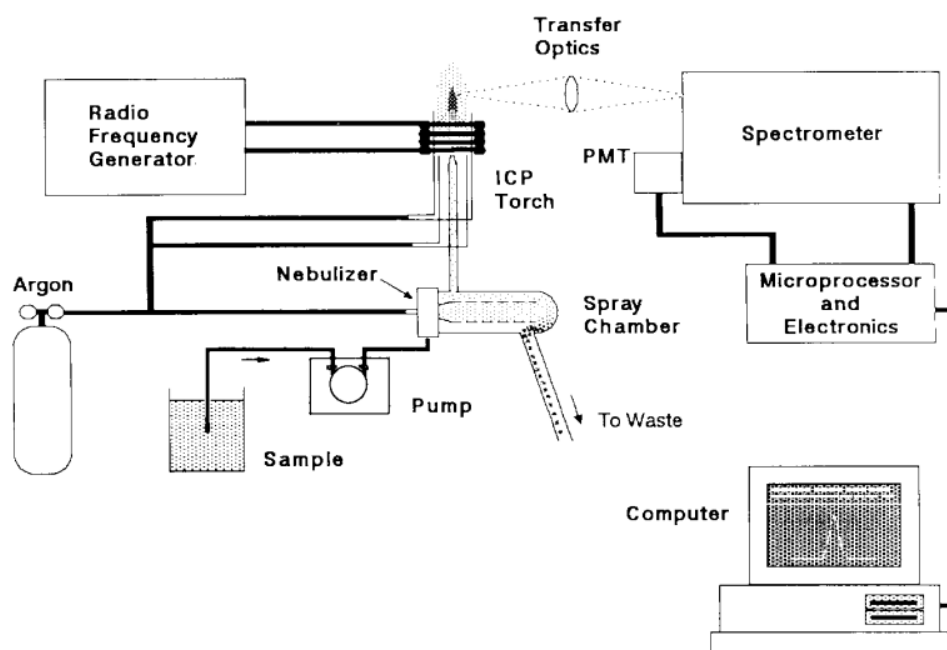


Figure 2.6: Overview of an ICP-AES spectrometer. The solution is pumped into a nebulizer which sprays the sample into a stream of argon. The mist is converted into a plasma using the ICP torch, and the intensities of the species are recorded by the spectrometer (Boss and Fredeen, 2004).

Two preparations were used for the ICP-AES analyses. In the case of determining the cation exchange capacity of solid bentonites 1 g of bentonite was allowed to equilibrate in 5 ml of 1 M ammonium acetate for 24 hours before vacuum filtration, and washed with a further 5 ml of 1M ammonium acetate (Chapman, 1965). The resulting solution was then diluted 10-fold in 2.2 % nitric acid. Samples collected to determine montmorillonite dissolution and introduced species concentration were prepared by centrifuging (14,800 rpm, 10 mins) the bentonite slurry, and then diluting the resulting supernatant 10 times in 2.2 % nitric acid.

2.3.3. Spectrophotometry

Spectrophotometry is the measurement of the absorbance of specific wavelengths of light to determine the concentration of an analyte in solution. Here, spectrophotometry was used to measure the concentration of the key analytes, 0.5 M HCl extractable Fe(II) and total iron, as well as the concentration of *Geobacter sulfurreducens* cells added to experiments. The analyte of interest is reacted with a molecule that forms a strongly colored complex (Stookey, 1970). The sample is diluted to the required concentration then introduced into the spectrophotometer, which is enclosed to prevent interference from natural light. A LED generates the required wavelength, passing it through the sample where it is then recorded by a detector (Figure 2.7). For solutions, the more concentrated the analyte is, the more light it absorbs, and the higher the peak absorption known as lambda max (λ_{\max}) (Figure 2.9). When measuring suspensions, such as bacterial cells, transmittance is affected by scattering of light, i.e. turbidity (Lewis et al., 2014), rather than absorption of light. The transmittance (T) of light through the sample is calculated using the following equation with I_t the intensity of light produced by the LED, and I_o the intensity of light detected after it has passed through the sample:

$$T = \frac{I_t}{I_o}$$

The absorbance (A) of light by the sample, and therefore the concentration of the analyte is related to transmittance in the following manner:

$$A = -\log(T) = -\log\left(\frac{I_t}{I_o}\right)$$

All spectrophotometric work was conducted using a Jenway 6850 UV Vis spectrophotometer (Stone, UK). Details for individual analytes are described below and, in all cases, a blank sample was initially used to calculate the background signal. A calibration curve was generated by measuring a series of standards with known concentrations. These standards were used to derive a linear equation, where y is absorbance, m the gradient, x concentration, and c where y intercepts 0:

$$y = mx + c$$

This equation was rearranged to solve for x (concentration) and used to calculate the concentration of the samples being analyzed.

$$x = (y - c) \div m$$

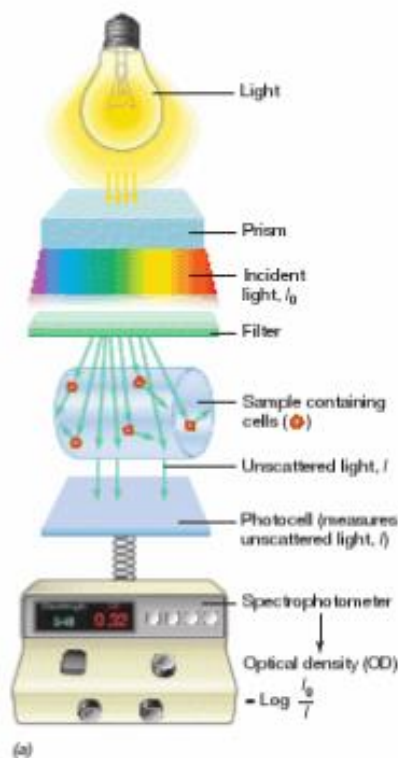


Figure 2.7: Diagram of a spectrophotometer being used to calculate the optical density of a cell solution (Madigan, 2015).

2.3.3.1. Ferrozine assay

Ferrozine (3-(2-Pyridyl)-5,6-diphenyl-1,2,4-triazine-p,p'-disulfonic acid) (Figure 2.8) is a ligand that produces a magenta color with a λ_{max} of 562 nm (Figure 2.9) in the presence of Fe(II) (Stookey, 1970). This assay is used in conjunction with an extractant to determine microbial Fe(III)-reduction in soil samples (Newsome et al., 2014), and pure mineral systems (Brown et al., 2014). The Ferrozine solution is prepared by adding 1 g of Ferrozine and 12 g of HEPES (4-(2-hydroxyethyl)-1-piperazineethanesulfonic acid) (a buffering agent) to 1 liter of deionized water and correcting the pH to 7 using 10 M sodium hydroxide. The bioavailable Fe(II) present in the sample is determined by adding 20 μl of bentonite slurry to 980 μl of 0.5 M hydrochloric acid, and allowing it to react for one hour. If bioavailable Fe(III) is of interest the total bioavailable iron is extracted by adding 20 μl of bentonite slurry to 0.25 M hydroxylamine hydrochloride dissolved in 0.5 M hydrochloric acid (Lovley and Phillips, 1987). These extraction techniques leave a solid residue in the Eppendorf. In the case of bentonite this includes suspended particles (Schramm and Kwak, 1982) that will increase the turbidity of the sample, decreasing transmission. The solid residue was removed

from the samples with centrifugation (16,126 g, 10 mins) before 80 μ l of supernatant was added to 920 μ l of Ferrozine solution in a semi-micro cuvette. Typical standards used for this procedure are iron sulfate heptahydrate of concentrations 0.5 mM, 1 mM, 5 mM, 10 mM, and 20 mM stored in 0.5 M hydrochloric acid, with detection limits (using the above ratio of Ferrozine to sample) of approximately 0.02 mM to 23 mM. This technique was used to monitor microbial Fe(III)-reduction in bentonite, however it is also known to underestimate the amount of bioavailable iron in phyllosilicates (Brookshaw et al., 2014). Quantitative evaluation of microbial Fe(III)-reduction in bentonites was supported further with Mössbauer spectroscopy (Ribeiro et al., 2009).

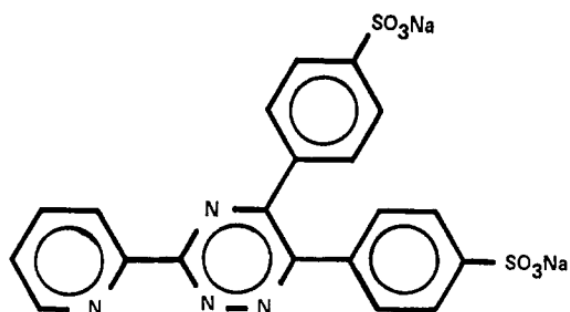


Figure 2.8: Chemical structure of Ferrozine (3-(2-Pyridyl)-5,6-diphenyl-1,2,4-triazine-p,p'-disulfonic acid) (Stookey, 1970).

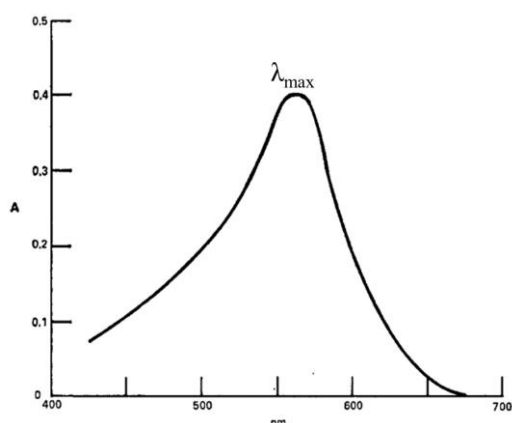


Figure 2.9: Absorption spectrum for Fe(II) complexed with Ferrozine (Stookey, 1970). Lambda max (λ_{max}) has been annotated.

2.3.3.2. Cell density

For particulate suspensions, such as cell suspensions, optical density was used to measure the scattered light, i.e. the turbidity of a sample, to provide a measure of the number of cells present (Lewis et al., 2014). The optical density of *Geobacter sulfurreducens* cell suspensions was determined by adding 100 µl of the bacterial suspension to 900 µl of 30 mM MOPS and comparing it to a 30 mM MOPS standard at 600 nm. This optical density was used to confirm that a known concentration of *G. sulfurreducens* cells was added to each experiment.

2.4. References

- Andrews, N., 2016. FastQC: A quality control tool for high throughput sequence data (Version 0.11.3) [Software]. Available at <https://bioinformatics.babraham.ac.uk/projects/fastqc/> (08/12/18).
- Bengtsson, A., Pedersen, K., 2017. Microbial sulphide-producing activity in water saturated Wyoming MX-80, Asha and Calcigel bentonites at wet densities from 1500 to 2000 kg m⁻³. *Applied Clay Science*, 137: 203-212.
- Boss, C.B., Fredeen, K.J., 2004. Concepts instrumentation and techniques in inductively coupled plasma optical emission spectrometry, Perkin Elmer, Shelton, Connecticut.
- Brookshaw, D.R., Lloyd, J.R., Vaughan, D.J., Patrick, R.A.D., 2014. Bioreduction of biotite and chlorite by a *Shewanella* species. *American Mineralogist*, 99(8-9): 1746-1754.
- Brown, A.R., Wincott, P.L., Laverne, J.A., Small, J.S., Vaughan, D.J., Pimblott, S.M., Lloyd, J.R., 2014. The Impact of gamma radiation on the bioavailability of Fe(III) minerals for microbial respiration. *Environmental Science and Technology*, 48(18): 10672-10680.
- Caporaso, J.G., Kuczynski, J., Stombaugh, J., Bittinger, K., Bushman, F.D., Costello, E.K., Fierer, N., Pena, A.G., Goodrich, J.K., Gordon, J.I., Huttley, G.A., Kelley, S.T., Knights, D., Koenig, J.E., Ley, R.E., Lozupone, C.A., McDonald, D., Muegge, B.D., Pirrung, M., Reeder, J., Sevinsky, J.R., Tumbaugh, P.J., Walters, W.A., Widmann, J., Yatsunenko, T., Zaneveld, J., Knight, R., 2010. QIIME allows analysis of high-throughput community sequencing data. *Nature Methods*, 7(5): 335-336.
- Chapman, H.D., 1965. Cation Exchange Capacity. *Methods of Soil Analysis Part 2*, 9. American Institute of Agronomy, Madison, Wisconsin.
- Chatterjee, A.K., 2001. 8 - X-ray diffraction. In: Ramachandran, V.S., Beaudoin, J.J. (Eds.), *Handbook of analytical techniques in concrete science and technology*, William Andrew Publishing, Norwich, New York, pp. 275-332.
- Cutting, R.S., Coker, V.S., Telling, N.D., Kimber, R.L., Van der Laan, G., Patrick, R.A.D., Vaughan, D.J., Arenholz, E., Lloyd, J.R., 2012. Microbial reduction of arsenic-doped schwertmannite by *Geobacter sulfurreducens*. *Environmental Science and Technology*, 46(22): 12591-12599.
- de Man, J.C., 1983. MPN tables, corrected. *European Journal of Applied Microbiology and Biotechnology*, 17(5): 301-305.
- Direito, S.O.L., Marees, A., Roling, W.F.M., 2012. Sensitive life detection strategies for low-biomass environments: optimizing extraction of nucleic acids adsorbing to terrestrial and Mars analogue minerals. *FEMS Microbiology Ecology*, 81(1): 111-123.

- Edgar, R.C., 2010. Search and clustering orders of magnitude faster than BLAST. *Bioinformatics*, 26(19): 2460-2461.
- Edgar, R.C., 2013. UPARSE: highly accurate OTU sequences from microbial amplicon reads. *Nature Methods*, 10(10): 996-998.
- Fritz, J.S., 2000. Ion chromatography, Wiley-VCH, Weinheim.
- Gonzalez, J.M., 1996. A general purpose program for obtaining most probable number tables. *Journal of Microbiological Methods*, 26(3): 215-218.
- Gütlich, P., 2011. Mössbauer spectroscopy and transition metal chemistry fundamentals and applications, Springer, Berlin.
- Haas, B.J., Gevers, D., Earl, A.M., Feldgarden, M., Ward, D.V., Giannoukos, G., Ciulla, D., Tabbaa, D., Highlander, S.K., Sodergren, E., Methe, B., Desantis, T.Z., Petrosino, J.F., Knight, R., Birren, B.W., 2011. Chimeric 16S rRNA sequence formation and detection in Sanger and 454-pyrosequenced PCR amplicons. *Genome Research*, 21(3): 494-504.
- Hammond, C., 2015. The basics of crystallography and diffraction, Oxford University Press, Oxford.
- Joshi, N.A., Fass, J.N., 2011. Sickel: A sliding-window, adaptive, quality-based trimming tool for FastQ files (Version 1.33) [Software]. Available at <https://github.com/najoshi/sickle> (08/12/18).
- Kanso, S., Greene, A.C., Patel, B.K.C., 2002. *Bacillus subterraneus* sp.-nov., an iron- and manganese-reducing bacterium from a deep subsurface Australian thermal aquifer. *International Journal of Systematic and Evolutionary Microbiology*, 52: 869-874.
- Kozich, J.J., Westcott, S.L., Baxter, N.T., Highlander, S.K., Schloss, P.D., 2013. Development of a dual-index sequencing strategy and curation pipeline for analyzing amplicon sequence data on the MiSeq Illumina sequencing platform. *Applied and Environmental Microbiology*, 79(17): 5112-5120.
- Lewis, C.L., Craig, C.C., Senecal, A.G., 2014. Mass and density measurements of live and dead Gram-negative and Gram-positive bacterial populations. *Applied and Environmental Microbiology*, 80(12): 3622-3631.
- Lovley, D.R., Fraga, J.L., Coates, J.D., Blunt-Harris, E.L., 1999. Humics as an electron donor for anaerobic respiration. *Environmental Microbiology*, 1(1): 89-98.
- Lovley, D.R., Holmes, D.E., Nevin, K.P., 2004. Dissimilatory Fe(III) and Mn(IV) reduction. *Advances in Microbial Physiology*, Vol. 49, 49: 219-286.
- Lovley, D.R., Phillips, E.J.P., 1986. Organic-matter mineralization with reduction of ferric iron in anaerobic sediments. *Applied and Environmental Microbiology*, 51(4): 683-689.
- Lovley, D.R., Phillips, E.J.P., 1987. Rapid assay for microbially reducible ferric iron in aquatic sediments. *Applied and Environmental Microbiology*, 53(7): 1536-1540.
- Madigan, M.T., 2015. Brock Biology of Microorganisms, Pearson Education Limited, Upper Saddle River, New Jersey.
- Martin, M., 2011. Cutadapt removes adapter sequences from high-throughput sequencing reads. *EMBnet*, 17(1): 3.
- Masella, A.P., Bartram, A.K., Truszkowski, J.M., Brown, D.G., Neufeld, J.F., 2012. PANDAseq: PAired-eND Assembler for Illumina sequences. *BMC Bioinformatics*, 13.
- Moore, D.M., Reynolds Jr, R.C., 1997. X-Ray diffraction and the identification and analysis of clay minerals. Oxford University Press, Oxford.
- Mosser-Ruck, R., Devineau, K., Charpentier, D., Cathelineau, M., 2005. Effects of ethylene glycol saturation protocols on XRD patterns: A critical review and discussion. *Clays and Clay Minerals*, 53(6): 631-638.

- Newsome, L., Morris, K., Trivedi, D., Atherton, N., Lloyd, J.R., 2014. Microbial reduction of uranium(VI) in sediments of different lithologies collected from Sellafield. *Applied Geochemistry*, 51(0): 55-64.
- Novinscak, A., Filion, M., 2011. Effect of soil clay content on RNA isolation and on detection and quantification of bacterial gene transcripts in soil by quantitative reverse transcription-PCR. *Applied and Environmental Microbiology*, 77(17): 6249-6252.
- Nurk, S., Bankevich, A., Antipov, D., Gurevich, A.A., Korobeynikov, A., Lapidus, A., Prjibelski, A.D., Pyshkin, A., Sirotkin, A., Sirotkin, Y., Stepanauskas, R., Clingenpeel, S.R., Woyke, T., McLean, J.S., Lasken, R., Tesler, G., Alekseyev, M.A., Pevzner, P.A., 2013. Assembling single-cell genomes and mini-metagenomes from chimeric MDA products. *Journal of Computational Biology*, 20(10): 714-737.
- Pearce, C.I., Patrick, R.A.D., Law, N., Charnock, J.M., Coker, V.S., Fellowes, J.W., Oremland, R.S., Lloyd, J.R., 2009. Investigating different mechanisms for biogenic selenite transformations: *Geobacter sulfurreducens*, *Shewanella oneidensis* and *Veillonella atypica*. *Environmental Technology*, 30(12): 1313-1326.
- Postgate, J.R., 1979. The sulphate-reducing bacteria, Cambridge University Press, Cambridge.
- Rancourt, D.G., Ping, J.Y., 1991. Voigt-based methods for arbitrary-shape static hyperfine parameter distributions in Mössbauer-spectroscopy. *Nuclear Instruments and Methods in Physics Research Section B-Beam Interactions with Materials and Atoms*, 58(1): 85-97.
- Ribeiro, F.R., Fabris, J.D., Kostka, J.E., Komadel, P., Stucki, J.W., 2009. Comparisons of structural iron reduction in smectites by bacteria and dithionite: II. A variable-temperature Mössbauer spectroscopic study of Garfield nontronite. *Pure and Applied Chemistry*, 81(8): 1499-1509.
- Schramm, L.L., Kwak, J.C.T., 1982. Influence of exchangeable cation composition on the size and shape of montmorillonite particles in dilute suspension. *Clays and Clay Minerals*, 30(1): 40-48.
- Shindo, D., Oikawa, T., 2002. Energy dispersive X-ray spectroscopy, *Analytical Electron Microscopy for Materials Science*, Springer Japan, Tokyo, pp. 81-102.
- Stookey, L.L., 1970. Ferrozine - a new spectrophotometric reagent for iron. *Analytical Chemistry*, 42: 779-781.
- Tanaka, N., 2017. Electron nano-imaging : basics of imaging and diffraction for TEM and STEM, Springer, Tokyo, Japan.
- Wang, Q., Garrity, G.M., Tiedje, J.M., Cole, J.R., 2007. Naive bayesian classifier for rapid assignment of rRNA sequences into the new bacterial taxonomy. *Applied and Environmental Microbiology*, 73(16): 5261-5267.
- Weber, R.T., Jiang, J., Barr, D.P., 1998. EMX users manual, Bruker, Billerica Massachusetts.

3. Response of Bentonite Microbial Communities to Stresses Relevant to Geodisposal of Radioactive Waste

Haydn M. Haynes^a, Carolyn I. Pearce^b, Chris Boothman^a, Jonathan R. Lloyd^a

^a *Williamson Research Centre for Molecular Environmental Science and Research Centre for Radwaste Disposal, School of Earth, and Environmental Sciences, University of Manchester, Manchester, M13 9PL, UK*

^b *Geosciences Group, Pacific Northwest National Laboratory, Richland, WA, 99354, US*

Keywords:

Bentonite, sulfate-reducing bacteria, Fe(III)-reducing bacteria, geological disposal facility

3.1. Preface

Question: Will the impact of stresses encountered during geological disposal on IRB, and SRB communities, influence cell numbers, and diversity?

During the writing of the literature review for this thesis Fe(III)- and sulphate-reducing bacteria were focused on as they had been shown to have an effect on bentonite buffers, or other components of a geological disposal facility. Fe(III)-reducers can influence the physical, and chemical properties of bentonites (Kim et al., 2004). Meanwhile, sulfate reducers produce sulfide which can corrode metallic containers (Pedersen, 2010). A greater understanding of bentonite microbial communities was required as although the activity of Fe(III) and sulphate reducers has been reported, the identities of the microorganisms responsible is less clear. Several other groups of bacteria may also be supporting their activity. For example fermentative organisms such as *Clostridia* can produce additional electron donors (e.g. organic acids and hydrogen) for utilization in the reduction of Fe(III) and sulphate. As well as identifying the microorganisms present in bentonite, it was also important to consider whether they would be viable under geological disposal conditions.

Using microbiological culturing techniques, and a routine counting method (MPN enumerations), we were able to investigate the influence of heating, gamma radiation, and pelletisation on the viability of sulfate- and Fe(III)-reducing microbial communities in bentonites. Furthermore, using state of the art DNA sequencing technologies we were able to identify the bacteria responsible, and the ancillary bacteria that may be supporting their activity. The results showed that viable Fe(III)- and sulfate-reducing bacteria remained in the bentonites after the treatments (in lower numbers). Differences in communities were

observed between different bentonites and appeared to influence the number of viable bacterial cells that remained. The screening of microbial communities in bentonites intended for geological disposal could potentially be used to identify a bentonite with a minimal chance of microbial activity. Further research should look at a combination of the treatments to see if this has a further impact on microbial viability, and the role of bentonite density/swelling pressure was considered in chapter 7.

3.2. Abstract

Microbes have been isolated previously from bentonite materials that may be used as barriers for the disposal of radioactive waste. Actively respiring microbes in such barrier materials, within a repository environment, have the potential to adversely affect waste container corrosion rates. Additionally, they could potentially alter the properties of the bentonite barrier itself. This is of significance, since the integrity of the waste container and properties of the bentonite barrier are required to fulfil defined safety functions. To help identify the critical factors that affect microbial activity in bentonite materials, this study examines the impact of a range of parameters that could affect microbial metabolism in a geodisposal environment. Several bentonites from different sources (bentonite mined from locations in Spain and the USA, along with commercially-sourced bentonite) were subjected to increased pressure (74 MPa, 30 seconds), heat (90 °C, 24 hours), and irradiation (1000 Gy, 24.17 Gy min⁻¹), before incubation in growth media selective for sulfate-reducing bacteria (SRB) or iron-reducing bacteria (IRB). The amount of SRB, and IRB were counted using the most probable number method and identified by 16S rRNA gene sequencing. The bentonites initially contained 660-6600 SRB cells g⁻¹, and the number of SRB was correlated with the initial water content of the bentonite. A similar number of IRB was also present (400-4000 cells g⁻¹), and the number of IRB was correlated with the ratio of bioavailable Fe(II)/Fe(Total) present in the bentonite. The bentonites hosted sulfate-reducing species from two bacterial genera, with *Desulfotomaculum* dominating the SRB communities in the Spanish bentonite used in the Full-scale Engineered Barriers Experiment (FEBEX), while the other communities contained *Desulfosporosinus* species. The nature of the SRB community played a significant role in the microbial community response to different stresses, with the FEBEX material producing high SRB cell counts in response to pressure and irradiation but yielding low numbers in response to heat. Initially, the IRB communities contained a mixture of Gram-negative bacteria such as *Geobacter*, and Gram-positive spore-forming bacteria such

as *Bacillus* and *Desulfosporosinus*, with an increase in the number of Gram-positive spore-formers in response to stress. The ability of Gram-positive spore-formers to grow, despite exposure to pressure, heat and irradiation, highlights the need to generate a swelling pressure sufficient to minimize microbial activity. In addition, we suggest that the microbial communities naturally present in the bentonite should be considered as part of the selection process for buffer materials in a geological disposal facility for radioactive waste.

3.3. Introduction

The preferred disposal route for most countries generating radioactive waste is via a highly-engineered underground facility known as a Geological Disposal Facility (GDF) (Baldwin et al., 2008). Bentonite is a clay-based material being considered for use as a buffer in a range of GDF concepts (Bengtsson et al., 2015). The properties of bentonite that make it suitable for use as a buffer material include the ability to swell, offering low permeability (restricting contaminant transport), in addition to amphoteric and ion exchange sites able to adsorb radionuclides. The optimization of swelling processes results in very small pores which inhibit colloid transport and minimize microbial colonization and activity (Wilson et al., 2011). The presence of active microbial populations in bentonite barriers is of concern, as they may influence the physical, and chemical properties of the buffer material, and its performance as a barrier material (Mulligan et al., 2009).

Microbes have been isolated from natural bentonite horizons (Lopez-Fernandez et al., 2015), bentonites prepared for commercial use (Masurat et al., 2010a), as well as being identified in bentonites under simulated geodisposal conditions (Pedersen, 2010). Sulfate-reducing bacteria (SRB) are particularly significant, due to their role in hydrogen sulfide production, a potent corroding agent implicated in nuclear waste canister corrosion (El Mendili et al., 2013). The reduction of structural Fe(III) in bentonites by Fe(III)-reducing bacteria (IRB) is also a concern, as it could lead to dissolution of the buffer material and a loss of structural integrity (Kim et al., 2004). The extent of Fe(III)-reduction in bentonites is debated with other studies suggesting minimal Fe(III)-reduction (Perdrial et al., 2009), with little effect on the stability of smectite (Dong, 2012). In addition to direct impacts on bentonite materials, microbes are also known to influence the speciation and solubility of radionuclides, and in the event of radionuclide release may prevent their transport by precipitating insoluble forms

of priority radionuclides, or could promote transport by bioadsorbing the radionuclides and subsequently migrating as planktonic cells in groundwaters (Newsome et al., 2014).

A range of stresses will be imposed on microorganisms growing in and around a GDF including heat, pressure, and irradiation (Wilson et al., 2011). Several disposal agencies have placed a 100 °C exposure limit on disposal scenarios involving a bentonite buffer, in order to avoid drying of the barrier, thermal alteration (illitization), and to minimize *in-situ* canister corrosion rates (Hicks et al., 2009). However, the current thermal upper limit for microbial growth in laboratory culture is 121 °C (Kashefi and Lovley, 2003), and viable SRB have been identified in bentonite materials following treatment at 120 °C for 15 hours (Masurat et al., 2010b), as well as after exposure to 110 °C for 170 hours (Bengtsson et al., 2015). At high temperatures cell membranes become more fluid, and key biomolecules are denatured (Morozkina et al., 2010) resulting in a loss in viability. Microbes can overcome these challenges by: (i) producing heat-resistant proteins; (ii) rapidly turning over sensitive molecules (Daniel and Cowan, 2000); and (iii) by producing spores which can remain viable for long periods of time (Yi and Setlow, 2010).

To restrict permeability, and to seal gaps within the buffer, a swelling pressure exceeding 0.1 to 1.0 MPa is essential (Sellin and Leupin, 2013). Such a swelling pressure will develop through the absorbance of incoming groundwaters. Bacteria have been identified in the Mariana Trench (10898 m), where hydrostatic pressure surpasses 100 MPa (Kato et al., 1998). Increased pressure reduces the fluidity of membranes, which is compensated for by including more flexible unsaturated fatty acids in the membrane structure (Bartlett, 2002). However, increased swelling pressure introduces an additional mechanical stress which causes a reduction in water activity, through the interactions of water with solutes, and water adsorption to clay surfaces (Stroes-Gascoyne et al., 2010). The decrease in permeability also reduces microbial transport, and access to nutrients, with the smallest known bacteria being approximately 0.1 to 0.2 µm in size (Lopez-Fernandez et al., 2018). Increased salinity reduces the availability of water to bacterial cells, potentially introducing more Na⁺ ions into the cytoplasm which can inhibit enzymes. High salinity is countered by accumulating non-detrimental solutes in the cell, thus balancing the gradient between the cell and the pore fluid (Cockell and Nixon, 2013). Desiccation, induced by water adsorption to clays, also leads to nutrient depletion (Potts, 1994), provoking spore formation in Gram-positive spore-forming bacteria as a survival strategy (Paredes-Sabja et al., 2011). Desiccation is also associated with the build-up of free radicals (Crowe and Crowe, 1992), an issue that is compounded by high

radiation fluxes (Daly, 2009). Highly penetrating gamma radiation is emitted from high level waste (Weber et al., 1998), and gamma-emitting radionuclides could also be adsorbed to the bentonite barrier (Park et al., 2012). Free radicals and other reactive oxygen species produced by the radiolysis of water molecules, cause damage to biomolecules, especially to nucleic acids, lipids, and proteins (Daly, 2009). Resistance to free radical stress is achieved via a range of mechanisms including free radical removal via the intracellular manganese redox cycle (Daly et al., 2007), the efficient repair of genetic damage by DNA repair mechanisms (Minton, 1994), and by maintaining multiple copies of the genome (polydiploidy) (Hansen, 1978).

The aim of this study was to characterize the microbial communities present within a broad range of bentonite samples and determine how they respond to the stresses imparted by temperature, pressure, and gamma radiation, relevant to geological disposal. The direct extraction of DNA from clays typically yields less than 1 % of the total amount present (Direito et al., 2012), so this study used selective growth media, to promote microbial growth, and therefore allow microbial quantification using more traditional most probable number (MPN) culturing techniques (Collins and Lyne, 2004), while increasing the yield of DNA for microbial community analysis. The results of this study highlight the variability in the bacterial content of bentonites, and how the indigenous bacterial communities respond to stresses relevant to geological disposal. A key observation is that spore-forming Gram-positive Fe(III)- and sulfate-reducing bacteria are both prevalent in bentonite materials, and highly resistant to the stresses of high temperatures, pressures and radiation.

3.4. Material and methods

3.4.1. Selection of bentonites

Four bentonites were used in this study including a southern (Mississippi, USA), and western (Wyoming, USA) bentonite, a commercial bentonite purchased from Thermo Fisher Scientific (Waltham, MA, USA), and bentonite from Almeria, Spain, used in the full-scale engineered barriers experiment (FEBEX) designed by Empresa Nacional de Residuos Radiactivos (ENRESA) to investigate the manufacture and construction of a bentonite buffer for use in a GDF (Lanyon and Gaus, 2016). The southern, western, and commercial

bentonites were received in powder form and used as-received; the FEBEX was received in granular form and was disaggregated using a mortar and pestle.

3.4.2. Analytical methods

3.4.2.1. X-ray Diffraction (XRD)

To identify the mineral phases, samples of each bentonite (0.1 g) were ground with a pestle and mortar, mixed with 1 ml of amyl acetate, mounted onto a low background sample holder, and identified using a Bruker (Billerica, MA, USA) D8 Advance diffractometer with CuK α radiation with a wavelength of 1.5406 Å. A step size of 0.02° 2 θ with a counting time of 0.02 s per step over a 2 θ range of 5–70° was used. Powder patterns were fitted using a search/match routine (EVA software program version 4 (Bruker, Billerica, MA, USA), with recorded peaks compared to standards from the ICDD (International Centre for Diffraction Data) database.

3.4.2.2. Brunauer-Emmett-Teller (BET) surface area analysis

Calculation of the surface area of the bentonites was carried out using nitrogen adsorption at -196 °C. 0.2 g of bentonite was purged for 18 hours at 100 °C under a constant flow of nitrogen before analysis (Micrometrics (Norcross, GA, USA) Flowprep 060).

3.4.2.3. X-ray Fluorescence (XRF), H₂O(–) and Loss on Ignition (LOI)

Major-element analyses were obtained with a wavelength dispersive, PANalytical (Royston, UK) Axios spectrometer using the standard glass AUSMON (B255). Finely powdered rock sample (12 g) and fine powdered wax (3 g) were milled for 7 min at 350 rpm in a TEMA (Woodford Halse, UK) mill and pressed into a pellet at 10 tonnes. Uncertainty on the XRF instrument was approximately 2.6 %. Samples (1 g) were dried at 105 °C for 1 hour, cooled in a desiccator and weight loss recorded to determine the loosely held water, H₂O(–). Samples were then heated for 1 hour at 1100 °C, cooled in a desiccator and reweighed. The loss on ignition is due to dehydroxylation of clay minerals and the release of CO₂ by breakdown of carbonates and oxidation of organic matter.

3.4.2.4. Ferrozine analysis

The Ferrozine method (Lovley and Phillips, 1987) was used to measure 0.5 M hydrochloric acid extractable Fe(II), and total iron (after reaction with hydroxylamine) in the bentonite samples. Samples (0.2 g) were placed in 0.5 M hydrochloric acid (5 ml), and allowed to equilibrate for an hour, then 20 μ l of the resulting slurry was transferred to 980 μ l of 0.5 M hydrochloric acid for Fe(II), or 980 μ l of 0.5 M hydroxylamine hydrochloride for total bioavailable iron. After a further hour of digestion, 80 μ l of the sample was added to 920 μ l of Ferrozine and measured using a spectrophotometer (Jenway (Stone, UK)) at 562 nm. The uncertainty limit of the Ferrozine assay is approximately 3.2 % (Stookey, 1970). Ferrozine was also used to measure Fe(III) reduction in the MPN experiments targeting IRB, in this instance 20 μ l of the sample was added to the hydrochloric acid solution (0.5 M, 980 μ l).

3.4.2.5. Ion Chromatography (IC) and pH

Ion chromatography was used to determine the concentration of sulfate in the bentonites. Samples (0.2 g) were placed in 5 ml of deionized water (18.2 M Ω) and allowed to equilibrate on a roller mixer for one hour. Afterwards 1ml of the slurry was transferred to an Eppendorf tube, and the supernatant was separated from the bentonite using a centrifuge (16,162 g, 10 minutes). The pH of the supernatant was measured (Denver Instrument (Sartorius, Göttingen, Germany)), then being diluted four times with deionized water, and analyzed using a Dionex (Sunnyvale, CA, USA) ICS5000. The uncertainty limit of the measurements was approximately 4.1 %.

3.4.2.6. Inductively Coupled Plasma Atomic Emission Spectroscopy (ICP-AES)

The interlayer cations in the bentonite samples were analyzed by ICP-AES. 1 g of each substrate was added to 5 ml of 1 M ammonium acetate, before being placed on a shaker for 24 hours. An extra 5 ml of 1M ammonium acetate was added to the slurries before being vacuum filtered (Chapman, 1965). The remaining solid was discarded, and the supernatant was collected. The solutions were acidified by adding 1 ml aliquots to 9 ml of 2.2% HNO₃. The acidified supernatants were then analyzed with a Perkin-Elmer (Waltham, MA, USA) Optima 5300 dual view ICP-AES. The uncertainty limit of the measurements was approximately 3.4 %.

3.4.3. Sample and media preparation

3.4.3.1. Pelletisation

Pelletisation was used to simulate the effects of compaction on the bentonite microbial communities. 0.3 g of each substrate was loaded into a pellet press (SpecAc, Orpington, Kent) between two 13 mm die (SpecAc, Orpington, Kent), before the addition of approximately 9 tonnes of load (~ 74 MPa), producing a 2.7 g cm^{-3} pellet. After being compressed for 30 seconds the load was released. The process was repeated until 9 pellets of each bentonite were produced. The pellets were subsequently powdered using a 70% ethanol sterilized mortar and pestle, before incubation in the growth medium.

3.4.3.2. Heat treatment

The effects of heat being created by high-heat generating wastes (HHGW) were replicated inside an incubator. Each bentonite sample was divided into 0.45 g aliquots, and placed inside sterilized 10 ml serum bottles, before being stoppered, and sealed. The bottles were then flushed with filter sterilized nitrogen to generate an unreactive atmosphere and sealed. Following the de-aeration, the bottles were placed in an incubator for 24 hours, at a temperature of 90°C .

3.4.3.3. Gamma irradiation

Along with heat, HHGW also produce gamma irradiation, which was simulated in this study using a Cobalt-60 irradiator (812 Co-60 irradiator, Foss Therapy Services Inc, North Hollywood, CA, USA). The bentonite substrates were transferred into sterile glass vials each holding 1 g. The bentonite was trapped in the vials with glass wool, and the air was removed using a vacuum. Whilst under vacuum the vials were sealed using an oxygen torch. Fricke dosimetry (Fricke and Hart, 1935) was used to calculate the dose rate within the Cobalt-60 irradiator, and the samples were subjected to 1000 Gy, at a dose rate of $24.17 \text{ Gy min}^{-1}$. The vials were subsequently opened in a laminar flow cabinet (Labcaire, Clevedon, UK) to prevent contamination and transferred to sterile 10 ml serum bottles ready for incubation.

3.4.3.4. Media preparation

The bentonites were added to selective growth media, to promote the growth of specific groups of anaerobic bacteria. Postgate Medium B was used to selectively enrich for SRB, and a fully defined growth medium was selected for IRB (Lovley and Phillips, 1986). While the media selected contain compounds to promote the growth of the organisms highlighted, some SRB are known to reduce iron (Liu et al., 2012), and may therefore appear in both media. The Postgate B medium was formulated according to its original specifications (Postgate, 1979). The pH of the Postgate B medium was amended to 7.0 using 10 M sodium hydroxide. The fully defined growth medium contained the equivalent of 4 mM ferrihydrite (as the sole electron acceptor) with 3.9 mM of nitrilotriacetic acid to increase the bioavailability of the Fe(III), as well as 2 mM of acetate and lactate as electron donors, the pH of the media was amended to 7.0 using 10 M sodium hydroxide. The Fe(III)-containing medium lacks the strong reducing agent sodium thioglycolate present in the Postgate B medium and was therefore degassed with nitrogen for 10 minutes to impose anaerobic conditions. Both media were divided into 9 ml aliquots within 10 ml serum bottles. The fully defined IRB growth medium was decanted inside an anaerobic glovebox (Coylab, Grass Lake, MI, USA) to preserve the anaerobic headspace, whilst the Postgate Medium B was decanted under atmospheric conditions. The media were sealed, and autoclaved (126 °C, 1.1 bar, 20 minutes) to ensure their sterility.

3.4.4. Microbiology methods

3.4.4.1. Most Probable Number (MPN) enumerations

The changes in the SRB, and IRB quantities following the individual treatments were tracked using MPN enumerations (de Man, 1983). To do this, 0.45 g of each substrate was inoculated into 9 ml of the media described in the previous section. The resulting slurry (1 ml) was transferred to fresh media (9 ml) using a nitrogen-gassed syringe; this was repeated until a 10^{-5} dilution was achieved. The serial dilutions were incubated at 20 °C in the dark, and a positive result was confirmed in the Postgate Medium B by the presence of a black precipitate after 25 days, while the fully defined Fe(III)-containing growth medium bottles were left for 70 days, and a positive result for Fe(III)-reducing bacteria was confirmed by the enrichment of 0.5 M hydrochloric acid extractable Fe(II)/Fe(total), using the Ferrozine

method described above. The number of SRB, and IRB were calculated by comparing the number of positive serial dilutions to a MPN chart, and correcting for the initial dilution (de Man, 1983). The MPN enumerations were conducted in triplicate.

3.4.4.2. Microbial analyses (16S rRNA gene sequencing)

The microorganisms that dominated in the MPN tubes that had scored positive for SRB or IRB were identified by extracting, amplifying and sequencing DNA from the samples showing the strongest positive result, after the initial incubation time. 200 µl of the slurries was treated using a PowerSoil DNA Isolation Kit (MO BIO Laboratories INC, Carlsbad, CA, USA). The 16S rDNA gene was amplified via PCR (polymerase chain reaction) using 8F (5'-AGAGTTTGATCCTGGCTCAG-3'), and 1492R (5'-TACGGYTACCTTGTTACGACTT-3') primers and the methods of (Rizoulis et al., 2016). Following amplification via PCR, a DNA stain (SYBR Safe DNA Gel Stain, Invitrogen, Carlsbad, CA, USA) was added before placement in an agarose gel, where it was subsequently separated using electrophoresis. The stained DNA was viewed under UV light, and target 1600 base pair products were identified by comparison to a ladder of DNA fragments of varying lengths.

3.4.4.3. Sequencing

A second PCR run was completed targeting the V4 hyper variable region (515F, 5'-GTGYCAGCMGCCGCGGTAA-3'; 806R, GGACTACHVGGGTWTCTAAT-3') (Caporaso et al., 2011) belonging to the successfully amplified 16S rRNA gene. The amplification of the region was completed with the Roche FastStart High Fidelity PCR System (Roche Diagnostics Ltd, Basel, SUI) using the following procedure; initial denaturation (95 °C, 2 mins), followed by 36 cycles (95 °C, 30 s; 55 °C, 30 s; 72 °C, 1 min), and then a final extension step (72 °C, 5 mins). Purification of the resulting products was completed, and then standardized to approximately 20 ng (SequalPrep Normalization Kit, Fisher Scientific). The products of the PCR were then pooled in equimolar proportions, and sequenced (Illumina MiSeq platform, Illumina, San Diego, CA, USA). The sequencing run was implemented using a 4 pM sample library, spiked with 4 pM of PhiX in a ratio producing a final PhiX concentration of 10% v/v (Kozich et al., 2013).

3.4.4.4. Bioinformatics

The sequences that were generated were identified by barcodes allowing for one mismatch before Cutadapt (v1.8.1) (Martin, 2011), FastQC (v11.3) (Andrews, 2016), and Sickle (v1.33) (Joshi and Fass, 2011) were used for quality control, and trimming. Errors from sequencing were corrected using SPADes (v3.5.0) (Nurk et al., 2013), and the forward, and reverse reads were amalgamated into complete sequences using Pandaseq (v2.8) (Masella et al., 2012). ChimeraSlayer (Haas et al., 2011) was used to remove chimeras, and operational taxonomic units (OTUs) were produced using UPARSE (Edgar, 2013). Usearch (v8.0.1623) (Edgar, 2010) was then used to remove singletons, and to classify the OTUs at a similarity of 95% or higher. OTUs were taxonomically classified using RDP classifier (v2.2) (Wang et al., 2007), and rarefaction curves were generated using Qiime (v1.8.0) (Caporaso et al., 2010).

3.5. Results

3.5.1. Characterization of the bentonites

The key characteristics of the bentonite samples were determined using a variety of techniques and are summarized in Table 3.1. The substrates consisted mostly of the clay mineral montmorillonite (a dioctahedral smectite), with accessory quartz and plagioclase feldspar; the southern bentonite also contained calcite, and biotite. The FEBEX, and commercial bentonites contained approximately 10 % water, while the southern, and western were about 6 %. The bentonite samples consisted of ~ 4 % iron, with the 0.5 M HCl extractable fraction consisting of ~ 100 % Fe(II) in the commercial, and western bentonites, and ~ 30 % in the FEBEX, and southern samples. The substrates had comparable surface areas of between 27.4, and 52.3 m² g⁻¹, measured by BET. In the commercial and western bentonites, sodium was the dominant interlayer cation, whereas the FEBEX bentonite contained more calcium.

Table 3.1: Key chemical characteristics, including the water content, loss on ignition (LOI), pH, surface area (SA), concentration of key interlayer cations (sodium, calcium, potassium, magnesium), along with the concentration of sulphate, the redox state of 0.5 M HCl extractable iron, and the mineralogy.

Sample	Commercial	FEBEX	Southern	Western
H ₂ O (%)	10.4	9.9	5.5	6.5
LOI (%)	6.2	8.0	9.8	6.3
pH	10.1	9.5	9.9	10.1
SA (m ² g ⁻¹)	27.4 ± 0.3	52.3 ± 0.5	44.9 ± 0.5	30.3 ± 0.3
Na ⁺ (mg g ⁻¹)	10.7	5.8	5.6	11.7
Ca ²⁺ (mg g ⁻¹)	4.9	7.3	5.4	5.0
K ⁺ (mg g ⁻¹)	0.5	0.7	0.3	0.5
Mg ²⁺ (mg g ⁻¹)	1.0	3.8	2.8	1.0
SO ₄ ²⁻ (mg g ⁻¹)	69.0	17.3	28.5	60.9
Fe (%)	3.8	3.8	4.2	3.9
0.5 M HCl extractable Fe(II)/Fe(total) (%)	99.2	29.8	36.6	100.0
Mineralogy (XRD)	Montmorillonite, Quartz, Labradorite	Montmorillonite, Quartz, Labradorite	Montmorillonite, Quartz, Sanidine, Calcite, Biotite	Montmorillonite, Quartz, Labradorite

3.5.2. Most Probable Number (MPN) enumerations

To determine the number of culturable SRB and IRB present in the bentonites, each sample was inoculated into Postgate medium B (25 days), and a fully defined growth medium containing ferrihydrite as the sole electron acceptor (70 days), targeting SRB and IRB respectively. The number in the starting inoculum was determined using MPN enumerations (de Man, 1983). The results indicate that the samples typically hosted 660-6600 SRB cells g⁻¹, and 400-4000 IRB cells g⁻¹ (Table 3.2), a few orders of magnitude lower than a typical soil. The commercial bentonite yielded the largest number of SRB cells (6600 g⁻¹), while the FEBEX, and southern substrates yielded approximately ~ 3000 g⁻¹; the western bentonite had the lowest (660 g⁻¹). IRB numbers were lower compared to SRB, with the most being found in the western substrate (4000 g⁻¹), an intermediate amount in the commercial bentonite (1880 g⁻¹), and minor amounts in the FEBEX (400 g⁻¹), and southern (660 g⁻¹) samples. Following analysis of the as received bentonite samples they were then subjected to increased pressure, gamma radiation, and temperatures to determine the impact on culturable SRB and IRB.

Table 3.2: Number of IRB and SRB per gram in each of the substrates, along with the 95% confidence intervals (MPN, most probable number; CI, confidence interval; LL, lower limit; UL, upper limit).

	MPN g ⁻¹	95 % CI LL	95 % CI UL
IRB			
Commercial	1880	460	7600
FEBEX	400	104	1620
Southern	660	184	2400
Western	4000	1020	16400
SRB			
Commercial	6600	1840	24000
FEBEX	4000	1020	16400
Southern	1880	460	7600
Western	660	184	2400

The change in the quantity of SRB after each treatment is shown in Figure 1, confidence intervals can be found in supplementary 3.1. The average MPN g⁻¹ of SRB decreased across all treatments, however the amount of SRB in the southern bentonite remained the same following irradiation (1880 g⁻¹) but doubled in number after the heat treatment (90 °C) to 4000 g⁻¹. Following pelletisation, the southern bentonite samples saw a reduction in SRB numbers (1700 g⁻¹); a decrease of approximately 60% was seen in the FEBEX (1880 g⁻¹), and western (196 g⁻¹) bentonites, while the commercial bentonite saw a reduction to 940 g⁻¹. SRB numbers in the western bentonite also saw a ~ 60 % reduction following the heat treatment, and recorded the poorest growth following irradiation (44 g⁻¹). The FEBEX bentonite maintained reasonable cell counts across the experiments, but a ten-fold loss (400 g⁻¹) was observed following the heat treatment. The commercial bentonite maintained a large cell count after the heat treatment (4000 g⁻¹) but saw a significant reduction in cell numbers after irradiation (500 g⁻¹).

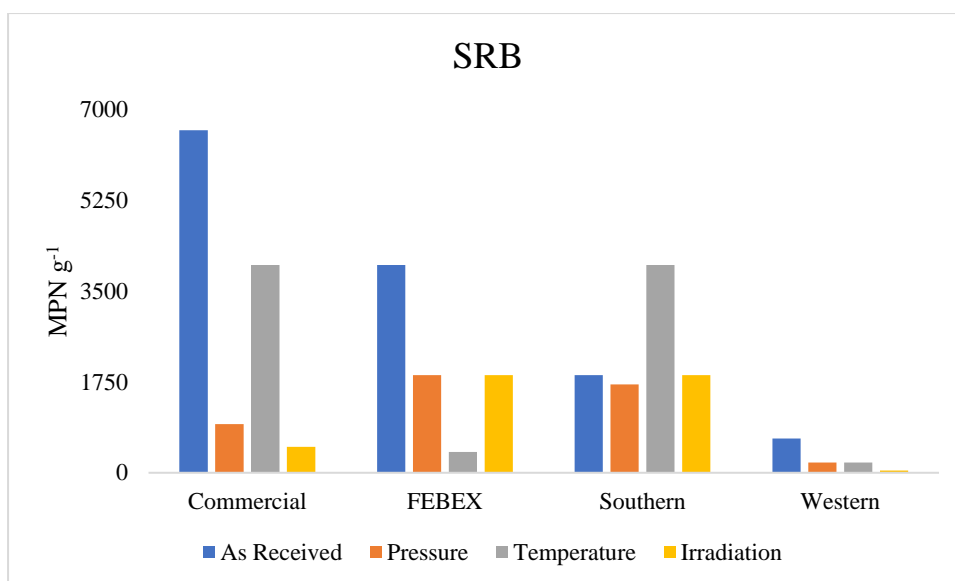


Figure 3.1: Number of SRB in the Postgate B enrichments (MPN g^{-1}) following no treatment (as received), pelletisation at $\sim 74 \text{ MPa}$ (pressure), heating at 90°C for 24 hours (temperature), and a gamma radiation dose of 1000 Gy (irradiation).

The quantities of IRB in the samples are shown in Figure 3.2, confidence intervals can be found in supplementary 3.1. Despite the as received FEBEX containing low numbers of IRB (400 g^{-1}), a substantial increase was observed following the heat treatment (1880 g^{-1}), a trend which was not reflected after exposure to pressure (176 g^{-1}), or irradiation (94 g^{-1}). There was also a moderate increase in IRB numbers in the Southern bentonite, to 1700 g^{-1} after pressure and 1020 g^{-1} after heating, but low MPN counts were recorded after irradiation (140 g^{-1}). After exposure to pressure, the commercial bentonite maintained its original cell count for IRB (1880 g^{-1}), and a reduction of just under 50% was observed after heating (1020 g^{-1}), and irradiation (1020 g^{-1}). The western bentonite samples had the highest initial IRB cell count (4000 g^{-1}), but a 58% reduction was observed following exposure to pressure (1700 g^{-1}), and larger losses in IRB were seen after heating (400 g^{-1}), and after irradiation (196 g^{-1}).

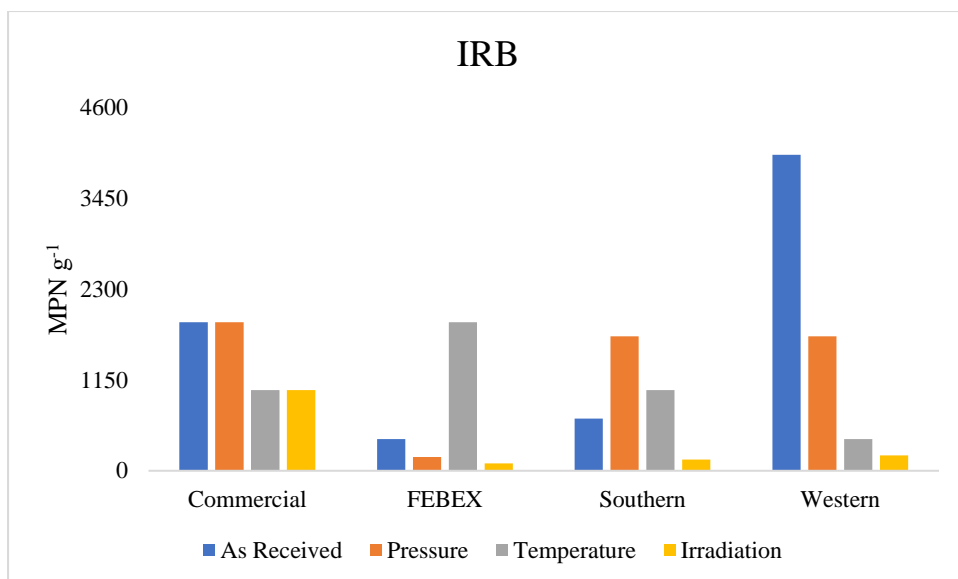
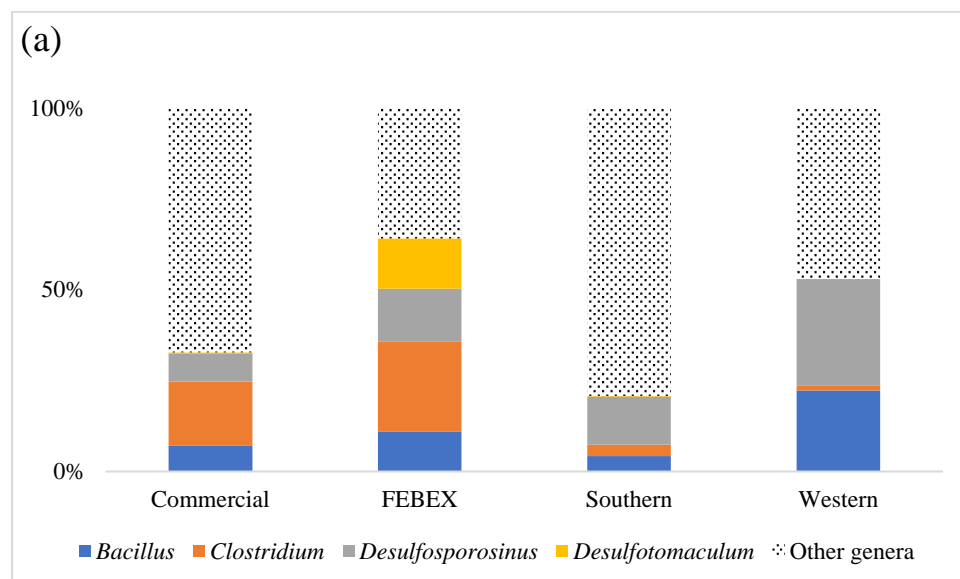


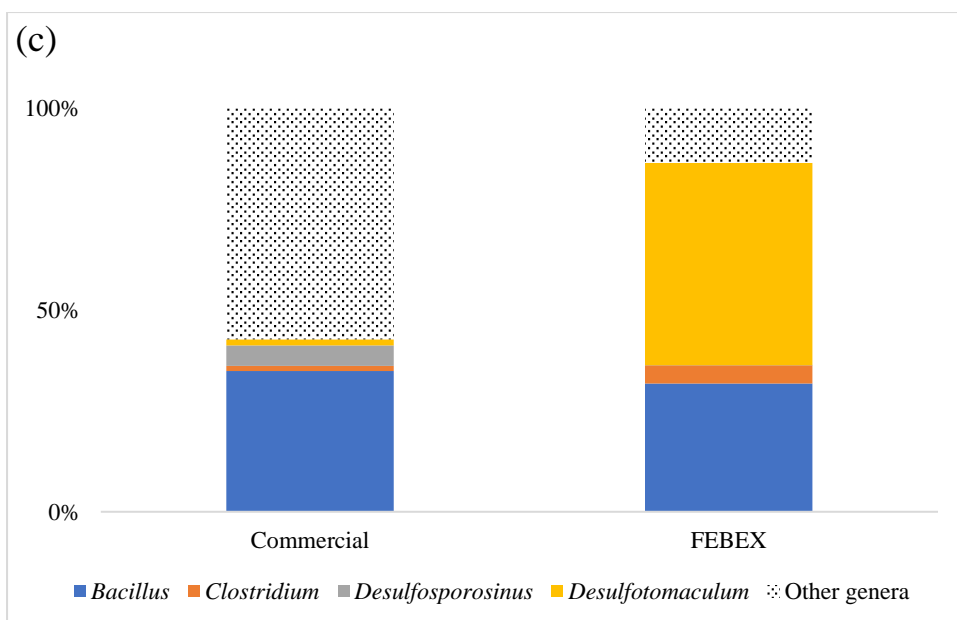
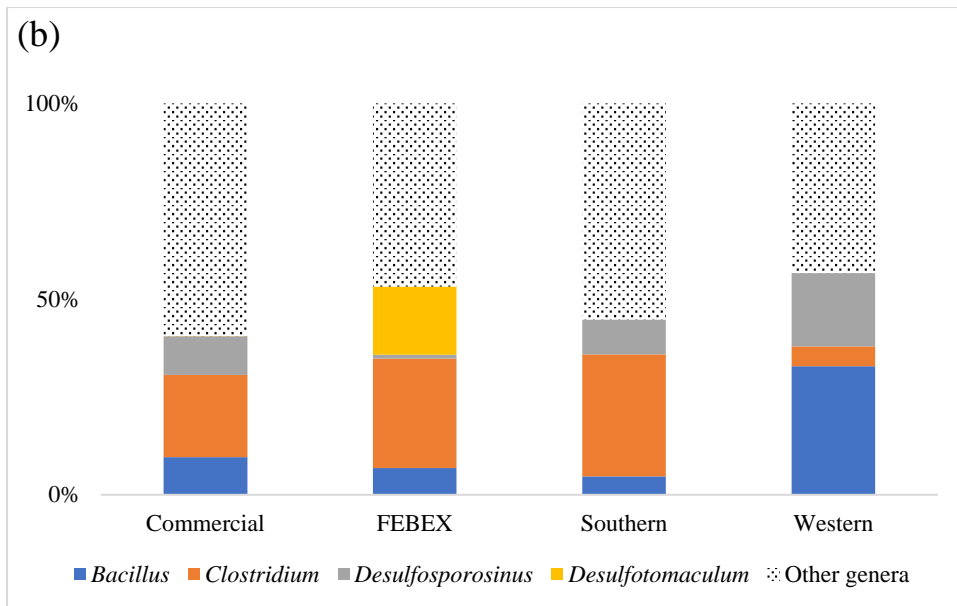
Figure 3.2: Number of IRB cells (MPN g⁻¹) in the fully defined growth medium for the as received bentonite, and for bentonite after exposure to pressure at ~74 MPa (pressure), after heating at 90 °C for 24 hours (temperature), and after a gamma radiation dose of 1000 Gy (irradiation).

3.5.3. Molecular ecology

Following the growth of the microbial communities in the respective media, DNA was extracted from the dilution displaying the strongest reaction (typically the first ten-fold dilution), and the effect of the treatments on the relative makeup of the communities was analyzed (Figure 3.3). Before treatment, enrichment in Postgate B medium produced nine original taxonomic units (OTU's) that were identified as being most closely related to known SRB. Six of the OTU's were closely related to *Desulfosporosinus* species making up approximately 10 % of the FEBEX, commercial, and southern communities, along with 29 % of the western. The other three OTU's were related to *Desulfotomaculum* species, making up 14 % of the FEBEX community. Other key non SRB genera included *Clostridium* species in the FEBEX (25 %), and commercial (18 %) bentonites, as well as *Bacillus* species which were abundant in the FEBEX (11 %), and western (22 %) bentonites. Eight OTU's related to SRB were present following pelletisation, and enrichment in the first MPN dilution into Postgate B medium, with seven being related to *Desulfosporosinus* species, these species were distributed in similar proportions in the commercial, and southern (10 %) samples, while a reduction in relative abundance of these species from 29 % to 19 % was observed in the western bentonite. The FEBEX bentonite harbored minimal *Desulfosporosinus* species after pelletisation, but contained a strain related to a *Desulfotomaculum* species (17 %). *Clostridium* levels increased to >20 % in the FEBEX, commercial, and southern bentonites

after pelletisation and MPN enumeration, and an increase in relative abundance of *Bacillus* species was observed in the western bentonite (33 %). Heating of the bentonites to 90 °C had no discernible impact on the number of OTU's related to SRB after MPN enrichments (compared to non-heated controls), however an increase in species related to *Desulfotomaculum* species was observed in the FEBEX (50 %) substrate, and a reduction in species related to *Desulfosporosinus* in the commercial bentonite (5 %). The proportion of organisms related to the non SRB *Bacillus* genera increased to 30 % in both samples, while *Clostridium* species decreased to below 5 %. After the irradiation treatment, and subsequent MPN enumeration the FEBEX, and commercial bentonites contained similar percentages of bacteria related to sulfate-reducing genera, with the FEBEX containing 27 % *Desulfotomaculum* species, and the commercial 25 % *Desulfosporosinus* species. Small proportions of *Bacillus* species, and *Clostridium* species were also identified in both samples (4-8 %).





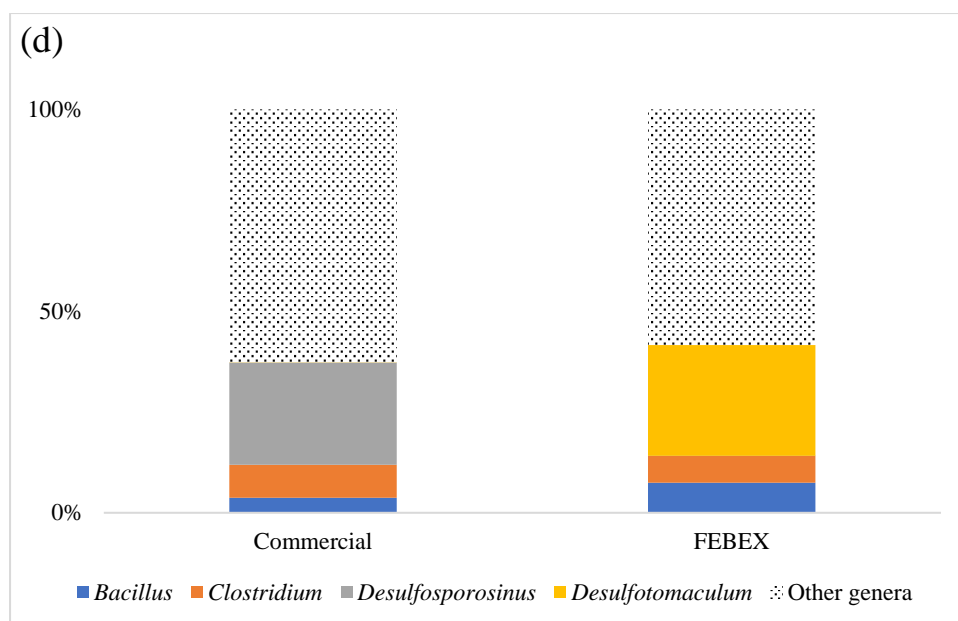
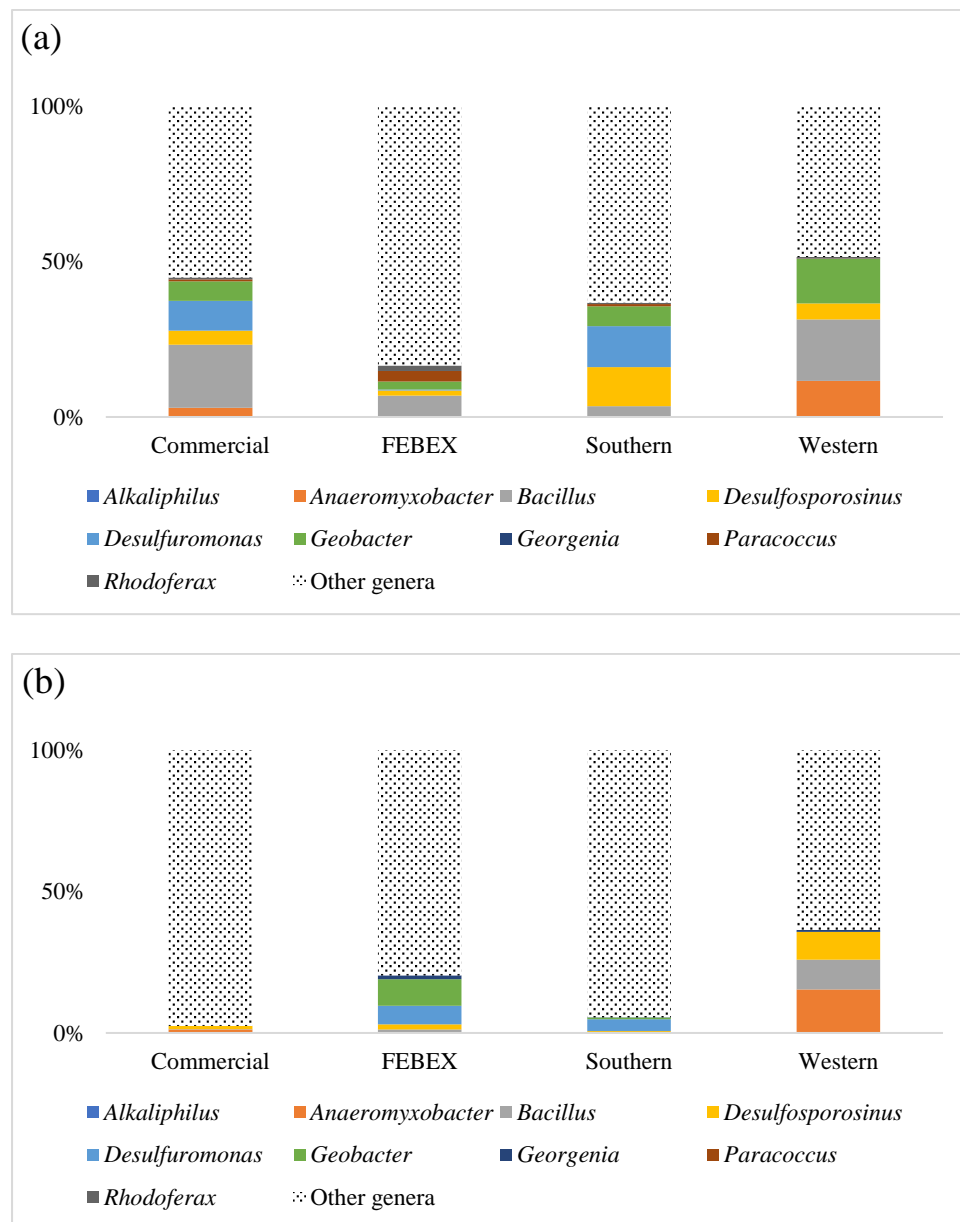


Figure 3.3: Comparison of SRB (*Desulfosporosinus*, *Desulfotomaculum*), and other key bacteria (*Bacillus*, *Clostridium*) contained in the Postgate B MPN enrichments (first dilution in series, scored positive). (A) As received bentonite (As Received). (B) Bentonite after exposure to pressure at ~74 MPa (Pressure). (C) Bentonite after heating at 90 °C for 24 hours (Temperature). (D) Bentonite after exposure to gamma irradiation (1000 Gy) (Irradiation).

A range of bacteria with the potential for Fe(III)-reducing activity were identified in the as received bentonites following enrichment in an Fe(III)-containing medium, with a total of seventeen OTU's related to documented Fe(III)-reducing species. Of these bacteria, organisms related to *Bacillus* species were the most abundant in the FEBEX (7 %), southern (20 %), and western bentonites (20 %), while 26 % of the species present in the southern bentonite were related to *Desulfosporosinus*, and *Desulfuromonas* (Figure 3.4). Species related to *Geobacter* were also identified in all the bentonites accounting for between 3 % and 14 % of the microbial community, along with *Anaeromyxobacter* species in the western bentonite (12 %) (Figure 3.4). Exposure to pressure resulted in a total of eighteen OTU's related to Fe(III)-reducing genera being picked up in the subsequent MPN dilutions, however a significant shift was observed in the community. The commercial, and southern bentonites were deficient in bacteria identified as having the potential to carry out Fe(III)-reduction, with species related to *Anaeromyxobacter* species being the most prevalent in the commercial bentonite (1 %), and *Desulfuromonas* species in the southern bentonite (4 %) (Figure 3.4). The western bentonite contained large proportions of strains related to *Anaeromyxobacter* species (15 %), *Bacillus* species (10 %), and *Desulfosporosinus* species (10 %) after enrichment in the MPN cultures, while the FEBEX bentonite MPNs contained *Geobacter*

species (9 %), and *Desulphuromonas* species (7 %) (Figure 3.4). Nine OTU's with Fe(III)-reducing potential were identified in the bentonites following exposure to heat and enrichment for IRB. Species related to *Desulfosporosinus* (40 %) dominated in MPN dilutions from heated commercial bentonite, while the heated FEBEX enrichments contained a mixture of species related to *Bacillus* (16 %), and *Desulfosporosinus* (18 %) species (Figure 3.4). Irradiation lead to preferential enrichment of four Fe(III)-reducing OTU's. Three of those strains were related to *Bacillus* species and were found in the FEBEX bentonite (73 %), while the other, related to a *Paracoccus* strain, was found in the commercial substrate (15 %) (Figure 3.4).



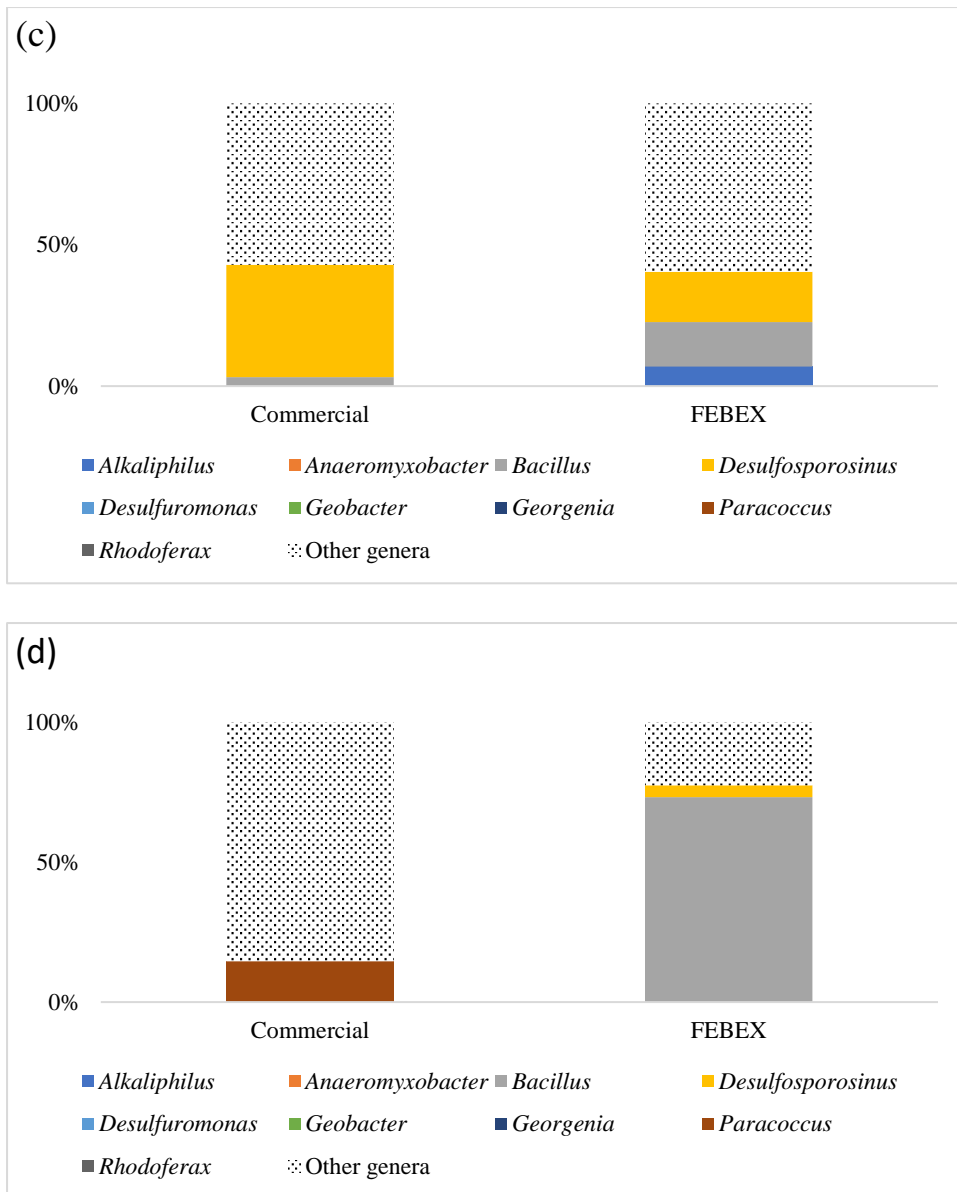


Figure 3.4: Bacteria affiliated with Fe(III)-reducing activity identified in the fully defined growth medium enrichments (dilution which provided the strongest result, typically first MPN dilution). (A) As received bentonite (As Received). (B) Bentonite after exposure to pressure at ~ 74 MPa (Pressure). (C) Bentonite after exposure to heat treatment at 90 °C for 24 hours (Temperature). (D) Bentonite after exposure to gamma irradiation (1000 Gy) (Irradiation).

3.6. Discussion

3.6.1. As received bentonite

While studies have looked at the impact of the various stresses that are imposed in a geological disposal facility for radioactive waste, more work on comparing these stresses, and their impact on microbial diversity and growth responses (especially with respect to IRB) is

required. This study combined the use of a cultivation-dependent technique (MPN) and complementary DNA-based molecular ecology tools, to assess the influence of temperature, pressure, and gamma irradiation on the microbial communities present in bentonites. Microbial characterization using 16S rRNA techniques in this study focused on MPN enrichments performed using selective media so that the viability of IRB and SRB (bacteria shown to have deleterious functions related to geodisposal) could be assessed. DNA recovery from untreated bentonites is low (Direito et al., 2012) so this enrichment culture methodology provided a greater DNA yield, with the added advantage of identifying IRB, and SRB (and the caveat of underestimating other bacteria such as aerobic heterotrophs). The amount of IRB and SRB cells in the bentonites was roughly 1000 cells per gram, which is several orders of magnitude lower than a typical soil bacterial content (Atlas and Bartha, 1998). Despite the bentonite materials being largely comparable in terms of chemistry and mineralogy, significant differences were seen in the water content, as well as the 0.5 M hydrochloric acid extractable Fe(II)/Fe(total) ratio (Table 3.1). Both factors seemed to influence the amount of culturable SRB and IRB present in the as received bentonite. A moderate correlation (R^2 0.77) was observed between the number of SRB identified from MPN counts in the untreated samples (Table 3.2), and the water content of the bentonites (Table 3.1). A key factor in controlling SRB numbers is water activity (Stroes-Gascoyne et al., 2010), so it is likely that when the substrates last supported an active microbial community the number of SRB was dictated by the water content of the substrates; when conditions became uninhabitable affiliates of the Gram-positive *Clostridia* class to which some Gram positive SRB such as *Desulfosporosinus* are affiliated would have formed spores (Xiao et al., 2011), and subsequently germinated in the Postgate B medium. Gram-positive bacteria affiliated with members of the *Clostridium* genus, also belonging to the Class *Clostridia*, can carry out fermentation to generate electron donors (but not sulfate reduction). *Clostridium* species were abundant in some of the bentonites following enrichment in Postgate B (Figure 3.3), with a moderate correlation (R^2 0.64) between their abundance, and the number of SRB (Table 3.2), suggesting that they were able to ferment some of the constituents of Postgate B medium, potentially providing alternative electron donors for the SRB. Gram-positive and Gram-negative bacteria, including those affiliated with *Desulfosporosinus* and *Geobacter* species respectively, dominated in the IRB MPN enrichments (Figure 3.4), and were therefore implicated in playing a role in Fe(III) reduction in these systems. A modest correlation was observed between the MPN counts in the Fe(III)-reducing samples (Table 3.2), and the raw bentonites with the highest 0.5 M HCl extractable Fe(II)/Fe(total) ratio (Table 3.1) (R^2 0.73).

This ratio is often used as a rough approximation for bioavailable iron in soil samples, however some silicates have been shown to have significantly more bioavailable iron (Brookshaw et al., 2014). It is likely that the bentonites with the greatest 0.5 M hydrochloric extractable Fe(II)/Fe(total) ratio promoted an environment more suitable for a microbial community enriched with Fe(III)-reducing bacteria. The variability in microbial communities observed in the bentonites is likely to have been influenced by the history, and chemistry of unsterile infiltrating waters.

3.6.2. Bentonite exposed to pressure

The influence of pressure was investigated by applying a load to the bentonite, and then using the bentonite to inoculate MPN enrichments to assess the impact of pressure on the number of culturable bacteria (and the diversity by subsequent DNA sequencing). SRB numbers decreased across all samples (Figure 3.1) with the most significant decrease observed in the Commercial bentonite (Supplementary 3.1). Decreases in the proportion of *Desulfosporosinus* cells detected in each sample highlighted the decrease in SRB (Figure 3.3). The Southern bentonite saw the least significant reduction in SRB (Supplementary 1), which coincided with an increase in *Clostridium* species (Figure 3.3). The pelletized FEBEX Postgate B enrichment contained a similar amount of *Desulfotomaculum* species to the as received FEBEX Postgate B enrichment (Figure 3.3) and had the highest MPN cell count after exposure to pressure (Figure 3.1). This suggests that *Desulfotomaculum* species were more resistant to pressure. *Desulfotomaculum*, and *Desulfosporosinus* have been identified in high pressure environments (Itavaara et al., 2011), but no previous studies have investigated SRB activity in bentonite exposed to the pressures in this study. All the SRB MPN enrichment communities maintained many potentially fermentative, and electron donor-producing *Clostridium*, apart from the western bentonite (Figure 3.3), which may explain why it produced the lowest MPN cell count (Figure 3.1). The extra stresses induced by pressure did not appear to restrict the proliferation of Gram-negative IRB in the Fe(III)-reducing MPN cultures, and the reduction in viable IRB cells was largely insignificant (Supplementary 3.1). The FEBEX, which was enriched in close relatives to Gram-negative *Geobacter* species (Figure 3.4), had the fewest IRB cells (by MPN counting) (Figure 3.2). The western bentonite had one of the highest IRB MPN cell counts (Figure 3.2), and the corresponding MPN IRB cultures were enriched in Gram-positive *Bacillus*, and *Desulfosporosinus*, along with some Gram-negative *Anaeromyxobacter* (Figure 3.4), which

have all been implicated in Fe(III) reduction. The commercial, and southern communities in the MPN enrichments contained fewer than 5 % known IRB (Figure 3.4), which suggests that the Fe(III)-reduction may have been carried out by organisms that have not been identified previously as IRB.

3.6.3. Bentonite exposed to heat

Following a heat treatment of 90 °C for 24 hours, the numbers of viable SRB and IRB were assessed by adding them to selective media, with further 16S rRNA sequencing focused on the commercial, and FEBEX bentonite MPNs. Decreases in SRB cell numbers were observed in all samples after heat treatment, except for the southern bentonite (Figure 3.1). A statistically insignificant reduction (Supplementary 3.1) in the SRB MPN counts in the commercial sample (Figure 3.1) coincided with a decrease in the percentage of *Desulfosporosinus* species detected in the subsequent MPN series (Figure 3.3). The FEBEX Postgate B enrichment was dominated by close relatives of a known *Desulfotomaculum* species (Figure 3.3) but saw a ten-fold reduction in MPN SRB counts (Figure 3.1), again suggesting a significant impact on cell viability, but the survival of a sub population of these SRB. Reductions in both SRB counts (Figure 3.1) also coincided with an enrichment in *Bacillus* species (Figure 3.3). *Bacillus* species are not known to respire sulfate; thus, growth of these Gram-positive spore formers could have been detrimental to SRB yields, competing for other growth substrates. This proliferation of *Bacillus* species was not apparent in the as received enrichments, and it is therefore likely that heat activation lead to a growth response by the *Bacillus* sp. stimulated by “germination nutrients” (Yi and Setlow, 2010). Heat activation of *Bacillus* sp., implicated in Fe(III) reduction (Kanso et al., 2002) coincides with a slight increase in IRB numbers in the FEBEX after heating, but this is likely not significant given the 46 % overlap in confidence intervals (Supplementary 3.1).

3.6.4. Bentonite exposed to gamma radiation

The bentonites used in this study were subjected to a gamma dose of 1 kGy, at a dose rate of 24 Gy min⁻¹, before placement in medium to determine the impact on SRB and IRB. Changes in the bacterial communities were investigated with 16S rRNA sequencing on the commercial, and FEBEX bentonite MPNs. Significant reductions in SRB MPN counts were observed in the commercial, and western bentonites (Supplementary 3.1), with the FEBEX

maintaining a reasonable number (1900 g^{-1}) (Figure 1). Both substrates had similar proportions of SRB in their communities (from analyses of positive MPN enrichments) (Figure 3.3), however the FEBEX MPN enrichments contained close relatives to *Desulfotomaculum* as opposed to *Desulfosporosinus* species found in the commercial enrichments (Figure 3.3). The closest relative of the *Desulfotomaculum* species detected in the FEBEX was *D. halophilum*, an endospore-forming, Gram-positive halophile that can tolerate NaCl concentrations of up to 14 % (Tardy-Jacquenod et al., 1998). The physiological response caused by oxidative stress is the same as that for desiccation and gamma radiation (Daly, 2009), which may explain why the FEBEX community displayed more resistance to gamma irradiation than the commercial bentonite. The SRB communities maintained a high diversity following irradiation with Shannon indexes around 3.6, compared to 4.1 in the as received bentonites. The Shannon indexes in the IRB communities on the other hand were greatly diminished decreasing from 4.26 in the commercial bentonite, and 6.15 in the FEBEX bentonite to less than 2 in both substrates after irradiation. Analysis of the IRB MPN cultures from the FEBEX samples identified Gram-positive *Bacillus* and *Desulfosporosinus* species, accounting for 77 % of the total community (Figure 3.4). However, the IRB MPN count remained low (98 g^{-1}) (Figure 3.2), suggesting that the IRB were ineffective at Fe(III)-reduction. The commercial bentonite maintained a larger loading of IRB (1020 g^{-1}) (Figure 3.2), and was dominated by a close relative of the Fe(III)-reducing, Gram-negative *Paracoccus denitrificans* (Mazoch et al., 2004), a bacterium belonging to a genera known to have desiccation tolerant species (Yu et al., 2015). The SRB communities are likely to have maintained their diversity due to the large number of Gram-positive spore-formers able to reduce sulfate. The lack of diversity in the irradiated Fe(III)-reducing communities suggests that typical IRB are less tolerant to oxidative stress, with the Fe(III)-reduction completed by the few radiation resistant organisms.

3.7. Conclusions

Bentonite chemistry influenced microbial presence, with correlations observed between SRB numbers and the initial water content, as well as correlations between the 0.5 M hydrochloric acid extractable Fe(II)/Fe(total) ratio and the number of IRB. There was also a distinction between the SRB communities in the different bentonites, with molecular analyses of MPN enrichments suggesting that *Desulfosporosinus* species were present as the dominant SRB in the commercial, southern, and western bentonites, while *Desulfotomaculum* species were the

dominant SRB in the FEBEX bentonite. This trend was particularly significant after exposure to stress, with *Desulfotomaculum* becoming enriched compared to *Desulfosporosinus* after pressure and irradiation but showing diminished viability after heat treatment. Such variabilities in SRB communities, as a function of both bentonite chemistry and response to pressure-, heat- and radiation-induced stress, may be an important consideration in the selection of the bentonite buffer used in a GDF for radioactive waste disposal, as SRB activity can promote corrosion of waste canisters (El Mendili et al., 2013). Fe(III)-reduction was most likely carried out in positive MPN cultures by a mixture of Gram-negative, and Gram-positive organisms cultured from the as received bentonite, however Gram-positive organisms (which generally have thicker cell walls and can form spores to aid long-term survival in harsh environments) were dominant after the bentonite was exposed to pressure and heat. The relative abundance of Gram-positive *Bacillus* and *Desulfosporosinus* species in MPN enrichments was significantly increased in response to these stresses, with *Bacillus* species present both under sulfate-reducing and Fe(III)-reducing conditions. The diversity of organisms catalyzing Fe(III)-reduction (and the underlying physiological mechanisms) is less well understood, compared to those involved in sulfate-reduction, and it is therefore more challenging to identify the organisms responsible for this process in the IRB MPNs in both the commercial and the southern bentonite after exposure to pressure. The broad range of IRB identified in this study provoke the question of whether pure culture Fe(III)-reduction studies using well studied model organisms such as *Geobacter*, and *Shewanella* species are appropriate in the context of engineered systems, including nuclear disposal barrier systems. Clearly a broader range of Fe(III)-reducing communities that can survive under GDF-relevant conditions, require attention, as they are more likely to survive and function despite challenges from the pressure, heat and radiation in such environments.

Overall, stress induced by pressure, heat and radiation did not completely inhibit microbial activity, but a reduction in cell numbers was seen in most cases, with increases observed in some bentonite, and treatment combinations. Microbes will be present in a bentonite barrier, so further research into their behavior in specific cases defined by waste repository implementers is crucial. Stress induced by the combination of high pressure, heat and radiation in a GDF will most likely inhibit microbial colonization, and the subsequent swelling pressure, induced by groundwater infiltration into the GDF, might play a further defining role in minimizing microbial activity. Although microbial colonization of bentonite barriers may help attenuate the release of priority radionuclides (Newsome et al., 2014a),

control of iron and sulfate-reducing bacterial activities will be important to maximize the physical integrity of the bentonite barrier and to prevent corrosion of the metal canisters. Thus, the careful selection of bentonite materials (e.g. with low microbial inocula) and achievement of appropriate swelling pressures (to control microbial proliferation (Pedersen, 2010) is crucial to bentonite buffer, and canister stability.

3.8. Acknowledgements

Funding for this work was provided by Radioactive Waste Management (RWM.). We thank Paul Lythgoe, and Alastair Bewsher for XRF, LOI, IC, and ICP-AES analysis, John Waters for the XRD, and BET work, Adam Sims for help sealing the irradiation vials, and Ruth Edge for carrying out the Fricke dosimetry, and irradiating the samples. JRL acknowledges the support of the European Commission Horizon 2020 MIND (Microbiology in Nuclear waste Disposal) project, which has received funding from the Euratom research and training programme 2014-2018 under Grant Agreement no. 861880, and funding from NERC (BIGRAD consortium, grant number NE/H007768/1L) and the Royal Society. CIP was supported by the Interfacial Geochemistry Group at Pacific Northwest National Laboratory.

3.9. References

- Andrews, N., 2016. FastQC: A quality control tool for high throughput sequence data (Version 0.11.3) [Software]. Available at [https://bioinformatics.babraham.ac.uk/projects/fastqc/ \(08/12/18\)](https://bioinformatics.babraham.ac.uk/projects/fastqc/ (08/12/18)).
- Atlas, R.M., Bartha, R., 1998. Microbial ecology: fundamentals and applications. Benjamin/Cummings, Menlo Park, California.
- Baldwin, T., Chapman, N., Neall, F., 2008. Geological disposal options for high-level waste and spent fuel, Radioactive Waste Management, Didcot.
- Bartlett, D.H., 2002. Pressure effects on *in-vivo* microbial processes. *Biochimica Et Biophysica Acta-Protein Structure and Molecular Enzymology*, 1595(1-2): 367-381.
- Bengtsson, A., Edlund, J., Hallbeck, B., Heed, C., Pedersen, K., 2015. Microbial sulphide-producing activity in MX-80 bentonite at 1750 and 2000 kg m⁻³ wet density. R-15-05, SKB, Stockholm.
- Brookshaw, D.R., Lloyd, J.R., Vaughan, D.J., Patrick, R.A.D., 2014. Bioreduction of biotite and chlorite by a *Shewanella* species. *American Mineralogist*, 99(8-9): 1746-1754.
- Caporaso, J.G., Kuczynski, J., Stombaugh, J., Bittinger, K., Bushman, F.D., Costello, E.K., Fierer, N., Pena, A.G., Goodrich, J.K., Gordon, J.I., Huttley, G.A., Kelley, S.T., Knights, D., Koenig, J.E., Ley, R.E., Lozupone, C.A., McDonald, D., Mugge, B.D., Pirrung, M., Reeder, J., Sevinsky, J.R., Tumbaugh, P.J., Walters, W.A., Widmann, J., Yatsuenko, T., Zaneveld, J., Knight, R., 2010. QIIME allows analysis of high-throughput community sequencing data. *Nature Methods*, 7(5): 335-336.
- Caporaso, J.G., Lauber, C.L., Walters, W.A., Berg-Lyons, D., Lozupone, C.A., Turnbaugh, P.J., Fierer, N., Knight, R., 2011. Global patterns of 16S rRNA diversity at a depth of millions of sequences per sample. *Proceedings of the National Academy of Sciences of the United States of America*, 108: 4516-4522.
- Chapman, H.D., 1965. Cation exchange capacity. *Methods of soil analysis part 2*, 9. American Institute of Agronomy, Madison, Wisconsin.

- Cockell, C.S., Nixon, S., 2013. The boundaries of life. In: Smith, I.W.M., Cockell, C.S., Leach, S. (Eds.), *Astrochemistry and Astrobiology*. Springer-Verlag, Berlin, pp. 211-241.
- Collins, C.H., Lyne, P.M., 2004. *Collins and Lyne's microbiological methods*, Arnold, London.
- Crowe, L.M., Crowe, J.H., 1992. Anhydrobiosis - A strategy for survival. *life sciences and space research xxiv (3) : planetary biology and origins of life. Advances in Space Research*, 12: 239-247.
- Daly, M.J., 2009. Opinion a new perspective on radiation resistance based on *Deinococcus radiodurans*. *Nature Reviews Microbiology*, 7(3): 237-245.
- Daly, M.J., Gaidamakova, E.K., Matrosova, V.Y., Vasilenko, A., Zhai, M., Leapman, R.D., Lai, B., Ravel, B., Li, S.M.W., Kemner, K.M., Fredrickson, J.K., 2007. Protein oxidation implicated as the primary determinant of bacterial radioresistance. *PLoS Biology*, 5(4): 769-779.
- Daniel, R.M., Cowan, D.A., 2000. Biomolecular stability and life at high temperatures. *Cellular and Molecular Life Sciences*, 57(2): 250-264.
- de Man, J.C., 1983. MPN tables, corrected. *European Journal of Applied Microbiology and Biotechnology*, 17(5): 301-305.
- Direito, S.O.L., Marees, A., Roling, W.F.M., 2012. Sensitive life detection strategies for low-biomass environments: optimizing extraction of nucleic acids adsorbing to terrestrial and Mars analogue minerals. *FEMS Microbiology Ecology*, 81(1): 111-123.
- Dong, H.L., 2012. Clay-microbe interactions and implications for environmental mitigation. *Elements*, 8(2): 113-118.
- Edgar, R.C., 2010. Search and clustering orders of magnitude faster than BLAST. *Bioinformatics*, 26(19): 2460-2461.
- Edgar, R.C., 2013. UPARSE: highly accurate OTU sequences from microbial amplicon reads. *Nature Methods*, 10(10): 996-998.
- El Mendili, Y., Abdelouas, A., Bardeau, J.F., 2013. Insight into the mechanism of carbon steel corrosion under aerobic and anaerobic conditions. *Physical Chemistry Chemical Physics*, 15(23): 9197-9204.
- Fricke, H., Hart, E., J., 1935. The oxidation of Fe(II) to Fe(III) by the irradiation with X-rays of solutions of ferrous sulfate in sulfuric acid. *The Journal of Chemical Physics*, 3(1): 60-61.
- Haas, B.J., Gevers, D., Earl, A.M., Feldgarden, M., Ward, D.V., Giannoukos, G., Ciulla, D., Tabbaa, D., Highlander, S.K., Sodergren, E., Methe, B., Desantis, T.Z., Petrosino, J.F., Knight, R., Birren, B.W., 2011. Chimeric 16S rRNA sequence formation and detection in Sanger and 454-pyrosequenced PCR amplicons. *Genome Research*, 21(3): 494-504.
- Hansen, M.T., 1978. Multiplicity of genome equivalents in radiation-resistant bacterium *Micrococcus radiodurans*. *Journal of Bacteriology*, 134(1): 71-75.
- Hicks, T.W., White, M.J., Hooker, P.J., 2009. Role of bentonite in determination of thermal limits on geological disposal facility design. 0883-1, Nuclear Decommissioning Authority-Radioactive Waste Management, Cumbria.
- Itavaara, M., Nyyssonen, M., Kapanen, A., Nousiainen, A., Ahonen, L., Kukkonen, I., 2011. Characterization of bacterial diversity to a depth of 1500 m in the Outokumpu deep borehole, Fennoscandian Shield. *FEMS Microbiology Ecology*, 77(2): 295-309.
- Joshi, N.A., Fass, J.N., 2011. Sickle: A sliding-window, adaptive, quality-based trimming tool for FastQ files (Version 1.33) [Software]. Available at <https://github.com/najoshi/sickle> (08/12/18).

- Kanso, S., Greene, A.C., Patel, B.K.C., 2002. *Bacillus subterraneus* sp nov., an iron- and manganese-reducing bacterium from a deep subsurface Australian thermal aquifer. *International Journal of Systematic and Evolutionary Microbiology*, 52: 869-874.
- Kashefi, K., Lovley, D.R., 2003. Extending the upper temperature limit for life. *Science*, 301(5635): 934-934.
- Kato, C., Li, L., Nogi, Y., Nakamura, Y., Tamaoka, J., Horikoshi, K., 1998. Extremely barophilic bacteria isolated from the Mariana Trench, Challenger Deep, at a depth of 11,000 meters. *Applied and Environmental Microbiology*, 64(4): 1510-1513.
- Kim, J., Dong, H.L., Seabaugh, J., Newell, S.W., Eberl, D.D., 2004. Role of microbes in the smectite-to-illite reaction. *Science*, 303(5659): 830-832.
- Kozich, J.J., Westcott, S.L., Baxter, N.T., Highlander, S.K., Schloss, P.D., 2013. Development of a dual-index sequencing strategy and curation pipeline for analyzing amplicon sequence data on the MiSeq Illumina sequencing platform. *Applied and Environmental Microbiology*, 79(17): 5112-5120.
- Lanyon, G.W., Gaus, I., 2016. Main outcomes and review of the FEBEX in-situ test (GTS) and mock-up after 15 years of operation. 15-04, National Cooperative for the Disposal of Radioactive Waste, Wettingen.
- Liu, D., Dong, H., Bishop, M.E., Zhang, J., Wang, H., Xie, S., Wang, S., Huang, L., Eberl, D.D., 2012. Microbial reduction of structural iron in interstratified illite-smectite minerals by a sulfate-reducing bacterium. *Geobiology*, 10(2): 150-162.
- Lopez-Fernandez, M., Cherkouk, A., Vilchez-Vargas, R., Jauregui, R., Pieper, D., Boon, N., Sanchez-Castro, I., Merroun, M.L., 2015. Bacterial diversity in bentonites, engineered barrier for deep geological disposal of radioactive wastes. *Microbial Ecology*, 70(4): 922-935.
- Lopez-Fernandez, M., Cherkouk, A., Vilchez-Vargas, R., Jauregui, R., Pieper, D., Boon, N., Sanchez-Castro, I., Merroun, M.L., 2018. Investigation of viable taxa in the deep terrestrial biosphere suggests high rates of nutrient recycling. *FEMS Microbiology Ecology*, 94(8).
- Lovley, D.R., Fraga, J.L., Blunt-Harris, E.L., Hayes, L.A., Phillips, E.J.P., Coates, J.D., 1998. Humic substances as a mediator for microbially catalyzed metal reduction. *Acta Hydrochimica et Hydrobiologica*, 26(3): 152-157.
- Lovley, D.R., Phillips, E.J.P., 1986. Organic-matter mineralization with reduction of ferric iron in anaerobic sediments. *Applied and Environmental Microbiology*, 51(4): 683-689.
- Lovley, D.R., Phillips, E.J.P., 1987. Rapid assay for microbially reducible ferric iron in aquatic sediments. *Applied and Environmental Microbiology*, 53(7): 1536-1540.
- Martin, M., 2011. Cutadapt removes adapter sequences from high-throughput sequencing reads. *EMBnet Journal*, 17(1): 3.
- Masella, A.P., Bartram, A.K., Truszkowski, J.M., Brown, D.G., Neufeld, J.D., 2012. PANDAseq: PAired-eND Assembler for Illumina sequences. *BMC Bioinformatics*, 13.
- Masurat, P., Eriksson, S., Pedersen, K., 2010a. Evidence of indigenous sulphate-reducing bacteria in commercial Wyoming bentonite MX-80. *Applied Clay Science*, 47(1-2): 51-57.
- Masurat, P., Eriksson, S., Pedersen, K., 2010b. Microbial sulphide production in compacted Wyoming bentonite MX-80 under *in-situ* conditions relevant to a repository for high-level radioactive waste. *Applied Clay Science*, 47(1-2): 58-64.
- Mazoch, J., Tesarik, R., Sedlacek, V., Kucera, I., Turanek, J., 2004. Isolation and biochemical characterization of two soluble iron(III) reductases from *Paracoccus denitrificans*. *European Journal of Biochemistry*, 271(3): 553-562.

- Minton, K.W., 1994. DNA-repair in the extremely radioresistant bacterium *Deinococcus radiodurans*. *Molecular Microbiology*, 13(1): 9-15.
- Morozkina, E.V., Slutsкая, E.S., Fedorova, T.V., Tugay, T.I., Golubeva, L.I., Koroleva, O.V., 2010. Extremophilic microorganisms: biochemical adaptation and biotechnological application (review). *Applied Biochemistry and Microbiology*, 46(1): 1-14.
- Mulligan, C.N., Yong, R.N., Fukue, M., 2009. Some effects of microbial activity on the evolution of clay-based buffer properties in underground repositories. *Applied Clay Science*, 42(3-4): 331-335.
- Newsome, L., Morris, K., Lloyd, J.R., 2014. The biogeochemistry and bioremediation of uranium and other priority radionuclides. *Chemical Geology*, 363: 164-184.
- Nurk, S., Bankevich, A., Antipov, D., Gurevich, A.A., Korobeynikov, A., Lapidus, A., Prjibelski, A.D., Pyshkin, A., Sirotkin, A., Sirotkin, Y., Stepanauskas, R., Clingenpeel, S.R., Woyke, T., McLean, J.S., Lasken, R., Tesler, G., Alekseyev, M.A., Pevzner, P.A., 2013. Assembling single-cell genomes and mini-metagenomes from chimeric MDA products. *Journal of Computational Biology*, 20(10): 714-737.
- Paredes-Sabja, D., Setlow, P., Sarker, M.R., 2011. Germination of spores of Bacillales and Clostridiales species: mechanisms and proteins involved. *Trends in Microbiology*, 19(2): 85-94.
- Park, Y., Shin, W.S., Choi, S.J., 2012. Sorptive removal of cobalt, strontium and cesium onto manganese and iron oxide-coated montmorillonite from groundwater. *Journal of Radioanalytical and Nuclear Chemistry*, 292(2): 837-852.
- Pedersen, K., 2010. Analysis of copper corrosion in compacted bentonite clay as a function of clay density and growth conditions for sulfate-reducing bacteria. *Journal of Applied Microbiology*, 108(3): 1094-1104.
- Perdrial, J.N., Warr, L.N., Perdrial, N., Lett, M.C., Elsass, F., 2009. Interaction between smectite and bacteria: implications for bentonite as backfill material in the disposal of nuclear waste. *Chemical Geology*, 264(1-4): 281-294.
- Postgate, J.R., 1979. *The sulphate-reducing bacteria*, Cambridge University Press, Cambridge.
- Potts, M., 1994. Desiccation tolerance of prokaryotes. *Microbiological Reviews*, 58(4): 755-805.
- Rizoulis, A., Milodowski, A.E., Morris, K., Lloyd, J.R., 2016. Bacterial diversity in the hyperalkaline Allas Springs (Cyprus), a natural analogue for cementitious radioactive waste repository. *Geomicrobiology Journal*, 33(2): 73-84.
- Sellin, P., Leupin, O.X., 2013. The use of clay as an engineered barrier in radioactive-waste management - a review. *Clays and Clay Minerals*, 61(6): 477-498.
- Stookey, L.L., 1970. Ferrozine - a new spectrophotometric reagent for iron. *Analytical Chemistry*, 42: 779-781.
- Stroes-Gascoyne, S., Hamon, C.J., Maak, P., Russell, S., 2010. The effects of the physical properties of highly compacted smectitic clay (bentonite) on the culturability of indigenous microorganisms. *Applied Clay Science*, 47(1-2): 155-162.
- Tardy-Jacquenod, C., Magot, M., Patel, B.K.C., Matheron, R., Caumette, P., 1998. *Desulfotomaculum halophilum* sp. nov., a halophilic sulfate-reducing bacterium isolated from oil production facilities. *International Journal of Systematic Bacteriology*, 48: 333-338.
- Wang, Q., Garrity, G.M., Tiedje, J.M., Cole, J.R., 2007. Naïve bayesian classifier for rapid assignment of rRNA sequences into the new bacterial taxonomy. *Applied and Environmental Microbiology*, 73(16): 5261-5267.

- Weber, W.J., Ewing, R.C., Catlow, C.R.A., de la Rubia, T.D., Hobbs, L.W., Kinoshita, C., Matzke, H., Motta, A.T., Nastasi, M., Salje, E.K.H., Vance, E.R., Zinkle, S.J., 1998. Radiation effects in crystalline ceramics for the immobilization of high-level nuclear waste and plutonium. *Journal of Materials Research*, 13(6): 1434-1484.
- Wilson, J., Savage, D., Bond, A., Watson, S., Pusch, R., Bennett, D., 2011. Bentonite: A review of key properties, processes and issues for consideration in the UK context, NDA, Harwell.
- Xiao, Y.H., Francke, C., Abee, T., Wells-Bennik, M.H., 2011. Clostridial spore germination versus bacilli: genome mining and current insights. *Food Microbiology*, 28(2): 266-274.
- Yi, X.A., Setlow, P., 2010. Studies of the commitment step in the germination of spores of *Bacillus* species. *Journal of Bacteriology*, 192(13): 3424-3433.
- Yu, L.Z.H., Luo, X.S., Liu, M., Huang, Q.Y., 2015. Diversity of ionizing radiation-resitant bacteria obtained from the Taklimakan Desert. *Journal of Basic Microbiology*, 55(1): 135-140.

3.10. Supplementary

Supplementary 3.1: Full summary of the MPN results for SRB, and IRB including 95 % confidence interval limits, and the overlap of confidence intervals between the as received bentonites, and the treatments (CI, confidence interval; LL, lower limit; UL, upper limit).

Substrate and Treatment	SRB				IRB			
	MPN/g	95 % CI LL	95 % CI UL	95 % CI Overlap (%)	MPN/g	95 % CI LL	95 % CI UL	95 % CI Overlap (%)
Commercial								
As Received	6600	1840	24000	-	1880	460	7600	-
Pressure	940	260	3200	22	1880	460	7600	100
Temperature	4000	1020	16400	79	1020	300	3600	83
Irradiation	500	136	1900	1	1020	300	3600	83
FEDEX								
As Received	4000	1020	16400	-	400	104	1620	-
Pressure	1880	460	7600	72	176	48	660	71
Temperature	400	104	1620	17	1880	460	7600	46
Irradiation	1880	460	7600	72	94	28	320	46
Southern								
As Received	1880	460	7600	-	660	184	2400	-
Pressure	1700	440	6600	98	1700	440	6600	66
Temperature	4000	1020	16400	72	1020	300	3600	81
Irradiation	1880	460	7600	100	140	40	500	40
Western								
As Received	660	184	2400	-	4000	1020	16400	-
Pressure	196	52	760	53	1700	440	6600	69
Temperature	196	52	760	53	400	104	1620	17
Irradiation	44	11	180	0	196	52	760	0

4. The Molecular Ecology of the FEBEX *in-situ* Project Along the Temperature/Evolving Resaturation Gradient

Haydn M. Haynes^a, Carolyn I. Pearce^b, Chris Boothman^a, Jonathan R. Lloyd^a

^a *Williamson Research Centre for Molecular Environmental Science and Research Centre for Radwaste Disposal, School of Earth, Atmospheric and Environmental Sciences, University of Manchester, Manchester, M13 9PL, UK*

^b *Geosciences Group, Pacific Northwest Laboratory, 902 Battelle Boulevard, Richland, WA, 99354, US*

Keywords:

FEBEX, bentonite, molecular ecology

4.1. Preface

Question: Using samples from the FEBEX *in-situ* test can we identify microbial communities in a bentonite buffer, and infer the effects of temperature, and evolving resaturation on the microbial communities?

One of the key aims of the original PhD proposal was to assess the microbial communities present in bentonite cores from the FEBEX *in-situ* test (Lanyon and Gaus, 2016).

Investigating samples from a field-scale experiment gave us a unique opportunity to observe the effect of real-world conditions (minus gamma radiation) on bentonite microbial communities. Having obtained bentonite cores from the underground laboratory *in situ* test, arranged along a temperature gradient (55 °C – 92 °C), we attempted to identify differences in the microbial communities relative to temperature/evolving resaturation. Similar to the work carried out in chapter 3 we started off by conducting MPN counts on the samples in an attempt to quantify the number of Fe(III)- and sulphate-reducing bacteria present at the temperatures encountered in the FEBEX *in-situ* test. Unfortunately, the MPN counts were unsuccessful, and therefore alternative methods for assessing the samples were sought.

Using a modified DNA extraction method (Direito et al., 2012), we were successfully able to extract DNA from the bentonite cores for DNA sequencing. An increase in the DNA yield with decreasing temperature suggested that viable bacteria were present at some point before, or during the 20-year *in situ* project at lower temperatures, but we were unable to establish when colonization occurred, due to a lack of time-points (samples were only available when the project was dismantled). Analysis of the microbial communities present in the bentonite

cores showed that several subsurface processes could have taken place, although growth temperatures for the identified bacteria ($-2\text{ }^{\circ}\text{C} - 55\text{ }^{\circ}\text{C}$) were lower than the predicted bentonite core temperatures ($55\text{ }^{\circ}\text{C} - 92\text{ }^{\circ}\text{C}$). This suggests that microbial growth, and viability in the near vicinity ($<0.55\text{ m}$) of a nuclear waste container would be inhibited by the elevated temperatures. This chapter of work could only partially answer the question posed. While we were able to identify bacteria and show increased DNA yields at lower temperatures it is unclear how reproducible these results are, and how much the microbial communities could be potentially influenced by local groundwater conditions (Pedersen et al., 2000). Microbial studies can be incorporated into existing long-term, and field-scale geological disposal tests, but input from the scientific community at the start of tests may be beneficial in producing more meaningful results.

4.2. Abstract

Nuclear waste is produced in many locations internationally during nuclear power generation and weapons manufacture, as well as by research and healthcare. Such wastes can present a high risk to human health, and the environment, and therefore a robust disposal solution is required. One solution favored by numerous countries is a geological disposal facility (GDF) where High Heat Generating Wastes (HHGW) are sealed in a metal canister, with a bentonite buffer filling the gap between the canister, and the host rock. Bentonite materials are known to contain microbial communities, that may persist through buffer fabrication processes, and while they have received much attention in lab-scale studies, little research has focused on field-scale studies. The FEBEX *in-situ* experiment was originally designed to test the feasibility of building a HHGW disposal gallery, consisting of a $100\text{ }^{\circ}\text{C}$ heater surrounded by a bentonite buffer. Samples were extracted from the gallery after 20 years and analyzed for viable microorganisms, and DNA to assess microbial colonization in relation to temperature, and evolving resaturation of the bentonite buffer. Most probable number (MPN) counts on the bentonite samples failed to yield a positive result, however DNA extraction from the cores was successful. DNA extractions from samples furthest away from the heater yielded the largest amount of DNA, with microorganisms responsible for terminal electron accepting processes from nitrate-reduction down to sulfate-reduction, along with fermentation, and sulfide production identified. The results presented here suggest microbial growth may potentially occur under geological disposal conditions, although levels of activity appear to be minimal. This study highlights the information that can be discerned from such field-scale

experiments, and that microbiological programs incorporated into experiments provide valuable information for the geological disposal knowledge base.

4.3. Introduction

The production of radioactive wastes via activities associated with the nuclear fuel cycle, and the manufacture of nuclear weapons has been occurring in many countries for the past eight decades. Radioactive wastes come in many forms with the most hazardous being high level waste (HLW) which in the United Kingdom accounts for 0.03 % of the total volume, and 95.4 % of the total radioactivity (NDA, 2016). HLW requires a highly engineered solution, able to withstand the radioactivity, and associated high temperatures, one such solution favored internationally by waste disposal agencies is the construction of a geological disposal facility (GDF). A GDF is a multi-barrier approach made up of the host rock, a buffer material, a metal overpack, and container, as well as the waste form itself (RWM, 2016a). A favored buffer material in many GDF concepts is bentonite. Among bentonite's advantageous properties as a buffer include its ability to swell in the presence of water minimizing permeability and pore sizes, the presence of surface sites which radionuclides can adsorb to, as well as being able to condition the near-field pH (Wilson et al., 2011).

The Full-Scale Engineered Barriers Experiment (FEBEX) was designed by Empresa Nacional de Residuos Radiactivos (ENRESA) to test the feasibility of constructing a HLW repository in crystalline rock, and to model the near-field conditions. The experiment consisted of a mock gallery constructed in Madrid (Spain), as well as an *in-situ* gallery constructed in Grimsel (Switzerland), along with complementary lab-based studies (Fuentes-Cantillana and Garcia-Sineriz, 1998). Construction of the *in-situ* gallery began in 1995 with the drilling of a 70.39 x 2.28 m tunnel into a granitic mass (Figure 4.1). The bentonite buffer in the *in-situ* gallery consisted of 5331 compacted blocks weighing between 20 to 25 kg each, with an average dry density once emplaced of 1.60 g cm⁻³ (Huertas et al., 2000). A series of mechanical processes were applied to the bentonite to produce a uniform granular material that was finally compacted to produce the blocks (Huertas et al., 2000). Emplaced in these blocks were two carbon steel dummy containers taking up 17.39 m (Figure 4.1). The gallery was sealed with a concrete plug (Figure 4.1). Operation of the *in-situ* gallery commenced in 1997, with the activation of heaters in the dummy containers producing a temperature of 100 °C at the bentonite interface. Partial dismantling of the *in-situ* gallery occurred in 2002 with

the removal of one of the dummy containers, and its associated bentonite blocks, the other heater remained fully operational during the partial dismantlement, and resealing of the gallery with concrete was completed in 2003 (Barcena et al., 2003). During the second operational phase of the *in-situ* gallery the knowledge base surrounding bentonite increased, especially in the field of microbiology.

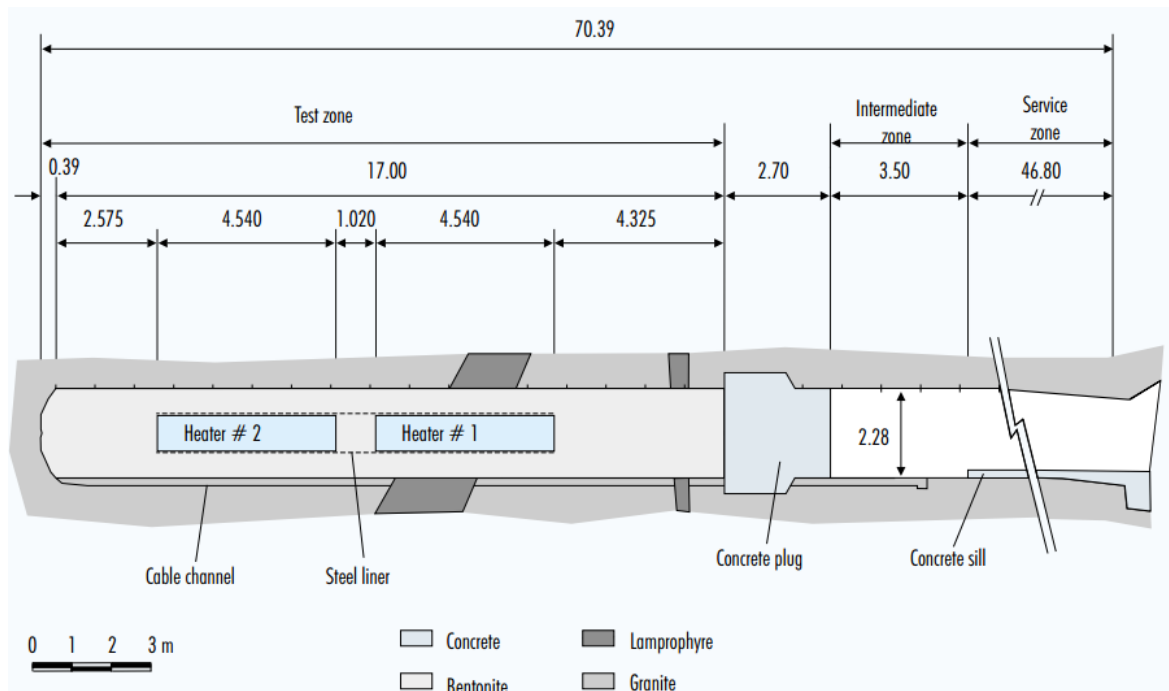


Figure 4.1: Diagrammatic representation of the FEBEX *in-situ* experiment (Huertas et al., 2000).

Advancements in molecular ecology identified diverse microbial communities in naturally occurring bentonite formations (Lopez-Fernandez et al., 2015), as well as under conditions pertinent to geological disposal (Stroes-Gascoyne et al., 2011). Several groups of bacteria have been identified as having potentially deleterious consequences in a GDF scenario including sulfate-reducing bacteria (SRB) (Bengtsson and Pedersen, 2017). SRB reduce sulfate present within the groundwater or near-field pore waters to hydrogen sulfide, which can cause container corrosion (El Mendili et al., 2013). Other bacterial groups that have not been investigated under GDF conditions include Fe(III)-reducing bacteria, which may also influence the structural integrity of the bentonite, by reducing structural Fe(III) to Fe(II) (Ribeiro et al., 2009). Final dismantling of the *in-situ* gallery occurred in 2015, 18 years after the experiment began (Lanyon and Gaus, 2016).

To assess the microbial ecology of the FEBEX *in-situ* experiment bentonite cores were extracted from the FEBEX gallery and sent to the University of Manchester for examination. DNA extraction from bentonite materials (even those not subjected to these experimental conditions) is challenging due to the relatively low abundance of biomass (Haynes et al., 2018) (Chapter 3), as well as the reduced efficiency of cell lysis, and the adsorption of DNA to clay particles (Novinscak and Fillion, 2011). Numerous methods have been devised to improve the yield of DNA from clay-rich, and other low biomass environments including the use of a concentrated phosphate buffer to compete with DNA for clay adsorption sites (Direito et al., 2012), and separation of microbial cells from foreign particles using density separation techniques (Morono et al., 2013).

DNA extraction from the bentonite cores was achieved using a routine soil extraction kit modified with a concentrated phosphate buffer, which was successful in isolating DNA from all the bentonite cores. Sequencing of the DNA from the bentonite cores suggested that microbial colonization may have occurred in the bentonites prior to the commencement of the experiment including photosynthetic *Cyanobacteria* during extraction at the quarry, along with the presence of psychrophilic (organisms that grow in cold conditions) to moderate temperature (1 °C – 42 °C) nitrate-reducing, Fe(III)-reducing, sulfate-reducing, and sulfide-producing bacteria that may have operated in the gallery before activation of the heaters. Moderately thermophilic (55 °C) sulfide-producers, and fermenters were also identified, and may have been viable in the cores furthest from the heater. Attempts to culture Fe(III), and sulfate-reducing bacteria from the cores at their experimental temperatures proved unsuccessful.

4.4. Methods

4.4.1. FEBEX core extraction and treatment

Bentonite cores were extracted from the Full-Scale Engineered Barriers Experiment (FEBEX) *in-situ* experiment located in Grimsel (Switzerland), after 18 years of exposure to a 100 °C canister surface, and the local geological environment. The samples used in this study were extracted from Section 48 of the FEBEX *in-situ* experiment (Figure 4.2). In total nine cores were extracted from the section, along three parallel to the temperature gradient (Figure 4.3). Removal of the cores from the experiment was achieved by drilling a circular outline

around the cores, and then extracting them using Shelby tubes (tubes commonly used in the collection of soil samples). Once extracted the tubes were sealed in foil packaging, under an atmosphere of argon. The tubes were then placed in a refrigerated container and transported to the University of Manchester where they were stored in a cold room (10 °C) until further use. Removal of the bentonite cores from the Shelby tubes was achieved using a hacksaw. Once extracted from the tubes the outer edges of the cores were removed in a laminar flow cabinet (Labcaire, Clevedon, UK), using an ethanol sterilized hammer, and chisel. Chips from the inside of the core were extracted and ground into a powder using an ethanol sterilized mortar, and pestle. The powders isolated from the cores were stored at -80 °C, ready for use in the most probable number (MPN) counts, and to identify the microbial communities using molecular ecology tools.

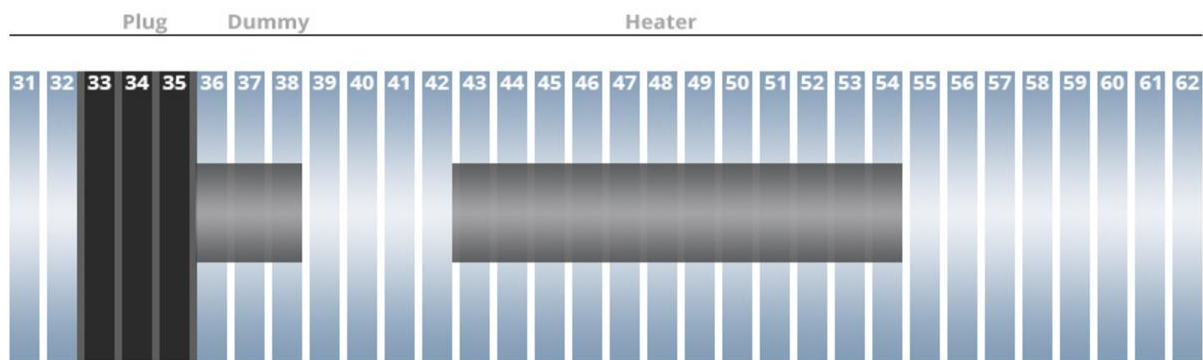


Figure 4.2: Breakdown of the FEBEX-DP sections (Wersin et al., 2017). Samples used in this work were taken from section 48, which was located at the halfway point of heater 2.

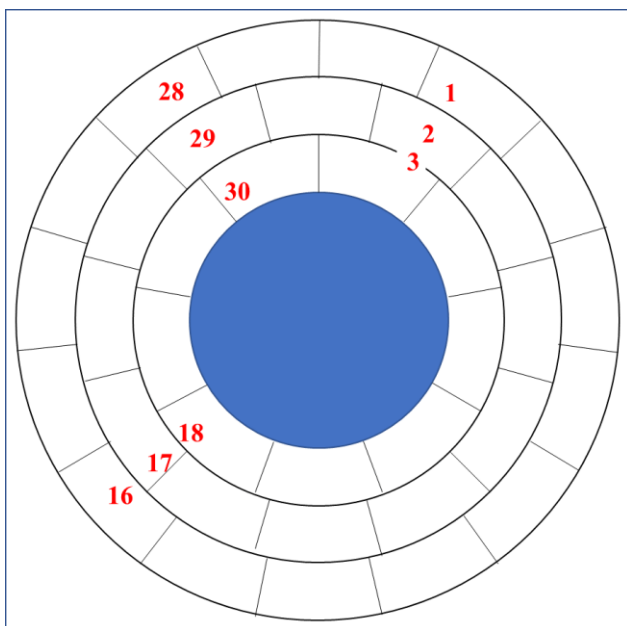


Figure 4.3: Location of the FEBEX cores extracted from section 48 of the FEBEX-DP.

4.4.2. Media preparation and MPN enumeration

Selective media in conjunction with most probable number (MPN) counts (de Man, 1983) were used to assess if there was any viable iron-reducing bacteria (IRB), and sulfate-reducing bacteria (SRB) in the cores after the FEBEX *in-situ* experiment. SRB were targeted using Postgate B medium (Postgate, 1979), while IRB were targeted with a fully defined growth medium (Lovley and Phillips, 1986) containing 4 mM ferrihydrite, 3.9 mM of nitrilotriacetic acid (NTA), 2 mM of sodium acetate, and 2 mM of sodium lactate. The fully defined growth medium was degassed using a mixture of N₂ and CO₂ before 9 ml aliquots were decanted into serum bottles under anaerobic conditions, the Postgate B contained the reductant sodium thioglycolate, and therefore 9 ml aliquots were decanted into serum bottles under atmospheric conditions. The media were sterilized in an autoclave (126 °C, 20 mins) after production. Powders from each core (0.45 g) were placed in the media in triplicate, and 1 ml of the resulting slurries was placed in fresh media using a nitrogen gassed syringe, this process was repeated until a dilution of 10⁻⁵ was achieved for each core. Once prepared the cores were stored at room temperature, along with separate batches stored at temperatures relevant to those found in the FEBEX *in-situ* experiment. The Postgate B samples were matured for 25 days before confirmation of a positive result by the formation of a black (iron sulfide) precipitate, the fully defined growth medium was left for 70 days, and a positive result was

verified by an enrichment in the 0.5 M HCl extractable Fe(II)/Fe(total), defined using the Ferrozine assay method (Lovley and Phillips, 1987).

4.4.3. Temperature prediction

During operation of the FEBEX *in-situ* experiment sensors were used to monitor the temperature of the bentonite buffer (Martinez et al., 2016), and other key variables. Data obtained from the sensors was provided by NAGRA and plotted against distance from the heater. A second order polynomial best fit was added and used to estimate the likely temperature the cores were exposed to during the experiment.

4.4.4. Molecular ecology methods

4.4.4.1. Microbial analyses (16S rRNA gene sequencing)

DNA was extracted from the bentonite cores to determine their molecular ecology. Four 0.25 g samples from each core were treated using the FastDNA™ Spin Kit (MP Biomedicals, Santa Ana, CA, USA) with a modified buffer step that replaced the buffer with a 1 M sodium phosphate buffer (Direito et al., 2012). Following the extraction procedure, the DNA extracts for each FEBEX core were combined, a DNA extraction was also carried out on the 1 M sodium phosphate buffer to ensure it was free from DNA. The 16S rDNA gene was targeted using PCR (polymerase chain reaction), with the forward primer 8F (5'-AGAGTTTGATCCTGGCTCAG-3'), and reverse primer 1492R (5'-TACGGYTACCTTGTTACGACTT-3'), as described previously by (Rizoulis et al., 2016). The amplified 16S rDNA sequences were stained using the SYBR Safe DNA Gel Stain (Invitrogen, Carlsbad, CA, USA) before setting in an agarose gel, and subsequent separation using electrophoresis. Confirmation that 1600 base pair products had been successfully amplified was achieved by viewing the stain under UV light, and comparing it to a ladder of known DNA fragment lengths.

4.4.4.2. Sequencing

After confirming the presence of DNA using the first PCR run a second was initiated focusing on the V4 hyper variable region (515F, 5'-GTGYCAGCMGCCGCGGTAA-3';

806R, GGACTACHVGGGTWTCTAAT-3') (Caporaso et al., 2011), a region of the previously amplified 16S rRNA gene that can be used to distinguish individual bacterial genera, and species. The V4 hyper variable region was amplified using the Roche FastStart High Fidelity PCR System (Roche Diagnostics Ltd, Basel, SUI) which utilized an initial denaturation step (95 °C, 2 mins), a further 36 temperature cycles (95 °C, 30 s; 55 °C, 30 s; 72 °C, 1 min) were then initiated, and then finally an extension step (72 °C, 5 mins). DNA products from the amplification were purified and then standardized to approximately 20 ng (SequalPrep Normalization Kit, Fisher Scientific, Loughborough, UK). The PCR products were subsequently pooled in equimolar proportions prior to sequencing (Illumina MiSeq platform, Illumina, San Diego, CA, USA). The sequencing run was executed with a 4 pM sample library, spiked with 4 pM of PhiX in a ratio which produced a final PhiX concentration of 10 % v/v (Kozich et al., 2013).

4.4.4.3. Bioinformatics

Sequences obtained from the Illumina sequencing run were set apart by barcodes, with one mismatch allowed. Cutadapt (v1.8.1) (Martin, 2011), FastQC (v1.1.3) (Andrews, 2016), and Sickle (v1.33) (Joshi and Fass, 2011) were utilized for trimming, and quality control purposes. Errors generated during sequencing were accounted for using SPADes (v3.5.0) (Nurk et al., 2013), and the forward, and reverse reads were merged into complete sequences using Pandaseq (v2.8) (Masella et al., 2012). Chimeras were removed using ChimeraSlayer (Haas et al., 2011), and UPARSE (Edgar, 2013) was used to produce operational taxonomic units (OTUs). Usearch (v8.0.1623) (Edgar, 2010) was used to remove singletons, and the OTUs classified with a similarity of 97 % or greater. The OTUs were taxonomically classified using RDP classifier (v2.2) (Wang et al., 2007), and rarefaction curves generated using Qiime (v1.8.0) (Caporaso et al., 2010).

4.4.4.4. Quantitative Polymerase Chain Reaction (qPCR)

The quantity of DNA in the extracts from the DNA extraction was calculated using qPCR. The qPCR reaction mixture consisted of 9.3 µl of sterile water, 0.4 µl of 25 µM forward primer 8F (5'-AGAGTTTGATCCTGGCTCAG-3'), 0.4 µl of 25 µM reverse primer 519R (5'-GWATTACCGCGGCKGCTG-3'), 0.4 µl 1 in 500 diluted Rox reference dye (Invitrogen, Carlsbad, CA, USA), and 12.5 µl of 2x qPCR SYBR Green master mix (Invitrogen,

Carlsbad, CA, USA), along with 2 μ l of the DNA extract. A negative control containing 2 μ l of PCR grade water was also produced along with a dilution series containing known quantities of DNA. The samples were loaded onto a MX3000P (Agilent Technologies, Stockport, UK) qPCR machine before exposure to an initial denaturation step at 94 °C for 4 minutes, followed by 36 cycles of 94 °C for 30 seconds, 50 °C for 30 seconds, and 72 °C for 45 seconds.

4.5. Results

4.5.1. Geophysical conditions

The geophysical conditions of the bentonite were approximated using a combination of data obtained from probes within the experiment (Martinez et al., 2016), along with modelling data (Lanyon and Gaus, 2016a). The water content of the bentonite blocks increased from the initial value, with the driest blocks being found in the inner ring (~ 17.5 %), and the wettest in the outer ring (~ 28.0 %) (Table 4.1). The density of the bentonite blocks increased towards the heater, with the inner blocks being less dense than the original blocks (1.50 g cm^{-3}), the middle blocks having a comparable dry density to the starting blocks (1.60 g cm^{-3}), and the inner blocks being the densest (1.63 g cm^{-3}) (Table 4.1). The inner blocks were also the hottest with the temperature in the center of the blocks being approximately 92 °C, this decreased to 72 °C in the middle ring, and 55 °C in the outer ring (Table 4.1).

Table 4.1: Approximations of the geophysical conditions encountered during the FEBEX in-situ project using data obtained from published sources: 1, (Lanyon and Gaus, 2016). 2, (Martinez et al., 2016).

	Pre-closure	Inner Ring	Middle Ring	Outer Ring
Water content (%) ¹	14.4	17.5	21.5	28
Dry density (g cm^{-3}) ¹	1.6	1.63	1.6	1.5
Temperature (°C) ²	16	92	72	55

4.5.2. Most Probable Number (MPN) enumerations

Most probable number (MPN) counts were conducted to assess the number of viable Fe(III)-reducing, and sulphate-reducing microbes present in the bentonite cores, at their

corresponding temperatures during the FEBEX experiment. None of the samples tested produced a positive result suggesting counts of less than 14.8 g⁻¹.

4.5.3. Transect 1-3

DNA was extracted from the cores to determine the type of organisms that may have been present during the experiment. BC-48-1 the core furthest away from the heater mostly consisted of *Clostridia* (51 %), *Betaproteobacteria* (22 %), *Actinobacteria* (9 %), *Bacteroidia* (7 %), *Deltaproteobacteria* (6 %) (Figure 4.4). The two cores closest to the heater had similar assemblages to each other with large proportions of *Betaproteobacteria* (~32 %), *Alphaproteobacteria* (~16 %), *Sphingobacteriia* (~17 %), and *Planctomycetacia* (~6 %) observed, which coincided with a large reduction in *Clostridia* to 2 % (Figure 4.4). A close relative of the thermophilic, fermentative *Clostridium* sp. JC3 (AB093456) was abundant in BC-48-1 (48 %), with close relatives of the nitrate-reducing *Dechlorosoma suillum* PS (NR_074103, 6 %), Fe(III)-reducing *Ferribacterium limneticum* strain cda-1 (NR_026464) (3 %), and the Fe(III), and sulfate-reducing *Desulfovibrio arcticus* (NR_115726) (5 %) identified as well. BC-48-2, and BC-48-3 contained close relatives of the psychrophilic nitrate-reducer *Polaromonas glacialis* strain Cr4-12 (NR_109013) (~ 24 %), and the sulfide-producing *Sediminibacterium salmoneum* strain NJ-44 (NR_044197) (4 %).

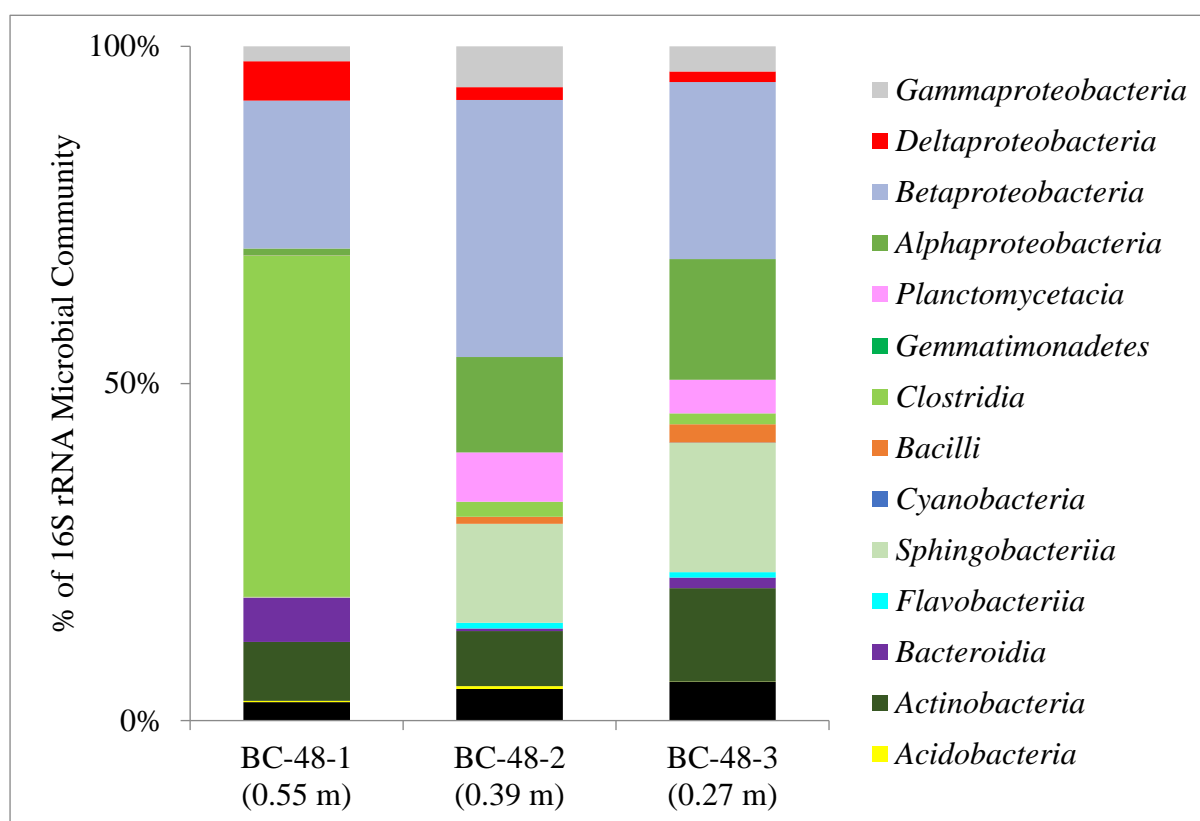


Figure 4.4: Breakdown of classes identified in the bentonite core transect made up of BC-48-1 (55 °C), BC-48-2 (72 °C), and BC-48-3 (83 °C), and the distance of the cores from the heater.

4.5.4. Transect 16-18

BC-48-16, and BC-48-17 were like each other and were mostly composed of *Gammaproteobacteria* (~28 %), *Betaproteobacteria* (~24 %), *Clostridia* (~14 %), *Bacilli* (~12 %), and *Alphaproteobacteria* (~8 %) (Figure 4.5). BC-48-18 the core closest to the heater contained large proportions of *Cyanobacteria* (38 %), *Betaproteobacteria* (31 %), and *Alphaproteobacteria* (11 %), but saw reductions in *Gammaproteobacteria* (11 %), *Clostridia* (4 %), and *Bacilli* (2 %) (Figure 4.5). A close relative of the nitrate-reducing bacterium *Pseudomonas zhaodongensis* strain NEAU-ST5-21 (NR_134795) was identified in BC-48-16, and BC-48-17 making up approximately 19 % of the communities. Small amounts of a close relative of the Fe(III), and nitrate-reducing bacterium *Albidiferax ferrireducens* strain T118 (NR_074760) (1 %) were also identified in the two cores, as well as a close relatives of the sulfide-producing *Sporacetigenium mesophilum* strain ZLJ115 (NR_043101) in BC-48-16 (2 %), along with the sulfide-producing *Massilia alkalitolerans* strain YIM 31775 (NR_043094) (4 %), and the sulfate-reducing bacterium *Desulfotomaculum* sp. clone

RC8C70 (EU921199) (2 %) in BC-48-17. BC-48-18 contained sequences related to several nitrate-reducing bacteria making up 6 % of the total amount.

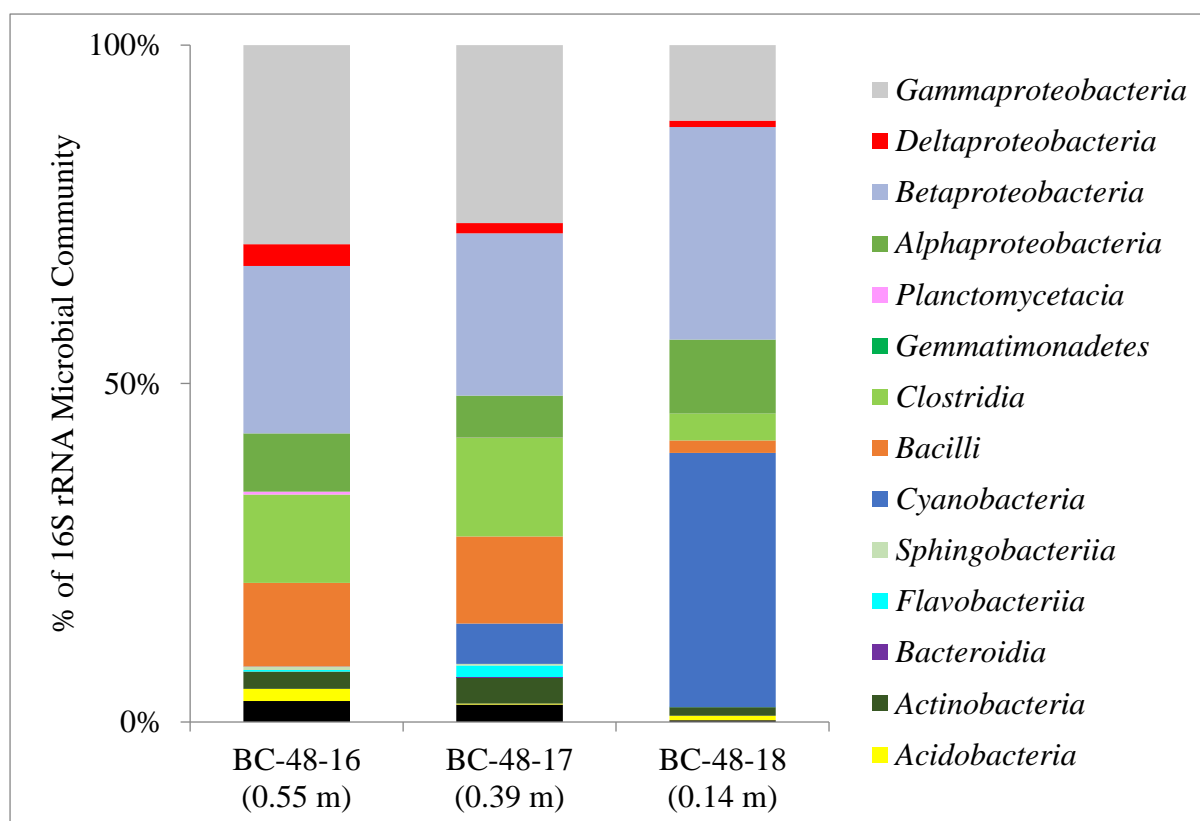


Figure 4.5: Classes present in bentonite cores BC-48-16 (55 °C), BC-48-17 (72 °C), BC-48-18 (92 °C), and the distance of the cores from the heater.

4.5.5. Transect 28-30

Transect 28-30 showed the greatest variability across the cores. BC-48-28, and BC-48-29 contained similar proportions of *Betaproteobacteria* (~29 %), *Gammaproteobacteria* (~18 %), and *Deltaproteobacteria* (5%), however BC-48-28 contained a higher percentage of *Alphaproteobacteria* (14 %), and *Clostridia* (14 %), while BC-48-29 had more reads related to *Bacilli* (11 %), and *Cyanobacteria* (14 %) (Figure 4.6). BC-48-30-1, and BC-48-30-2 contained similar amounts of *Betaproteobacteria* (~37 %), and *Gammaproteobacteria* (9 %), with *Deltaproteobacteria* (6 %), *Alphaproteobacteria* (17 %), and *Cyanobacteria* (24 %) being the other key classes in BC-48-30-1, and *Alphaproteobacteria* (6 %) and *Cyanobacteria* (39 %) in BC-48-30-2 (Figure 4.6). Several close relatives of nitrate-reducing bacteria were identified in BC-48-28 (8 %), and BC-48-29 (14 %), including close relatives of *Pseudomonas zhadongensis* strain NEAU-ST5-21 (NR_134795), and *Polaromonas*

glacialis strain Cr4-12 (NR_109013). Both of the cores also contained sequences related to Fe(III)-reducing (~ 2%), and sulfate-reducing (~ 2%) bacteria. Both BC-48-30-1, and BC-48-30-2 contained close relatives of the nitrate-reducing bacteria *Aquabacterium fontiphilum* strain CS-6 (NR_044322) (2 %), and *Methylothermobacter versatilis* strain 301 (NR_074693) (~4 %). However, BC-48-30-1 also contained close relatives of the nitrate-reducing *Acidovorax defluvii* strain BSB411 (NR_026506) (5 %), and the Fe(III)-reducing *Ferribacterium limneticum* strain cda-1 (NR_026464) (1 %).

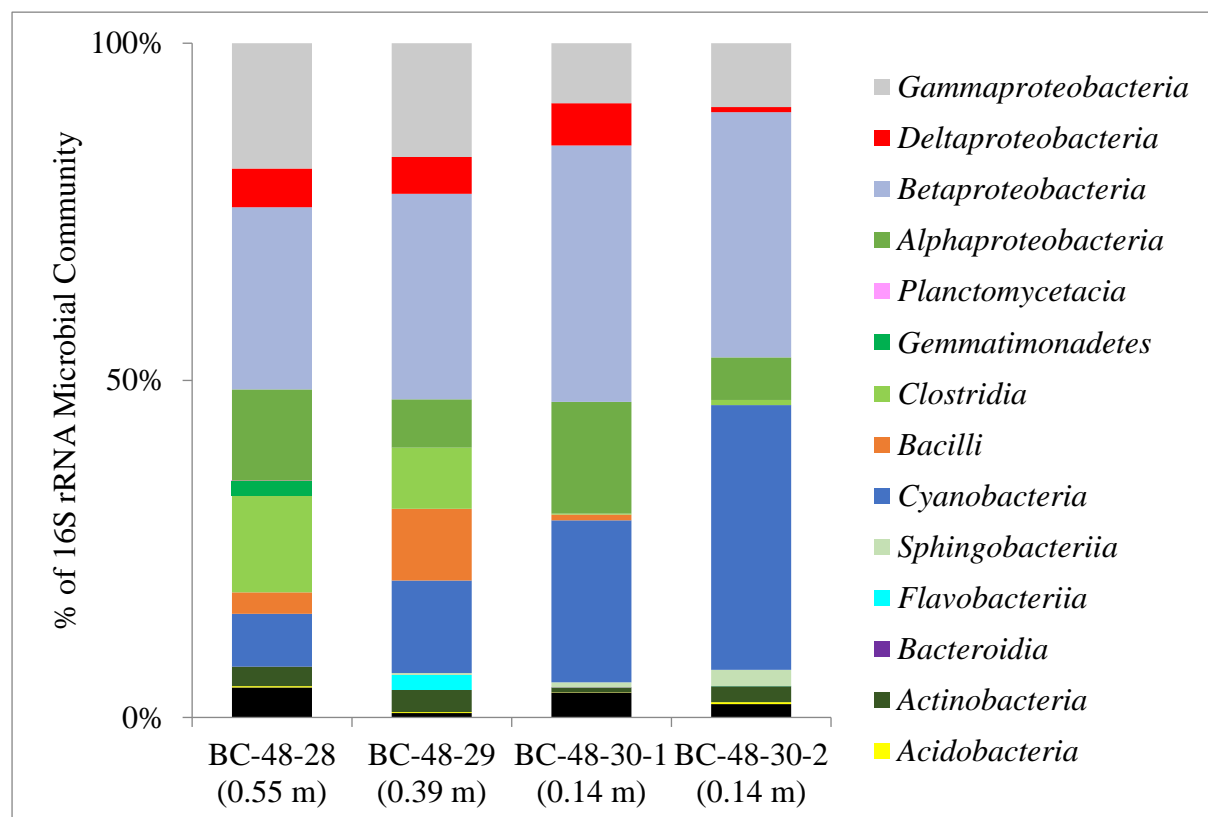


Figure 4.6: Overview of the classes present in the transect containing the bentonite cores BC-48-28 (55 °C), BC-48-29 (72 °C), BC-48-30-1 (92 °C), BC-48-30-2 (92 °C), and the distance of the cores from the heater.

4.5.6. Potential for microbially-driven processes

The potential metabolism and physiology of the microorganisms identified by Illumina sequencing of the bentonite cores was assessed by collating data from type strain papers of their closest relative. The majority of the cores contained DNA that suggested they had at some point supported nitrate, and iron-reduction, as well as hydrogen sulfide production, and fermentation in the range of psychrophilic (2 °C) to above room temperature (32 °C), with

sulfate-reduction at similar temperatures observed in BC-48-1, BC-48-16, BC-48-29 (Table 4.2). Sulfate-reduction capability was also observed in BC-48-17, BC-48-18, and BC-48-28 although no temperature data was available for these close relatives (Table 4.2). Hydrogen sulfide-producing behavior was observed at thermophilic temperatures (55 °C) in BC-48-1, BC-48-2, BC-48-16, BC-48-17, BC-48-29, and BC-48-30-1, as well as fermentation capability (55 °C) in BC-48-1, BC-48-2, BC-48-16, BC-48-17, BC-48-18, and BC-48-30-1 (Table 4.2).

Table 4.2: Key metabolic processes, and their temperature limits under optimum growth conditions as inferred from type strain papers of the closest relatives identified by Illumina sequencing of the bentonite core DNA extracts. x denotes the identification of a close relative carrying out a metabolic process, but no temperature constraints available.

Bentonite core	Nitrate-reduction	Iron-reduction	Sulfate-reduction	Sulfide-production	Fermentative
BC-48-1	1-42 °C	-2-28 °C	-2-28 °C	4-55 °C	55 °C
BC-48-2	1-42 °C	4-35 °C	-	4-55 °C	37, 55 °C
BC-48-3	1-42 °C	4-35 °C	-	18-37 °C	6-20 °C
BC-48-16	1-42 °C	4-25 °C	8-39 °C	4-55 °C	20-54 °C
BC-48-17	1-42 °C	4-35 °C	x	4-55 °C	6-20, 37, 55 °C
BC-48-18	1-42 °C	25 °C	x	6-30 °C	55 °C
BC-48-28	1-42 °C	4-32 °C	x	6-30 °C	37 °C
BC-48-29	1-42 °C	4-32 °C	8-39 °C	4-55 °C	6-20 °C
BC-48-30-1	15-42 °C	25 °C	-	4-55 °C	55 °C
BC-48-30-2	15-42 °C	30-35 °C	-	6-30 °C	-

4.5.7. qPCR

The quantity of DNA extracted from each sample was determined using qPCR. Overall BC-48-1 contained the most DNA with 1.3E+05 copies per gram, this decreased along the transect to 3.4E+04 copies per gram in BC-48-2, and 1.9E+04 copies per gram in BC-48-3 (Figure 4.7). The quantity detected in BC-48-16, and BC-48-17 was similar (~ 5.0E+04), while BC-48-18 produced the lowest amount across all the samples (1.6E+03) (Figure 4.7). Despite being further from the heater BC-48-28 produced less copies per gram (1.6E+04), than BC-48-29 (2.2E+04) (Figure 4.7). BC-48-30-2 contained almost double the amount of copies per gram (1.7E+04), compared to BC-48-30-1 (9.4E+03) despite them coming from the same core (Figure 4.7).

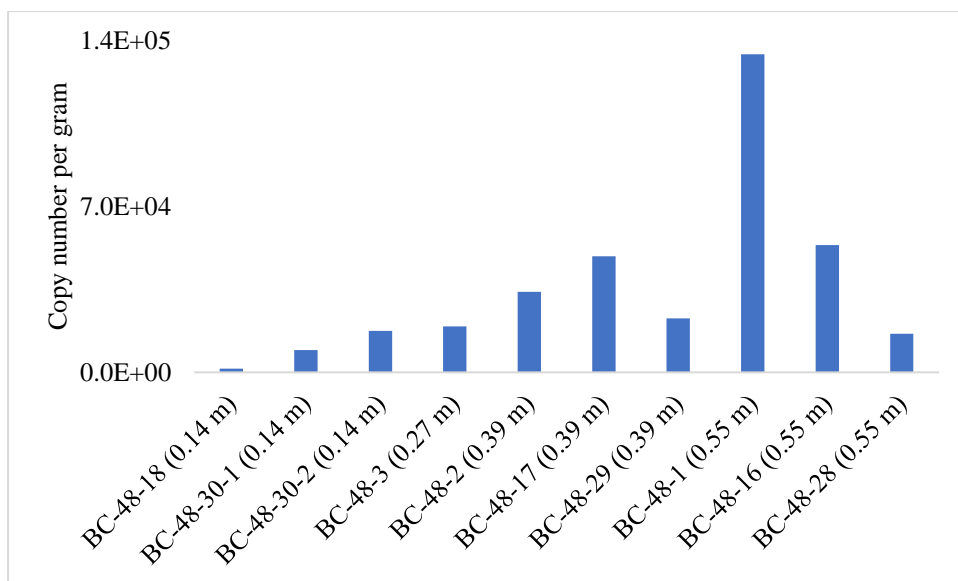


Figure 4.7: The number of copies present in each DNA extract from the bentonite cores, and the distance of the cores from the heater.

4.6. Discussion

4.6.1. Most Probable Number (MPN) enumerations

The presence of microbes in bentonite buffers intended for the disposal of nuclear waste has been of interest for the last two decades, due to the potential impacts on near-field chemistry, container corrosion and radionuclide speciation (RWM 2016b). Microbial analyses over this period have typically focused on short-term lab-scale studies, making it difficult to assess the impact of microbial activity on a bentonite buffer containing high-level waste (HLW). Using samples obtained from the FEBEX-DP we were able to investigate the microbial communities present in long-term samples that accurately reflect a geological disposal environment, minus the gamma radiation. Most probable number (MPN) analyses on the samples were conducted to determine the number of SRB, and Fe(III)-reducing bacteria present at the temperatures they were exposed to during the experiment. None of the MPNs conducted produced a positive result, suggesting active cell concentrations of less than 14.8 g^{-1} , a value which is considerably lower than a typical bentonite (Haynes et al., 2018) (Chapter 3). This suggests that following the operating period of the experiment (~20 years) the activity of SRB, and Fe(III)-reducing bacteria was minimal. The lack of activity in the MPNs does not confirm whether the bentonites are sterile or not, as there are other test conditions and media that may have yielded a positive result, and while sulfate-reduction is a

highly conserved function, there are other ways biological sulfide production can occur, for instance via thiosulfate reduction (Surkov et al., 2000), and the metabolism of amino acids (Madigan, 2015). There is also the potential that any microbial communities that developed in such a high swelling pressure regime may struggle to adapt back to a nutrient-rich, atmospheric pressure environment used in the MPN cultures.

4.6.2. Molecular ecology

Along with assessing the viability of key microbes in the cores following the FEBEX-DP, molecular ecology techniques were also used to establish if microbial activity may have occurred during the operation of the experiment. DNA extraction from all the cores was successful, and variability between individual samples, and transects was high. qPCR on the cores showed that BC-48-1 yielded double the DNA of the next closest result. Sequencing of DNA from this core identified close relatives of nitrate-, Fe(III)-, sulfate-reducing bacteria; capable of the key terminal electron accepting processes (apart from methanogenesis) found in an anaerobic environment, along with close relatives of other bacterium that are fermentative, as well as hydrogen sulfide producers (Table 4.2). TEAP chains of varying completeness were identified in the rest of the samples, with a decrease in completion of the chain towards the heater (Table 4.1), as would be expected as the temperature increased, and the water content of the bentonite decreased (Table 4.1).

Further analysis of the close relatives allowed us to generate a table of likely temperatures these TEAPs would be operating at (Table 4.2). It appears that most TEAP activity in the cores would be unlikely at the temperatures they were exposed to, and therefore microbial activity is likely to have occurred before the experiment was closed, as well as during the partial dismantlement (Barcena et al., 2003). Some of the cores contained DNA of close relatives that were capable of sulfide-production, and fermentation at 55 °C (Table 4.2) which suggests that these metabolic processes may be possible in the cores that were furthest from the heater.

The presence of close relatives of photosynthetic *Cyanobacteria* (Figure 4.5, Figure 4.6) also adds to the question about when these processes were occurring, and whether the microbial communities we are observing are one community, or several operating at different times in the bentonite's history that have been preserved together. The *Cyanobacteria* signal is likely to have been introduced into the bentonite cores when the bentonite was exposed in the

quarry to the atmosphere, as the block fabrication precluded the introduction of water to the bentonite (Huertas et al., 2000). Homogenization of the material before block preparation would have distributed the *Cyanobacteria* DNA throughout the starting material, and it therefore seems plausible that the *Cyanobacteria* signal could be used as a reference for microbial activity, with an increase in microbial activity decreasing the contribution from the *Cyanobacteria*. The preferential preservation of certain bacteria mainly spore-forming species (Madigan, 2015) versus the difficulty of extracting DNA from said cells (Wielinga et al., 2011) is something that was not quantifiable in this research, however these factors may explain the prominent *Cyanobacteria* signal observed in some of the cores, as well as the close relative of *Clostridium sp.* JC3 found in BC-48-1 (Figure 4.4).

Analyzing the data from samples extracted from BC-48-30-1, and BC-48-30-2 (Figure 4.6) highlighted the variability that can exist between individual core sub-samples and coupled with the low total yield of DNA observed in montmorillonite-containing samples (Direito et al., 2012) adds a lot of uncertainty to the predictions we have made. The data used in this study was also obtained from 1 g aliquots of 10 bentonite samples, out of a total of 115.7 tonnes used in the FEBEX-DP (Huertas et al., 2000). Several sources of variability in the system were also unable to be accounted for. These included the influx of groundwater into the bentonite barrier which could influence local geochemical parameters, and potentially be a source of microbial cells (Pedersen et al., 2000). Inconsistency in individual bentonite blocks may also occur due to a decrease in density at interfaces between individual blocks, the surrounding geological host, and the canister wall (Stroes-Gascoyne et al., 2011), although we were unable to establish that during this experiment, as 9 of the samples were from the center of blocks, while only one was from an interface. Future studies could provide a better understanding of the variability in individual blocks by profiling bentonite block cross sections.

4.7. Conclusions

A concentrated phosphate buffer with a routine soil DNA extraction kit was used to extract DNA from bentonite samples, to probe the molecular ecology of bentonite cores extracted from the FEBEX-DP, along the temperature gradient. Attempts to culture, and count Fe(III)-, and sulfate-reducing bacteria using the MPN technique were unsuccessful. This suggests that the potential for near-container Fe(III)-reducing bacteria to alter the bentonite, and sulfate-

reducing bacteria to contribute to container corrosion during the first 20 years of operation (duration of the FEBEX experiment), and potentially longer is low. Molecular ecology techniques identified DNA from a range of organisms that play a role in nitrate-, Fe(III), sulfate-reduction, sulfide-production, and fermentation suggesting that microbial communities could have been active (in low numbers) at some stage of the experiment. Information obtained from the type strain papers of the closest relatives of these microbes suggests that most of these processes are likely to have occurred during periods where the buffer was not heated, while sulfide-producing, and fermentative bacteria may have been viable at 55 °C a temperature observed in the bentonite cores furthest from the heater.

Applying molecular ecology techniques to the large-scale FEBEX-DP experiment proved to be a unique challenge, with bentonite providing a positively charged, low permeability environment conducive to DNA preservation, but at the same time increasing the difficulty of extraction. It is also challenging to draw reproducible, and gallery-wide conclusions using a single time-point from the 10 cores. These limitations increased the uncertainty that the communities extracted were representative of the whole system; this was compounded by the likelihood that a low proportion of the total DNA was extracted (Direito et al., 2012). These data probably represent communities preserved from different times in the bentonite's history, as shown by incompatible microbes being found together i.e. strict anaerobes such as *Clostridium*, and the photosynthetic *Cyanobacteria*. It must be acknowledged that reliable DNA extraction from bentonites is not a routine endeavor, and that the field of geomicrobiology was still in its infancy when the FEBEX experiment was proposed. Future field-scale disposal experiments can have microbiological programs implemented in them from the start, with the tools available to assess the molecular ecology before experiments commence. As molecular ecology techniques continue to develop, and more powerful sequencing platforms become available, the ease by which data is collected, and the data quality, will improve. Other issues, such as the limited number of time-points available to assess the molecular ecology of the barrier may prove to be more difficult to implement in field-scale experiments, and therefore bespoke microbiological field tests, as well as natural analogues must be considered.

The original aim of this research was to identify how temperature and evolving resaturation influence the molecular ecology of bentonites in the *in-situ* FEBEX experiment and, while it does not provide a thorough assessment of these effects, it does provide evidence for the potential existence of microbial communities under geological disposal conditions. With

increasing DNA yields away from the heater, it can be inferred that activity is more likely to occur at lower temperatures. However, a combination of the inability to culture microbes from the samples, and access to one time point makes it difficult to assess the role of evolving resaturation in microbial colonization.

4.8. Acknowledgements

Funding for this work was provided by Radioactive Waste Management (RWM). We thank Florian Kober for arranging transport of the samples from the Grimsel Test Site, and Barry Gale for removing the cores from their packaging.

4.9. References

- Andrews, N., 2016. FastQC: A quality control tool for high throughput sequence data (Version 0.11.3) [Software]. Available at <https://bioinformatics.babraham.ac.uk/projects/fastqc/> (08/12/18).
- Barcena, I., Fuentes-Cantillana, J.L., Garcia-Sineriz, J.L., 2003. Dismantling of the Heater 1 at the FEBEX in-situ Test, ENRESA, Madrid.
- Bengtsson, A., Pedersen, K., 2017. Microbial sulphide-producing activity in water saturated Wyoming MX-80, Asha and Calcigel bentonites at wet densities from 1500 to 2000 kg m⁻³. *Applied Clay Science*, 137: 203-212.
- Caporaso, J.G., Kuczynski, J., Stombaugh, J., Bittinger, K., Bushman, F.D., Costello, E.K., Fierer, N., Pena, A.G., Goodrich, J.K., Gordon, J.I., Huttley, G.A., Kelley, S.T., Knights, D., Koenig, J.E., Ley, R.E., Lozupone, C.A., McDonald, D., Muegge, B.D., Pirrung, M., Reeder, J., Sevinsky, J.R., Tumbaugh, P.J., Walters, W.A., Widmann, J., Yatsunenkov, T., Zaneveld, J., Knight, R., 2010. QIIME allows analysis of high-throughput community sequencing data. *Nature Methods*, 7(5): 335-336.
- Caporaso, J.G., Lauber, C.L., Walters, W.A., Berg-Lyons, D., Lozupone, C.A., Turnbaugh, P.J., Fierer, N., Knight, R., 2011. Global patterns of 16S rRNA diversity at a depth of millions of sequences per sample. *Proceedings of the National Academy of Sciences of the United States of America*, 108: 4516-4522.
- de Man, J.C., 1983. MPN tables, corrected. *European Journal of Applied Microbiology and Biotechnology*, 17(5): 301-305.
- Direito, S.O.L., Marees, A., Roling, W.F.M., 2012. Sensitive life detection strategies for low-biomass environments: optimizing extraction of nucleic acids adsorbing to terrestrial and Mars analogue minerals. *FEMS Microbiology Ecology*, 81(1): 111-123.
- Edgar, R.C., 2010. Search and clustering orders of magnitude faster than BLAST. *Bioinformatics*, 26(19): 2460-2461.
- Edgar, R.C., 2013. UPARSE: highly accurate OTU sequences from microbial amplicon reads. *Nature Methods*, 10(10): 996-1000.
- El Mendili, Y., Abdelouas, A., Bardeau, J.F., 2013. Insight into the mechanism of carbon steel corrosion under aerobic and anaerobic conditions. *Physical Chemistry Chemical Physics*, 15(23): 9197-9204.
- Fuentes-Cantillana, J., L., Garcia-Sineriz, J., L., 1998. FEBEX Full-scale engineered barriers experiment in crystalline host rock: final design and installation of the "in situ" test at Grimsel, ENRESA, Madrid.

- Haas, B.J., Gevers, D., Earl, A.M., Feldgarden, M., Ward, D.V., Giannoukos, G., Ciulla, D., Tabbaa, D., Highlander, S.K., Sodergren, E., Methe, B., Desantis, T.Z., Petrosino, J., F., Knight, R., Birren, B.W., 2011. Chimeric 16S rRNA sequence formation and detection in Sanger and 454-pyrosequenced PCR amplicons. *Genome Research*, 21(3): 494-504.
- Haynes, H.M., Pearce, C.I., Boothman, C., Lloyd, J.R., 2018. Response of bentonite microbial communities to stresses relevant to geodisposal of radioactive waste. *Chemical Geology*, 501: 58-67.
- Huertas, F., Fuentes-Cantillana, J.L., Jullien, F., 2000. Full-scale engineered barriers experiment for a deep geological repository for high-level radioactive waste in crystalline host rock, ENRESA, Madrid.
- Kozich, J.J., Westcott, S.L., Baxter, N.T., Highlander, S.K., Schloss, P.D., 2013. Development of a dual-index sequencing strategy and curation pipeline for analyzing amplicon sequence data on the MiSeq Illumina sequencing platform. *Applied and Environmental Microbiology*, 79(17): 5112-5120.
- Lanyon, G.W., Gaus, I., 2016. Main outcomes and review of the FEBEX in situ test (GTS) and mock-up after 15 years of operation, NAGRA, Wettingen.
- Lopez-Fernandez, M., Cherkouk, A., Vilchez-Vargas, R., Jauregui, R., Pieper, D., Boon, N., Sanchez-Castro, I., Merroun, M.L., 2015. Bacterial diversity in bentonites, engineered barrier for deep geological disposal of radioactive wastes. *Microbial Ecology*, 70(4): 922-935.
- Lovley, D.R., Phillips, E.J.P., 1986. Organic matter mineralization with reduction of ferric iron in anaerobic sediments. *Applied and Environmental Microbiology*, 51(4): 683-689.
- Lovley, D.R., Phillips, E.J.P., 1987. Rapid assay for microbially reducible ferric iron in aquatic sediments. *Applied and Environmental Microbiology*, 53(7): 1536-1540.
- Madigan, M.T., 2015. *Brock Biology of Microorganisms*. Pearson Education Limited, Upper Saddle River, New Jersey.
- Martin, M., 2011. Cutadapt removes adapter sequences from high-throughput sequencing reads. *EMBnet Journal*, 17(1): 3.
- Martinez, V., Abos, H., J.L., G.-S., 2016. FEBEXe: Final sensor data report (FEBEX in situ experiment), NAGRA, Wettingen.
- Masella, A.P., Bartram, A.K., Truszkowski, J.M., Brown, D.G., Neufeld, J.D., 2012. PANDAsq: PAired-eND Assembler for Illumina sequences. *BMC Bioinformatics*, 13.
- Morono, Y., Terada, T., Kallmeyer, J., Inagaki, F., 2013. An improved cell separation technique for marine subsurface sediments: applications for high-throughput analysis using flow cytometry and cell sorting. *Environmental Microbiology*, 15(10): 2841-2849.
- NDA, 2016. 2016 UK radioactive waste and materials inventory: UK radioactive waste inventory report, NDA, Harwell.
- Novinscak, A., Filion, M., 2011. Effect of soil clay content on RNA isolation and on detection and quantification of bacterial gene transcripts in soil by quantitative reverse transcription-PCR. *Applied and Environmental Microbiology*, 77(17): 6249-6252.
- Nurk, S., Bankevich, A., Antipov, D., Gurevich, A.A., Korobeynikov, A., Lapidus, A., Prjibelski, A.D., Pyshkin, A., Sirotkin, A., Sirotkin, Y., Stepanauskas, R., Clingenpeel, S.R., Woyke, T., McLean, J.S., Lasken, R., Tesler, G., Alekseyev, M.A., Pevzner, P.A., 2013. Assembling single-cell genomes and mini-metagenomes from chimeric MDA products. *Journal of Computational Biology*, 20(10): 714-737.

- Pedersen, K., Motamedi, M., Karnland, O., Sanden, T., 2000. Mixing and sulphate-reducing activity of bacteria in swelling compacted bentonite clay under high-level radioactive waste repository conditions. *Journal of Applied Microbiology*, 89: 1038-1047.
- Postgate, J.R., 1979. *The sulphate-reducing bacteria*. Cambridge University Press, Cambridge.
- Ribeiro, F.R., Fabris, J.D., Kostka, J.E., Komadel, P., Stucki, J.W., 2009. Comparisons of structural iron reduction in smectites by bacteria and dithionite: II. a variable-temperature Mössbauer spectroscopic study of Garfield nontronite. *Pure and Applied Chemistry*, 81(8): 1499-1509.
- Rizoulis, A., Milodowski, A.E., Morris, K., Lloyd, J.R., 2016. Bacterial diversity in the hyperalkaline Allas springs (Cyprus), a natural analogue for cementitious radioactive waste repository. *Geomicrobiology Journal*, 33(2): 73-84.
- RWM, 2016a. Geological disposal: Generic disposal facility design, RWM, Didcot.
- RWM, 2016b. Geological disposal: Generic environmental safety case main report, RWM, Didcot.
- Stroes-Gascoyne, S., Hamon, C.J., Maak, P., 2011. Limits to the use of highly compacted bentonite as a deterrent for microbiologically influenced corrosion in a nuclear fuel waste repository. *Physics and Chemistry of the Earth*, 36(17-18): 1630-1638.
- Surkov, A.V., Bottcher, M.E., Kuever, J., 2000. Stable sulfur isotope fractionation during the reduction of thiosulfate by *Dethiosulfovibrio russensis*. *Archives of Microbiology*, 174(6): 448-451.
- Wang, Q., Garrity, G.M., Tiedje, J.M., Cole, J.R., 2007. Naive bayesian classifier for rapid assignment of rRNA sequences into the new bacterial taxonomy. *Applied and Environmental Microbiology*, 73(16): 5261-5267.
- Wersin, P., Spahiu, K., Bruno, J., 2017. FEBEX-DP: Metal corrosion and iron-bentonite interaction studies, NAGRA, Wettingen.
- Wielinga, P.R., de Heer, L., de Groot, A., Hamidjara, R.A., Bruggeman, G., Jordan, K., van Rotterdam, B.J., 2011. Evaluation of DNA extraction methods for *Bacillus anthracis* spores spiked to food and feed matrices at biosafety level 3 conditions. *International Journal of Food Microbiology*, 150(2-3): 122-127.
- Wilson, J., Savage, D., Bond, A., Watson, S., Pusch, R., Bennett, D., 2011. Bentonite: A review of key properties, processes and issues for consideration in the UK context, NDA, Harwell.

5. Monitoring Bioreduction of Iron (III) in Bentonites Using a Magnetic Approach

Haydn M. Haynes^a, Carolyn I. Pearce^b, Anke Neumann^c, Adam Brookfield^d, Jonathan R. Lloyd^a

^a *Williamson Research Centre for Molecular Environmental Science and Research Centre for Radwaste Disposal, School of Earth, Atmospheric and Environmental Sciences, University of Manchester, Manchester, M13 9PL, UK*

^b *Pacific Northwest National Laboratory, Richland, WA, 99354, US*

^c *Newcastle University, Newcastle, NE1 7RU, UK*

^d *School of Chemistry, University of Manchester, Manchester, M13 9PL, UK*

Keywords

Bentonite, Fe(III)-reduction, electron paramagnetic resonance, Mössbauer, *Geobacter sulfurreducens*

5.1. Preface

Following on from the results encountered during chapter 3, it was clear that bentonites contain a wide variety of microorganisms that can contribute towards microbial Fe(III)- and sulphate-reduction. The consequences of sulphate-reducing activity are well known, and this has received a lot of attention in recent years (El mendili et al., 2013, Bengtsson et al., 2015). Fe(III)-reducing bacteria on the other hand have had less coverage, with much of the literature being over a decade old (Kostka et al., 1999, Kim et al., 2004). This chapter sought to provide a greater insight into the impacts of microbial Fe(III) reduction on a pure montmorillonite (SWy-2), and then comparing the results to a bentonite (FEBEX). The impact of microbial Fe(III) reduction on these two substrates was assessed by treating them with the Fe(III)-reducing bacterium *Geobacter sulfurreducens*. Changes to the speciation of the iron in the substrates was then investigated using a variety aqueous (Ferrozine assay), and solid-state techniques (EPR, Mössbauer).

Mössbauer spectroscopy showed that the two substrates had contrasting susceptibilities to microbial Fe(III)-reduction with the majority of the Fe(III) in the SWy-2 montmorillonite being reduced (88 %), and only a minor amount in the FEBEX bentonite (17 %). The differences in Fe(III) bio-availability were investigated using EPR spectroscopy. In the case of the FEBEX bentonite two forms of Fe(III) were identified, structural Fe(III) in the octahedral layer of the montmorillonite, and amorphous Fe(III) whose identity was not

known. The SWy-2 montmorillonite only contained the structural Fe(III). The difference in susceptibility to Fe(III) reduction appears to be due to the iron speciation, with the structural Fe(III) being reducible, and the amorphous Fe(III) being recalcitrant to reduction. Fe(III)-reduction in the SWy-2 montmorillonite caused a small decrease in pH, and an increase in cation exchange capacity. These effects were not observed in the FEBEX bentonite. However, a decrease in sulphate was observed which suggests that the lack of reducible Fe(III), allowed the conditions for sulphate reduction to develop faster. In terms of geological disposal, this shows that two montmorillonite-based materials can have comparable iron concentrations but can behave differently. The FEBEX bentonite is recalcitrant to Fe(III)-reduction, and may be more susceptible to sulphate-reduction which could promote canister corrosion. Meanwhile, the SWy-2 montmorillonite is amenable to Fe(III)-reduction which influences the bentonite's chemical properties. It is therefore important to consider the influence of these properties when selecting a candidate bentonite for geological disposal.

5.2. Abstract

Bentonites are montmorillonite-based clays that are being considered for use as a buffer material for the geological disposal of radioactive waste. Biological iron (III)-reduction can influence the chemical and physical properties of bentonites. Fe(III)-bioreduction in montmorillonites has been studied, but a comparison with industry relevant bentonite materials is required to understand the effects of accessory minerals. To address this issue, the impact of microbial Fe(III) reduction by *G. sulfurreducens* cells stimulated with electron donor (10 mM acetate) was assessed in slurries of pure montmorillonite (SWy-2) and bentonite (FEBEX). Initial results showed an increase in 0.5 M HCl extractable Fe(II) by 9 % in the SWy-2, and minimal Fe(III) reduction in the FEBEX. However, further studies using Mössbauer spectroscopy indicated that 88 % of the Fe(III) in SWy-2, and 17 % in the FEBEX had been reduced. It is clear that 0.5 M hydrochloric acid extraction is not an accurate measurement of bioavailable Fe(II) in montmorillonites. Electron paramagnetic resonance (EPR) spectroscopy identified isolated Fe(III) ($g = 4.2$) substituted into the octahedral sheet of montmorillonite in both SWy-2 and FEBEX. A broad band at $g = 2$, which is typical of nanostructured Fe(III)-oxides and -oxyhydroxides, was also present in the EPR spectrum for FEBEX. The unidentified iron oxide phase may be present in the interlayer of the montmorillonite or may be present as a coating on the clay particles. The limited Fe(III)-bioreduction observed with the FEBEX bentonite suggests that the Fe(III) is present

in a form that is inaccessible to the *G. sulfurreducens* cells, such as in a recalcitrant Fe(III) oxide coating, e.g. hematite, or trapped as nanoscale Fe(III)-oxide precipitates in the interlayer space. The presence of calcium ions in the interlayer space may also have limited the exposure of the basal surface. Analysis of the solution phase by inductively coupled plasma-atomic emission spectroscopy revealed that neither SWy-2 nor FEBEX showed signs of dissolution. However, the large amount of Fe(III)-reduction in the SWy-2 montmorillonite increased the CEC which may have knock-on impacts for the swelling behavior. The FEBEX bentonite was more susceptible to sulphate-reduction. Sulfate-reduction in a bentonite buffer could encourage microbially-induced container corrosion under geodisposal conditions. These differences highlight the need to characterize microbial interactions with the iron species present in bentonites intended for geological disposal.

5.3. Introduction

Biological Fe(III)-reduction is a process widespread in many environmental systems (Dong et al., 2009). Recent studies have identified microbial Fe(III)-reduction in bentonites (Esnault et al., 2013), and this can affect key properties of clay minerals, including their ability to reduce contaminants (Hofstetter et al., 2006), their ability to swell (Kostka et al., 1999), and their susceptibility to illitisation (Kim et al., 2004). Bentonite is a clay-based material and its major constituent is the dioctahedral smectite, montmorillonite. Bentonite has many advantageous properties that can be manipulated, depending on industry requirements, including pH buffering, amphoteric adsorption, and ion exchange sites, as well as swelling in the presence of water. The nuclear disposal industry is exploring bentonite's beneficial properties for use as a buffer and backfill material in a geological disposal facility (GDF) for nuclear waste (Bengtsson et al., 2015). The buffer is an engineered barrier surrounding the waste containers. It is an important component of the GDF, as it provides a low permeability barrier, limiting the transportation of corrosive substances to the waste container, and the release of radionuclides from the waste container into the surrounding geological environment (RWM, 2016). Iron (III)-reducing bacteria (IRB) have been identified in natural bentonite formations (Lopez-Fernandez et al., 2014), as well as under conditions designed to replicate geological disposal (Pedersen, 2010). There is therefore a need to understand the impacts IRB have on bentonites intended for use as a buffer in a GDF.

The mechanisms of Fe(III)-reduction in smectite materials have been studied for several decades. Chemical reduction of Fe(III) in smectite minerals is typically achieved using dithionite as a reducing agent (Komadel et al., 1990). Meanwhile, biological Fe(III)-reduction has been achieved with a range of bacteria including *Shewanella putrefaciens* (Luan et al., 2015), and *Methanothermobacter thermautotrophicus* (Zhang et al., 2013). Comparisons between the chemical and biological reduction of smectite minerals typically show that a greater extent of Fe(III)-reduction is observed through chemical means (Ribeiro et al., 2009). Aside from the reducing agent used, a number of factors influence the proportion of Fe(III) reduced, the mechanism by which it is reduced, and the reversibility of the reaction. The most important factors appear to be the structure of the smectite mineral, and the total amount of iron present. Two contrasting examples are iron-poor montmorillonites (2-3 % Fe), and iron-rich nontronites (> 20 %). A bioreduction study where Fe(III)-reduction was tracked using the Ferrozine assay showed 27 % of the total iron in NAu-2 nontronite was reducible, compared to 14 % in SWy-2 montmorillonite, with a rapid stage of reduction followed by a slower stage in the montmorillonite, and the reverse observed in the nontronite (Zhang et al., 2013). Electrochemical studies on the other hand have showed that 96.5 % of the iron in SWy-2 montmorillonite is redox-active, compared to 81.8 % in NAu-1 nontronite (Gorski et al., 2012). Upon reoxidation the SWy-2 is almost fully restored to its original state, but in the case of NAu-2 significant structural changes are observed (Gorski et al., 2013). The structural changes in NAu-2 and other nontronites are caused by the formation of trioctahedral Fe(II) clusters (Manceau et al., 2000) which lead to the distortion of the Fe(III) environment after reoxidation (Komadel et al., 1995). These structural changes affect the surface properties of the nontronite, changing the redox reactivity towards organics (Stucki et al., 2002). However, these irreversible reactions do not occur in montmorillonites as trioctahedral Fe(II) clusters require: (i) a high structural iron content (> 12 %); (ii) *trans*-vacant configuration of hydroxyl groups; and (iii) tetrahedral layer charging, none of which are present in montmorillonite (Neumann et al., 2011). The iron content of a smectite mineral also dictates how electrons are transferred to the iron atoms. In the case of nontronites electrons have been shown to hop between iron atoms (Alexandrov et al., 2013), with electron transfer to Fe(III) in montmorillonites occurring through the basal plane (Latta et al., 2017). In natural systems electron-shuttling compounds, such as humic acids (HA) and anthraquinone disulfonic acid (AQDS), have been shown to increase the rate and extent of Fe(III)-reduction by shuttling electrons to iron atoms inaccessible to bacterial cells (Nevin and Lovley, 2000). Similar results might be expected in montmorillonite, however research appears to show that while

the rate of Fe(III)-reduction increases in the presence of these electron-shuttling compounds, the extent does not (Zhang et al., 2013).

While the studies above provide a lot of insight into biological Fe(III)-reduction in smectite minerals, the focus has tended to be on pure mineral systems which raises questions about the relevance of these studies to the natural environment, as well as to materials for engineering projects. Research has shown that the distribution of iron in smectites can vary greatly depending on the deposit, with Wyoming smectites having an ordered distribution of iron atoms, while other deposits have random distributions, or clustering of iron atoms (Vantelon et al., 2003). This study compares biological Fe(III)-reduction in SWy-2 montmorillonite to that in FEBEX bentonite. FEBEX bentonite has been used as a buffer in a test to demonstrate the feasibility of constructing a high heat generating waste (HHGW) disposal gallery (Fuentes-Cantillana et al., 2000), and therefore provides a unique opportunity to investigate Fe(III)-reduction in a bentonite material relevant to the geological disposal of radioactive waste. State of the art magnetic spectroscopic tools, including electron paramagnetic resonance (EPR) and Mössbauer spectroscopy, were used to track, and characterize the end points of biological Fe(III)-reduction in SWy-2 montmorillonite and FEBEX bentonite. EPR is a powerful tool for investigating Fe(III) in clays due to its selectivity towards paramagnetic species, of which Fe(III) is one. EPR has been used to investigate a variety of phenomena including the transformation of bentonites by gamma radiation (Galambos et al., 2012), the pillaring of bentonites for use as catalysts (Carriazo et al., 2005), as well as probing interactions with radionuclides (Verma et al., 2014), and biomolecules (de Santana et al., 2010). Fe(III) features typically observed in smectite EPR spectra are a peak at $g = 4.3$ attributed to isolated Fe(III) atoms in the octahedral layer (Galambos et al., 2012), and a peak at $g = 2.0$ attributed to the presence of hydrated Fe(III) in the form of amorphous, or nanoparticulate iron oxyhydroxides (Bensimon et al., 1999; Carbone et al., 2005). Non Fe(III) features typically observed in EPR spectra include a Mn(II) sextet at $g = 2.04$ (Jung et al., 2002), and radical ions in the montmorillonite structure at $g = 2.005$ often used for dating the age of the smectite (Bensimon et al., 1999).

⁵⁷Fe-Mössbauer spectroscopy provides information on iron oxidation states and binding environment. Mössbauer spectroscopy is typically used to identify the extent of Fe(III)-reduction in reduced smectites, as well as to study mixed bentonite/iron oxide systems (Kristan et al., 2013), during catalysis (Komlosi et al., 2005) and interactions with aqueous species such as Np(V) (Verma et al., 2017) and Fe(II) (Latta et al., 2017). Variable

temperature Mössbauer spectrometry has been used to show that abiotic and biotic Fe(III)-reduction, the latter using *Shewanella oneidensis* strain MR-1, produces different iron structural arrangements (Ribeiro et al., 2009). When octahedral Fe(III) in Garfield nontronite was reduced to similar extents using microbes or the chemical reductant dithionite, a doublet belonging to octahedral Fe(II) was observed in both cases in the resulting Mössbauer spectra collected at 77 K. At 4 K the abiotic system looked similar with flaring on the Fe(III) doublet, however the biotic system displayed magnetic ordering suggesting separate Fe(II), and Fe(III) domains. Overall the results suggested that abiotic reduction occurs through the basal plane producing Fe(III)-Fe(II) links, while biological reduction occurs at the edge of the smectite producing separate Fe(II)-Fe(II), and Fe(III)-Fe(III) links.

Direct Fe(III)-reduction of the FEBEX bentonite and the SWy-2 montmorillonite by the Fe(III)-reducing bacterium *G. sulfurreducens* was assessed in this research, as well as indirect biological Fe(III)-reduction utilizing the soluble electron shuttle 9,10-anthraquinone-2,6-disulphonic acid (AQDS). The Ferrozine assay method identified a 10 % increase in 0.5 M hydrochloric acid extractable Fe(II) in the SWy-2 montmorillonite, while little measurable Fe(III)-reduction occurred in the FEBEX bentonite. Identification of the oxidation states of the iron in the materials using Mössbauer spectroscopy, showed that almost all the Fe(III) in the SWy-2 montmorillonite had been reduced to Fe(II), with minimal increase in Fe(II) in the FEBEX bentonite. Electron paramagnetic resonance spectroscopy (EPR) on the raw materials identified structural Fe(III) in both materials, and identified the presence of iron oxides in the FEBEX bentonite. This observation leads us to believe that the iron oxides in the FEBEX bentonite were recalcitrant to biological Fe(III)-reduction, and inhibited Fe(III)-reduction in the montmorillonite. This shows significant differences in Fe(III)-reduction can occur even in montmorillonite-based materials with a comparable iron content. Further investigation is therefore required to understand the nature of iron speciation in bentonite.

5.4. Materials and methods

5.4.1. Material selection, and clay suspension preparation

5.4.1.1. Material selection

The aim of this study was to investigate the extent of bacterial Fe(III)-reduction on a pure montmorillonite, and a bentonite using *G. sulfurreducens*, assessing the mineralogical changes that take place. A sodium montmorillonite, SWy-2, excavated in Wyoming, USA was purchased from the Clay Minerals Society (Chantilly, VA, USA). Calcium bentonite (FEBEX), retrieved from a quarry in Almeria, Spain was provided by Empresa Nacional de Residuos Radiactivos (ENRESA), Spain. The SWy-2 arrived in powder form and received no further treatment prior to experimentation, while the FEBEX came in a granular form, and was ground up using an ethanol sterilized mortar and pestle.

5.4.1.2. Preparation of *Geobacter sulfurreducens* cultures

Active *G. sulfurreducens* cells were prepared by transferring 10 ml of stationary phase cells into three sterile 90 ml bottles of a modified fresh water medium (NBAF), which contained 20 mM of sodium acetate acting as the sole electron donor, and 40 mM of fumarate as the sole electron acceptor (Cutting et al., 2012). Sodium hydroxide (10 M) was added to the growth media to obtain a pH of 7, and the air removed by flushing with a mix of nitrogen and carbon dioxide (Cutting et al., 2012). The amended NBAF medium was placed in an incubator in the dark at 30 °C, and the *G. sulfurreducens* cells were grown for 48 hours. These three bottles of starter culture were transferred into sterile media (900 ml) in an anaerobic cabinet (Coylab, Grass Lake, MI, USA), and grown for a further 48 hours at 30 °C. The *G. sulfurreducens* cells were then transferred to a set of centrifuge tubes under a sterile stream of pure nitrogen. The tubes were placed in a centrifuge for 20 minutes (4920 g, 4 °C) before the supernatant was discarded, and the cell pellets resuspended in 30 mM of sterile MOPS solution, corrected to pH 7 using 10 M sodium hydroxide. The cells were washed in a 30 mM MOPS solution twice more before being suspended in 50 ml of the solution. The optical density (OD_{600nm}) of the cell solution was measured using a Jenway (Stone, UK) spectrophotometer.

5.4.1.3. Clay suspension preparation

All glassware used in the experiment was washed in a 5 % nitric acid bath, and thoroughly rinsed with deionized water (18.2 M Ω) prior to use. Three different media compositions were prepared for the experiment: (i) a solution without electron donor, containing 30 mM MOPS; (ii) a solution containing 30 mM MOPS and 10 mM sodium acetate as an electron donor; and (iii), a solution containing 30 mM MOPS, 10 mM sodium acetate, and 10 μ M AQDS as an electron shuttle. Sodium hydroxide (10 M) was added to the media to obtain a pH of 7, and the media was degassed with nitrogen before being transferred into 100 ml serum bottles in an anaerobic chamber, and autoclaved (126 °C, 20 mins). After autoclaving each serum bottle was supplemented with either 4 g of FEBEX, or SWy-2, resulting in a clay mineral concentration of 40 g l⁻¹. In total five treatments were prepared in triplicate for each substrate, a no added electron donor triplicate with, and without 0.5 OD_{600nm} of *G. sulfurreducens*, an added acetate (electron donor) triplicate containing 0.5 OD_{600nm} of *G. sulfurreducens*, and an acetate (electron donor) plus AQDS (electron shuttle) triplicate with, and without 0.5 OD_{600nm} of *G. sulfurreducens*. Transfer of *G. sulfurreducens* into the bottles was completed using a degassed syringe, and the bottles were subsequently stored in a 20 °C incubator. The serum bottles were stored for 41 days with aliquots removed aseptically for further examination at appropriate time points.

5.4.2. Solution analysis

5.4.2.1. pH and Eh

pH and Eh were monitored in this experiment to ensure that conditions remained suitable for Fe(III)-reduction by *G. sulfurreducens*. The rest of the bentonite slurry extracted during the Ferrozine analysis was centrifuged (16,162 g, 5 mins), before insertion of the pH probe (Denver Instrument (Sartorius, Göttingen, Germany)) calibrated with pH 4, and pH 7 standards, and an Eh probe (Denver Instrument (Sartorius, Göttingen, Germany)) calibrated with a 220 mV standard. The initial pH of the substrates was also analyzed by allowing 2 g of sample to equilibrate in deionized water for an hour, before centrifuging (16,162 g, 5 mins) and monitoring the supernatant.

5.4.2.2. Ion chromatography (IC)

The concentration of key electron acceptors (nitrite, nitrate, sulphate) and the utilization of the added electron donor (sodium acetate) in solution were tracked using IC. For the clay suspensions 50 µl of the supernatant from the centrifuged clay slurry (16,162 g, 5 mins) was added to 950 µl of deionized water (18.2 MΩ). The starting materials were measured by allowing a 0.2 g sample to equilibrate in 5 ml of deionized water (18.2 MΩ) for an hour before centrifugation (16,162 g, 5 mins), and dilution of 250 µl of the supernatant in 750 µl of deionized water (18.2 MΩ). Both were analyzed using a Dionex ICS5000 instrument (Sunnyvale, CA, USA).

5.4.2.3. Inductively Coupled Plasma – Atomic Emission Spectroscopy (ICP-AES)

The impact of Fe(III)-reduction on the cation exchange capacity (CEC) on the bentonites, as well as the dissolution of the main bentonite constituents was analyzed using the concentrations of key interlayer cations (sodium, calcium, magnesium, potassium), along with key montmorillonite constituents (silicon, iron, aluminium) in the supernatant over the course of the experiment using ICP-AES. The initial CEC of the substrates was determined by adding 1 g of the unreduced sample to 5 ml of 1 M ammonium acetate solution and allowing it to equilibrate for 24 hours on a shaker. The samples were then vacuum filtered, and 1 ml of the solution was added to 9 ml of 2.2% nitric acid. Time-points during the experiment were also analyzed. Sample slurries were centrifuged (16,162 g, 5 mins), and 500 µl aliquots of the supernatant acidified in 9.5 ml of 2.2 % nitric acid. After acidification the samples were evaluated using a Perkin-Elmer Optima 5300 Dual View (Waltham, MA, USA) ICP-AES.

5.4.3. Solid phase analysis

5.4.3.1. X-ray diffraction (XRD)

The mineralogical characteristics of the starting materials, and their reduced equivalents were evaluated using XRD. The reduced samples were prepared by removing 2 ml of clay suspension from the serum bottles in an anaerobic cabinet (Coylab, Grass Lake, MI, USA), and allowing them to dry in a weigh boat for 24 hours. The samples were then ground using a pestle and mortar before mixing ~ 0.1 g with nitrogen flushed amyl acetate and placing on a

glass slide inside an airtight specimen holder. A 0.1 g sample of the starting materials was ground with a pestle and mortar before dispersal in amyl acetate and mounting on a low background sample holder. All samples were analyzed using a Bruker (Billerica, MA, USA) D8 Advance diffractometer. The diffractometer used a $\text{CuK}\alpha$ radiation source with a wavelength of 1.5406 Å, and the step size during the analysis was $0.02^\circ 2\theta$ with a counting time of 0.02 s per step, over a range of $5\text{--}70^\circ$. Patterns were fitted with a search/match routine (EVA software program version 4 ((Bruker, Billerica, MA, USA), with peaks matched to standards in the ICDD (International Centre for Diffraction Data) database.

5.4.3.2. Brunauer-Emmett-Teller (BET) surface area analysis

The surface area of the two substrates was determined by measuring nitrogen adsorption at -196°C . A 0.2 g sample of the materials was initially purged under a constant flow of nitrogen at 100°C for 18 hours before quantification (Micrometrics Flowprep 060, Norcross, GA, USA).

5.4.3.3. X-ray Fluorescence (XRF), H_2O content and loss on ignition (LOI)

The percentage makeup of elements in the FEBEX bentonite and SWy-2 montmorillonite was determined using XRF. In both cases a 12 g batch of substrate was mixed together with 3 g of fine powdered wax before milling at 350 rpm for 7 minutes using a TEMA (Woodford Halse, UK) mill, and a pellet formed using a press. The pellet was analyzed using a wavelength dispersive, PANalytical (Royston, UK) Axios spectrometer with a standard glass AUSMON (B255). The water content, and carbon present in the samples was determined by placing 1.0 g of the two substrates in clean, dry pre-ignited crucibles. The samples were then heated to 110°C for an hour before cooling in a desiccator and weighed to determine the water content. The samples were then heated again to 1000°C and cooled in a desiccator once more before being reweighed to determine the amount of carbon lost.

5.4.3.4. Ferrozine assay

The Ferrozine assay was used to measure the 0.5 M hydrochloric acid extractable Fe(II), and Fe(total) in the clay suspensions. Ferrozine solution was made by adding 0.5 g of 3-(2-Pyridyl)-5,6-diphenyl-1,2,4-triazine-*p,p'*-disulfonic acid (Ferozine), and 5.98 g of 4-(2-

hydroxyethyl)-11piperazineethanesulfonic acid (HEPES) to 500 ml of deionized water (18.2 MΩ), before neutralizing with 10 M sodium hydroxide. At each time-point 1 ml of bentonite slurry was extracted from the serum bottles using a sterile syringe degassed with nitrogen, and then 20 µl of this slurry was added to 980 µl of 0.5 M hydrochloric acid for Fe(II) measurements, or 980 µl of 0.25 M hydroxylamine hydrochloride dissolved in 0.5 M hydrochloric acid for total bioavailable Fe measurements, and allowed to react for one hour. The acidified solutions were then centrifuged (16,162 g, 5 mins) to remove the solids from solution, and 80 µl was added to 920 µl of Ferrozine solution. The Ferrozine solutions were examined using a spectrophotometer (Jenway (Stone, UK)) at 562 nm, and compared to a series of known standards.

5.4.3.5. Electron Paramagnetic Resonance (EPR)

The presence of unpaired electron species in the bentonites before, and after Fe(III)-reduction was determined using EPR. A 2 ml sample was removed from the acetate and *G. sulfurreducens* clay suspensions, along with another 2 ml aliquot from the no donor, and no *G. sulfurreducens* clay suspensions in an anaerobic chamber (Coylab, Grass Lake, MI, USA) using a sterile syringe and left to dry for 24 hours. The samples were then ground using a pestle and mortar and a 0.05 g sample was placed in a capillary tube with a J Young tap fitting (GPE Scientific (Leighton Buzzard, UK)) to prevent exposure to the air. The capillary tubes were then transferred to a Bruker (Billerica, MA, USA) EMX Micro X-Band (~ 9.9 GHz) spectrometer. The signal channel had a receiver gain of 30 dB, and a modulation amplitude of 10 G. The microwaves had a power of 2 mW and were attenuated to 20 dB. The capillary tubes were run empty prior to use to confirm the absence of species that may interfere with the results. The g values of the scans were corrected by measuring the error on a strong pitch standard, and the field of individual samples was normalized to a fixed frequency (9.8718 GHz).

5.4.3.6. Mössbauer

The local chemical environment of iron species in the bentonite slurries was examined using Mössbauer spectroscopy and the abundance of the iron oxidation state was determined. In the case of the reduced bentonites, approximately 5 ml of bentonite slurry was passed through a filter and the supernatant discarded. The solid was placed in a holder and sealed with Kapton

tape to prevent oxidation during transfer to the Mössbauer spectrometer. Untreated bentonites (0.2 g of powder bentonite) were deposited directly onto Kapton tape and sealed. Mössbauer spectra were collected in transition mode at 13 K, using a MS4 Mössbauer spectrometer (SEE Co, Edina, MN, USA) equipped with a closed-cycle cryostat (SHI-850, Janis Research Co, Wilmington, MA, USA). Calibration was carried out against 7 μm Fe(0)-foil and spectral fitting was performed using the Voigt-based fitting routine of the Recoil software (Rancourt and Ping, 1991).

5.5. Results

5.5.1. Material characterization

The mineralogy, as well as the physical and chemical properties of the two materials was determined to see if they had an influence on the rate, and extent of Fe(III)-reduction that took place. Both substrates had similar water contents ($\sim 9.4\%$), and pH (~ 9.1), but the FEBEX bentonite contained more organic carbon (8.0%), and a higher surface area ($44.9\text{ m}^2\text{ g}^{-1}$) compared to the SWy-2 montmorillonite which contained 6.4% organic carbon, and a surface area of $24.7\text{ m}^2\text{ g}^{-1}$ (Table 5.1). The two materials had similar iron ($\sim 26.2\text{ mg g}^{-1}$), and manganese ($\sim 0.1\text{ mg g}^{-1}$) contents (Table 5.1). However, the amount of 0.5 M hydrochloric acid extractable iron in the SWy-2 montmorillonite was 0.7 mg g^{-1} (0.2 mg g^{-1} Fe(II)), while the FEBEX bentonite contained 0.2 mg g^{-1} ($<0.1\text{ mg g}^{-1}$), which accounted for 2.7% , and 0.8% of the total iron in the two substrates (Table 5.1). The two substrates were mostly composed of montmorillonite, and quartz, with some anorthite in the FEBEX bentonite (Table 5.1), no change to the mineralogy was observed after reduction.

Table 5.1: Chemical and physical properties of the FEBEX bentonite, and SWy-2 montmorillonite including water content, loss on ignition, pH, surface area, the key interlayer cation concentrations (sodium, calcium, potassium, magnesium), sulphate, manganese, and iron contents, as well as 0.5 M hydrochloric acid extractable iron (Fe(II) and total), and the mineralogy.

Sample	FEBEX	SWy-2
H ₂ O (%)	9.9	8.8
LOI (%)	8	6.4
pH	8.7	9.4
SA (m ² g ⁻¹)	44.9 ± 0.4	24.7 ± 0.2
Na ⁺ (mg g ⁻¹)	5.8	>5.7
Ca ²⁺ (mg g ⁻¹)	7.3	4.2
K ⁺ (mg g ⁻¹)	0.7	0.5
Mg ²⁺ (mg g ⁻¹)	1	1.6
SO ₄ ²⁻ (mg g ⁻¹)	0.7	1.8
Mn (mg g ⁻¹)	0.2	0.1
Fe (mg g ⁻¹)	26.6	25.7
0.5 M HCl extractable Fe(II) (mg g ⁻¹)	<0.1	0.2
0.5 M HCl extractable total Fe (mg g ⁻¹)	0.2	0.7
Mineralogy (XRD)	Montmorillonite, Quartz, Anorthite	Montmorillonite, Quartz

5.5.2. Microbial Fe(III)-reduction in the substrates

The rate of Fe(III)-reduction taking place in the clay suspensions was determined using the Ferrozine assay. 0.5 M hydrochloric acid extractable Fe(II) levels in the FEBEX bentonite remained relatively constant (Figure 5.1). However in the SWy-2 montmorillonite, a sharp increase in 0.5 M hydrochloric acid extractable Fe(II) from 0.3 mg g⁻¹ to 2.2 mg g⁻¹ occurred over the course of 10 days in the acetate + AQDS incubations amended with *G.*

sulfurreducens, with a similar value being achieved in the acetate, and *G. sulfurreducens* amended incubations over a 41-day period (Figure 5.1). The amount of bioavailable Fe(II) after the experiment was approximately 9 % of the total iron in the SWy-2 montmorillonite (Figure 5.1). The increase in bioavailable Fe(II) in the SWy-2 montmorillonite treatments coincided with a change in the color of the sediment from a light brown color, to a light grey.

Minor amounts of Fe(III) reduction were also observed in the SWy-2 montmorillonite control containing *G. sulfurreducens* but no electron donor (0.3 mg g⁻¹) (Figure 5.1).

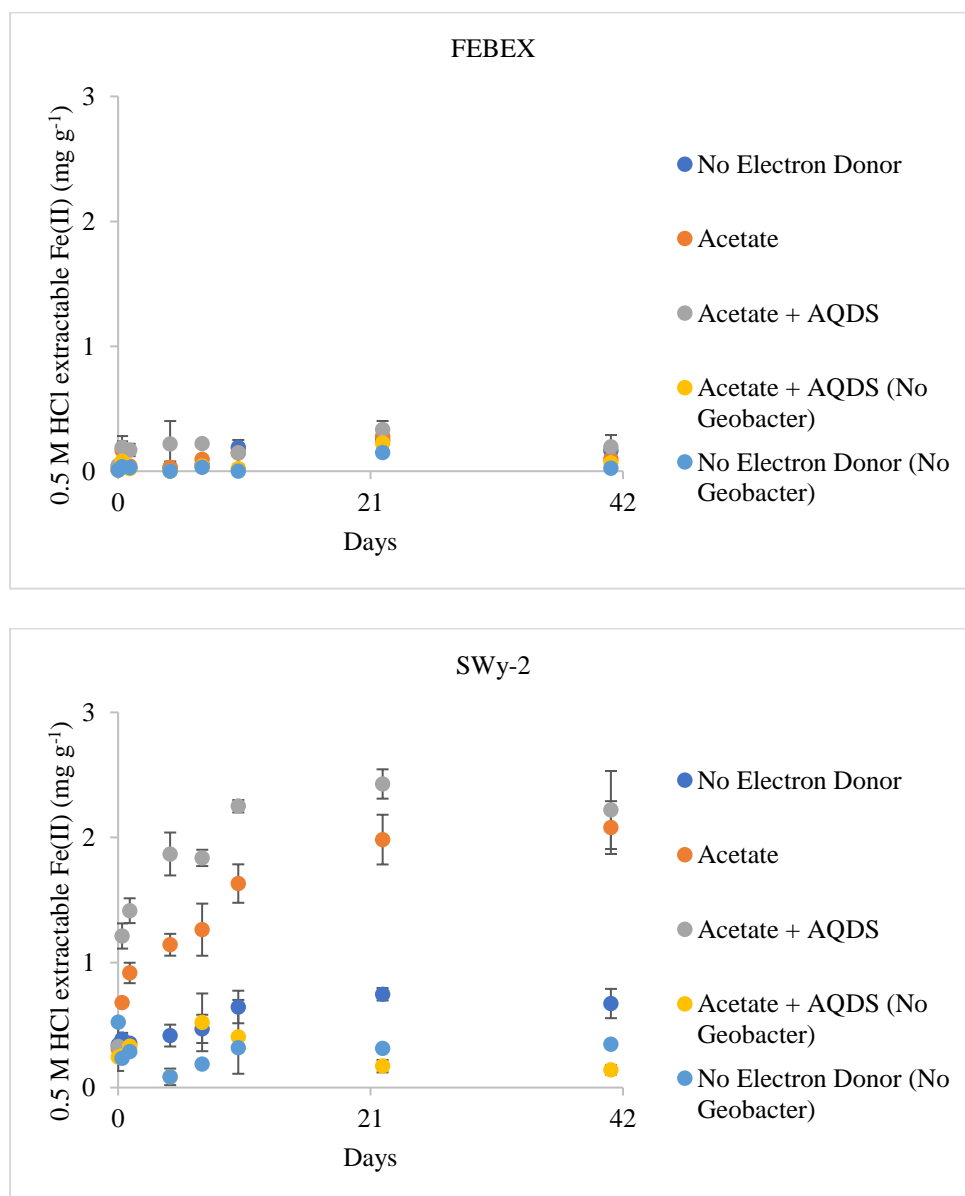


Figure 5.1: The amount of 0.5 M hydrochloric acid extractable Fe(II) in the FEBEX bentonite, and the SWy-2 montmorillonite as determined by Ferrozine assay.

5.5.3. pH and Eh

The pH of all the clay suspensions remained circumneutral, with a slight decrease in pH observed in the clay suspensions that had exhibited Fe(III) reduction (Supplementary 5.1). Eh in the FEBEX bentonite clay suspensions amended with acetate and AQDS decreased to

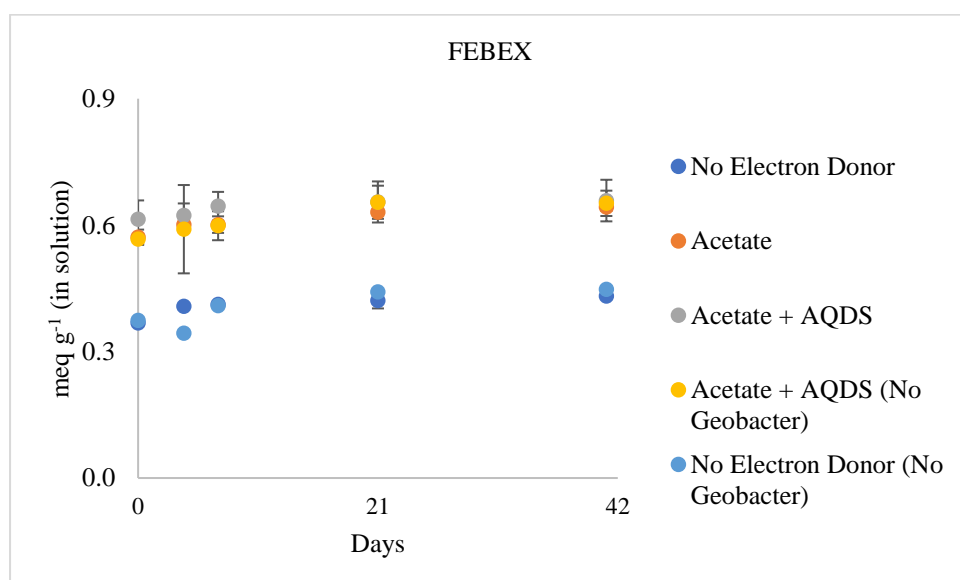
approximately -300 mV over the course of the experiment, while the rest decreased to -400 mV (Supplementary 5.2). In the SWy-2 montmorillonite the Eh of the clay suspensions containing both acetate, and *G. sulfurreducens* decreased to -325 mV, while the other treatments decreased to -200 mV (Supplementary 5.2).

5.5.4. Electron donor, and electron acceptor utilization

IC was used to track the consumption of the key electron acceptors (nitrite, nitrate, sulphate), and the electron donor (acetate) over the course of the experiment. The levels of nitrite and nitrate, in the supernatants for both substrates was low, with no nitrite detected in solution in any of the samples. Approximately 0.02 mg g⁻¹ of nitrate in solution was detected in the FEBEX bentonite samples, which was removed within seven days in the acetate amended treatments, while 0.01 mg g⁻¹ was left in the no electron donor supernatants at the end of the experiment. The SWy-2 montmorillonite samples contained more nitrate in solution than the FEBEX bentonite (0.05 mg g⁻¹), with the *Geobacter sulfurreducens* amended samples removing it in seven days, while the acetate + AQDS (no *G. sulfurreducens*) control removed it in 41 days, with 0.01 mg g⁻¹ in solution remaining in the no electron donor (no *G. sulfurreducens*) control at the end of the experiment. Approximately 0.8 mg g⁻¹ of sulphate was found in solution in the FEBEX bentonite samples at the beginning of the experiment, with nearly all of it consumed in the *G. sulfurreducens* amended clay suspensions over the course of the experiment (Supplementary 5.3). Concentrations in solution in the FEBEX bentonite no *Geobacter* controls also decreased to 0.6 mg g⁻¹ by day 41 (Supplementary 5.3). The SWy-2 montmorillonite suspensions contained 1.8 mg g⁻¹ of sulphate in solution which remained steady across most of the samples, although a decrease to 1.4 mg g⁻¹ was observed in the acetate + AQDS treatment, and a decrease to 1.6 mg g⁻¹ in the other acetate amended clay suspensions (Supplementary 5.3). The level of acetate utilization in the FEBEX clay suspensions was negligible, while 2 mg g⁻¹ was utilized in the two sets of SWy-2 montmorillonite suspensions containing acetate, and *G. sulfurreducens* cells (Supplementary 5.4).

5.5.5. Changes in the cation exchange capacity of the substrates (CEC) and mineral dissolution

The cation exchange capacity, and the dissolution of key constituents from the FEBEX bentonite, and the SWy-2 montmorillonite was monitored using ICP-AES. The concentrations of the key interlayer cations (sodium, potassium, magnesium, calcium) were initially elevated in all the acetate amended clay suspensions (due to the acetate being added as a sodium salt) with the FEBEX bentonite acetate containing clay suspensions having 0.58 meq g⁻¹ in solution, and the SWy-2 montmorillonite acetate containing clay suspensions having 0.74 meq g⁻¹ in solution (Figure 5.2). Meanwhile the FEBEX bentonite no electron donor clay suspensions contained 0.37 meq g⁻¹ of the cation species described above in solution, and the SWy-2 montmorillonite no electron donor clay suspensions contained 0.51 meq g⁻¹ in solution (Figure 5.2). Over the course of the experiment the concentration of interlayer cations in solution in the FEBEX bentonite clay suspensions increased by approximately 0.07 meq g⁻¹ (Figure 5.2). In the case of the SWy-2 montmorillonite clay suspensions negligible change was observed in the clay suspensions that did not contain *G. sulfurreducens* and decreases of 0.07 meq q⁻¹ in solution were observed in the suspensions that contained *G. sulfurreducens* (Figure 5.2).



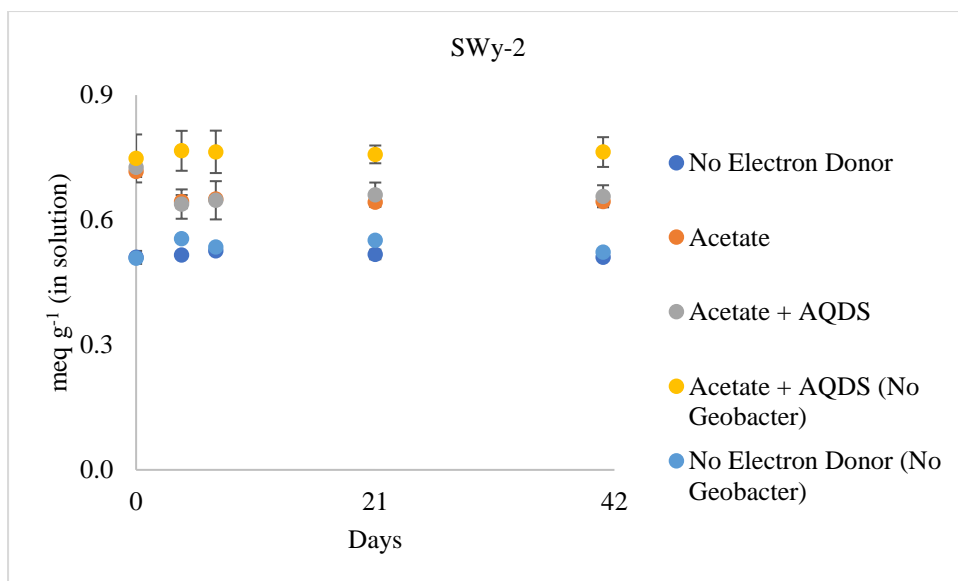


Figure 5.2: The change in key interlayer cations (sodium, calcium, potassium, magnesium) expressed as milliequivalents per gram in solution over the course of the experiment.

Dissolution of silicon across the treatments occurred at similar rates with an increase of approximately 0.20 mg g^{-1} (0.01%) in solution observed across all samples, with slightly more released in the two sets of acetate, and *G. sulfurreducens* amended SWy-2 montmorillonite clay suspensions (0.25 mg g^{-1}). No dissolution of aluminium was observed in the clay suspensions, however 0.02 mg g^{-1} ($\sim 0.08 \%$) of iron was released into solution in both sets of acetate, and *G. sulfurreducens* amended SWy-2 montmorillonite bottles.

5.5.6. EPR investigation of bioreduction-induced changes in Fe(III) speciation

EPR was used to examine the speciation of Fe(III), and other paramagnetic species in the substrates, before and after microbial Fe(III)-reduction. The SWy-2 montmorillonite displayed a sharp peak at $g = 4.2$ which was attributed to structural Fe(III) in the montmorillonite (Galambos et al., 2012) (Figure 5.3). A sextet of peaks was also identified at $g = 2.0$ belonging to Mn(II), as well as a sharp peak at $g = 2.0$ due to electron holes (defects) on the oxygen associated with Si in the tetrahedral sheet of the montmorillonite (Sorieul et al., 2005) (Figure 5.3). Following biological Fe(III)-reduction of the SWy-2 montmorillonite, a decrease in the intensity of the structural Fe(III) and Mn(II) signals was observed, as well as an increase in the defect signal (Figure 5.3). The FEBEX bentonite has two paramagnetic features identified as structural Fe(III) at $g = 4.2$ (Galambos et al., 2012), and nanostructured Fe(III)-oxides and -oxyhydroxides at $g = 2.1$ (Carbone et al., 2005) (Figure 5.3). After the

FEBEX was biologically reduced a decrease was observed in the overall intensity of the sample, with some distortion to the iron oxide signal at $g = 2.4$, along with the emergence of a new peak at $g = 2.3$ (Figure 5.3).



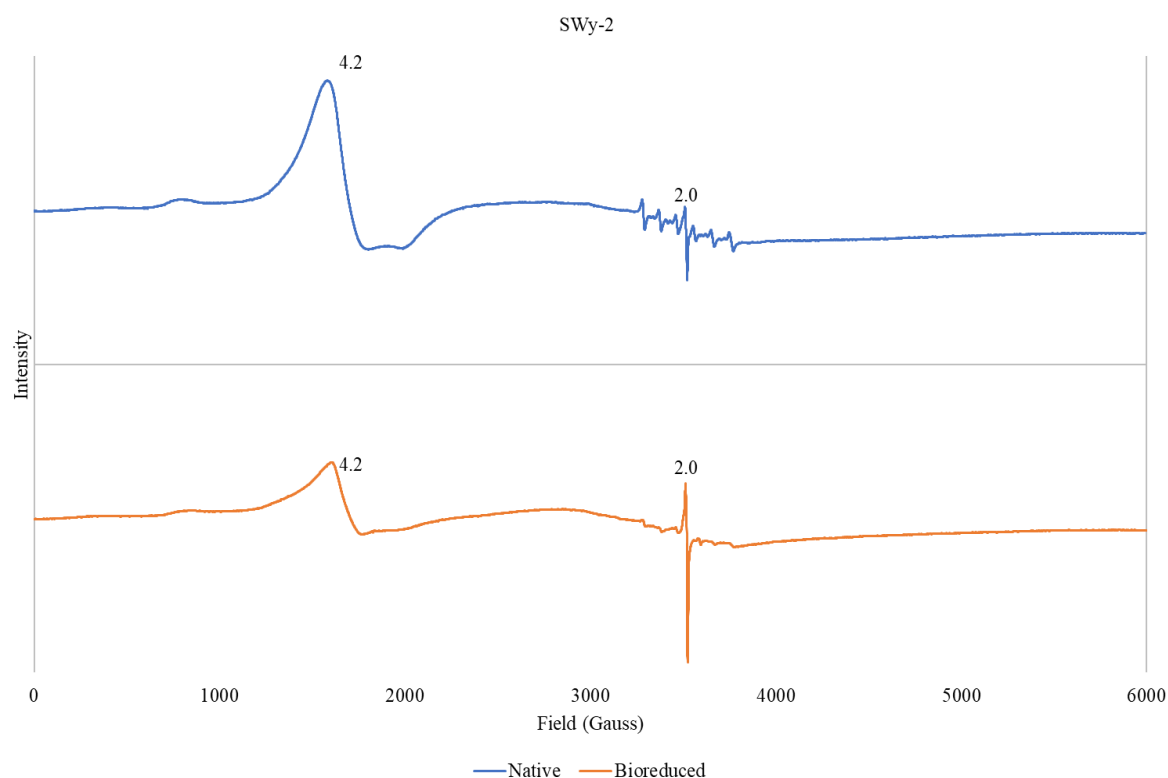


Figure 5.3: EPR spectrum of the native, and reduced FEBEX bentonite, and SWy-2 montmorillonite. The spectra were normalized to a frequency of 9.8718 GHz, and instrument error was corrected by comparing to a standard (strong pitch) of known g value.

5.5.7. Iron speciation using Mössbauer spectroscopy

The iron oxidation state and binding environment in the substrates was studied before and after 41 days of bioreduction. Spectra of both untreated substrates exhibited a large central doublet at 0.46-0.47 mm/s (Figure 5.4), indicative of octahedral Fe(III) in smectites. The broad Fe(III) doublets were fit with two overlapping distributions of quadrupole split (QS) values and the resulting parameter values (isomer shift (IS), and QS) were highly similar for both substrates, yet present in different proportions (Table 5.2). While the spectrum of the untreated FEBEX bentonite contained only the Fe(III) doublet, additional peaks were observed in the spectrum of the untreated SWy-2 montmorillonite (Figure 5.4). The shoulder at around 2.65 mm/s is characteristic for the presence of Fe(II) and spectral fitting yielded Mössbauer parameters similar to those observed for siderite or vivianite (Muehe et al., 2013). The two peaks at around -4.2 mm/s and 5.3 mm/s are indicative of the presence of a magnetically ordered Fe(III) phase (Figure 5.4), which was, not entirely captured during the measurement (velocity range: -6 to +6 mm/s) and its Mössbauer parameters can therefore only be indirectly estimated, after fitting of all the other components. The most probable

Mössbauer parameters for the Fe(III) sextet component (IS:0.5 mm/s, QS:-0.05 mm/s, hyperfine field H:50 T; Table 5.2) are consistent with the presence of ferrihydrite (IS:0.35 mm/s, QS:-0.02 to -0.07 mm/s, H:47-50 T) or goethite (IS:0.37 mm/s, QS:-0.25 mm/s, H:50.6 T) (Murad and Cashion, 2004). Combined, the two non-montmorillonite components make up 15% of the spectral area (Table 5.2).

After reduction, the FEBEX bentonite Mössbauer spectrum exhibited a new peak around 2.8 mm/s and a shoulder at -0.25 mm/s, distinctive of the presence of Fe(II) in the sample (Mössbauer parameters in Table 5.2) (Figure 5.4). Spectral fitting revealed that 17% of the solid-bound Fe was present as Fe(II) (Table 5.2). In contrast, the Mössbauer spectrum of the bio-reduced SWy-2 montmorillonite was dramatically different from that of the untreated sample and was dominated by an intensive Fe(II) doublet (Figure 5.4). The Fe(II) doublet had identical Mössbauer parameters as found for Fe(II) associated with bio-reduced FEBEX bentonite (IS: 1.27 mm/s, QS: 3.03 mm/s; Table 5.2) and comprised 88% of the spectral area (Table 5.2). The Fe(III) sextet as well as the Fe(II) phase detected in the untreated SWy-2 montmorillonite were absent in the spectrum of the bio-reduced sample and the remaining Fe was present as Fe(III), with Mössbauer parameters consistent with clay mineral octahedral Fe(III) (Figure 5.4).

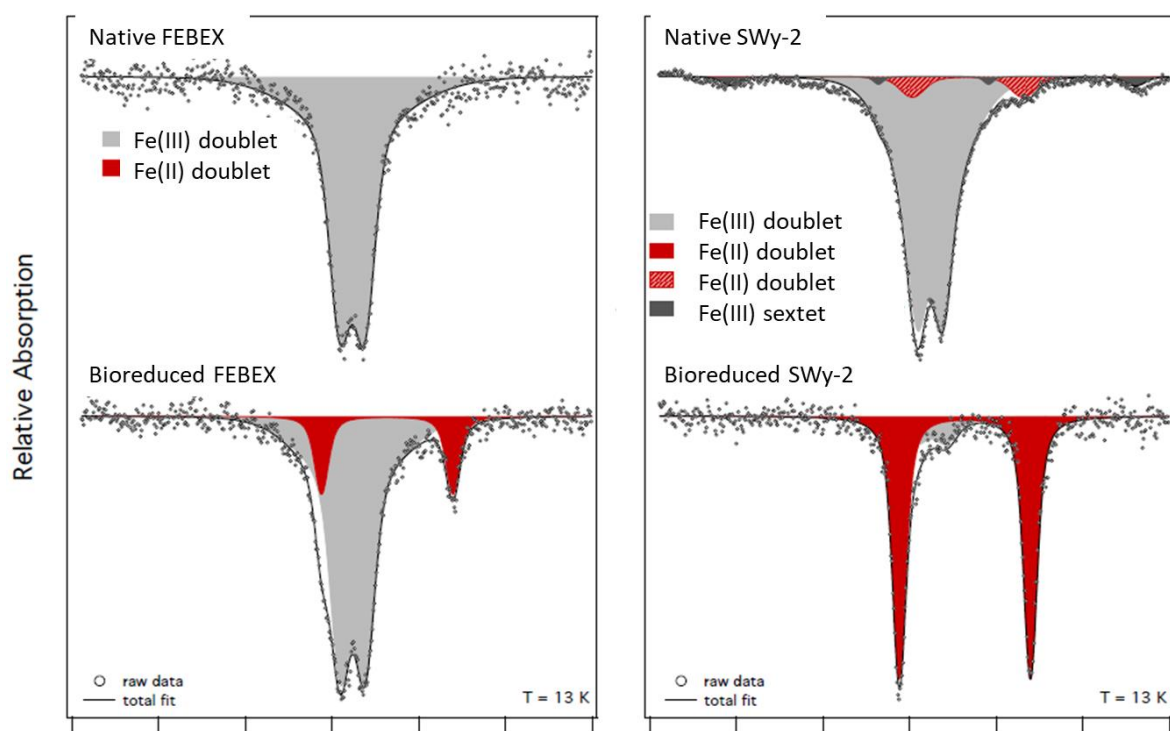


Figure 5.4: Mössbauer spectra of the native and bio-reduced FEBEX bentonite, and SWy-2 montmorillonite, along with fitted iron species.

Table 5.2: Parameters and statistical data for the fitted Mössbauer spectra, χ^2 , chi-squared; CS, center shift relative to α -Fe(0); QS, quadrupole splitting.

Sample (χ^2) and feature	CS (mm s ⁻¹)	QS (σ)	Area (σ) (%)
Native FEBEX (0.59)			
Fe(III) doublet	0.46	1.08 (1.15)	100
Bio-reduced FEBEX (0.60)			
Fe(II) doublet	1.27	3.03 (0.21)	16.6 (1.3)
Fe(III) doublet	0.47	0.96 (0.89)	83.4 (1.3)
Native Swy-2 (1.46)			
Fe(II) doublet	1.34	2.56 (0.47)	6.8 (0.4)
Fe(III) doublet	0.47	0.97 (0.78)	85.2 (0.8)
Fe(III) sextet	0.5	-0.05	8.0 (0.8)
Bio-reduced Swy-2 (0.80)			
Fe(II) doublet	1.27	3.03 (0.20)	87.5 (1.4)
Fe(III) doublet	0.5	0.69 (0.38)	12.5 (1.4)

5.6. Discussion

The aim of this study was to investigate the extent of microbial Fe(III) reduction achievable in bentonites using *G. sulfurreducens*. FEBEX bentonite, and SWy-2 montmorillonite were

exposed to microbial treatments (and appropriate controls), and then the materials assessed using the Ferrozine assay, EPR and Mössbauer spectroscopy. Initial analysis of 0.5 M hydrochloric acid extractable Fe(II) using the Ferrozine assay to quantify Fe(III)-reduction in the system showed that the amount of bioavailable Fe(II) in the SWy-2 montmorillonite increased by 9 % of the total iron content (Figure 5.1), with a similar trend occurring in the total bioavailable iron as well. A rapid rate of Fe(III)-reduction was observed over the first day followed, by a much slower rate of reduction for the rest of the experiment, as observed in previous studies (Figure 5.1) (Zhang et al., 2013). Previous research has suggested that iron in silicates is recalcitrant to 0.5 M hydrochloric acid extraction (Brookshaw et al., 2014) so the extent of biological Fe(III)-reduction was also investigated using Mössbauer spectroscopy which showed that 88 % of the iron was reduced after biological reduction had taken place (Table 5.2). This extent of Fe(III)-reduction was ten times the reported value from the Ferrozine assay, and therefore highlights the need for solid phase characterization, along with analysis of the solution phase using the Ferrozine assay, to interpret bioavailable iron in montmorillonite systems. The Ferrozine assay was still able to distinguish a difference in the FEBEX bentonite, and the SWy-2 montmorillonite, and is a quick method for showing that Fe(III)-reduction is occurring. However, it should not be used to measure the total extent of Fe(III)-reduction, and the findings in previous studies such as Zhang et al., (2013) should be viewed in a way that takes this information into account.

The consumption of acetate in the acetate, and *G. sulfurreducens* amended SWy-2 montmorillonite clay suspensions accounted for approximately 43 % of the Fe(III)-reduction, and 65 % in the acetate, AQDS, and *G. sulfurreducens* amended clay suspensions. These values do not match the Mössbauer data (Table 5.2), but we cannot rule out the *G. sulfurreducens* utilizing reduced co-factors. Fitting of the native SWy-2 montmorillonite Mössbauer data identified the presence of an Fe(II) doublet comparable to vivianite, or siderite (Table 5.2). However, despite accounting for 7 % of the spectrum, the 0.5 M hydrochloric acid extractable iron content was less than 1 % (Table 5.1). Vivianite, and siderite are susceptible to dissolution in 0.5 M hydrochloric acid which suggests either heterogeneity in the SWy-2 montmorillonite, or the doublet was present due to a different source of Fe(II). A sextet of peaks attributable to iron oxides (Murad and Cashion, 2004) was also present in the Mössbauer spectra accounting for 8 % of the sample (Table 5.2), and matched the amount of Fe(III)-reduction at the end of the experiment discerned by the Ferrozine assay (Figure 5.1). Further identification of the Fe(III) species in the SWy-2

montmorillonite was carried out using EPR. The EPR spectrum showed the presence of octahedral Fe(III) in the montmorillonite, but the broad and partially structured band at $g = 2.00$ was very weak, suggesting very little in the way of nanostructured Fe(III)-oxides and –oxyhydroxides associated with SWy-2 (Figure 5.3). Analysis of the bio-reduced SWy-2 montmorillonite using EPR also identified an increase in the defect signal (Figure 5.3), which implies that Fe(III) might not be the only sink for electrons in the montmorillonite.

Negligible Fe(III)-reduction was detected in the FEBEX bentonite using the Ferrozine assay, but once again a greater amount was identified in the Mössbauer spectrum (17 %) (Table 5.2), reinforcing the need for solid phase analysis of bioavailable iron in montmorillonite systems. Analysis of the native FEBEX bentonite using Mössbauer spectroscopy identified all of the iron was present as Fe(III) (Table 5.2). Meanwhile, the EPR spectrum contained two Fe(III) features, one attributed to structural Fe(III) in the montmorillonite, and another attributed to an iron oxide phase (Figure 5.3). If the Fe(III) oxide phase was partitioned into another mineral we would expect it to be detectable using XRD, which suggests it was present as an amorphous or nano-sized phase associated with the montmorillonite (Carbone et al., 2005), potentially in the interlayer space or as a coating on the clay particles. The presence of trioctahedral iron clusters as seen in nontronites can be discounted, because the iron content of the FEBEX bentonite is too low (Neumann et al., 2011). Changes to the shape of the Fe(III) oxide feature in the EPR spectrum were observed after biological Fe(III)-reduction (Figure 5.3). This suggests it may have been the target of biological Fe(III)-reduction in the FEBEX bentonite. The iron oxide phase may have prevented access to the structural Fe(III) in the FEBEX bentonite preventing more extensive Fe(III)-reduction. However, the FEBEX bentonite may also have been recalcitrant to biological Fe(III)-reduction due to the calcium ions in the interlayer space reducing the exposure of the basal surface to the *G. sulfurreducens* cells (Norrish, 1954). The unidentified iron oxide phase in the FEBEX bentonite requires further study. One consequence of the lack of biological Fe(III)-reduction appears to be an earlier onset of sulphate-reducing conditions in the FEBEX bentonite (Supplementary 5.3). The bioavailable Fe(III) in the SWy-2 montmorillonite would have acted as a competing electron acceptor reducing the activity of sulphate-reducing bacteria.

As well as assessing the impact on iron chemistry in the two substrates, attempts were also made to identify any wider associated mineralogical, and chemical changes that occurred because of the change in the iron redox state. ICP-AES was used to determine the changes in

key interlayer cations in solution, and therefore changes in the CEC during the experiment. Data from the acetate amended SWy-2 clay suspensions showed a decrease in the key interlayer cations in solution (Figure 5.2), and therefore Fe(III)-reduction enhanced the CEC of SWy-2. This is due to an increase in the interlayer charge accompanying the reduction of the Fe(III) (Kostka et al., 1999). A relatively consistent increase in the number of cations in solution was observed across all of the FEBEX treatments (Figure 5.2), suggesting the minimal Fe(III)-reduction that did take place did not have a significant impact on the interlayer charge. This might be further evidence that microbial Fe(III)-reduction was impacting the iron oxide species rather than the structural Fe(III) responsible for the interlayer charge. A lack of dissolution of key montmorillonite components was confirmed using ICP-AES. Minor increases (~0.01%) in the amount of silicon in solution was observed across all samples, meanwhile aluminium concentrations remained constant. A minor amount of iron dissolution (~0.01%) was also observed in the two sets of acetate, and *G. sulfurreducens* amended SWy-2 montmorillonite clay suspensions, which is unlikely to impart significant mineralogical change.

5.7. Conclusions

The extent of microbial Fe(III) reduction in montmorillonite-based materials can vary greatly, even between materials with comparable iron contents. The FEBEX bentonite appeared to have two Fe(III) species in the form of structural Fe(III), and an interlayer iron oxide, or iron oxide coating. It was not clear if this iron oxide phase was disrupting electron transfer through the montmorillonite (preventing extensive Fe(III)-reduction) or if calcium ions in the interlayer were decreasing the basal surface accessible to the *G. sulfurreducens*. Further study is required to identify the iron oxide form and if it has an influence on electron transfer. SWy-2, a pure montmorillonite containing mostly structural Fe(III), was amenable to biological Fe(III)-reduction. The Ferrozine assay showed that AQDS increased the rate of biological Fe(III) reduction, but not the extent, as has been shown previously (Zhang et al., 2013). However, the bioavailable Fe(II) concentrations were tenfold lower than the extent of Fe(III)-reduction identified by Mössbauer spectroscopy. It is clear that 0.5 M hydrochloric extractable Fe is not a reliable measure of bioavailable Fe in montmorillonite systems, and this needs to be taken into consideration when understanding the extent of Fe(III)-reduction in previous studies, and when planning future work. The EPR spectrum of bio-reduced SWy-2 also saw an increase in defects present as electron holes. The increase in the defect content

may provide insights into the transfer of electrons through the montmorillonite, and suggests Fe(III) might not be the only electron sink present.

Sulfate-reduction was observed in the FEBEX bentonite, with a minimal amount in the SWy-2 montmorillonite. This shows the bioavailable iron in the SWy-2 montmorillonite acts as a competing electron acceptor preventing sulfate-reduction. However, the Fe(III)-reduction increased the interlayer charge, and the CEC, which may influence the swelling ability of a bentonite buffer (Fitch et al., 1995; Kostka et al., 1999). Therefore, the two materials have advantages, and disadvantages when it comes to nuclear waste disposal. The FEBEX bentonite is more recalcitrant to geochemical changes imparted by biological Fe(III)-reduction, but is more susceptible to sulfate-reduction, and therefore could encourage microbially-induced corrosion (El Mendili et al., 2013). The SWy-2 montmorillonite will be less likely to promote microbially-induced corrosion, but its swelling pressure may be altered under reducing conditions. These differences highlight the requirement to characterize bentonite materials intended for use in geological disposal. As subtle differences in their iron speciation appears to influence their geochemistry under reducing conditions.

5.8. Acknowledgements

The authors would like to thank Radioactive Waste Management (RWM) for the funding provided for this work. We would also like to thank Paul Lythgoe, and Alastair Bewsher for the IC, ICP-AES, LOI, and XRF analyses, Adam Brookfield, and David Collison for assistance with collecting the EPR data, and John Waters for the BET analysis, James Entwistle for help preparing the Mössbauer samples and collecting the data.

5.9. References

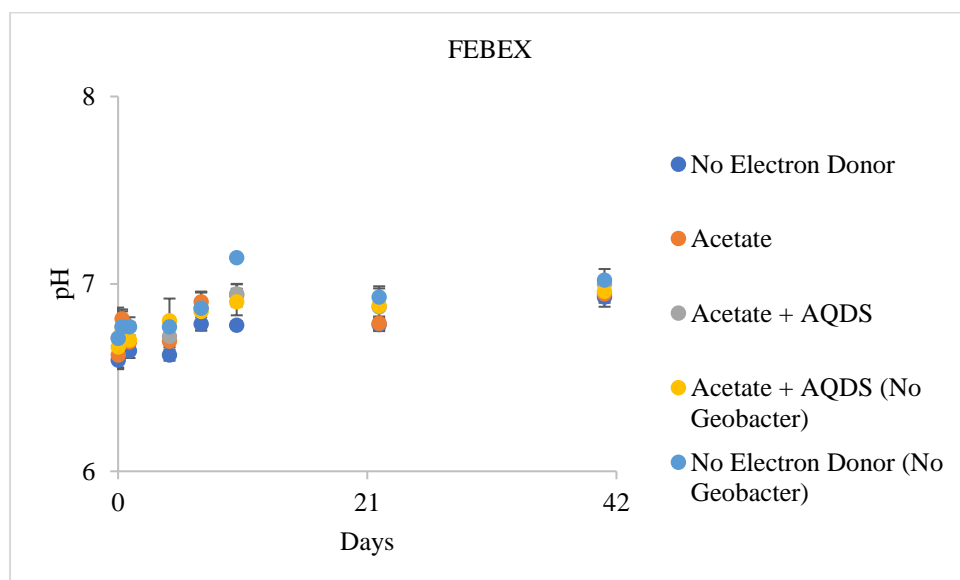
- Alexandrov, V., Neumann, A., Scherer, M.M., Rosso, K.M., 2013. Electron exchange and conduction in Nontronite from first-principles. *Journal of Physical Chemistry C*, 117(5): 2032–2040.
- Bengtsson, A., Edlund, J., Hallbeck, B., Heed, C., Pedersen, K., 2015. Microbial sulphide-producing activity in MX-80 bentonite at 1750 and 2000 kg m⁻³ wet density, SKB, Stockholm.
- Bensimon, Y., Deroide, B., Zanchetta, J.V., 1999. Comparison between the electron paramagnetic resonance spectra obtained in X- and W-bands on a fired clay: a preliminary study. *Journal of Physics and Chemistry of Solids*, 60(6): 813-818.
- Brookshaw, D.R., Lloyd, J.R., Vaughan, D.J., Pattrick, R.A.D., 2014. Bioreduction of biotite and chlorite by a *Shewanella* species. *American Mineralogist*, 99(8-9): 1746-1754.
- Carbone, C., Di Benedetto, F., Marescotti, P., Sangregorio, C., Sorace, L., Lima, N., Romanelli, M., Lucchetti, G., Cipriani, C., 2005. Natural Fe-oxide and -oxyhydroxide

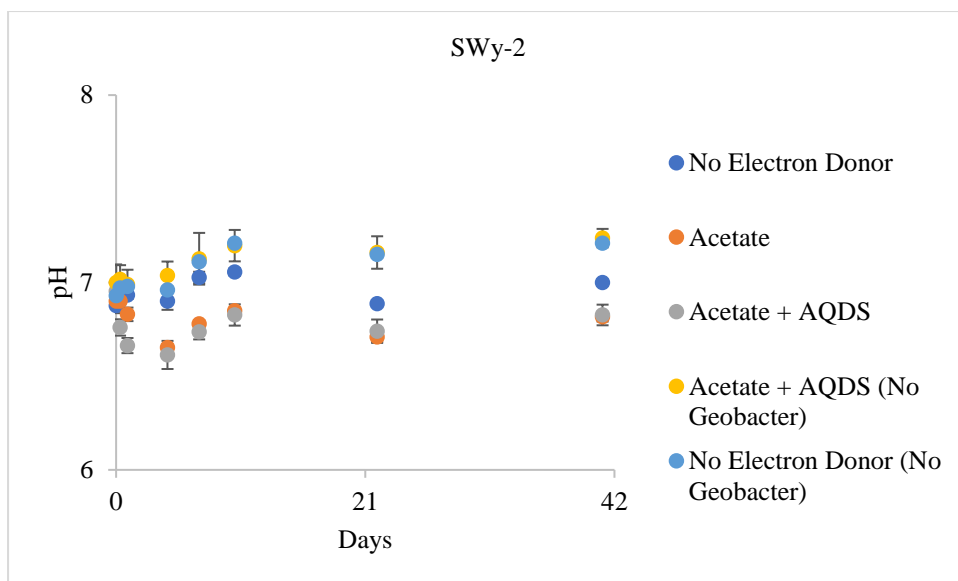
- nanoparticles: an EPR and SQUID investigation. *Mineralogy and Petrology*, 85(1-2): 19-32.
- Carriazo, J., Guelou, E., Barrault, J., Tatibouet, J.M., Molina, R., Moreno, S., 2005. Synthesis of pillared clays containing Al, Al-Fe or Al-Ce-Fe from a bentonite: characterization and catalytic activity. *Catalysis Today*, 107-08: 126-132.
- Cutting, R.S., Coker, V.S., Telling, N.D., Kimber, R.L., van der Laan, G., Patrick, R.A.D., Vaughan, D.J., Arenholz, E., Lloyd, J.R., 2012. Microbial reduction of arsenic-doped Schwertmannite by *Geobacter sulfurreducens*. *Environmental Science & Technology*, 46(22): 12591-12599.
- de Santana, H., Paesano, A., Da Costa, A.C.S., Di Mauro, E., De Souza, I.G., Ivashita, F.F., De Souza, C.M.D., Zaia, C., Zaia, D.A.M., 2010. Cysteine, thiourea and thiocyanate interactions with clays: FT-IR, Mössbauer and EPR spectroscopy and X-ray diffractometry studies. *Amino Acids*, 38(4): 1089-1099.
- Dong, H., Jaisi, D.P., Kim, J., Zhang, G., 2009. Microbe-clay mineral interactions. *American Mineralogist*, 94(11-12): 1505-1519.
- El Mendili, Y., Abdelouas, A., Bardeau, J.F., 2013. Insight into the mechanism of carbon steel corrosion under aerobic and anaerobic conditions. *Physical Chemistry Chemical Physics*, 15(23): 9197-9204.
- Esnault, L., Libert, M., Bildstein, O., Mustin, C., Marsal, F., Jullien, M., 2013. Impact of iron-reducing bacteria on the properties of argillites in the context of radioactive waste geological disposal. *Applied Clay Science*, 83-84: 42-49.
- Fitch, A., Du, J., Gan, H.M, Stucki, J.W., 1995. Effect of clay charge on swelling: a clay-modified electrode study. *Clays and Clay Minerals*, 43(5): 607-614.
- Fuentes-Cantillana, J.L., Garcia-Sineriz, J.L., Franco, J.J., Obis, J., Perez, A., 2000. FEBEX project: full-scale engineered barriers experiment for a deep geological repository for high-level radioactive waste in crystalline host rock, CIEMAT, Madrid.
- Galambos, M., Dano, M., Rosskopfova, O., Sersen, F., Kufcaková, J., Adamcova, R., Rajec, P., 2012. Effect of gamma-irradiation on adsorption properties of Slovak bentonites. *Journal of Radioanalytical and Nuclear Chemistry*, 292(2): 481-492.
- Gorski, C.A., Aeschbacher, M., Soltermann, D., Voegelin, A., Baeyens, B., Fernandes, M.M., Hofstetter, T.B., Sander, M., 2012. Redox properties of structural Fe in clay minerals. 1. electrochemical quantification of electron-donating and -accepting capacities of smectites. *Environmental Science & Technology*, 46(17): 9360-9368.
- Gorski, C.A., Kluepfel, L.E., Voegelin, A., Sander, M., Hofstetter, T.B., 2013. Redox properties of structural Fe in clay minerals: 3. relationships between smectite redox and structural properties. *Environmental Science & Technology*, 47: 13477-85.
- Hofstetter, T.B., Neumann, A., Schwarzenbach, R.P., 2006. Reduction of nitroaromatic compounds by Fe(II) species associated with iron-rich smectites. *Environmental Science & Technology*, 40(1): 235-242.
- Jung, J., Yoo, D.H., Lee, M.J., 2002. Radiation treatment of TCE and PCE in the presence of anatase, P25 and bentonite. *Journal of Radioanalytical and Nuclear Chemistry*, 251(3): 423-425.
- Kim, J., Dong, H.L., Seabaugh, J., Newell, S.W., Eberl, D.D., 2004. Role of microbes in the smectite-to-illite reaction. *Science*, 303(5659): 830-832.
- Komadel, P., Lear, P.R., Stucki, J.W., 1990. Reduction and reoxidation of Nontronite - extent of reduction and reaction-rates. *Clays and Clay Minerals*, 38(2): 203-208.
- Komadel, P., Madejova, J., Stucki, J.W., 1995. Reduction and reoxidation of Nontronite - questions of reversibility. *Clays and Clay Minerals*, 43(1): 105-110.

- Komlosi, A., Kuzmann, E., Homonnay, Z., Nagy, N.M., Kubuki, S., Konya, J., 2005. Effect of FeCl₃ and acetone on the structure of Na-montmorillonite studied by Mössbauer and XRD measurements. *Hyperfine Interactions*, 166(1-4): 643-649.
- Kostka, J.E., Wu, J., Nealson, K.H., Stucki, J.W., 1999. The impact of structural Fe(III) reduction by bacteria on the surface chemistry of smectite clay minerals. *Geochimica Et Cosmochimica Acta*, 63(22): 3705-3713.
- Kristan, P., Chilan, V., Stepankova, H., Reznicek, R., Kouril, K., Stepanek, J., Polakova, K., Prochazka, V., Cuda, J., Medrik, I., 2013. Bentonite/iron oxide composites: preparation and characterization by hyperfine methods. *Journal of Nanomaterials*.
- Latta, D.E., Neumann, A., Premaratane, W., Scherer, M.M., 2017. Fe(II)-Fe(III) electron transfer in a clay mineral with low Fe content. *ACS Earth and Space Chemistry*, 1(4): 197-208.
- Lopez-Fernandez, M., Fernandez-Sanfrancisco, O., Moreno-Garcia, A., Martin-Sanchez, I., Sanchez-Castro, I., Merroun, M.L., 2014. Microbial communities in bentonite formations and their interactions with uranium. *Applied Geochemistry*, 49: 77-86.
- Luan, F.B., Liu, Y., Griffin, A.M., Gorski, C.A., Burgos, W.D., 2015. Iron(III)-bearing clay minerals enhance bioreduction of nitrobenzene by *Shewanella putrefaciens* CN32. *Environmental Science & Technology*, 49(3): 1418-1426.
- Manceau, A., Drits, V.A., Lanson, B., Chateignern D., Wu, J., Huo, D., Gates, W.P., Stucki, J.W., 2000. Oxidation-reduction mechanism of iron in dioctahedral smectites: II. crystal chemistry of reduced Garfield nontronite. *American Mineralogist*, 85(1): 153-172.
- Muehe, E.M., Obst, M., Hitchcock, A., Tyliszczak, T., Behrens, S., Schroder, C., Byrne, J.M., Michel, F.M., Kramer, U., Kapplert, A., 2013. Fate of Cd during microbial Fe(III) mineral reduction by a novel and Cd-tolerant *Geobacter* Species. *Environmental Science & Technology*, 47(24): 14099-14109.
- Murad, E., Cashion, J., 2004. Mössbauer spectroscopy of environmental materials and their industrial utilization, Springer, New York.
- Neumann, A., Petit, S., Hofstetter, T.B., 2011. Evaluation of redox-active iron sites in smectites using middle and near infrared spectroscopy. *Geochimica Et Cosmochimica Acta*, 75(9): 2336-2355.
- Nevin, K.P., Lovley, D.R., 2000. Potential for nonenzymatic reduction of Fe(III) via electron shuttling in subsurface sediments. *Environmental Science & Technology*, 34(12): 2472-2478.
- Norrish, K., 1954. The swelling of montmorillonite. *Discussions of the Faraday Society*(18): 120-134.
- Pedersen, K., 2010. Analysis of copper corrosion in compacted bentonite clay as a function of clay density and growth conditions for sulfate-reducing bacteria. *Journal of Applied Microbiology*, 108(3): 1094-1104.
- Rancourt, D.G., Ping, J.Y., 1991. Voigt-based methods for arbitrary-shape static hyperfine parameter distributions in Mössbauer-spectroscopy. *Nuclear Instruments and Methods in Physics Research Section B-Beam Interactions with Materials and Atoms*, 58(1): 85-97.
- Ribeiro, F.R., Fabris, J.D., Kostka, J.E., Komadel, P., Stucki, J.W., 2009. Comparisons of structural iron reduction in smectites by bacteria and dithionite: II. a variable-temperature Mössbauer spectroscopic study of Garfield nontronite. *Pure and Applied Chemistry*, 81(8): 1499-1509.
- RWM, 2016. Geological disposal: generic disposal facility design, RWM, Didcot.

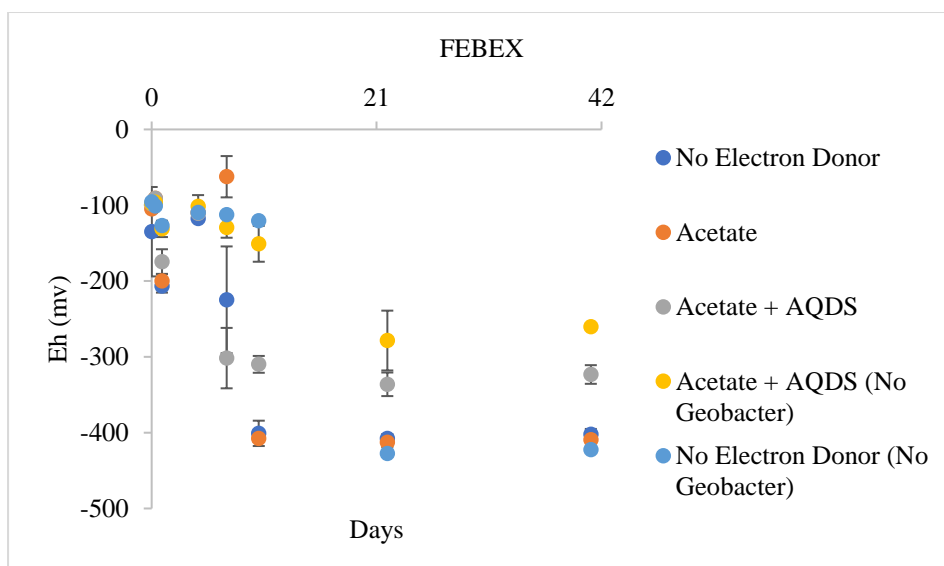
- Sorieul, S., Allard, T., Morin, G., Boizot, B., Calas, G., 2005. Native and artificial radiation-induced defects in montmorillonite. An EPR study. *Physics and Chemistry of Minerals*, 32(1): 1-7.
- Stucki, J.W., Lee, K., Zhang, L.Z., Larson, R.A., 2002. Effects of iron oxidation state on the surface and structural properties of smectites. *Pure and Applied Chemistry*, 74(11): 2145-2158.
- Vantelon, D., Montarges-Pelletier, E., Michot, L.J., Briois, V., Pelletier, M., Thomas, F., 2003. Iron distribution in the octahedral sheet of dioctahedral smectites. an FeK-edge X-ray absorption spectroscopy study. *Physics and Chemistry of Minerals*, 30(1): 44-53.
- Verma, P.K., Pathak, P.N., Mohapatra, P.K., Godbole, S.V., Kadam, R.M., Veligzhanin, A.A., Zubavichus, Y.V., Kalmykov, S.N., 2014. Influences of different environmental parameters on the sorption of trivalent metal ions on bentonite: batch sorption, fluorescence, EXAFS and EPR studies. *Environmental Science-Processes & Impacts*, 16(4): 904-915.
- Verma, P.K., Romanchuk, A.Y., Vlasova, I.E., Krupskaya, V.V., Zakusin, S.V., Sobolev, A.V., Egorov, A.V., Mohapatra, P.K., Kalmlycov, S.N., 2017. Np(V) uptake by bentonite clay: effect of accessory Fe oxides/hydroxides on sorption and speciation. *Applied Geochemistry*, 78: 74-82.
- Zhang, J., Dong, H.L., Liu, D., Agrawal, A., 2013. Microbial reduction of Fe(III) in smectite minerals by thermophilic methanogen *Methanothermobacter thermautotrophicus*. *Geochimica Et Cosmochimica Acta*, 106: 203-215.

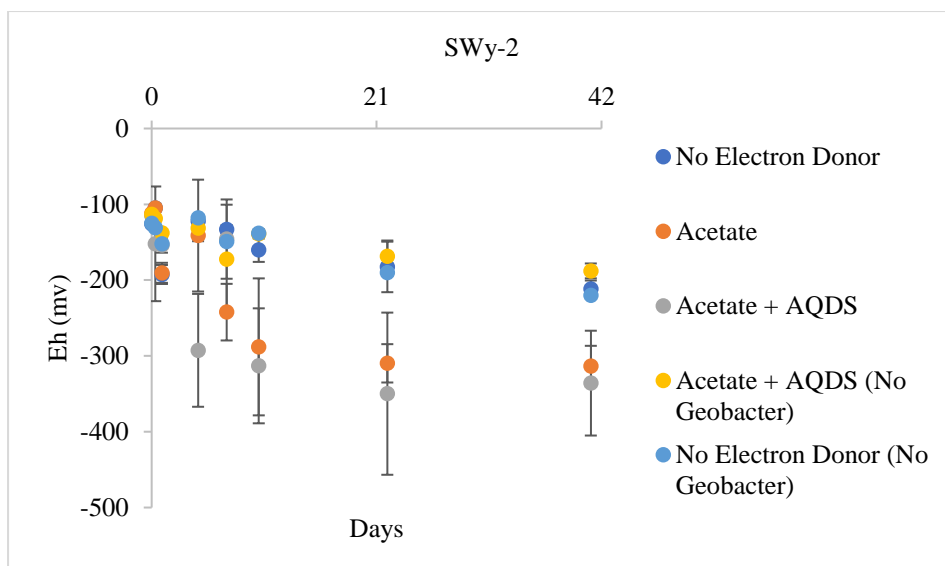
5.10. Supplementary



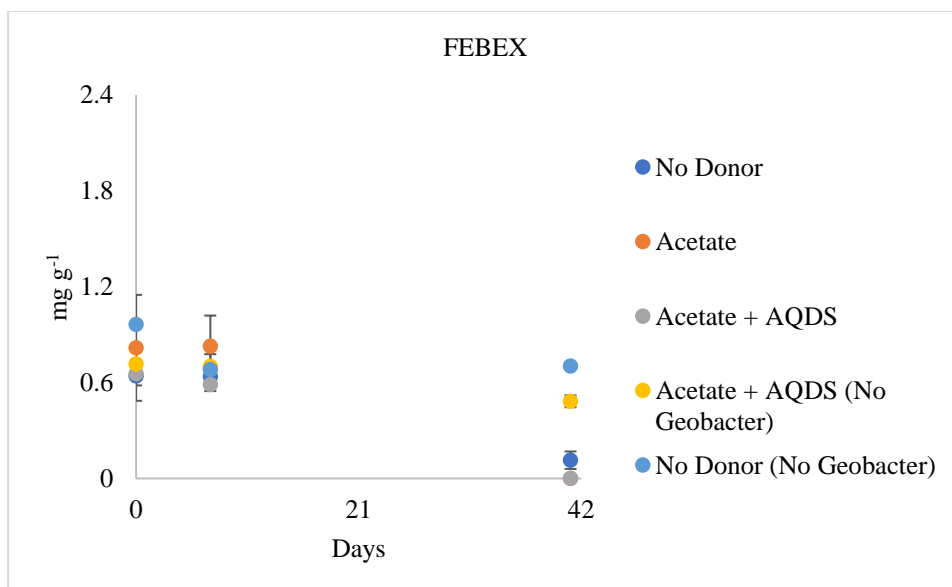


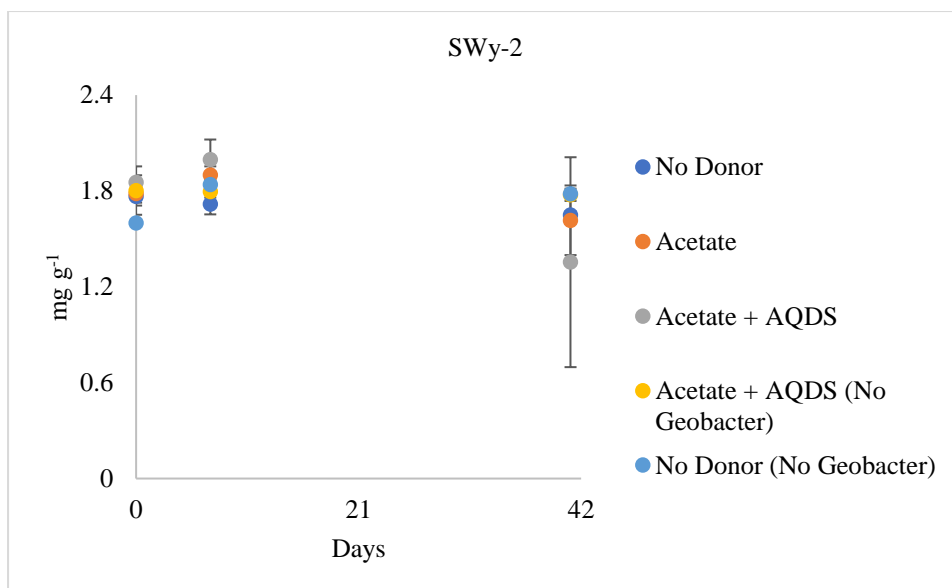
Supplementary 5.1: pH of the FEBEX bentonite, and SWy-2 montmorillonite clay suspensions.



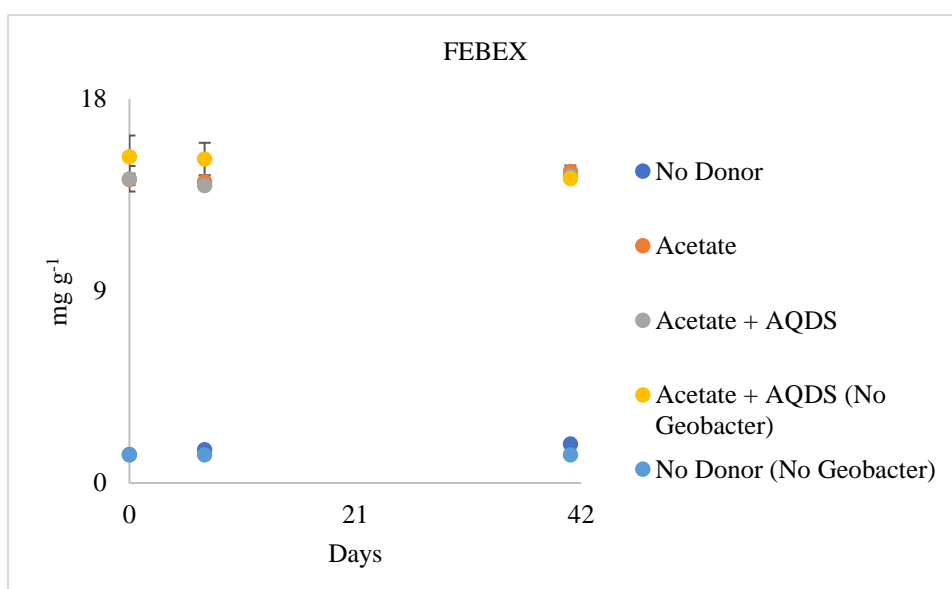


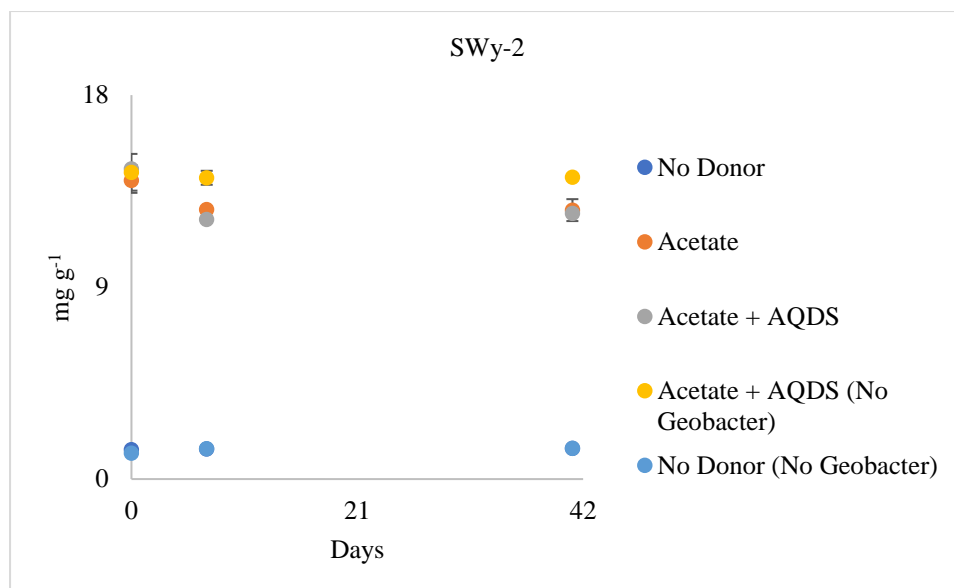
Supplementary 5.2: Eh of the FEBEX bentonite, and SWy-2 montmorillonite clay suspensions.





Supplementary 5.3: Concentration of sulphate in the FEBEX bentonite and SWy-2 montmorillonite clay suspensions.





Supplementary 5.4: Acetate concentrations in the FEBEX bentonite, and SWy-2 montmorillonite clay suspensions.

6. Selenium Speciation in Microbially Reduced SWy-3 Montmorillonite

Haydn M. Haynes^a, Carolyn I. Pearce^b, Jonathan R. Lloyd^a

^a *Williamson Research Centre for Molecular Environmental Science and Research Centre for Radwaste Disposal, School of Earth, Atmospheric and Environmental Sciences, University of Manchester, Manchester, M13 9PL, UK*

^b *Geosciences Group, Pacific Northwest National Laboratory, Richland, WA, 99354, US*

Keywords

Montmorillonite, Fe(III)-reducing bacteria, Selenium, Geological Disposal

6.1. Preface

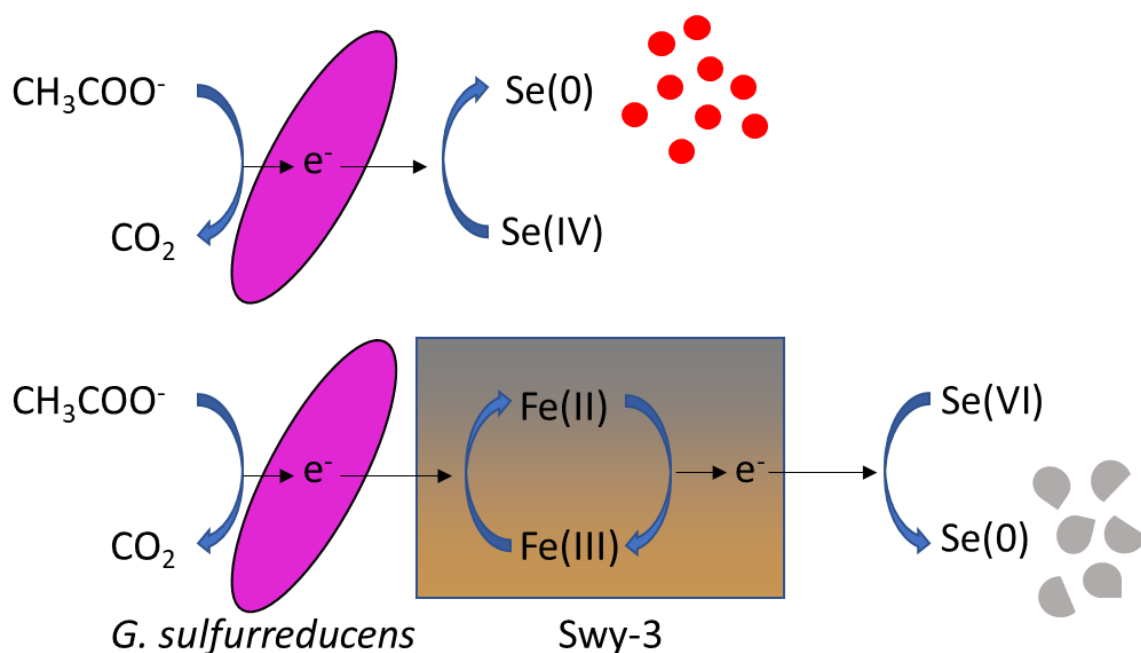
Question: If *Geobacter sulfurreducens* can cause mineralogical transformations in bentonite materials, do these transformations influence the speciation of priority radionuclides (selenium)?

Experimental data in chapter 5 showed that the majority of Fe(III) in SWy-2 montmorillonite was reducible to Fe(II). Other research in the field has shown that the reduction of Fe(III) in montmorillonites, and other smectite minerals is partially, or even fully reversible (Gorski et al., 2013). This reversibility implies that montmorillonite and other smectite minerals in their reduced forms may serve as electron donors. This could potentially be used to reduce redox-active radionuclides in the event of release in a geological disposal facility. We investigated this further using the selenium oxyanions selenite and selenate. Similar to the methodology used in chapter 5, we inoculated SWy-3 montmorillonite with *Geobacter sulfurreducens* and supplemented it with selenite or selenate.

Geobacter sulfurreducens can reduce selenite to elemental selenium, with the product being red nanospheres (Pearce et al., 2009). This was also observed in our experiments. Selenate on the other hand is not reducible by *Geobacter sulfurreducens*, but its removal from solution still occurred. The selenate product was once again elemental selenium. However, this time it was observed in a grey/black crystalline form. This difference in product is consistent with the selenite being reduced microbially by *Geobacter sulfurreducens*, and the selenate by a different process whose workings remain unknown. The most plausible mechanism for the selenate removal is via electron transfer from the reduced SWy-3 montmorillonite. Further research is required to prove that the selenate product is indeed produced by the reduced

montmorillonite. This could be tested via several ways, for instance by chemically reducing the montmorillonite, or pasteurizing the reduced montmorillonite, and introducing the selenium oxyanions afterwards. These results highlight a microbial activity that could be beneficial to a geological disposal facility. The absorption of selenium oxyanions (and other anions) is very poor (Kim et al., 2012), and therefore indirect microbial reduction could offer a plausible mechanism for their immobilization.

6.2. Graphical abstract



6.3. Abstract

Selenium is a toxic element commonly found in nuclear wastes and is typically found in the form of the two oxyanions selenite (SeO_3^{2-}), and selenate (SeO_4^{2-}). In the case of canister failure following the geological disposal of nuclear wastes, bentonite buffers are expected to retard radionuclide transport. However, selenium oxyanions have a low affinity for adsorption to bentonites. The presence of Fe(III)-reducing bacteria in a bentonite buffer may directly (enzymatically) reduce selenium oxyanions, as well as increasing the Fe(II) content of the bentonite providing indirect Fe(II)-mediated reduction mechanisms as well. This experiment investigated the fate of selenium oxyanions in the presence of SWy-3 montmorillonite, and cultures of the Fe(III)-reducing bacterium *G. sulfurreducens*. Selenite reduction occurred concurrently with Fe(III)-reduction forming red elemental selenium

nanospheres approximately 30 nm in size, meanwhile selenate remained in solution for several days before rapid precipitation occurred in most of the *G. sulfurreducens* amended microcosms, producing black subhedral crystallites approximately 150 nm in size. These results suggest that selenite removal occurred via direct enzymatic reduction by *G. sulfurreducens*, but the selenate was likely removed via a chemical reaction with structurally-bound Fe(II) in the SWy-3 montmorillonite. The occurrence of biological Fe(III)-reduction in a bentonite buffer would likely alter the geochemical conditions promoting the reduction, and precipitation of selenium oxyanions. Other redox-active radionuclides such as uranium may exhibit similar behaviors and require further investigation. Along with the impacts on the geological disposal of nuclear waste this may also be of relevance to selenium speciation in the natural environment, and the development of novel techniques to clean-up selenium contaminated land.

6.4. Introduction

The accumulation of radioactive wastes has been occurring in many countries for decades through the production of nuclear power, weapons, medical treatments, and for research purposes. The process of nuclear fission produces a diverse range of radionuclide species with a wide variety of half-lives and chemical properties (RWM, 2016). Amongst these radioactive wastes are high heat generating wastes (HHGW) which contain long-lived radioisotopes, many of which also have a toxicological component (Domingo, 2001). Geological disposal of HHGW is being considered in many countries using a multi-barrier concept comprised of the waste form, a metal canister, a buffer, and the surrounding geological host (SKB, 2006). One material being considered as a buffer in a geological disposal facility (GDF) is the montmorillonite-based material bentonite which has a low permeability, as well as ion exchange, and surface complexation sites which can capture radionuclides (Wilson et al., 2011).

Selenium is a member of the chalcogens, and several stable selenium isotopes are formed by nuclear fission, as well as unstable ^{79}Se which has a half-life of 3.27×10^5 years. Selenium is a sulfur analogue commonly existing in four oxidation states (-2, 0, +4, +6). Under oxidizing conditions, selenium exists as the toxic, and soluble selenate (SeO_4^{2-}), and selenite (SeO_3^{2-}) oxyanions, while under reducing conditions it typically exists as the insoluble, and less toxic elemental selenium ($\text{Se}(0)$), sulfide (S_2Se), metal selenide (FeSe) forms, as well as soluble,

and highly toxic hydrogen selenide (H_2Se) (Orucoglu and Hacıyakupoglu, 2015). Research into selenium interactions with bentonite have mostly focused on the oxyanion forms. The negative interlayer charge associated with bentonites means they have limited adsorption capacity for selenium oxyanions (Kim et al., 2012). Selenate shows minimal adsorption to bentonite (Loffredo et al., 2011), meanwhile the limited sorption capacity that bentonite displays for selenite, appears to be dominated by surface complexes (H_2SeO_3) at pH 5-7, and by ternary surface complexes with Ca^{2+} , and Mg^{2+} above pH 7 (Montavon et al., 2009). Attempts to improve the adsorption capacity of selenium have focused on modifying the bentonite with zero valent iron (Li et al., 2015), aluminium oxocations (Wang et al., 2015), and other specialist cations (Orucoglu and Hacıyakupoglu, 2015). Such strategies while useful in the treatment of effluents, and contaminated land, would be expensive, and difficult to implement in a geological disposal environment, due to the large amount of bentonite required. For example, an underground research laboratory (URL) experiment aimed at assessing the technical feasibility, and behavior of a geological disposal facility (GDF) used 115.7 tonnes of bentonite in a single disposal gallery (Fuentes-Cantillana et al., 2000).

Bentonites have been shown to support a range of microbial cells and spores (Lopez-Fernandez et al., 2015), some of which can persist under simulated geological disposal conditions (Pedersen, 2010). Many groups of bacteria have been shown to reduce selenium oxyanions, whether it be a pathway for detoxification, or as a source for energy, and growth (Eswayah et al., 2016); SRB partially reduce selenium using sulfate-reduction pathways (Tomei et al., 1995). The transformation of selenite into elemental selenium has been observed in cultures of *Geobacter sulfurreducens*, with some further reduction to selenide occurring in the presence of AQDS (Pearce et al., 2009). The elemental product of selenite-respiring bacteria is typically homogenous, red $\text{Se}(0)$ nanospheres, arranged into monoclinic crystalline structures (Oremland et al., 2004). Bacterial selenate reduction is less documented, but has been observed with *Enterobacter cloacae*, and a few other species, with the product being selenite (Yee et al., 2007). As well as the potential for direct biological reduction of selenium oxyanions there may also be indirect reactions that can immobilize selenium. Fe(III)-reducing bacteria have been shown to reduce selenate indirectly using humic acids (Lovley et al., 1999). *G. sulfurreducens* can also reduce structural Fe(III) in bentonites to Fe(II) (Chapter 5), which can influence the physical, and chemical properties of bentonites (Stucki et al., 2002). Structurally bound Fe(II) in smectite minerals has also been shown to reduce a number of environmental contaminants including nitroaromatic compounds

(Hofstetter et al., 2003), pertechnetate ions (Bishop et al., 2011), and polychlorinated ethanes (Neumann et al., 2009). While the reduction of selenium oxyanions by structural Fe(II) in smectite minerals has not been documented several studies have shown selenium oxyanions can be reduced by Fe(II)-bearing minerals such as green rust (Borsig et al., 2018).

Instead of investigating costly modification strategies to improve the sorption of selenium oxyanions to bentonites, this paper investigates the impact of microbial Fe(III)-reduction in bentonites (Chapter 5) on selenium oxyanion sequestration, as well as the potential for biomineralisation of these contaminants (Zannoni et al., 2008). The identification of microbially-driven selenium oxyanion immobilization would build confidence in a geological disposal safety case, by showing selenium species will not be mobile in the event of canister failure. This study examined the interactions between SWy-3 montmorillonite, *Geobacter sulfurreducens*, and selenium oxyanions. *G. sulfurreducens* was chosen for this work after previous research highlighted its ability to reduce structural Fe(III) in SWy-2 (Chapter 5), as well as undertaking direct, and indirect reactions with selenite oxyanions (Pearce et al., 2009). Direct reduction of selenate oxyanions by *G. sulfurreducens* has not been reported. However, based on the literature cited it was hypothesized that microbially reduced structurally bound Fe(II) in bentonites may be able to reduce selenate oxyanions, in a similar manner to humic acid-mediated selenate reduction (Lovley et al., 1999). This chapter investigated the reduction of selenite, and selenate in the presence of SWy-3 montmorillonite, and *Geobacter sulfurreducens*. Results from this study indicated that both selenium oxyanions were reduced to insoluble elemental selenium forms. The selenite oxyanions appeared to be reduced by direct interactions with the *G. sulfurreducens* cells, while the selenate oxyanions appeared to be reduced indirectly by the reduced SWy-3 montmorillonite.

6.5. Materials and methods

6.5.1. Experiment preparation

6.5.1.1. Material selection

This study investigated the speciation of selenite, and selenate, in the presence of the source clay SWy-3 montmorillonite (Van Olphen and Fripiat, 1979), and *Geobacter sulfurreducens* cells. The SWy-3 sodium montmorillonite was bought from the Clay Minerals Society

(Chantilly, VA, USA) having been excavated in Wyoming, USA. The SWy-3 montmorillonite arrived in powdered form and received no treatment before adding to the microcosms.

6.5.1.2. *Geobacter sulfurreducens* culture preparation

Geobacter sulfurreducens cells (Caccavo et al., 1994) were prepared by adding 10 ml of early stationary cells to 90 ml of sterile NBAF medium containing 20 mM of sodium acetate (electron donor), and 40 mM of fumarate (electron acceptor) (Cutting et al., 2012) in a serum bottle. The NBAF medium was adjusted to a pH of 7 using 10 M sodium hydroxide, and was flushed with nitrogen, and carbon dioxide prior to use. The serum bottle was incubated in the dark at 30 °C for 48 hours, to allow the *G. sulfurreducens* culture to grow. After 48 hours the *G. sulfurreducens* starter culture was transferred into 900 ml of sterile NBAF medium in an anaerobic cabinet (Coylab, Grass Lake, MI, USA), and left to grow for a further 48 hours at 30 °C. The *G. sulfurreducens* containing NBAF medium was transferred into a set of centrifuge tubes under a flow of filter-sterilized nitrogen gas. The *G. sulfurreducens* cells were centrifuged for 20 minutes (4920 g, 4 °C) before the supernatant was discarded; this step was repeated before concentrating the cells in a single tube. Once in a single tube the cells were washed in sterile, anaerobic 30 mM MOPS solution twice, before re-suspension in 50 ml of the 30 mM MOPS in a sterile serum bottle. The optical density (OD_{600nm}) of the cell suspension was determined using a Jenway (Stone, UK) spectrophotometer.

6.5.1.3. Clay suspension preparation

Serum bottles were prepared by washing them in a 5% nitric acid bath for 24 hours, before rinsing them with deionized water (18.2 MΩ). A total of five treatments were set up to monitor the fate of the selenium species, including no cell, no clay, and no donor treatments consisting of 30 mM MOPS, as well as acetate-amended, and autoclaved (sterile) treatments containing 30 mM MOPS, and 10 mM sodium acetate. These media were supplemented further with either 0.12 mM sodium selenate, or 0.12 mM sodium selenite. After the addition of the selenium species, and autoclaving (126 °C, 20 mins), 0.2 g (2 g l⁻¹) of SWy-3 montmorillonite was added to the serum bottles (except for the no clay treatment) in an anaerobic chamber (Coylab, Grass Lake, MI, USA), the autoclave treatment bottles were once again autoclaved, and finally the *G. sulfurreducens* cell suspension was added to the no

donor, and acetate treatments using a sterile nitrogen flushed syringe. The serum bottles were stored at 20 °C and examined over a 21-day period.

6.5.2. Analytical Methods

6.5.2.1. X-ray Diffraction (XRD)

The SWy-3 montmorillonite was characterized using XRD. A 0.1 sample of the SWy-3 montmorillonite was ground with a pestle, and mortar, and dispersed in amyl acetate, before mounting onto a low background sample holder. The sample was analyzed using a Bruker (Billerica, MA, USA) D8 Advance diffractometer using a CuK α radiation source with a 1.5406 Å wavelength. The step size during the analysis was 0.02° 2 θ with a counting time of 0.02 s per step, using a 2 θ range of 5-70°. The pattern generated was fitted using a search/match routine (EVA software program version 4 (Bruker, Billerica, MA, USA)), and the peaks were matched to standards in the ICDD (International Centre for Diffraction Data) database.

6.5.2.2. Brunauer-Emmett-Teller (BET) surface analysis

The surface area of the SWy-3 montmorillonite was calculated using nitrogen adsorption at -196 °C. A 0.2 g sample of the montmorillonite was heated to 100 °C and purged under a constant flow of nitrogen for 18 hours before analysis (Micrometrics (Norcross, GA, USA) Flowprep 060).

6.5.2.3. X-ray Fluorescence (XRF), H₂O, and loss on ignition (LOI)

Elemental composition of the SWy-3 montmorillonite was determined using XRF. A 12 g sample of the montmorillonite was mixed with 3 g of fine powdered wax and milled for 7 min at 350 rpm using a TEMA (Woodford Halse, UK) mill, before being pressed into a pellet at 10 tonnes. The water content was determined by heating a 1 g sample of the montmorillonite at 105 °C for an hour before cooling in a desiccator and reweighing the sample. The carbon content of the sample was then determined by returning the sample to a furnace and heating at 1100 °C before being cooled in a desiccator, and reweighed.

6.5.2.4. Ferrozine assay

The amount of 0.5 M hydrochloric acid extractable Fe(II), and total Fe in the starting material, and the microcosms was determined using Ferrozine assay (Lovley and Phillips, 1987). The Ferrozine solution was prepared by adding 0.5 g of Ferrozine, and 5.98 g of HEPES to 500 ml of deionized water (18.2 MΩ), before adjusting the solution to pH 7 using 10 M sodium hydroxide. For the starting material, a 0.2 g sample was dispersed in 0.5 M hydrochloric acid, and mixed for an hour, while in the clay suspensions a 1 ml aliquot of slurry was removed from each of the clay suspensions at each time-point using a nitrogen flushed sterile syringe. In both cases a subaliquot of the slurries (20 µl) were added to 980 µl of 0.5 M hydrochloric acid to establish the amount of bioavailable Fe(II) present in the samples. A further 20 µl subaliquot was treated with 980 µl of 0.25 M hydroxylamine hydrochloride dissolved in 0.5 M hydrochloric acid to determine the total bioavailable iron. After an hour of periodic shaking the solutions were centrifuged (16,162 g, 5 mins) to remove any solid from the solution before 80 µl of supernatant was added to 920 µl of Ferrozine solution. The samples were measured on a spectrophotometer (Jenway, Stone, UK) at 562 nm (Stookey, 1970) before comparison to a calibration curve made up of iron sulphate standards in 0.5 M hydrochloric acid.

6.5.2.5. Ion Chromatography (IC), pH and Eh

The pH of the starting material was analyzed, along with the clay suspensions at each time-point. In the case of the clay suspensions the remainder of the slurry extracted for the Ferrozine assay was centrifuged (16162, 5 mins), and the pH checked with a pH probe (Denver Instrument (Sartorius, Göttingen, Germany) calibrated with pH 4 and pH 7 standards, as well as the Eh with an Eh probe calibrated using a 220 mV standard (Denver Instrument (Sartorius, Göttingen, Germany)). For the starting material a 0.2 g portion of the SWy-3 was dispersed in 5 ml of deionized water (18.2 MΩ) and allowed to equilibrate for an hour. The slurry was then centrifuged (16162 g, 5 mins), and the pH checked with a pH probe (Denver Instrument (Sartorius, Göttingen, Germany)) using the same standards as before. The supernatants in both cases were also analyzed for sulphate and acetate using IC. A 50 µl aliquot of the clay suspension supernatant was diluted in 950 µl of deionized water (18.2 MΩ), and 250 µl of the starting material supernatant was diluted in 750 µl of deionized water (18.2 MΩ) before both were analyzed using a Dionex (Sunnyvale, CA, USA) ICS5000.

6.5.2.6. Inductively Coupled Plasma Atomic Emission Spectroscopy (ICP-AES)

The concentration of key interlayer cations (sodium, potassium, magnesium, calcium), key montmorillonite constituents (silicon, iron, aluminium), as well as selenium were determined in the solid starting material, and in the clay suspension supernatants using ICP-AES. A 1 g sample of the starting material was added to 5 ml of 1 M ammonium acetate and left to equilibrate on a shaker for 24 hours. A further 5 ml of ammonium acetate was added to the starting material, and the supernatant recovered using vacuum filtration (Chapman, 1965). For the clay suspensions supernatant collected for IC analyses was also used for ICP-AES. In both cases 500 μ l of supernatant was added to 9.5 ml of 2.2 % nitric acid and analyzed using a Perkin-Elmer Optima 5300 Dual View (Waltham, MA, USA) ICP-AES.

6.5.2.7. Transmission Electron Microscopy (TEM), and Energy Dispersive X-ray Spectroscopy (EDS)

The fate of selenium in the reduced samples was tracked using TEM. A 1 ml aliquot was removed from acetate, and *G. sulfurreducens* treated selenite, and selenate clay suspensions on day 21 using a nitrogen flushed syringe, and centrifuged (16162, 5 mins). The supernatant was discarded, and the solid was dispersed in 800 μ l of deionized water (18.2 M Ω) before a further ten-fold dilution in deionized water (18.2 M Ω). A 1.3 μ l aliquot of the diluted samples were deposited on carbon coated copper TEM grids (Agar Scientific (Stansted, UK)) using a pipette. The copper grids were examined using a FEI (Hillsboro, OR, USA) TF30 FEG TEM operating at 300 kV, and EDS spectra were generated using an Oxford (Abingdon, UK) XMax EDS detector, and analyzed using Oxford (Abingdon, UK) INCA software.

6.6. Results

6.6.1. Material characterization

A series of analyses were conducted on the SWy-3 montmorillonite to determine key physical, and chemical properties (Table 6.1). XRD showed that the material was mostly montmorillonite, with some minor amounts of quartz impurities (Table 6.1). The montmorillonite had a water content of 9.7 % and had a similar percentage of carbon (9.5 %) as determined by LOI (Table 6.1). The pH of the montmorillonite was mildly alkaline (8.7), and the total iron content was 23.5 mg g⁻¹ (2.4 %) (Table 6.1).

Table 6.1: Physical and chemical characteristics of the SWy-3 montmorillonite including water content, loss on ignition, pH, surface area (SA), key interlayer cations (sodium, calcium, potassium, magnesium), sulphate, 0.5 M hydrochloric acid extractable Fe(II), as well as the mineralogy.

Sample	SWy-3
H ₂ O (%)	9.7
LOI (%)	9.5
pH	8.7
SA (m ² g ⁻¹)	29.0 ± 0.2
Na ⁺ (mg g ⁻¹)	> 5.7
Ca ²⁺ (mg g ⁻¹)	5.1
K ⁺ (mg g ⁻¹)	0.3
Mg ²⁺ (mg g ⁻¹)	1.5
SO ₄ ²⁻ (mg g ⁻¹)	8.1
Fe (mg g ⁻¹)	23.5
0.5 M HCl extractable Fe(II) (mg g ⁻¹)	0.9
Mineralogy (XRD)	Montmorillonite, Quartz

6.6.2. Selenite removal

Selenium removal from solution in the clay suspensions was determined using ICP-AES. Selenite was completely removed from solution in all the *G. sulfurreducens* amended clay suspensions, taking 3 days in the acetate amended microcosms, and 21 days in the no donor microcosms (Figure 6.1). The disappearance of selenium from the selenite and acetate-amended cultures coincided with the formation of red particles in solution. Minor amounts of selenium removal were reported in the other clay suspensions (<0.7 mg l⁻¹) (Figure 6.1). Selenite removal coincided with an increase in 0.5 M hydrochloric acid extractable Fe(II) from 0.34 mg g⁻¹ to 2.71 mg g⁻¹ in the acetate clay suspensions amended with *G. sulfurreducens*, while an increase from 0.24 mg g⁻¹ to 1.46 mg g⁻¹ was observed in the no donor clay suspensions amended with *G. sulfurreducens* (Figure 6.1). The concentration of 0.5 M hydrochloric acid extractable Fe(II) remained constant in the rest of the clay suspensions (Figure 6.1). The pH of the clay suspensions remained circumneutral over the course of the experiment (Supplementary 6.1). Eh in the clay suspensions was between -100 and 0 mV with a decrease to -180 mV by day 14 in the acetate clay suspensions amended with *G. sulfurreducens* (Supplementary 6.1). No sulfate-removal was observed in any of the clay suspensions during the experiment (Supplementary 6.1). Acetate levels remained

constant in all the clay suspensions apart from in the acetate clay suspensions amended with *G. sulfurreducens* which decreased from 38.0 mg g⁻¹ to 32.6 mg g⁻¹ (Supplementary 6.1). The insoluble selenium product was identified in the selenite-amended cultures using TEM, and consisted of spherical deposits, approximately 30 nm in size, with no apparent internal structure (Figure 6.2). EDS spectra collected from the same area consisted mostly of selenium, and copper, with minor amounts of carbon, oxygen, cobalt, silicon, sulphur, calcium, and iron observed (Figure 6.2).

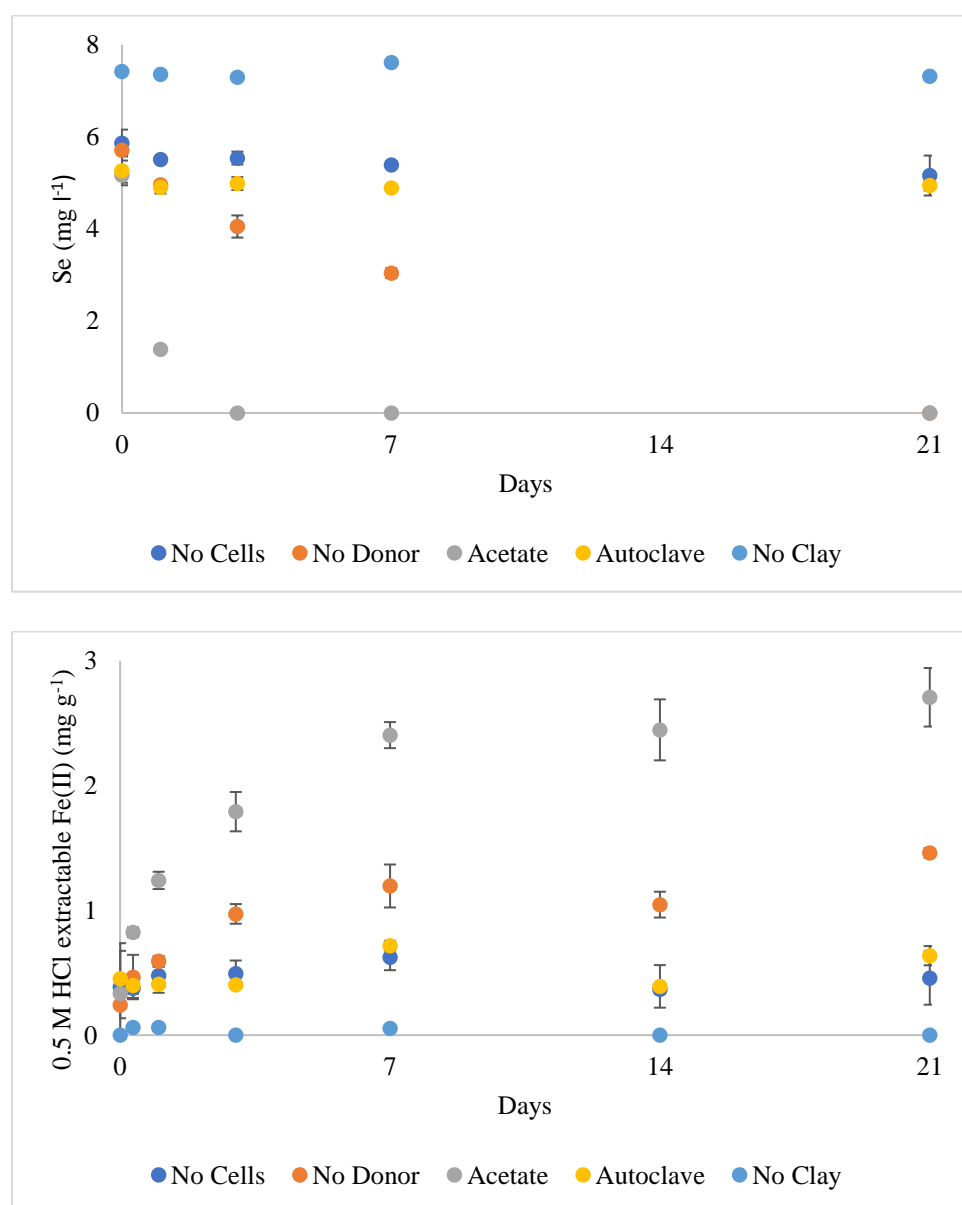


Figure 6.1: The amount of soluble selenium, and 0.5 M hydrochloric acid extractable Fe(II) present in the selenite clay suspensions.

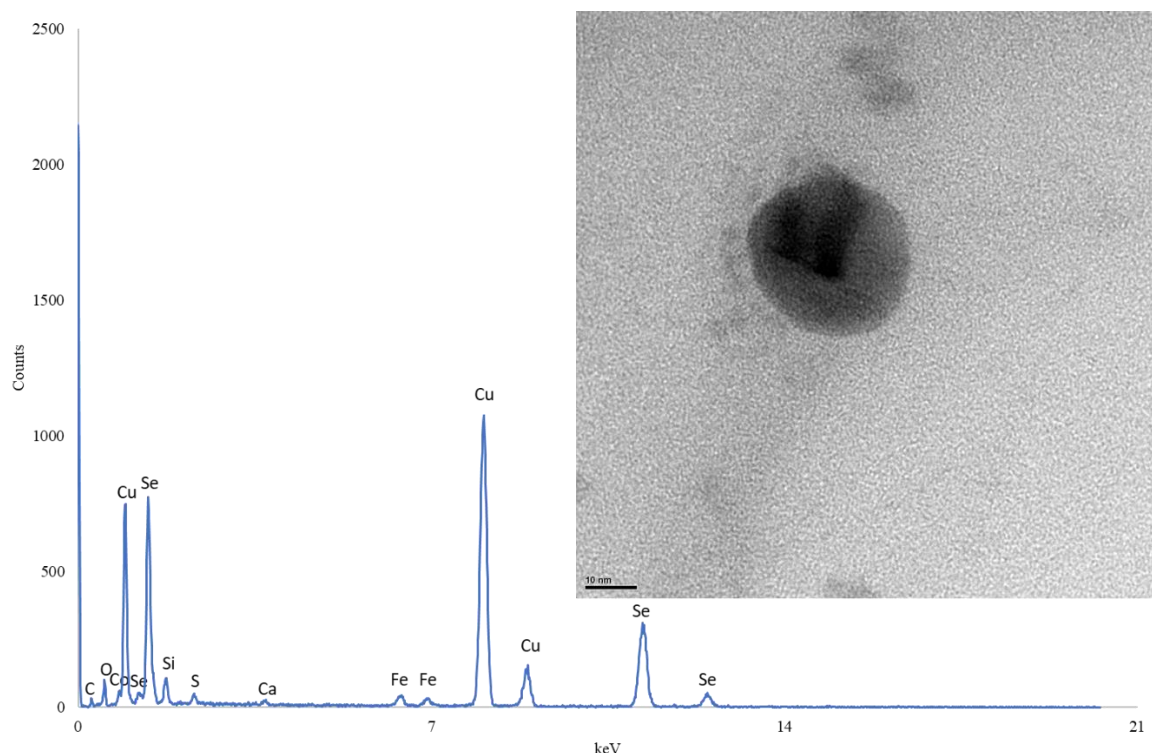
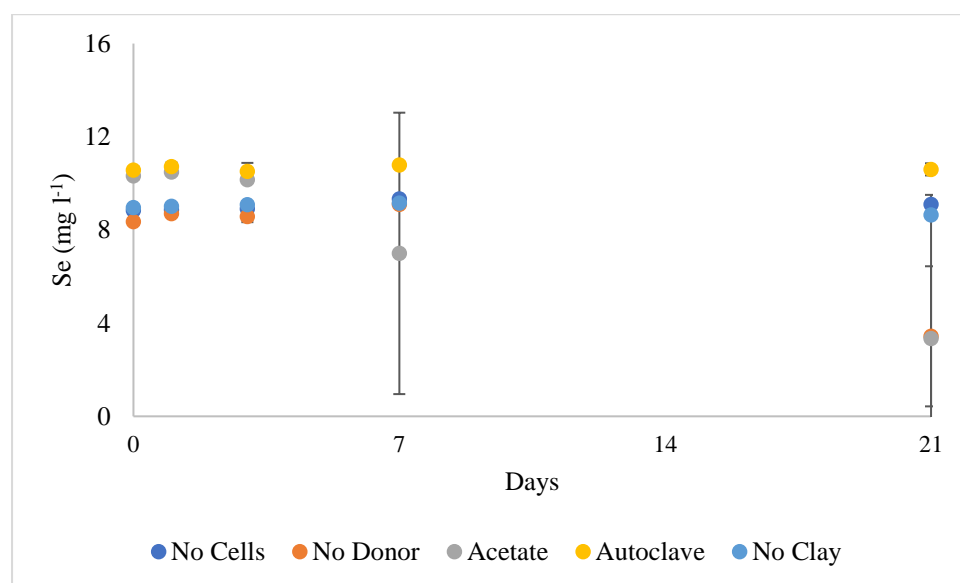


Figure 6.2: TEM image of the selenium phase in the acetate, and *G. sulfurreducens* amended selenite clay suspensions, along with the EDS spectra for the associated area.

6.6.3. Selenate removal

Unlike the selenite experiments no selenium removal from solution was detected in the selenate experiments during the first 4 days (Figure 6.3). After this period, the biogeochemistry of the different replicates diverged. In the acetate and *G. sulfurreducens* amended clay suspensions, complete removal of selenium in solution was observed in a single replicate suspension by day 7, followed by another of the triplicate suspensions at day 21 (Figure 6.3). The other acetate and *G. sulfurreducens* clay suspension showed no removal of selenium from solution over the course of the experiment (Figure 6.3). Full removal of selenium from solution was also observed in a no added electron donor clay suspension amended with *G. sulfurreducens* by day 21, with partial removal (~40%) in the other two no donor clay suspensions amended with *G. sulfurreducens* (Figure 6.3). The removal of selenate from solution coincided with an increase in black/grey particles in solution. None of the other selenate clay suspensions displayed signs of selenium removal from solution (Figure 6.3). The concentration of 0.5 M hydrochloric acid extractable Fe(II) in the selenate clay suspensions was initially ~0.43 mg g⁻¹, apart from in the no clay treatment which remained below detection (< 0.06 mg g⁻¹) (Figure 6.3). Increases in 0.5 M hydrochloric acid

extractable Fe(II) over 21 days were observed in the no donor clay suspensions, amended with *G. sulfurreducens*, and acetate clay suspensions, amended with *G. sulfurreducens* to 1.44 mg g⁻¹, and 2.80 mg g⁻¹ respectively (Figure 6.3). No enrichment in 0.5 M hydrochloric acid extractable Fe(II) was observed in any of the other selenate clay suspensions (Figure 6.3). The pH of the selenate clay suspensions remained circumneutral over the course of the experiment (Supplementary 6.2). The Eh of the microcosms was between -100 mV and 0 mV but decreased to -180 mV in the acetate microcosms amended with *G. sulfurreducens* after 14 days (Supplementary 6.2). Sulfate concentrations in all the clay suspensions remained constant over the course of the experiment (Supplementary 6.2). Acetate also remained constant in the clay suspensions apart from in the acetate clay suspensions amended with *G. sulfurreducens* which saw a decrease from 36.2 mg g⁻¹ to 33.2 mg g⁻¹ (Supplementary 6.2). Analysis of the selenium precipitates using TEM showed they had a subhedral texture and were approximately 150 nm in size (Figure 6.4). Analysis of the crystallites using EDS showed a strong selenium, and copper signal, with minor amounts of carbon, oxygen, cobalt, silicon, sulphur (Figure 6.4).



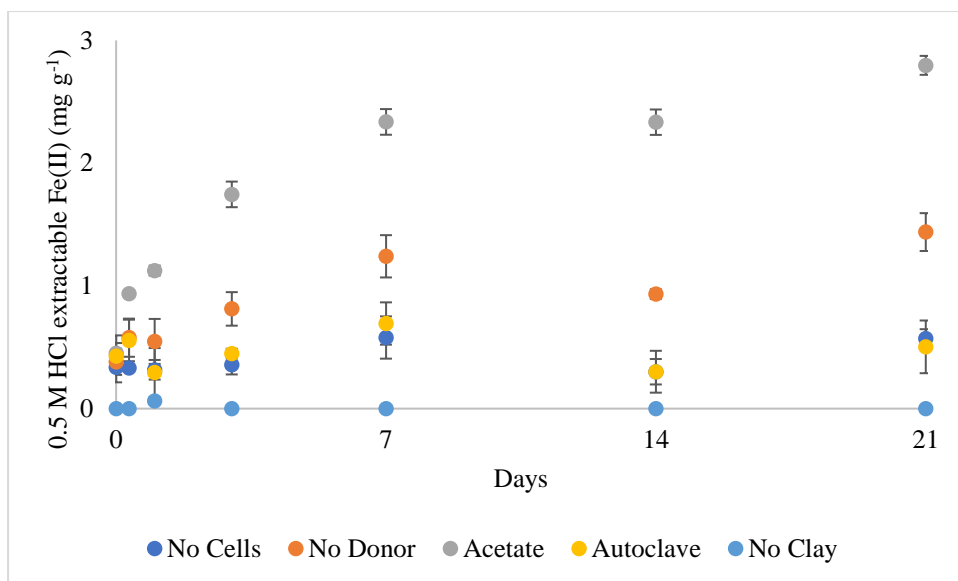


Figure 6.3: The concentration of soluble selenium, and 0.5 M hydrochloric acid extractable Fe(II) in the selenate clay suspensions.

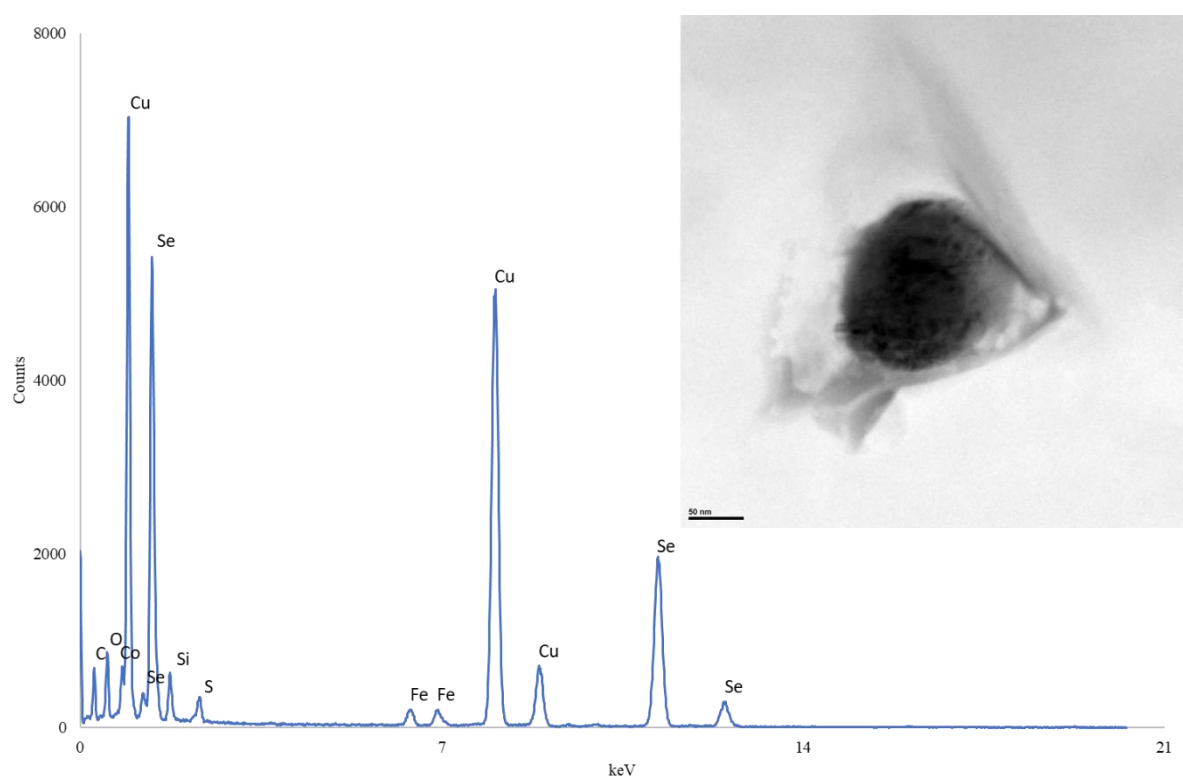


Figure 6.4: TEM image of the selenium product in the acetate, and *G. sulfurreducens* amended Se(VI) microcosms, as well as the EDS spectra for the associated area.

6.7. Discussion

Selenium is a component of radioactive wastes and under oxic conditions exists as the selenite (SeO_3^{2-}), and selenate oxyanions (SeO_4^{2-}). In the presence of SWy-3 montmorillonite, and the Fe(III)-reducing bacterium *G. sulfurreducens* selenite was reduced to red nanospheres approximately 30 nm in size (Figure 6.2). The EDS spectra was mostly comprised of copper (from the TEM grid) as well as selenium, and minor amounts of other elements, that could be attributed to phases close to the nanoparticles or the TEM grid itself (Figure 6.2). The lack of other strong elemental signals in the EDS spectra suggests the nanospheres were pure selenium. Red elemental selenium nanospheres are a product of biological selenite-reduction by *G. sulfurreducens* (Pearce et al., 2009), which suggests direct biological reduction was responsible for selenium removal from solution. Unlike the selenite microcosms the removal of selenate from solution was not concurrent with Fe(III)-reduction confirming previous studies that have shown *G. sulfurreducens* can only reduce selenate in the presence of an electron shuttle (Lovley et al., 1999). However, selenate removal from solution was observed after 7 to 21 days in most of the experimental cultures amended with *G. sulfurreducens*, but not all of them (Figure 6.3). It is unclear what the mechanism behind the selenate removal from solution was, but the product was crystalline (Figure 6.4) with the EDS spectra suggesting it was once again pure elemental selenium (Figure 6.4). Although the electron transfer process here remains obscure, a possible mechanism could be the transfer of electrons from Fe(II) in the reduced montmorillonite to the selenate oxyanions. This has not been demonstrated for selenate before, but other oxyanion contaminants such as pertechnetate (TcO_4^-) display this behavior (Bishop et al., 2011), and selenate is also known to be reduced via Fe(II) minerals (Borsig et al., 2018). It is not clear why this process was not reproducible across all the *G. sulfurreducens* microcosms but may have been due to heterogeneity in the cell cultures or SWy-3 montmorillonite. The selenium oxyanion solubility appeared to be unaffected by the presence of the SWy-3 montmorillonite as observed in previous selenium studies (Loffredo et al., 2011; Montavon et al., 2009), meaning any selenium removal from solution must have been the result of a direct interaction with *G. sulfurreducens*, or as a result of Fe(III)-reduction in the SWy-3 montmorillonite. Fe(III)-reduction in both selenium systems occurred at comparable rates to that seen in Chapter 5 suggesting no toxicological effects were noted at the selenium concentration used (0.12 mM). Fe(III)-reduction was also observed in the no donor microcosms amended with *G. sulfurreducens*, this is likely due to a reducing potential (reduced co-factors) present in the *G. sulfurreducens* cells. Sulphate-reduction in the microcosms was not noted (Supplementary 6.1, Supplementary 6.2), even in

the acetate microcosms amended with *G. sulfurreducens* despite a significant amount of acetate remaining in the system (Supplementary 6.1, Supplementary 6.2). The excess acetate would be expected to promote sulfate-reducing activity as seen in Chapter 5. However, the presence of the selenium oxyanions may have interfered with the metabolic pathways of the indigenous sulfate-reducing bacteria (Tomei et al., 1995).

6.8. Conclusions

The fate of selenium oxyanions in a montmorillonite subjected to biological Fe(III)-reduction was investigated. The selenium oxyanions displayed no signs of removal from solution in the presence of the SWy-3 montmorillonite when *G. sulfurreducens* was not present. If a high enough bentonite density is used the transport of selenium will be restricted to diffusion processes (Wilson et al., 2011). However, if a flow regime develops (due to bentonite erosion etc.) it is unlikely selenium oxyanions will be captured in the bentonite buffer unless microbial activity is occurring. In the presence of *G. sulfurreducens* the selenite was reduced to amorphous, red elemental selenium nanoparticles (~ 30 nm), meanwhile the selenate was reduced to grey/black crystalline elemental selenium approximately 150 nm in size. The removal of selenite occurred at a similar rate to Fe(III)-reduction, and the formation of red elemental selenium nanoparticles suggest that direct-enzymatic reduction by *G. sulfurreducens* was occurring. Despite *G. sulfurreducens* being unable to reduce selenate, its removal occurred rapidly at either the day 7, or day 21 timepoints in the presence of SWy-3 montmorillonite. The delay in selenate removal followed by its precipitation in a crystalline form suggests chemical reduction had taken place, likely due to an electron-transfer process mediated by the reduced SWy-3 montmorillonite. The inconsistency of selenate removal between microcosms suggests there is heterogeneity in the cell culture or the SWy-3 montmorillonite, and further research is required. Along with examining the mechanism of selenate removal follow up analyses on the products are required to confirm their identity, such as X-ray absorption spectroscopy which would confirm the oxidation state of the selenium and provide information on the local bonding environment.

Overall the research shows that biological Fe(III)-reduction in bentonite may have beneficial properties when it comes to the retention of directly, and indirectly-reducible soluble radionuclide species such as selenium oxyanions. In the case of canister failure in a geological disposal environment a reduced bentonite would be expected to retard the

transport of oxyanions that are not typically adsorbed by montmorillonite-based materials, and therefore reduce the mobility of selenium in a repository. However, further study is required to understand the long-term stability of the elemental selenium particles, as well as their susceptibility to reoxidation. The investigation of other redox-active priority radionuclides such as uranium in the presence of reduced montmorillonite-based materials should also be considered. Outside of geological disposal this research may also be of relevance to the behavior of selenium in the natural environment, and fluids supplemented with montmorillonite, and slow release electron donors (Newsome et al., 2017) could also provide a novel method of treating selenium contaminated land.

6.9. Acknowledgements

The authors would like to thank Radioactive Waste Management for financial support, via a PhD bursary. Assistance with XRD and BET analyses were provided by John Waters, Heath Bagshaw provided help with the TEM and EDS work, Alastair Bewsher ran the IC and LOI samples, and Paul Lythgoe conducted the ICP-AES, and XRF analysis.

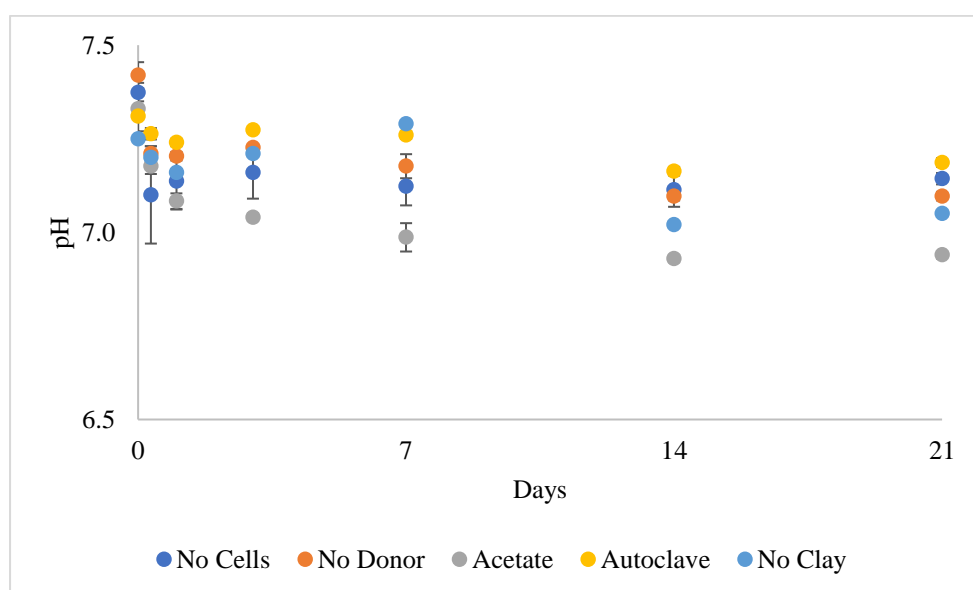
6.10. References

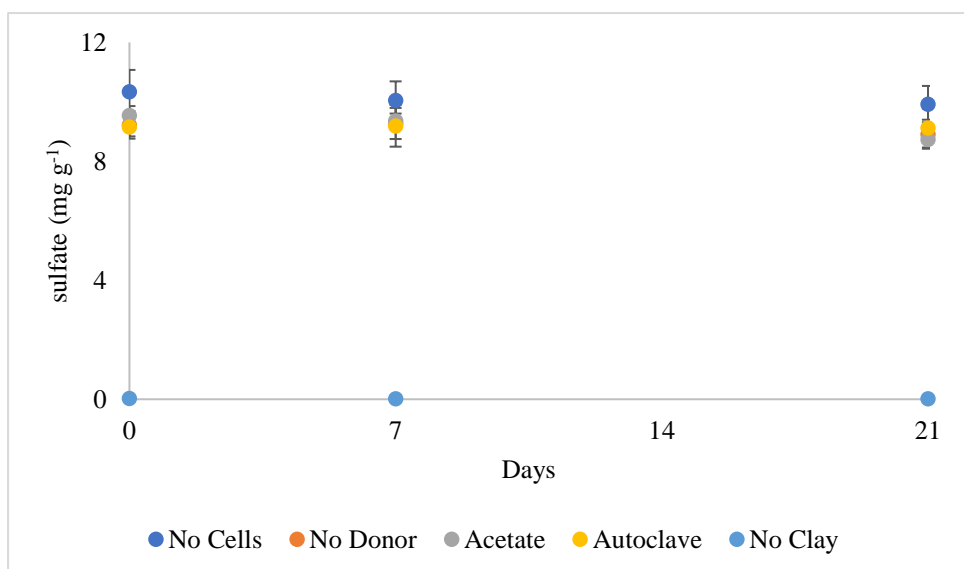
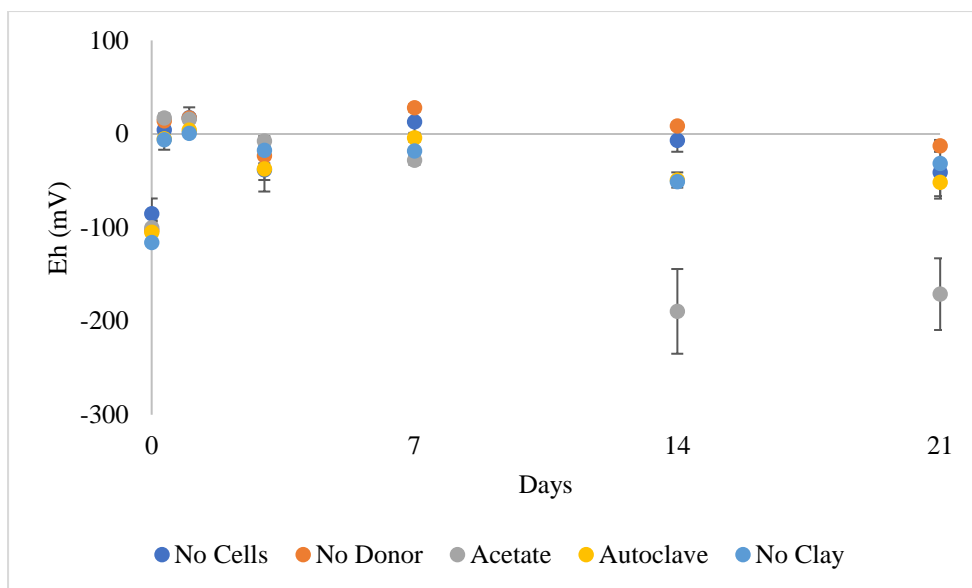
- Bishop, M.E., Dong, H.L., Kukkadapu, R.K., Liu, C.X., Edelman, R.E., 2011. Bioreduction of Fe-bearing clay minerals and their reactivity toward pertechnetate (Tc-99). *Geochimica Et Cosmochimica Acta*, 75(18): 5229-5246.
- Borsig, N., Scheinost, A.C., Shaw, S., Schild, D., Neumann, T., 2018. Retention and multiphase transformation of selenium oxyanions during the formation of magnetite via iron(II) hydroxide and green rust. *Dalton Transactions*, 47(32): 11002-11015.
- Caccavo, F., Lonergan, D.J., Lovley, D.R., Davis, M., Stolz, J.F., McInerney, M.J., 1994. *Geobacter sulfurreducens* sp-nov, a hydrogen-oxidizing and acetate-oxidizing dissimilatory metal-reducing microorganism. *Applied and Environmental Microbiology*, 60(10): 3752-3759.
- Chapman, H.D., 1965. Cation exchange capacity. *Methods of Soil Analysis Part 2*, 9. American Institute of Agronomy, Madison, Wisconsin.
- Cutting, R.S., Coker, V.S., Telling, N.D., Kimber, R.L., van der Laan, G., Patrick, R.A.D., Vaughan, D.J., Arenholz, E., Lloyd, J.R., 2012. Microbial reduction of arsenic-doped schwertmannite by *Geobacter sulfurreducens*. *Environmental Science & Technology*, 46(22): 12591-12599.
- Domingo, J.L., 2001. Reproductive and developmental toxicity of natural and depleted uranium: a review. *Reproductive Toxicology*, 15(6): 603-609.
- Eswayah, A.S., Smith, T.J., Gardiner, P.H.E., 2016. Microbial transformations of selenium species of relevance to bioremediation. *Applied and Environmental Microbiology*, 82(16): 4848-4859.
- Fuentes-Cantillana, J.L., Garcia-Sineriz, J.L., Franco, J.J., Obis, J., Perez, A., 2000. FEBEX project: full-scale engineered barriers experiment for a deep geological repository for high-level radioactive waste in crystalline host rock, CIEMAT, Madrid.

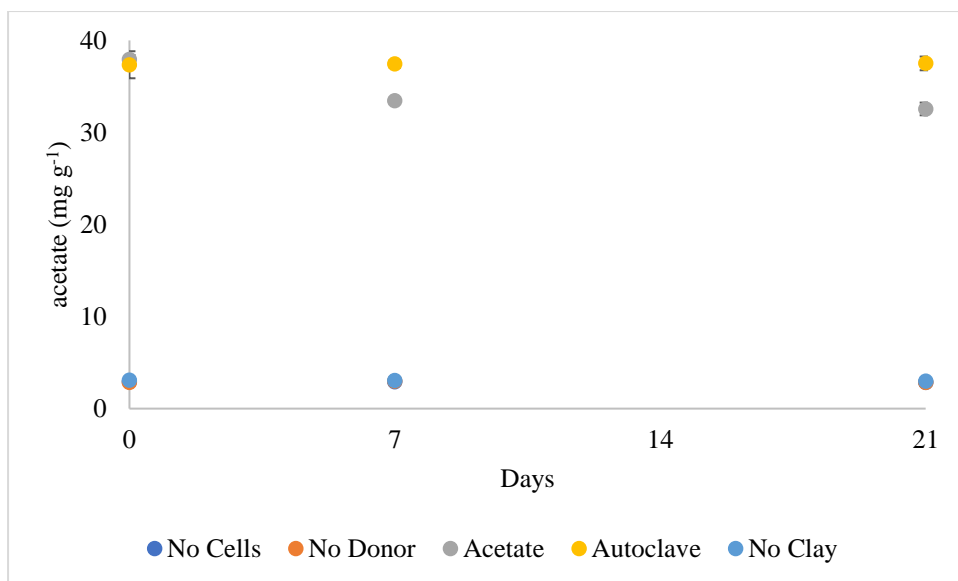
- Gorski, C.A., Kluepfel, L.E., Voeglin, A., Sander, M., Hofstetter, T.B., 2013. Redox properties of structural Fe in clay minerals: 3. Relationships between smectite redox and structural properties. *Environmental Science and Technology*, 47(23): 13477-13485.
- Hofstetter, T.B., Schwarzenbach, R.P., Haderlein, S.B., 2003. Reactivity of Fe(II) species associated with clay minerals. *Environmental Science & Technology*, 37(3): 519-528.
- Kim, S.S., Min, J.H., Baik, M.H., Kim, G.N., Choi, J.W., 2012. Estimation of the behaviors of selenium in the near field of repository. *Nuclear Engineering and Technology*, 44(8): 945-952.
- Li, Y.M., Cheng, W., Sheng, G.D., Li, J.F., Dong, H.P., Chen, Y., Zhu, L.Z., 2015. Synergetic effect of a pillared bentonite support on Se(VI) removal by nanoscale zero valent iron. *Applied Catalysis B-Environmental*, 174: 329-335.
- Loffredo, N., Mounier, S., Thiry, Y., Coppin, F., 2011. Sorption of selenate on soils and pure phases: kinetic parameters and stabilisation. *Journal of Environmental Radioactivity*, 102(9): 843-851.
- Lopez-Fernandez, M., Cherkouk, A., Vilchez-Vargas, R., Jauregui, R., Pieper, D., Boon, N., Sanchez-Castro, I., Merroun, M. L., 2015. Bacterial diversity in bentonites, engineered barrier for deep geological disposal of radioactive wastes. *Microbial Ecology*, 70(4): 922-935.
- Lovley, D.R., Fraga, J.L., Coates, J.D., Blunt-Harris, E.L., 1999. Humics as an electron donor for anaerobic respiration. *Environmental Microbiology*, 1(1): 89-98.
- Lovley, D.R., Phillips, E.J.P., 1987. Rapid assay for microbially reducible ferric iron in aquatic sediments. *Applied and Environmental Microbiology*, 53(7): 1536-1540.
- Montavon, G., Guo, Z., Lutzenkirchen, J., Alhajji, E., Kedziorek, M.A.M., Bourg, A.C.M., Grambow, B., 2009. Interaction of selenite with MX-80 bentonite: effect of minor phases, pH, selenite loading, solution composition and compaction. *Colloids and Surfaces a-Physicochemical and Engineering Aspects*, 332(2-3): 71-77.
- Neumann, A., Hofstetter, T.B., Skarpeli-Liati, M., Schwarzenbach, R.P., 2009. Reduction of polychlorinated ethanes and carbon tetrachloride by structural Fe(II) in smectites. *Environmental Science & Technology*, 43(11): 4082-4089.
- Newsome, L., Cleary, A., Morris, K., Lloyd, J.R., 2017. Long-term immobilization of technetium via bioremediation with slow-release substrates. *Environmental Science & Technology*, 51(3): 1595-1604.
- Oremland, R.S., Herbel, M.J., Blum, J.S., Langley, S., Beveridge, T.J., Ajayan, P.M., Sutto, T., Ellis, A.V., Curran, S., 2004. Structural and spectral features of selenium nanospheres produced by Se-respiring bacteria. *Applied and Environmental Microbiology*, 70(1): 52-60.
- Orucoglu, E., Hacıyakupoglu, S., 2015. Bentonite modification with hexadecylpyridinium and aluminum polyoxy cations and its effectiveness in Se(IV) removal. *Journal of Environmental Management*, 160: 30-38.
- Pearce, C.I., Patrick, R.A.D., Law, N., Charnock, J.M., Coker, V.S., Fellowes, J.W., Oremland, R.S., Lloyd, J.R., 2009. Investigating different mechanisms for biogenic selenite transformations: *Geobacter sulfurreducens*, *Shewanella oneidensis* and *Veillonella atypica*. *Environmental Technology*, 30(12): 1313-1326.
- Pedersen, K., 2010. Analysis of copper corrosion in compacted bentonite clay as a function of clay density and growth conditions for sulfate-reducing bacteria. *Journal of Applied Microbiology*, 108(3): 1094-1104.
- RWM, 2016. Geological disposal: derived inventory report, RWM, Didcot.
- SKB, 2006. Long-term safety for KBS-3 repositories at Forsmark and Laxemar - a first evaluation, SKB, Stockholm.

- Stookey, L.L., 1970. Ferrozine - a new spectrophotometric reagent for iron. *Analytical Chemistry*, 42: 779-781.
- Stucki, J.W., Lee, K., Zhang, L.Z., Larson, R.A., 2002. Effects of iron oxidation state on the surface and structural properties of smectites. *Pure and Applied Chemistry*, 74(11): 2145-2158.
- Tomei, F.A., Barton, L.L., Lemanski, C.L., Zocco, T.G., Fink, N.H., Sillerud, L.O., 1995. Transformation of selenate and selenite to elemental selenium by *Desulfovibrio desulfuricans*. *Journal of Industrial Microbiology*, 14(3-4): 329-336.
- Van Olphen, H., Fripiat, J., J, 1979. Data handbook for clay materials and other non-metallic minerals, Pergamon Press, Oxford.
- Wang, H., Wu, T., Chen, J., Zheng, Q., He, C., Zhao, Y.L., 2015. Sorption of Se(IV) on Fe- and Al-modified bentonite. *Journal of Radioanalytical and Nuclear Chemistry*, 303(1): 107-113.
- Wilson, J., Savage, D., Bond, A., Watson, S., Pusch, R., Bennett, D., 2011. Bentonite: A Review of key properties, processes and issues for consideration in the UK context, NDA, Harwell.
- Yee, N., Ma, J., Dalia, A., Boonfueng, T., Kobayashi, D.Y., 2007. Se(VI) reduction and the precipitation of Se(0) by the facultative bacterium *Enterobacter cloacae* SLD1a-1 are regulated by FNR. *Applied and Environmental Microbiology*, 73(6): 1914-1920.
- Zannoni, D., Borsetti, F., Harrison, J.J., Turner, R.J., 2008. The bacterial response to the chalcogen metalloids Se and Te. *Advances in Microbial Physiology*, Vol 53, 53: 1-72.

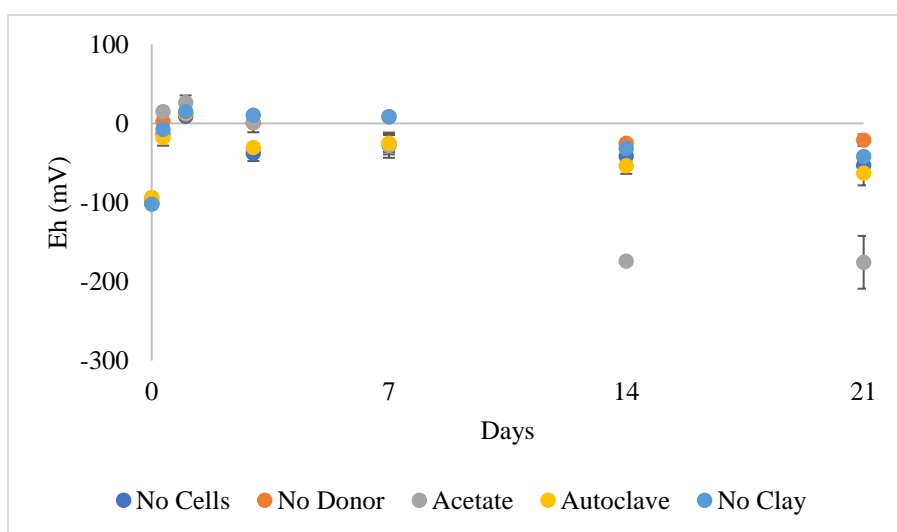
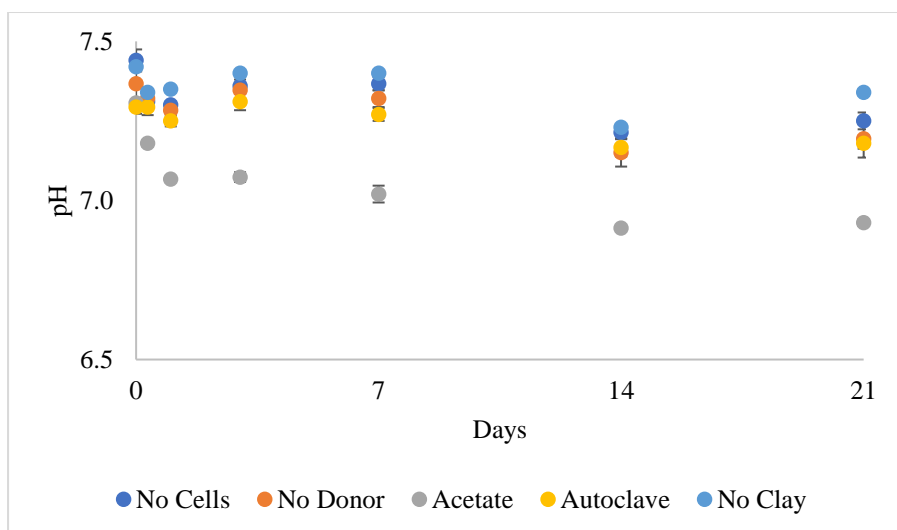
6.11. Supplementary

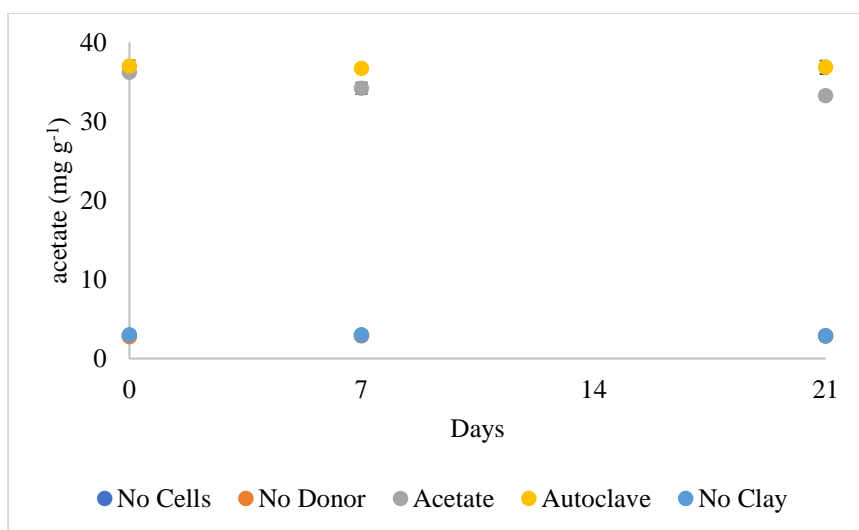
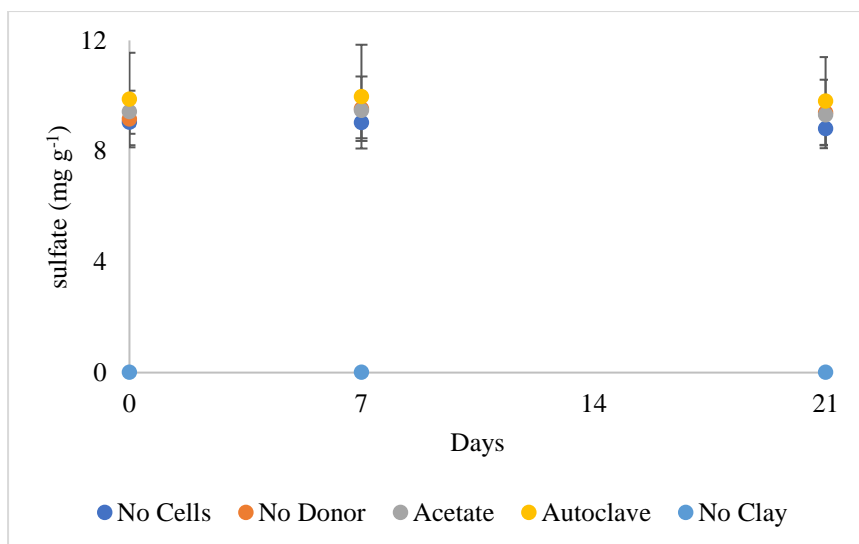






Supplementary 6.1: The evolution of pH, Eh, sulphate, and acetate over the course of the experiment in the selenite microcosms.





Supplementary 6.2: Changes in the Eh, pH, sulphate and acetate of the selenate microcosms during the experiment.

7. The Viability and Activity of Fe(III)-reducing Bacteria in Response to Bentonite Density and Swelling Pressure

Haydn M. Haynes^a, Carolyn I. Pearce^b, Jon Harrington^c, Jonathan R. Lloyd^a

^a *Williamson Research Centre for Molecular Environmental Science and Research Centre for Radwaste Disposal, School of Earth, Atmospheric and Environmental Sciences, University of Manchester, Manchester, M13 9PL, UK*

^b *Geosciences Group, Pacific Northwest National Laboratory, Richland, WA, 99354, US*

^c *British Geological Survey, Keyworth, NG12 5GG, UK*

Keywords

Bentonite, Swelling Pressure, Fe(III)-reducing bacteria

7.1. Preface

Question: Can IRB activity in bentonite materials be restricted by a sufficient bentonite density?

Chapters 5 and 6 showed that Fe(III) in bentonites was potentially reducible, and could be used to reduce redox-active contaminants. However, it is important to consider if such reactions are possible in bentonite buffers, where the bentonite density is considerably higher than in the experiments we carried out. Previous research has shown that copper corrosion instigated by sulphate-reducing bacteria in bentonite buffers can be prevented if a high enough bentonite density is used and maintained (Bengtsson and Pedersen, 2017). Such restrictions on microbial activity have also been documented in other groups of bacteria (Stroes-Gascoyne et al., 2010), and therefore there is also likely a bentonite density limit for microbial Fe(III)-reduction.

We investigated the restrictions placed on microbial Fe(III) reduction by increased bentonite density using specialized pressure vessels (Bengtsson and Pedersen, 2017). SWy-3 montmorillonite was supplemented with the Fe(III)-reducing bacterium *Bacillus subterraneus*, and then compacted to produce several montmorillonite wet densities (1500 kg m⁻³, 1750 kg m⁻³, 1900 kg m⁻³). Having been compacted the montmorillonites were attached to a fluid delivery system and left to saturate with an artificial groundwater for 34 days. After saturation an electron donor (lactate) was added to the compacted montmorillonites to promote microbial Fe(III) reduction, and the samples were incubated for 34 days. Samples

were extracted and a series of analyses were conducted in an attempt to identify Fe(III) reduction in the samples.

The results suggested that the greatest extent of Fe(III)-reduction took place in the 1500 kg m⁻³ sample, with microbial Fe(III) reduction decreasing with increased density, and halted at 1900 kg m⁻³. Interestingly, a visual inspection of the samples also showed significant amounts of iron sulfide (synonymous with sulphate-reducing bacteria) covering the 1750 kg m⁻³ sample, and to a smaller degree in the 1500 kg m⁻³ sample. This indicates that a viable sulphate-reducing bacterial population in the SWy-3 montmorillonite was able to use the added electron donor to support sulphate reduction. This increase in sulphate-reducing bacterial activity between the 1500 kg m⁻³, and 1750 kg m⁻³ samples suggest the Fe(III)-reducing bacteria were in competition for resources, and were unable to adapt to increased bentonite density/swelling pressure. It is impossible to determine if the *Bacillus subterraneus* would have been more active at the higher bentonite density if the sulphate-reducing bacteria were not present. This chapter was successful in developing a system that can be used to determine the effects of bentonite density/swelling pressure on Fe(III)-reducing bacteria (and other microorganisms). However, the methodology requires refinement to produce more meaningful results, and a greater range of densities would be useful in determining a more accurate cut off value. This work adds to previous research suggesting that a high enough bentonite density will suppress microbial activity, which is a key aim in ensuring the optimum functioning of a geological disposal facility.

7.2. Abstract

The presence of IRB in a bentonite buffer intended for use in a geological disposal facility may have deleterious effects on the buffer. A key factor in determining if IRB will be active or not is the density of the bentonite buffer, and the swelling pressure generated due to the intrusion of groundwater. The activity and viability of the Fe(III)-reducing bacterium *Bacillus subterraneus* was investigated at bentonite wet densities of 1500 kg m⁻³, 1750 kg m⁻³, and 1900 kg m⁻³. SWy-3 montmorillonite doped with ~1200 *B. subterraneus* cells per gram was saturated for 34 days with an artificial groundwater before sodium lactate was inserted, as an electron donor for Fe(III) reduction, and the pressure reset. The experimental stage of the experiment was conducted for a further 34 days, before the pressure vessels were disassembled, and MPN counts, and geochemical analyses were completed. MPN counts

showed that the 1500 kg m⁻³ pressure vessel which was under a mechanical pressure of 475 kPa contained the most IRB, with approximately a ten-fold decrease in cell numbers in the 1750 kg m⁻³ (541 kPa), and 1900 kg m⁻³ (1845 kPa) pressure vessels. Ferrozine assays targeting bioavailable Fe(II) showed that biological Fe(III)-reduction decreased when the montmorillonite density increased. The 1750 kg m⁻³ pressure vessel also displayed large amounts of SRB activity, with small amounts of SRB activity observed in the 1500 kg m⁻³ pressure vessel. These results suggest that the *Bacillus subterraneus* cells outcompeted sulphate-reducing bacteria in the 1500 kg m⁻³ pressure vessel but could not tolerate the pressures in the 1750 kg m⁻³ pressure vessel allowing the naturally occurring SRB to proliferate. IRB can colonize montmorillonites, and potentially reduce structural Fe(III). However, this research suggests that a sufficient bentonite density would generate a swelling pressure and halt IRB activity.

7.3. Introduction

The issue of nuclear wastes produced through power generation, weapon manufacturing, research, and medicine is a concern to many nations. One solution supported by numerous waste-producing countries is to construct a geological disposal facility (GDF) containing nuclear waste forms housed in metallic containers, separated from the local geology by a buffer material (RWM, 2016). One proposed buffer for high-heat generating waste (HHGW) is bentonite, a clay-based material mostly composed of the smectite mineral montmorillonite. Bentonite is a candidate buffer due to its low permeability, ability to buffer pH, as well as a mixture of ion exchange, and amphoteric adsorption sites. This provides an environment where corroding agents cannot access the nuclear waste container, and radionuclides are not able to leave the GDF (Wilson et al., 2011). A critical criterion in ensuring low permeability is achieved is swelling pressure, with a value of 0.1 - 1.0 MPa required (Sellin and Leupin, 2013). Swelling pressure is generated when smectite minerals absorb water (and other polarized fluids) in a confined space; the higher the bentonite density, the greater the swelling pressure (Karnland, 1998). The uptake of water occurs because cations are drawn to the negatively charged interlayers in the montmorillonite, with water required to satisfy the charge (Moore and Reynolds Jr, 1997).

As well as ensuring a low permeability environment, swelling pressure also restricts microbial activity (Bengtsson and Pedersen, 2017). Microbial communities do however exist

in bentonite deposits (Lopez-Fernandez et al., 2015), and may also be encountered under GDF conditions (Pedersen, 2010). Anaerobic microorganisms, especially iron- and sulfate-reducing bacteria may influence the corrosion rate of the metallic canisters (El Mendili et al., 2013), and may also affect the structural integrity of the bentonite buffer (Kim et al., 2004). Swelling bentonite places stress on these microorganisms by decreasing pore size, and connectivity in the clay matrix, which restricts microbial movement, access to nutrients, and space to grow in (Stroes-Gascoyne et al., 2010). Increased bentonite density also decreases water activity (a_w) (Motamedi et al., 1996). a_w is the measurement of water vapor pressure in a system and is expressed as a fraction of the water vapor pressure of pure water, at the same temperature and pressure. The a_w of a system can decrease for many reasons, but in the context of a bentonite barrier, decreases are due to interactions with solutes, and adsorption of water to mineral surfaces (Stroes-Gascoyne et al., 2010). The optimal a_w for microbial growth is 0.98, with some bacteria such as *Bacillus* species known to tolerate water activities as low as 0.91 (Brown, 1976). Research has shown that an a_w of 0.96 in combination with a swelling pressure of 2.0 MPa is enough to suppress indigenous microorganisms in bentonites (Stroes-Gascoyne et al., 2010). Investigations into the roles bentonite density, and swelling pressure play in restricting microbial activity have focused on *in-situ* field experiments such as the FEBEX-DP project (Chapter 4), as well as lab studies using specialized confining vessels (Bengtsson and Pedersen, 2017). Lab studies have investigated the viability of aerobic heterotrophs (Stroes-Gascoyne et al., 2010), as well as anaerobes including sulfate-reducing bacteria (SRB) (Bengtsson et al., 2015). SRB are of particular concern due to their ability to produce hydrogen sulfide, which can cause corrosion of steel (El Mendili et al., 2013), and copper container materials (Pedersen, 2010). Recent research into the activity of SRB at elevated bentonite densities has shown that the wet density cutoff value for sulfide-producing activity is between 1740 and 1880 kg m⁻³ depending on the bentonite used (Bengtsson and Pedersen, 2017).

One group of bacteria that have not been investigated at varying bentonite densities are Fe(III)-reducing bacteria (IRB). Microbial Fe(III)-reduction has been observed in smectite-based materials (Esnault et al., 2013), and can potentially increase the sensitivity of the material to illitisation (Kim et al., 2004), increase the cation exchange capacity (Khaled and Stucki, 1991), reduce swelling pressure (Kostka et al., 1999), and influence the reduction of contaminants (Chapter 6) (Hofstetter et al., 2006). This study intended to develop and test a system to determine the viability, and activity of IRB as a function of bentonite density.

Despite bentonite materials containing IRB (Haynes et al., 2018), the presence of SRB can cause indirect Fe(III)-reduction via sulfide-formation (Berner, 1984; Coleman et al., 1993), making it difficult to understand the direct contribution from the IRB in the reduction of Fe(III) in bentonites. To facilitate these studies, SWy-3 montmorillonite was dosed with known concentrations of a well-defined spore forming Fe(III)-reducing bacterium. Most pure culture studies on IRB have focused on the Gram-negative, non-spore-forming *Shewanella* genera (Liu et al., 2014; Ribeiro et al., 2009) commonly found in Fe(III)-reducing environments (Jeong et al., 2019). However, along with the swelling pressure described above, microorganisms in a GDF are likely to encounter high temperatures, and gamma radiation doses, so the relevance of Gram-negative bacteria such as *Shewanella* species to a GDF scenario is questionable (Haynes et al., 2018). In this study we used the Gram-positive Fe(III)-reducing bacterium *Bacillus subterraneus* instead (Kanso et al., 2002) as it had attributes more suited to a geological disposal scenario. These attributes included the tolerance of mildly alkaline conditions, a Gram-positive cell wall, and the tolerance of up to 9 % NaCl (Kanso et al., 2002). The *Bacillus subterraneus* cells were used to dope SWy-3 montmorillonite before compaction to wet densities of 1500 kg m⁻³, 1750 kg m⁻³, and 1900 kg m⁻³ (dry densities of 784 kg m⁻³, 1176 kg m⁻³, 1411 kg m⁻³). Having been incubated with sodium lactate geochemical, and microbiological analyses were completed. After incubation, a combination of geochemical and microbiological analyses suggested that Fe(III)-reduction was occurring in the 1500 kg m⁻³ pressure vessel, but the IRB were outcompeted by SRB at a wet density of 1750 kg m⁻³.

7.4. Materials and methods

7.4.1. Material preparation

7.4.1.1. Material selection

The montmorillonite chosen for this experiment was SWy-3, a sodium montmorillonite excavated in Wyoming, and purchased from the Clay Minerals society (Chantilly, VA, USA). The SWy-3 montmorillonite was provided in powder form, and was supplemented with a *Bacillus subterraneus* culture prior to use to ensure it contained viable Fe(III)-reducing bacterial cells.

7.4.1.2. Microbial culture preparation

B. subterraneus was obtained from DSMZ (Brunswick, Germany) and grown on metal-reduction (MR) medium (Kanso et al., 2002) modified with 20 mM of sodium lactate acting as an electron donor, and 4 mM of ferrihydrite acting as an electron acceptor, the medium was corrected to pH 7.35 using 10 M sodium hydroxide, before gassing with pure nitrogen, and autoclaving (126 °C, 20 mins). The ability for *B. subterraneus* to carry out Fe(III)-reduction was confirmed by the enrichment of Fe(II) in the medium using the Ferrozine assay detailed below. To prepare the cells for inoculation into the clay, a 100 ml aliquot of *B. subterraneus* containing MR medium was added to 1 l of sterile tryptone soya broth (TSB) medium and incubated on a shaker at 40 °C for 8 hours. The TSB medium was then centrifuged for 20 minutes (4920 g, 4 °C), and the resulting pellet washed twice with a sterile artificial groundwater (AGW) (Table 1). After washing, the pellet was dispersed in 10 ml of sterile AGW in a serum bottle, before sealing with a rubber stopper, and aluminium crimp.

Table 7.1: Concentrations of compounds in the artificial groundwater (AGW) (Bengtsson and Pedersen, 2017).

Compound	Concentration (mM)
Sodium chloride	120
Calcium chloride dihydrate	7
Potassium chloride	9
Ammonium chloride	18
Potassium orthophosphate	1
Magnesium chloride hexahydrate	2

7.4.1.3. Inoculation of the clay

Manipulation of the SWy-3 montmorillonite, and *B. subterraneus* culture was completed in a laminar flow cabinet under a flow of sterile air (Labcaire, Clevedon, UK). The *B. subterraneus* culture was removed in 2 ml aliquots using a sterile syringe and dispersed in a petri dish containing approximately 1 g of SWy-3 montmorillonite, this process was repeated producing 5 petri dishes in total. The resulting clumps of SWy-3 montmorillonite, and *B. subterraneus* cells were air dried for an hour, before being pushed through an ethanol sterilized fine sieve to return it to a powdered form. The cell-doped SWy-3 montmorillonite

was then mixed with approximately 90 g of fresh SWy-3 montmorillonite to produce a 100 g batch of SWy-3 montmorillonite doped with *B. subterraneus* cells.

7.4.1.4. Water content, and loss on ignition (LOI)

Water content of the *B. subterraneus* doped SWy-3 montmorillonite, and in the SWy-3 montmorillonite plugs after the experiment was determined by placing 1 g samples of the clay into preignited crucibles before heating them to 105 °C for an hour. The crucibles were cooled in a desiccator, and reweighed. The decrease in mass was attributed to the release of water from the mineral structure. The samples were then heated for a further hour at 1100 °C to determine the loss of carbon as a result of the breakdown of carbonates, and oxidation of organic matter.

7.4.1.5. Grain density

The grain density (p_s) of the SWy-3 montmorillonite was determined using a pycnometer. The SWy-3 montmorillonite was dried at 105 °C for an hour before adding approximately 1.0 g to a pre-weighed pycnometer. The pycnometer was then weighed again before being half-filled with water. The SWy-3 montmorillonite was agitated to release any trapped air, and then left for 24 hours. The pycnometer was then filled to the top and weighed, before finally weighing the pycnometer again with just water inside. The p_s was calculated using the below equation where m_1 is the pycnometer mass, m_2 the mass of the pycnometer and clay, m_3 the mass of the pycnometer, clay and solution, and m_4 the pycnometer and solution (BSI, 1990):

$$p_s = \frac{m_2 - m_1}{m_4 - m_1 - m_3 - m_2}$$

7.4.1.6. Bentonite mass calculations

The mass of bentonite required for each wet density was calculated using the following equations derived from relationships described in (Karnland, 2010)); the void ratio of the pressure vessels (e) was equal to the grain density (p_s) minus the wet density (p_m) divided into the wet density minus 1000:

$$e = \frac{p_s - p_m}{p_m - 1000}$$

The water ratio (w_{sat}) was calculated by adding 1 to the void ratio and multiplying it by the wet density divided by the grain density and subtracting 1:

$$w_{sat} = \frac{p_m}{p_s} \times (1 + e) - 1$$

The dry density (p_d) is determined by adding 1 to the water ratio and dividing it by the wet density:

$$p_d = \frac{p_m}{(1 + w_{sat})}$$

The unsaturated density (p_u) is equal to 1 plus the initial water content (w) multiplied by the dry density:

$$p_u = p_d \times (1 + w)$$

The mass of unsaturated bentonite (m_u) is then equal to the unsaturated density multiplied by the volume (V):

$$m_u = p_u \times V$$

Having determined the mass of the SWy-3 montmorillonite required the pressure vessels were placed in a laminar flow cabinet (Labcaire, Clevedon, UK), and bentonite wet densities of 1500 kg m^{-3} , 1750 kg m^{-3} , and 1900 kg m^{-3} (dry densities 784 kg m^{-3} , 1176 kg m^{-3} , 1411 kg m^{-3}) prepared. A piston was inserted into the pressure vessel and compressed to the appropriate volume using a G-clamp. An outlet housed in the piston allowed air in the pressure vessel to escape, whilst a sintered titanium filter prevented the clay from being extruded.

7.4.2. Pressure vessel preparation and use

7.4.2.1. Pressure vessel design

The SWy-3 montmorillonite used in these experiments was contained in titanium pressure vessels that confined the clay allowing a swelling pressure to develop (Bengtsson et al., 2015). The pressure vessels were purchased from MICANS (Molnlycke, Sweden) and consisted of a titanium cylinder with a bottom lid, and a piston (Figure 1). A top plate sits on top of the piston with space for a load cell (force transducer) to sit (Figure 1). The piston, and

base plate are sealed with O-rings to make them air tight. The pistons, and base plates come in two configurations, an impermeable configuration was used during the experimental stage, and consisted of a solid base plate, as well as a piston with a removable plug (so air can be removed from the cylinder). A permeable configuration was used during the saturation stage, and consisted of pistons, and base plates that permitted the movement of fluids into the cylinder. The piston, and base plate used during the saturation phase were equipped with sintered titanium filters to prevent the bentonite extruding from the cylinder.

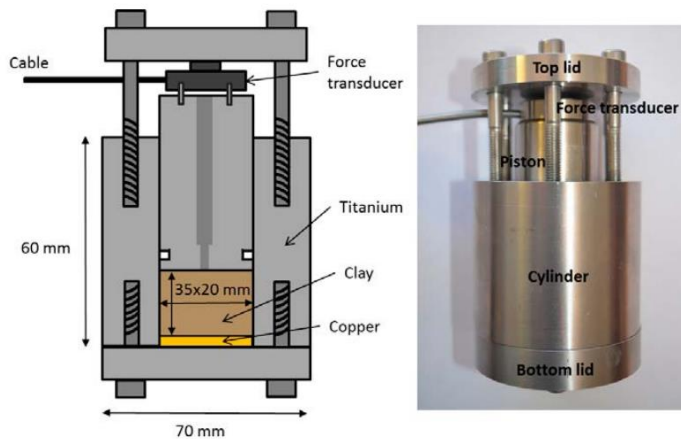


Figure 7.1: Schematic of the pressure vessels (image obtained from (Bengtsson et al., 2015)).

7.4.2.2. Swelling pressure measurement

Swelling pressure generated by the SWy-3 montmorillonite was determined using a load cell mounted between the top plate, and the piston. As the montmorillonite swelled the piston was pushed upwards pressing the load cell against the top plate, generating an electrical signal. The readings from the load cells were recorded and used to measure the swelling pressure over the saturation, and experimental stages of the work. Calibration of the load cells was achieved by mounting the pressure vessels to the saturation system in an empty configuration before inserting water at a known series of pressures using a Teledyne ISCO (Lincoln, NE, USA) 260D syringe pump. The pressure reading on the pressure pump was independently verified using a pressure gauge mounted to the saturation system. Calibration curves were produced for the individual load cells and used to calculate the swelling pressure in kPa.

7.4.2.3. Saturating the clay

Before the experiment could commence, the SWy-3 montmorillonite needed to be in a saturated state. The pressure vessels were mounted to a saturation system which allowed the infiltration of fluids via the base plate, and piston, whilst preventing the extrusion of the montmorillonite with a set of sintered titanium filters. Once mounted, the saturation system was gassed with nitrogen, and then purged using an Edwards (West Sussex, UK) E2M8 Rotary Vane High Vacuum Two Stage Pump in three cycles over the course of an hour, before being purged for a further 23 hours. Having been purged a sterile, nitrogen-gassed AGW (Table 1) was introduced into the saturation system at a constant pressure of 200 kPa, using a Teledyne ISCO (Lincoln, NE, USA) 260D syringe pump that was treated with methanol, and washed with sterile deionized water prior to use. The pressure vessels were left to saturate for 34 days, with complete saturation determined by the presence of a stable swelling pressure over a prolonged period.

7.4.2.4. Addition of electron donor

Having allowed the SWy-3 montmorillonite to saturate the pressure vessels were disconnected from the saturation system and transferred to an anaerobic cabinet (Coylab, Grass Lake, MI, USA). The base plates were swapped out for the impermeable versions, and the pistons were removed exposing the clay surface. Individual sodium lactate solutions were prepared for each of the pressure vessels. Sodium lactate solutions of different concentrations were prepared by diluting a 60 % sodium lactate solution in deionized water (18.2 MΩ) the concentrations used were 30 mM for the 1500 kg m⁻³ pressure vessel, 57 mM for the 1750 kg m⁻³ pressure vessel, and 80 mM for 1900 kg m⁻³ pressure vessel, equivalent to the amount of electrons required to reduce all of the Fe(III) in the pressure vessels. The sodium lactate solutions were gassed with nitrogen in serum bottles before being autoclaved (126 °C, 20 mins). A 900 µl aliquot of the sterile electron donor solutions were deposited on the surface of the SWy-3 montmorillonite plugs using a nitrogen gassed syringe. Following the addition of the sodium lactate the impermeable pistons equipped with a ventilation hole (to remove air) were inserted into the pressure vessels at the original volume, and the ventilation holes were sealed with plugs. After reassembly the pressure vessels were removed from the anaerobic chamber, and load cells were inserted between the pistons, and the top plates. The pressure registered by the load cells was reset to the readings displayed at the end of the saturation stage by tightening the screws on the top plates. Once the pressure vessels had

been reset, they were stored at room temperature for 35 days. The temperature was monitored over the course of the experimental phase, and the pressure on the pressure vessels was regularly reset to the required value.

7.4.2.5. Sample retrieval

Following the experimental stage, the pressure vessels were transferred to an anaerobic chamber, and the SWy-3 montmorillonite plugs removed. The plugs were dissected using disposable, sterile scalpels, and weighed out in preparation for further analysis.

7.4.3. Follow up analyses

7.4.3.1. Most Probable Number (MPN) enumerations

The number of Fe(III)-reducing bacteria (IRB) cells in the doped SWy-3 montmorillonite, and in the pressure vessels after the experimental stage was determined using most probable number (MPN) counts. The medium used for the MPN enumerations consisted of MR medium modified with 20 mM sodium lactate (electron donor), and 4 mM ferrihydrite (electron acceptor). The pH of the medium was corrected to 7.35 and gassed with nitrogen before transferal to an anaerobic chamber (Coylab, Grass Lake, MI, USA). The medium was then transferred in 9 ml aliquots to a series of serum bottles, and autoclaved (126 °C, 20 mins). In the case of the doped SWy-3 montmorillonite 0.45 g of the clay was transferred to 9 ml of MR medium in triplicate inside an anaerobic chamber, using a sterile spatula. The pressure vessel plug material was prepared by dispersing 0.5 g of the plugs in a sterile, anoxic 1 % sodium chloride solution inside the anaerobic chamber (Coylab, Grass Lake, MI, USA) for an hour, before 1 ml of the solutions was transferred to 9 ml of MR medium in triplicate using a nitrogen gassed, sterile syringe. In both cases serial dilutions were set up from the initial inoculation by transferring 1 ml of the slurry to a fresh 9 ml batch of modified medium. The transferal of slurry was repeated until five sequential ten-fold dilutions were achieved. The MPN serum bottles were stored at room temperature (20 °C) in an incubator for 2 weeks, and positive dilutions were detected by identifying an increase in the 0.5M hydrochloric acid extractable Fe(II)/Fe(total) ratio using the Ferrozine assay. MPN counts were calculated by comparing to a table of known values (de Man, 1983), and converted to dry weight.

7.4.3.2. X-ray Fluorescence (XRF)

The total iron content of the SWy-3 montmorillonite was determined using XRF. A 12 g portion of SWy-3 montmorillonite was mixed with 3 g of fine powdered wax and milled for 7 min at 350 rpm using a TEMA (Woodford Halse, UK) mill before being pressed into a pellet at 10 tonnes. The breakdown of major elements was collected using a wavelength dispersive, PANalytical (Royston, UK) Axios spectrometer using the standard glass AUSMON (B255). The carbon and water content of the SWy-3 montmorillonite was obtained using loss on ignition (LOI), and the XRF data corrected.

7.4.3.3. Ferrozine assay

The Ferrozine assay was used during the experiment to quantify Fe(II) and hence determine a positive reaction in the Fe(III)-reducing MPNs, along with changes in the 0.5 M hydrochloric acid extractable Fe(II)/Fe(total) ratio of the montmorillonites during the experiment (Lovley and Phillips, 1987). In the case of direct measurements on the montmorillonite, 1.0 g of the doped clay, or pelletized clay was left to equilibrate in 25 ml of 0.5 M hydrochloric acid for an hour before a 20 µl aliquot of the slurry was added to 980 µl of 0.5 M hydrochloric acid (Fe(II)), or 980 µl hydroxylamine hydrochloride (Fe(total)) followed by a further hour of equilibration. The acidified mixture was centrifuged (14800 rpm, 5 mins) before 80 µl of the supernatant was added to 920 µl of Ferrozine solution. The absorption of the solution was determined at 562 nm using a spectrophotometer (Jenway (Stone, UK). In the case of the MPNs a 20 µl aliquot was removed using a N₂ degassed syringe and treated like the slurry above. All results were compared to a calibration curve consisting of known standards.

7.4.3.4. Ion Chromatography (IC)

The concentration of volatile fatty acids (VFAs), and sulfate in the doped SWy-3 montmorillonite, and in the pressure vessel plugs was determined using IC. A 0.2 g sample was extracted in each case and washed in 5 ml of deionized water (18.2 MΩ) for an hour on a roller mixer. When the slurries were homogenous, a 1 ml aliquot was removed, and centrifuged (16,162 g, 10 mins). A 250 µl subaliquot was placed in an IC vial and diluted in 750 µl of deionized water (18.2 MΩ). IC samples were analyzed using a Dionex (Sunnyvale,

CA, USA) ICS5000. Values were corrected to the dry weight of SWy-3 montmorillonite present.

7.4.3.5. Inductively Coupled Plasma Atomic Emission Spectroscopy (ICP-AES)

ICP-AES was used to determine changes in key interlayer cations (sodium, potassium, calcium, magnesium) in extractions from the doped SWy-3 montmorillonite, as well as in the pressure vessel plugs. For all samples a 1 g portion of clay was added to 5 ml of 1 M ammonium acetate solution and placed on a shaker for 24 hours. Having been given time to homogenize, the samples were topped up with 5 ml more of the 1 M ammonium acetate solution, and passed through a 0.22 μm filter (Chapman, 1965). The solid was discarded, and a 1 ml aliquot of the supernatant was acidified in 9 ml of 2.2 % nitric acid. The samples were then measured using a Perkin-Elmer (Waltham, MA, USA) Optima 5300 dual view ICP-AES.

7.5. Results

7.5.1. Saturation stage

Prior to the addition of the sodium lactate (electron donor) the SWy-3 montmorillonite needed to be saturated. This was achieved by pumping AGW into the pressure vessels. A rapid increase in swelling pressure to 200 kPa, 320 kPa, and 1300 kPa in the 1500 kg m^{-3} , 1750 kg m^{-3} , and 1900 kg m^{-3} pressure vessels respectively occurred over the space of 4 hours (Figure 7.2). Following the initial increase, a small lag was observed, and then another rapid increase in swelling pressure occurred bringing the swelling pressures after 3 days to approximately 340 kPa (1500 kg m^{-3}), 610 kPa (1750 kg m^{-3}), and 2200 kPa (1900 kg m^{-3}) (Figure 7.2). A much slower increase in swelling pressure occurred over the rest of the experiment with final swelling pressures of 482 kPa, 737 kPa, and 2384 kPa in the 1500 kg m^{-3} , 1750 kg m^{-3} , and 1900 kg m^{-3} pressure vessels respectively (Figure 7.2). The average swelling pressure observed in the period between day 4, and day 34 was 381 kPa in the 1500 kg m^{-3} pressure vessel, 646 kPa in the 1750 kg m^{-3} pressure vessel, and 2278 kPa in the 1900 kg m^{-3} pressure vessel with standard deviations of 37 kPa, 35 kPa, and 50 kPa respectively (Table 7.2). The room temperature at the start of the experiment was 27.8 °C, and a gradual decrease (considering daily fluctuations) to 18.9 °C was observed over the course of the

experiment (Table 7.2). The average room temperature was 23.0 °C with a standard deviation of 1.6 °C (Table 7.2).

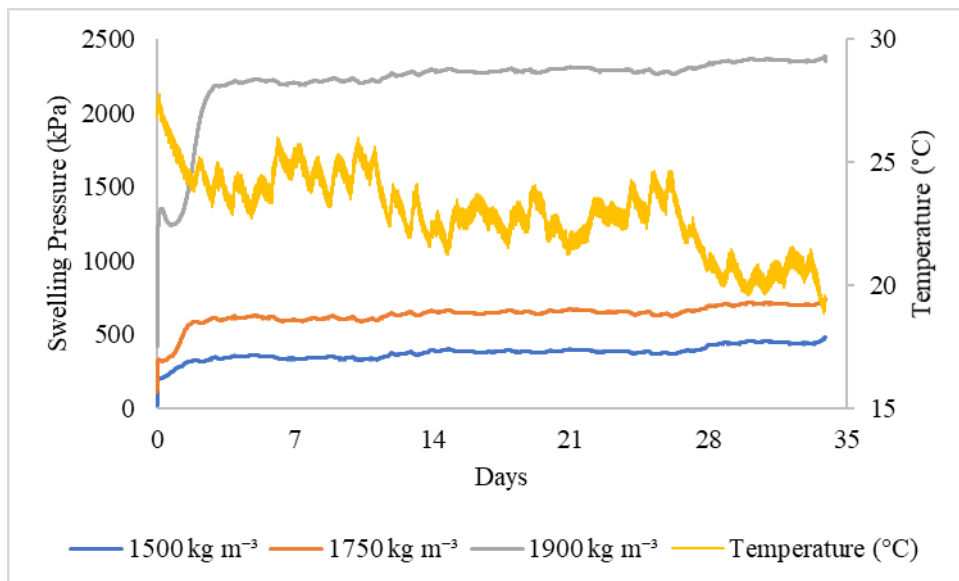


Figure 7.2: Changes in swelling pressure (kPa), and external temperature (°C) over the course of the saturation stage.

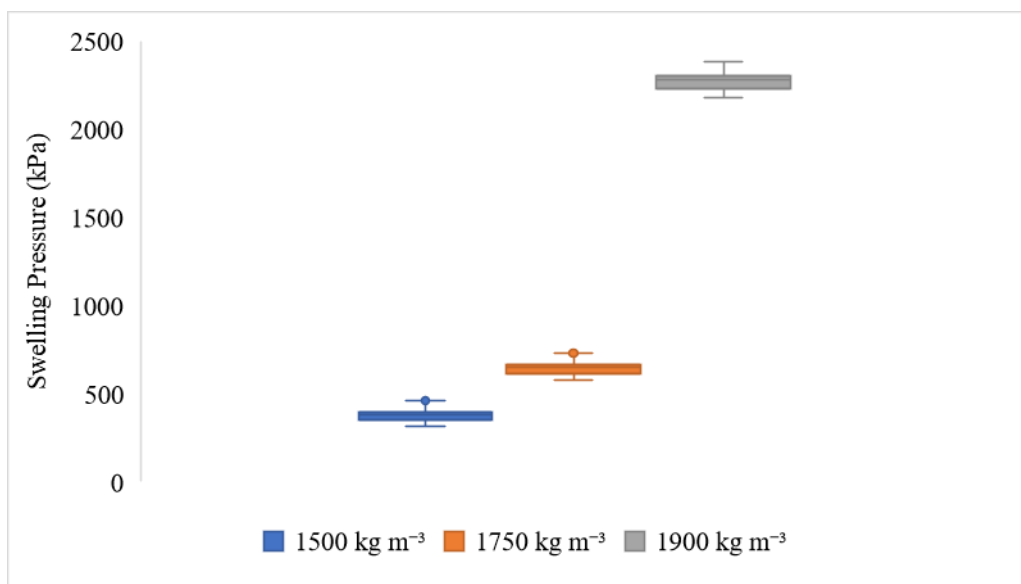


Figure 7.3: Box and whisker plots depicting the variability in the swelling pressure (kPa) once the pressure vessels had reached a steady state.

Table 7.2: Statistical data for the swelling pressure (kPa) in the pressure vessels when they reached a steady state, and the variation in external temperature (°C) during the saturation stage of the experiment.

	1500 kg m ⁻³ (kPa)	1750 kg m ⁻³ (kPa)	1900 kg m ⁻³ (kPa)	Temperature (°C)
Minimum	315.62	575.93	2179.61	18.87
Average	380.52	645.63	2277.76	22.98
Maximum	482.37	736.9	2383.75	27.75
Standard Deviation	36.57	35.4	50.15	1.61

7.5.2. Experimental stage

Following the addition of the sodium lactate electron donor, the mechanical pressure in the vessels was set to approximately the final swelling value observed during the saturation stage. These values were 474 kPa, 713 kPa, and 2451 kPa, in the 1500 kg m⁻³, 1750 kg m⁻³ and 1900 kg m⁻³ pressure vessels respectively (Figure 7.4). After 10 hours the mechanical pressure in the 1900 kg m⁻³ pressure vessel had decreased to 1151 kPa, with smaller decreases observed in the 1500 kg m⁻³ (450 kPa), and 1750 kg m⁻³ (605 kPa) pressure vessels (Figure 7.4). Regular adjustments were made to return the mechanical pressure to the swelling pressure that was observed at the end of the saturation stage. The average mechanical pressures recorded over the course of the experimental stage were 475 kPa in the 1500 kg m⁻³ pressure vessel, 541 kPa in the 1750 kg m⁻³ pressure vessel, and 1845 kPa in the 1900 kg m⁻³ pressure vessel with standard deviations of 21 kPa, 31 kPa, and 339 kPa respectively (Table 7.3). The average room temperature during the experimental stage was 20.0 °C, with a standard deviation of 1.2 °C (Table 7.3).

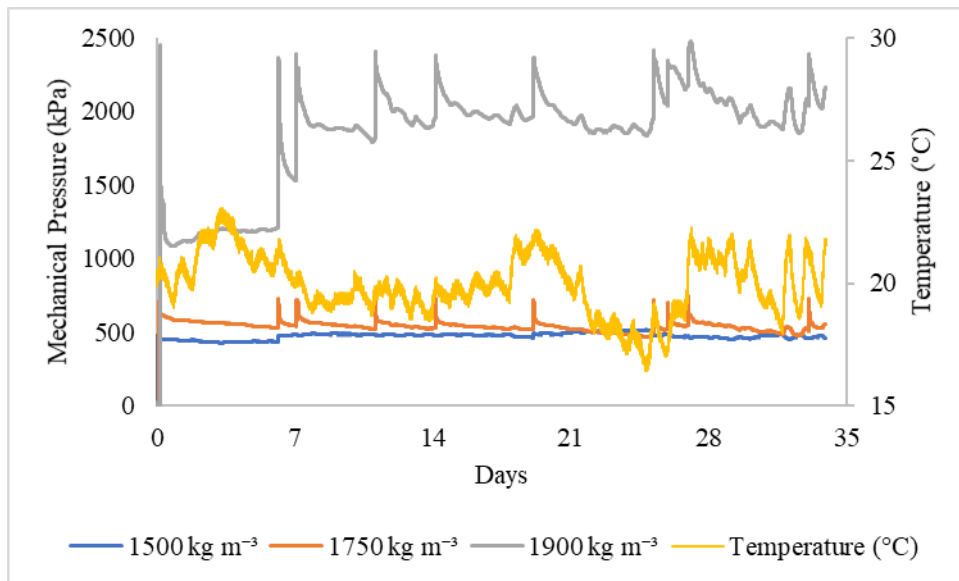


Figure 7.4: Mechanical pressure (kPa), and external temperature (°C) data from the experimental stage of the study.

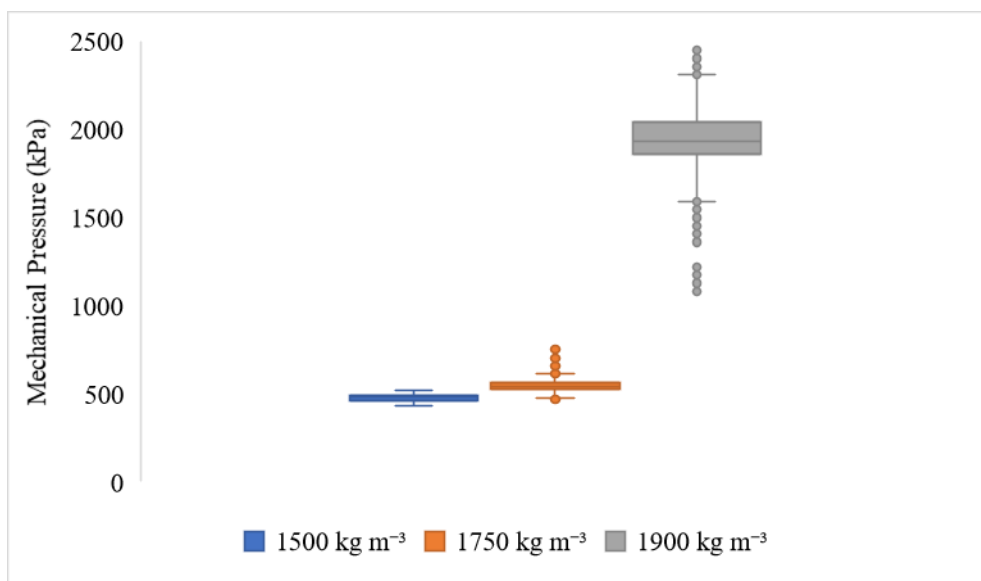


Figure 7.5: Variability in the mechanical pressure (kPa) of the pressure vessels during the experimental stage of the work.

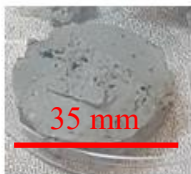
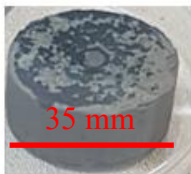

Table 7.3: Statistical data of the mechanical pressures (kPa) in the pressure vessels, as well as the external temperature (°C) during the experimental stage of the study.

	1500 kg m ⁻³ (kPa)	1750 kg m ⁻³ (kPa)	1900 kg m ⁻³ (kPa)	Temperature (°C)
Minimum	427.93	466.35	1081.51	16.44
Average	474.54	540.5	1844.54	19.99
Maximum	516.32	748.83	2474.55	23.06
Standard Deviation	20.92	30.56	339.28	1.23

7.5.3. Sample description and characterization

After the clay plugs were removed from their pressure vessels a visual inspection was conducted followed by geochemical, and microbiological analysis. The 1500 kg m⁻³ SWy-3 montmorillonite plug had the highest water content (35.1 %), and visible SRB communities (evidenced by black iron sulfide deposits) were sparsely distributed through the clay (Table 7.4). A large amount of iron sulfide staining was found throughout the 1750 kg m⁻³ SWy-3 montmorillonite plug, which had a water content of 29.3 % (Table 7.4). No visual signs of iron sulfide formation were found at 1900 kg m⁻³, and this sample had the lowest water content (20.9 %) (Table 7.4). The total iron content of the SWy-3 montmorillonite was 23.5 mg g⁻¹. The doped SWy-3 montmorillonite had a 0.5 M hydrochloric acid extractable Fe(II) content of 1.1 mg g⁻¹, with the 1500 kg m⁻³, 1750 kg m⁻³, and 1900 kg m⁻³ pressure vessels containing 1.9 mg g⁻¹, 2.6 mg g⁻¹, and 1.6 mg g⁻¹ respectively (Table 7.4). Meanwhile the concentration of VFAs was comparable in the doped SWy-3 montmorillonite, 1500 kg m⁻³, and 1750 kg m⁻³ pressure vessels (0.14mg g⁻¹), but higher in the 1900 kg m⁻³ pressure vessel (0.47 mg g⁻¹) (Table 7.4). Sulphate concentrations were the highest in the 1750 kg m⁻³ pressure vessel (7.2 mg g⁻¹), with the lowest concentration observed in the 1500 kg m⁻³ pressure vessel (5.2 mg g⁻¹) while the doped SWy-3 montmorillonite, and the 1900 kg m⁻³ pressure vessel contained approximately 5.7 mg g⁻¹ (Table 7.4).

Table 7.4: Images of the SWy-3 montmorillonite plugs after the experiment. Along with information on the plugs, and *Bacillus subterraneus* doped SWy-3 (Doped) including grain density of the bentonites (kg m^{-3}), water content (%), interlayer cation (sodium, calcium, potassium, magnesium) concentrations in solution per gram of substrate (mg g^{-1}), sulphate concentration in solution per gram of substrate (mg g^{-1}), volatile fatty acids (VFAs) in solution per gram of substrate (mg g^{-1}), the iron content of the SWy-3 montmorillonite, and the amount of Fe(II), and total Fe extracted using 0.5 M hydrochloric acid per gram of substrate (mg g^{-1}).

	Doped	1500 kg m^{-3}	1750 kg m^{-3}	1900 kg m^{-3}
Sample				
Grain density (kg m^{-3})	2735	2735	2735	2735
H ₂ O (%)	14.1	35.1	29.3	20.9
Na ⁺ (mg g^{-1})	>6.6	8.7	>8.0	>7.2
Ca ²⁺ (mg g^{-1})	6.2	6	7.1	6.6
K ⁺ (mg g^{-1})	0.4	0.5	0.6	0.5
Mg ²⁺ (mg g^{-1})	1.8	1.6	1.9	1.8
SO ₄ ²⁻ (mg g^{-1})	5.8	5.2	7.2	5.6
VFAs (mg g^{-1})	0.14	0.13	0.14	0.47
Fe (mg g^{-1})	23.5	23.5	23.5	23.5
0.5 M HCl extractable Fe(II) (mg g^{-1})	1.1	1.9	2.6	1.6
0.5 M HCl extractable Fe (mg g^{-1})	1.3	2.3	3	2

7.5.4. Most Probable Number (MPN) enumerations

The number of viable *Bacillus subterraneus* cells in the Doped SWy-3, and in the clay plugs after treatment were determined using MPN counts, in MR medium. MPN counts suggested that the starting concentrations of *Bacillus subterraneus* cells in the doped SWy-3 was approximately $1.1 \times 10^3 \text{ MPN g}^{-1}$, this increased to $1.3 \times 10^5 \text{ MPN g}^{-1}$ in the 1500 kg m^{-3} pressure vessel, to $1.2 \times 10^4 \text{ MPN g}^{-1}$ in the 1750 kg m^{-3} pressure vessel, and finally 1.0×10^4 in the 1900 kg m^{-3} pressure vessel (Table 7.5).

Table 7.5: The dry weight MPN g⁻¹ values for the doped SWy-3 montmorillonite, and the pressure vessel plugs. Along with 95 % confidence interval (CI), lower limits (LL), and upper limits (UL).

	MPN g ⁻¹	95 % CI LL	95 % CI UL
Doped Swy-3	1187	349	4191
1500 kg m ⁻³	1.3×10^5	3.0×10^4	4.9×10^5
1750 kg m ⁻³	1.2×10^4	2829	4.5×10^4
1900 kg m ⁻³	1.0×10^4	2528	4.0×10^4

7.6. Discussion

7.6.1. Saturation stage

Swelling pressure been shown by numerous studies to play a significant role in the viability, and therefore activity of microorganisms in a bentonite buffer intended for the geological disposal of nuclear waste. Studies into the effects of swelling pressure on microorganisms, have focused on aerobes (Stroes-Gascoyne et al., 2010), and SRB (Bengtsson and Pedersen, 2017), with little attention given to IRB that can alter the geochemistry of the bentonite buffer (Kostka et al., 1999). This study focused on developing a system to study Fe(III)-reduction at elevated swelling pressures. To ensure the SWy-3 montmorillonite was saturated before the addition of an electron donor (sodium lactate), load cells were used to track swelling pressure, as AGW was introduced into the pressure vessels. The evolution of swelling pressure in the pressure vessels proceeded in 3 stages, as observed in other montmorillonite swelling pressure experiments (Lloret et al., 2003). In the first stage an initial sharp rise in swelling pressure occurred due to a reduction in suction associated with the intake of water (Figure 7.2). In the second stage the swelling pressure overcame the forces generated by suction leading to macrostructure collapse, and a slight decrease in swelling pressure (Figure 7.2). In the final stage the montmorillonite starts to reach saturation, and the swelling pressure rapidly increased again as suction decreased to a minimum (Figure 7.2). During stage 3 of the swelling process a gradual increase in swelling pressure coincided with a decrease in temperature (Figure 7.2). To ensure that the clay was saturated, and that the variation was due to fluctuations in the room temperature, the swelling pressure over this period was plotted against temperature. Strong correlations were observed between swelling pressure, and temperature (Table 7.2) indicating the temperature was the cause of these fluctuations, and that the swelling pressure was stable. Furthermore, the equations derived

from the relationship between swelling pressure, and temperature can be used to predict the swelling pressure at a desired temperature (Table 7.6), and therefore can be used as a benchmark to identify saturation in future experiments.

Table 7.6: Relationships between swelling pressure (y, kPa), and temperature (x, °C) with predicted swelling pressures (including error margins) at 20 °C.

Density	Equation	R ²	20 °C swelling pressure	Error
1500 kg m ³	y = -22.73x + 900.15	0.91	445.65 kPa	± 40.11
1750 kg m ³	y = -22.13x + 1151.70	0.93	709.10 kPa	± 49.64
1900 kg m ³	y = -30.45x + 2972.20	0.85	2363.12 kPa	± 354.47

7.6.2. Variability in experimental swelling pressures

Having established that the montmorillonite in the pressure vessels had reached saturation, the pressure vessels were removed from the saturation system, and sodium lactate was added. Despite the volume of the pressure vessels being comparable during the saturation, and experimental stages, the pressures observed were remarkably different, with greater variation observed during the experimental stage (Figure 7.5). In the case of the saturation stage the pressure on the load cell is generated by swelling pressure as the clay absorbs the AGW, and suction decreases (Yigzaw et al., 2016). However, during the experimental stage there was no input of AGW into the pressure vessels, and therefore a high swelling pressure/low suction environment was not maintained. To compensate for the decrease in swelling pressure a mechanical load was applied to the clay plugs using the pressure vessel pistons. The mechanical pressure applied during the experimental stage is not a true reflection of the swelling pressure generated during the saturation stage. However, if the pressure vessels were attached to the saturation system during the experimental stage there is a risk of fouling of the pump and saturation system, as well as microbial activity in the saturation system altering the geochemistry of the SWy-3 montmorillonite plugs (Masurat et al., 2010). Previous research has shown that this mechanical force does prevent microbial activity (Bengtsson and Pedersen, 2017), but more research is required to see if it is an accurate representation of swelling pressure. Placement in a fixed temperature incubator may also reduce the amount of variability observed in the load cell readings, and the equations in Table 7.6 can be used to derive a target pressure at the chosen temperature.

7.6.3. Microbial viability and activity

After the addition of the sodium lactate, the pressure vessels were incubated for 35 days, and finally dismantled so geochemical, and microbiological analyses could be conducted.

Analysis of the water content of the SWy-3 montmorillonite plugs using loss on ignition showed a decrease in water content as the density of the sample increased. The large variation in water content between treatments highlighted the need to compare the geochemical, and microbiological parameters of the materials by dry weight so that the values were comparable. The MPN counts showed an increase in IRB numbers at all bentonite densities compared to the doped SWy-3 montmorillonite (Table 7.5). The highest MPN count was observed in the 1500 kg m⁻³ pressure vessel, with IRB cells reducing as a function of wet density, as observed in other studies (Bengtsson and Pedersen, 2017) (Table 7.5). One of the issues with the measurements was that the doped SWy-3 montmorillonite was placed into the MPNs with no further treatment, while the plugs were disaggregated in a sterile salt solution prior to use. This washing step may have increased the number of cells in the solution (rather than bound to the clay) increasing the number of cells transferred to the subsequent dilutions, and therefore providing a positive bias. This could be investigated by treating the doped SWy-3 with a salt solution as well. Another issue with the MPN counts is that *B. subterraneus* has alternative metabolisms that do not require an electron donor (Kanso et al., 2002) so even with the exclusion of sodium lactate the presence of TSB medium carried over from the initial preparation may have been enough to promote microbial growth during the saturation stage of the experiment

Evidence for Fe(III)-reduction was sought by looking for an increase in the concentration of 0.5 M hydrochloric acid extractable Fe(II) (bioavailable iron), compared to the doped SWy-3 montmorillonite using the Ferrozine assay method (Lovley and Phillips, 1987). Enrichment in bioavailable iron was observed in all the pressure vessels compared to the doped SWy-3 montmorillonite (Table 7.4). The largest enrichment was observed in the 1750 kg m⁻³ pressure vessel, with a moderate enrichment in the 1500 kg m⁻³ pressure vessel, and the lowest enrichment in the 1900 kg m⁻³ pressure vessel (Table 7.4). As Fe(III)-reducing activity was expected to be inversely correlated with swelling pressure, the enrichment in bioavailable Fe(II) should have been higher in the 1500 kg m⁻³ pressure vessel, compared to the 1750 kg m⁻³ pressure vessel. Research presented in Chapter 5 has shown that the 0.5 M hydrochloric acid extraction of Fe(II) underestimates bioavailable Fe(II) in montmorillonites, which makes it difficult to establish if the Fe(III)-reduction extents were significant or not. A

mechanical pressure of 1845 kPa in the 1900 kg m⁻³ pressure vessel (Table 7.3) would also be expected to prevent microbial activity as observed in other studies (Bengtsson and Pedersen, 2017). It is clear a more robust technique is required to identify the extent of biological Fe(III)-reduction in the pressure vessels such as Mössbauer spectroscopy (Ribeiro et al., 2009).

The enrichment of 0.5 M hydrochloric acid extractable Fe(II) in the SWy-3 montmorillonite plugs may have also been influenced by the formation of a black precipitate (iron sulfide) in the 1500 kg m⁻³, and 1750 kg m⁻³ pressure vessels (Table 7.4). SRB are commonly found in montmorillonite-based materials (Lopez-Fernandez et al., 2015), and would have used the lactate as an electron donor producing sulfide, and increasing the 0.5 M hydrochloric acid extractable Fe(II) (Berner, 1984). A greater amount of black precipitate indicative of iron sulfide formation was observed in the 1750 kg m⁻³ swelling vessel compared to the 1500 kg m⁻³ swelling vessel (Table 7.4). This suggests that the larger number of Fe(III)-reducing *B. subterraneus* cells in the 1500 kg m⁻³ pressure vessel were outcompeting the SRB and suppressing sulfate reduction. A similar effect was observed in Chapter 5 where Fe(III)-reduction in SWy-2 montmorillonite delayed the onset of sulfate reduction. This suggests that the swelling pressure tolerance of the *B. subterraneus* cells is less than the natural SRB community. Quantification of the amount of sulfate-reduction taking place was attempted using IC. The doped SWy-3 montmorillonite, and 1900 kg m⁻³ pressure vessel had similar concentrations of sulfate which suggests no sulfate-reduction, and therefore SRB activity had occurred in the 1900 kg m⁻³ pressure vessel (Table 7.4). However, the highest sulfate concentrations were found in the 1750 kg m⁻³ pressure vessel which is not consistent with the amount of sulfide fouling observed (Table 7.4). Removal of sulfate in the 1500 kg m⁻³ pressure vessel was observed, but these results appear to suggest the IC data is not representative of the clay plugs. A 0.2 g portion of the clay plugs was used for the IC analysis which accounts for approximately 1 % of the samples. Improvements could be made to the IC methodology by increasing the proportion of clay plug used, performing analyses in triplicate, and sampling a cross-section of the plugs to highlight sample variability. The concentration of VFAs was also tracked using IC and showed that the 1900 kg m⁻³ contained considerably more VFAs than the doped SWy-3 montmorillonite, and the 1500 kg m⁻³, and 1750 kg m⁻³ pressure vessels which all had similar values (Table 7.4). This suggests lactate was depleted in the 1500 kg m⁻³ and 1750 kg m⁻³ pressure vessels leaving behind a background VFA signal found in the original material. The 1900 kg m⁻³ pressure vessel

contained the most lactate initially as values were determined based on the amount of potentially reducible Fe(III). Perhaps using a fixed concentration of lactate based on the pore volume would be a more accurate way of quantifying lactate consumption, and reducing the lactate concentration in the 1500 kg m⁻³, and 1750 kg m⁻³ pressure vessels may reduce sulfide fouling, allowing for a better understanding of the Fe(III)-reduction process. Overall significant IRB and SRB activities were identifiable in the 1500 kg m⁻³, and 1750 kg m⁻³ pressure vessels, with a small increase in bioavailable Fe(II) in the 1900 kg m⁻³ pressure vessel (Table 7.4). Improvements could be made to the SWy-3 montmorillonite plug sampling, and pressure vessel preparation to provide more in-depth information on microbial activity in the samples. DNA sequencing of the microbial populations in the pressure vessel samples would provide invaluable information about the other microorganisms that may have been enriched during the experiment, and quantitative PCR would provide a stronger argument when it comes to proving minimal activity in the 1900 kg m⁻³ pressure vessel.

7.7. Conclusions

The activity of IRB can increase the CEC of montmorillonite-based materials as demonstrated in Chapter 5, which may impact a bentonite buffers ability to swell (Kostka et al., 1999). A reduction in swelling could allow restoration of microbial activity including deleterious processes such as canister corrosion. If a sufficient bentonite density is used, the swelling pressure in a bentonite buffer is expected to prevent microbial activity. This chapter sought to investigate IRB viability, and activity as a function of bentonite density. Pressure vessels were attached to an artificial groundwater (AGW) delivery system (saturation system), and the evolution of swelling pressure in the pressure vessels was tracked using load cells. Having reached saturation, the pressure vessels were removed from the saturation system, and a sodium lactate solution was added to the SWy-3 montmorillonite before the pressure inside the pressure vessels was reset by reducing the volume of the samples. The mechanical pressure deteriorated over time, showing it was not a true reflection of swelling pressure during the saturation stage. Inspection of the SWy-3 montmorillonite plugs showed that a large amount of iron sulfide precipitation (indicative of SRB activity) had occurred in the 1750 kg m⁻³ pressure vessel, with a small amount observed in the 1500 kg m⁻³ pressure vessel as well. The amount of IRB in the plugs was examined using MPN enumerations and showed that the 1500 kg m⁻³ plug had the highest MPN count with a decrease observed with increasing wet density. This suggests that IRB activity impeded SRB activity in the 1500 kg

m⁻³ plug, with SRB being more resistant to swelling pressure and displaying more activity at the 1750 kg m⁻³ wet density. The SWy-3 montmorillonite plugs contained more IRB than the doped montmorillonite, with a decrease observed with increasing wet density. Growth in the 1900 kg m⁻³ swelling vessel may have been as a result of *B. subterraneus* cells using an alternative metabolism, or due to differences in the MPN preparation between the starting material, and the pressure vessel plugs. Sulfate concentrations in the pressure vessels measured using IC were inconsistent with the amount of sulfide fouling observed, with irregularities observed in the bioavailable Fe(II), and ICP-AES measurements as well. These irregularities indicate that alterations to the methodologies are required to account for the higher solid/solution ratio in this chapter.

The results show that investigating IRB behavior at varying swelling pressures can be achieved using the setup devised, with revisions to the methodology required. Future research should also implement triplicate experiments, and multiple time-points so greater confidence in the results can be achieved. The research appears to suggest that IRB viability decreases as a function of montmorillonite density. With SRB activity appearing to supersede IRB activity at a wet density between 1500 kg m⁻³ and 1750 kg m⁻³ (dry densities 784 kg m⁻³, and 1176 kg m⁻³). Ferrozine assay data shows the total Fe(III)-reduction also decreased with increasing montmorillonite. However, attempts to deduce the impact of Fe(III)-reduction on the montmorillonite was complicated by irregularities in the geochemistry data. A sufficient bentonite density would be expected to halt IRB activity, but further research is required to constrain the required density, and to investigate the impacts of the IRB on the montmorillonite.

7.8. Acknowledgements

The authors would like to thank Radioactive Waste Management (RWM) for the funding to do this research. We would also like to thank Barry Gale for help with adapting the pressure cells, and assistance with setting up the saturation system, Julian Mecklenburgh, and Steven May for assisting with designing the saturation system, John Waters for help devising a risk assessment, as well as Katherine Daniels, and Matthew Kirkham for completing the grain density measurements.

7.9. References

Bengtsson, A., Edlund, J., Hallbeck, B., Heed, C., Pedersen, K., 2015. Microbial sulphide-producing activity in MX-80 bentonite at 1750 and 2000 kg m⁻³ wet density, SKB, Stockholm.

- Bengtsson, A., Pedersen, K., 2017. Microbial sulphide-producing activity in water saturated Wyoming MX-80, Asha and Calcigel bentonites at wet densities from 1500 to 2000 kg m⁻³. *Applied Clay Science*, 137: 203-212.
- Berner, R.A., 1984. Sedimentary pyrite formation - an update. *Geochimica Et Cosmochimica Acta*, 48(4): 605-615.
- Brown, A.D., 1976. Microbial water stress. *Bacteriological Reviews*, 40(4): 803-846.
- BSI, 1990. Methods of test for soils for civil engineering purposes part 2: classification tests, British Standards Institution, London.
- Chapman, H.D., 1965. Cation exchange capacity. methods of soil analysis part 2, 9. American Institute of Agronomy, Madison, Wisconsin.
- Coleman, M.L., Hedrick, D.B., Lovley, D.R., White, D.C., Pye, K., 1993. Reduction of Fe(III) in sediments by sulfate-reducing bacteria. *Nature*, 361(6411): 436-438.
- de Man, J.C., 1983. MPN tables, corrected. *European Journal of Applied Microbiology and Biotechnology*, 17(5): 301-305.
- El Mendili, Y., Abdelouas, A., Bardeau, J.F., 2013. Insight into the mechanism of carbon steel corrosion under aerobic and anaerobic conditions. *Physical Chemistry Chemical Physics*, 15(23): 9197-9204.
- Esnault, L., Libert, M., Bildstein, O., Mustin, C., Marsal, F., Jullien, M., 2013. Impact of iron-reducing bacteria on the properties of argillites in the context of radioactive waste geological disposal. *Applied Clay Science*, 83-84: 42-49.
- Haynes, H.M., Pearce, C.I., Boothman, C., Lloyd, J.R., 2018. Response of bentonite microbial communities to stresses relevant to geodisposal of radioactive waste. *Chemical Geology*, 501: 58-67.
- Hofstetter, T.B., Neumann, A., Schwarzenbach, R.P., 2006. Reduction of nitroaromatic compounds by Fe(II) species associated with iron-rich smectites. *Environmental Science & Technology*, 40(1): 235-242.
- Jeong, M., Kim, Y., Roh, Y., 2019. Biogenesis of magnetite nanoparticles using *Shewanella* species isolated from diverse regions. *Journal of Nanoscience and Nanotechnology*, 19(2): 963-966.
- Kanso, S., Greene, A.C., Patel, B.K.C., 2002. *Bacillus subterraneus* sp-nov., an iron- and manganese-reducing bacterium from a deep subsurface Australian thermal aquifer. *International Journal of Systematic and Evolutionary Microbiology*, 52: 869-874.
- Karnland, O., 1998. Bentonite swelling pressure in strong NaCl solutions: correlation of model calculations to experimentally determined data, Clay Technology, Lund, Sweden.
- Karnland, O., 2010. Chemical and mineralogical characterization of the bentonite buffer for the acceptance control procedure in a KBS-3 repository, SKB Stockholm.
- Khaled, E.M., Stucki, J.W., 1991. Iron oxidation-state effects on cation fixation in smectites. *Soil Science Society of America Journal*, 55(2): 550-554.
- Kim, J., Dong, H.L., Seabuagh, J., Newell, S.W., Eberl, D.D., 2004. Role of microbes in the smectite-to-illite reaction. *Science*, 303(5659): 830-832.
- Kostka, J.E., Wu, J., Nealson, K.H., Stucki, J.W., 1999. The impact of structural Fe(III) reduction by bacteria on the surface chemistry of smectite clay minerals. *Geochimica Et Cosmochimica Acta*, 63(22): 3705-3713.
- Liu, D., Donh, H.L., Zhao, L.D., Wang, H.M., 2014. Smectite reduction by *Shewanella* species as facilitated by cystine and cysteine. *Geomicrobiology Journal*, 31(1): 53-63.
- Lloret, A., Villar, M.V., Sanchez, M., Gens, A., Pintado, X., Alonso, E.E., 2003. Mechanical behaviour of heavily compacted bentonite under high suction changes. *Geotechnique*, 53(1): 27-40.

- Lopez-Fernandez, M., Cherkouk, A., Vilchez-Vargas, R., Jauregui, R., Pieper, D., Boon, N., Sanchez-Castro, I., Merroun, M.L., 2015. Bacterial diversity in bentonites, engineered barrier for deep geological disposal of radioactive wastes. *Microbial Ecology*, 70(4): 922-935.
- Lovley, D.R., Phillips, E.J.P., 1987. Rapid assay for microbially reducible ferric iron in aquatic sediments. *Applied and Environmental Microbiology*, 53(7): 1536-1540.
- Masurat, P., Eriksson, S., Pedersen, K., 2010. Microbial sulphide production in compacted Wyoming bentonite MX-80 under in situ conditions relevant to a repository for high-level radioactive waste. *Applied Clay Science*, 47(1-2): 58-64.
- Moore, D.M., Reynolds Jr, R.C., 1997. X-Ray diffraction and the identification and analysis of clay minerals. Oxford University Press, Oxford.
- Motamedi, M., Karland, O., Pedersen, K., 1996. Survival of sulfate reducing bacteria at different water activities in compacted bentonite. *FEMS Microbiology Letters*, 141(1): 83-87.
- Pedersen, K., 2010. Analysis of copper corrosion in compacted bentonite clay as a function of clay density and growth conditions for sulfate-reducing bacteria. *Journal of Applied Microbiology*, 108(3): 1094-1104.
- Ribeiro, F.R., Fabris, J.D., Kostka, J.E., Komadel, P., Stucki, J.W., 2009. Comparisons of structural iron reduction in smectites by bacteria and dithionite: II. a variable-temperature Mössbauer spectroscopic study of Garfield nontronite. *Pure and Applied Chemistry*, 81(8): 1499-1509.
- RWM, 2016. Geological disposal: generic disposal facility design, RWM, Didcot.
- Sellin, P., Leupin, O.X., 2013. The use of clay as an engineered barrier in radioactive-waste management - a review. *Clays and Clay Minerals*, 61(6): 477-498.
- Stroes-Gascoyne, S., Hamon, C.J., Maak, P., Russell, S., 2010. The effects of the physical properties of highly compacted smectitic clay (bentonite) on the culturability of indigenous microorganisms. *Applied Clay Science*, 47(1-2): 155-162.
- Wilson, J., Savage, D., Bond, A., Watson, S., Pusch, R., Bennett, D., 2011. Bentonite: a review of key properties, processes and issues for consideration in the UK context, NDA, Harwell.
- Yigzaw, Z.G., Cuisinier, O., Massat, L., Masrouri, F., 2016. Role of different suction components on swelling behavior of compacted bentonites. *Applied Clay Science*, 120: 81-90.

8. Conclusions and Future Directions

In a geological disposal environment, microbial processes within or associated with bentonite barriers could impact upon barrier properties and waste container corrosion rates. Microbial cells including spore-forming bacteria are naturally occurring in bentonite deposits (Lopez-Fernandez et al., 2015), with some evidence to suggest they may persist under geological disposal conditions (Pedersen, 2010). Microbial activities that are of particular relevance to geological disposal are sulfate-reduction which contributes to microbially influenced corrosion (MIC), and the degradation of canister materials (El Mendili et al., 2013); along with Fe(III)-reduction which is known to alter the geochemistry of smectite minerals (Kostka et al., 1999). Research into microbial processes occurring under geological disposal conditions have typically focused on the viability of sulfate-reducing bacteria (SRB), and their role in canister corrosion (Bengtsson and Pedersen, 2017). Less attention has been paid to microbial viability in response to stresses such as gamma radiation during geological disposal, as well as the presence and activity of microbes in long-term field experiments. The viability, and activity of Fe(III)-reducing bacteria (IRB) has also been overlooked, and it is therefore important to study their behavior in such systems.

The research in this thesis focused on the viability of IRB, and SRB communities in response to stresses that would be expected during the geological disposal of nuclear waste (Chapter 3), along with the general microbial communities found in a long-term bentonite buffer field study (Chapter 4). Attention was also focused on IRB, and their impact on bentonite materials in terms of geochemistry (Chapter 5), their influence on contaminants relevant to nuclear waste disposal (Chapter 6), as well as how they respond to a high swelling pressure regime likely to be found in a bentonite buffer under disposal conditions (Chapter 7). These areas of research will provide a greater understanding of the effectiveness of bentonite properties in retarding microbial growth and activity, as well as the potential transformations to the material that may occur.

8.1. Microbial viability

A range of stresses are expected to be imparted on microbial cells in a bentonite buffer during the geological disposal of nuclear waste. Swelling pressure has been the primary focus of previous viability studies (Masurat et al., 2010). However, other stresses including gamma

radiation, heat, and mechanical pressure have received less attention. Application of these stresses to a range of bentonite materials highlighted the differences in IRB, and SRB populations that exist between deposits (Chapter 3). All the materials tested were positive before, and after the treatments for both groups of bacteria with values between 44 MPN g⁻¹, and 6600 MPN g⁻¹. Sulfate-reduction in the materials was limited to members of the *Desulfotomaculum* which were dominant in one of the bentonites tested, and *Desulfosporosinus* genera in the other three substrates. This distinction appeared to greatly influence SRB viability with the *Desulfotomaculum* species displaying resistance to pressure, and radiation while the *Desulfosporosinus* species were resistant to the heat treatment. The viability of IRB in the bentonites appeared to be underpinned by their ability to form spores, with Gram-positive genera appearing in greater numbers following the individual treatments. The inability to suppress microbial viability in these bentonites highlighted the need to generate a sufficient swelling pressure during geological disposal conditions so that microbial activity can be minimized. The variation in communities between bentonites should also be considered during the selection process of bentonite buffer materials.

The microbial ecology of bentonite buffers under geological disposal conditions was also investigated using cores from the FEBEX *in-situ* experiment (Lanyon and Gaus, 2016) (Chapter 4). The cores were extracted along transects away from a heating element (100 °C) making it possible to profile how temperature, and evolving saturation may have affected the microbial populations. Attempts to cultivate IRB, and SRB from the cores failed. However, DNA extraction was successful, and the samples furthest from the heater showed enrichment in DNA amplified from the *Clostridia*, and *Bacilli* classes. This work suggests that microbial activity in the vicinity of the canisters will be minimal, but it is not possible to discount that microbial activity may be restored in lower temperature regions further from the canisters.

8.2. Fe(III)-reducing bacteria

Evaluation of the literature regarding microbial process during geological disposal highlighted significant gaps when it came to the viability, and activity of IRB. IRB became a focal point of this thesis, and their influences on the geochemistry of bentonites including contaminant speciation, as well as their viability and activity in response to swelling pressure were investigated. Fe(III)-reduction in montmorillonites, and other smectite minerals has been studied (Kostka et al., 1999; Neumann et al., 2011), but the investigation of bentonites,

especially in the context of geological disposal has received less attention. Bioreduction of Fe(III) in FEBEX bentonite by the Fe(III)-reducer *Geobacter sulfurreducens* was compared to SWy-2 montmorillonite (Chapter 5). Both materials had comparable iron contents, but the extent of Fe(III)-reduction was much greater in the SWy-2 montmorillonite, compared to the FEBEX bentonite. The differences in reactivity were attributed to either a smaller interlayer spacing in the FEBEX bentonite, reducing exposure to the *G. sulfurreducens* cells, or the presence of an iron oxide in the FEBEX bentonite that disrupted electron transfer to the structural iron in the montmorillonite. Despite Fe(III)-reduction occurring, no dissolution of the materials was observed. However Fe(III)-reduction in the SWy-2 montmorillonite caused an increase in the cation exchange capacity (CEC), which may influence the swelling pressure (Kostka et al., 1999). The rate of sulfate-reduction by indigenous microbes in the two materials was controlled by the amount of bioavailable iron, with little sulfate-reduction occurring in the SWy-2 montmorillonite, and a large amount in the FEBEX bentonite. It is clear the speciation of iron in montmorillonite-based materials can have a significant impact on the geochemical evolution. A trade off is present between the SWy-2 montmorillonite which is susceptible to Fe(III)-reduction, and therefore increased CEC and potentially a decrease in swelling pressure, and the FEBEX bentonite which is prone to sulphate-reduction, and therefore increased MIC.

The Fe(III)-reduction work suggested that the SWy-2 montmorillonite was acting as an insoluble electron sink, which posed the question can the reduced montmorillonite act as an electron donor in the presence of a reducible contaminant? Clarification was sought by repeating the Fe(III)-reduction experiments with *G. sulfurreducens* on the SWy-2 montmorillonite with the addition of selenium oxyanions (Chapter 6). Selenite (SeO_3^{2-}) oxyanions were reduced concurrently with the Fe(III) in the system by the *G. sulfurreducens* cells as expected; because the organism is known to reduce selenite (Pearce et al., 2009). However, selenate (SeO_4^{2-}) oxyanions (not directly reducible by *G. sulfurreducens* (Lovley et al., 1999)) were also removed over a longer time period. The selenate removal from solution was inconsistent across triplicate experiments, suggesting some heterogeneity in the system, but nevertheless highlights that reduced SWy-2 montmorillonite (at least in slurry form) can capture highly mobile and toxic selenium species.

Finally the reduction of Fe(III) in SWy-3 montmorillonite at increased swelling pressure was investigated to see if these processes would be possible in a geological disposal environment (Chapter 7). Bentonite wet densities of 1500 kg m^{-3} , 1750 kg m^{-3} and 1900 kg m^{-3} (equivalent

to dry densities of 784 kg m^{-3} , 1176 kg m^{-3} and 1411 kg m^{-3}) were chosen due to previous research surrounding SRB activity (Bengtsson and Pedersen, 2017)). The results suggested the number of IRB, and the amount of biological Fe(III)-reduction decreased with increasing montmorillonite density. The 1500 kg m^{-3} and 1750 kg m^{-3} wet densities also displayed signs of SRB activity. The results suggest that a sufficient swelling pressure should suppress the Fe(III)-reducing activities described above. However, further constraining of the limit of IRB activity is needed.

8.3. Overarching conclusions

Results from the FEBEX *in-situ* experiment cores (Chapter 4), and the IRB swelling pressure experiments (Chapter 7) show that microbial activity (in particular IRB) should be suppressed if a bentonite buffer maintains a suitable density. In the case of the IRB swelling pressure work, a dry density of above 1411 kg m^{-3} may be required, but in the case of the FEBEX *in-situ* experiment a dry density of 1500 kg m^{-3} was sufficient (Lanyon and Gaus, 2016). The montmorillonite content is a key factor in determining the density required (Karnland, 2010). If the bentonite density is not high enough, or in the event of a decrease in the bentonite density the results of Chapter 3 would suggest that microbial growth, and activity could be restored. The *in-situ* effects of temperature, irradiation, and mechanical pressure were not investigated, but exposure to these stresses in laboratory scale experiments did not prevent the restoration of microbial life (Chapter 3). IRB could potentially reduce the swelling pressure further encouraging more microbial activity, but this can be prevented if a bentonite recalcitrant to Fe(III)-reduction is chosen (Chapter 5). However, biological Fe(III)-reduction in montmorillonites also has beneficial effects such as sequestering highly mobile, and toxic selenium oxyanions, which may extend to other key radionuclides such as uranyl, and pertechnetate (Chapter 6).

8.4. Future directions

The work described in this thesis made it possible to explore the viability of microorganisms in bentonite barriers, and offers further insight into the effects of IRB on the geochemistry of montmorillonite-based materials, and contaminant speciation. However, some of these areas require further study, and complimentary studies could verify, and bolster some of the findings.

8.4.1. Microbe viability

While Chapter 3 was able to demonstrate that IRB, and SRB remain viable in bentonite materials following their treatment with heat, mechanical pressure, and gamma radiation this thesis did not assess their ability to grow in the presence of these stresses (which would be a requirement for them to be viable and active in a bentonite buffer). This is of particular importance to the gamma radiation treatment, where the microbes would be exposed to a low radiation dose over a prolonged period (1 Gy hr^{-1}), rather than the short-term single dose (1000 Gy , $24.17 \text{ Gy min}^{-1}$) used in Chapter 3. Samples from the FEBEX *in-situ* experiment tested negative for viable microbes, but DNA extraction suggested the enrichment of anaerobic classes Chapter 4. The research showed that invaluable microbial data can be obtained from field-scale, long-term experiments. However, the experiment was not initially intended with microbial analyses in mind. This means the initial bacterial content of the FEBEX bentonite could not be determined, and the various inputs of biological material during quarrying of the bentonite, bentonite fabrication, and gallery excavation could not be assessed. Further collaboration between geomicrobiology researchers, and nuclear waste disposal agencies through projects such as the EU MIND (Microbes in Nuclear Disposal) project will ensure the appropriate microbial analyses can be implemented in future long-term experiments.

8.4.2. Biological Fe(III)-reduction of bentonites

Differences in the bioavailability of Fe(III) in montmorillonite-based materials was identified in Chapter 5. The lack of Fe(III)-reduction in the FEBEX bentonite may have been due to an iron oxide phase associated with the montmorillonite. However, the identity of this iron oxide phase remains unknown, and requires further investigation. EPR spectroscopy on the reduced SWy-2 montmorillonite also showed an increase in radical ions in the structure after biological Fe(III)-reduction which could provide further insight into how electron transfer occurs in low iron content smectites. The electron donating capabilities of reduced SWy-2 montmorillonite were also demonstrated in the presence of selenate oxyanions (Chapter 6). A suitable control is required to prove the clay itself instigated the reduction rather than a biological reaction. This could be studied by pasteurising the montmorillonite after reduction, and then inserting the selenate. This process could also be investigated using a chemical reductant such as dithionite (Ribeiro et al., 2009). Outside of nuclear disposal reduced SWy-2 montmorillonite may be a novel way of immobilising oxyanions in contaminated land, and

also poses questions about the potential role of montmorillonite as an electron shuttle in the natural environment. The potential for biological Fe(III)-reduction in a bentonite buffer will be eliminated if a sufficient bentonite density is achieved. Chapter 7 appears to show that a wet density of more than 1900 kg m⁻³ in SWy-2 montmorillonite is required to prevent biological Fe(III)-reduction from occurring. However, experiments were not conducted in triplicate, and the methods employed to investigate the compacted bentonite did not appear to be representative of the material (as a result of sample heterogeneity). Work is required to optimise the methodology for high solid:solution samples so more significant results can be obtained. Moving on from that previous studies have shown that microbial activity can be restored in highly compacted bentonites in the event of a reduction in density which is particularly relevant to canister, and host rock interfaces (Stroes-Gascoyne et al., 2011) and requires further study. The impact of bentonite density on the reduction of selenium species (and other radionuclides) should also be a focus of further study.

8.5. References

- Bengtsson, A., Pedersen, K., 2017. Microbial sulphide-producing activity in water saturated Wyoming MX-80, Asha and Calcigel bentonites at wet densities from 1500 to 2000 kg m⁻³. *Applied Clay Science*, 137: 203-212.
- El Mendili, Y., Abdelouas, A., Bardeau, J.F., 2013. Insight into the mechanism of carbon steel corrosion under aerobic and anaerobic conditions. *Physical Chemistry Chemical Physics*, 15(23): 9197-9204.
- Karnland, O., 2010. Chemical and mineralogical characterization of the bentonite buffer for the acceptance control procedure in a KBS-3 repository, SKB, Stockholm.
- Kostka, J.E., Wu, J., Nealson, K.H., Stucki, J.W., 1999. The impact of structural Fe(III) reduction by bacteria on the surface chemistry of smectite clay minerals. *Geochimica Et Cosmochimica Acta*, 63(22): 3705-3713.
- Lanyon, G.W., Gaus, I., 2016. Main outcomes and review of the FEBEX in situ test (GTS) and mock-up after 15 years of operation, NAGRA, Wettingen.
- Lopez-Fernandez, M., Cherkouk, A., Vilchez-Vargas, R., Jauregui, R., Pieper, D., Boon, N., Sanchez-Castro, I., Merroun, M.L., 2015. Bacterial diversity in bentonites, engineered barrier for deep geological disposal of radioactive wastes. *Microbial Ecology*, 70(4): 922-935.
- Lovley, D.R., Fraga, J.L., Coates, J.D., Blunt-Harris, E.L., 1999. Humics as an electron donor for anaerobic respiration. *Environmental Microbiology*, 1(1): 89-98.
- Masurat, P., Eriksson, S., Pedersen, L., 2010. Microbial sulphide production in compacted Wyoming bentonite MX-80 under in situ conditions relevant to a repository for high-level radioactive waste. *Applied Clay Science*, 47(1-2): 58-64.
- Neumann, A., Sander, M., Hofstetter, T.B., 2011. Redox Properties of Fe in smectite clay minerals. In: Tratnyek, P. (Ed.), *Aquatic Redox Chemistry*. ACS Symposium Series.
- Pearce, C.I., Patrick, R.A.D., Law, N., Charnock, J.M., Coker, V.S., Fellowes, J.W., Oremland, R.S., Lloyd, J.R., 2009. Investigating different mechanisms for biogenic

- selenite transformations: *Geobacter sulfurreducens*, *Shewanella oneidensis* and *Veillonella atypica*. Environmental Technology, 30(12): 1313-1326.
- Pedersen, K., 2010. Analysis of copper corrosion in compacted bentonite clay as a function of clay density and growth conditions for sulfate-reducing bacteria. Journal of Applied Microbiology, 108(3): 1094-1104.
- Ribeiro, F.R., Fabris, J.D., Kostka, J.E., Komadel, P., Stucki, J.W., 2009. Comparisons of structural iron reduction in smectites by bacteria and dithionite: II. a variable-temperature Mössbauer spectroscopic study of Garfield nontronite. Pure and Applied Chemistry, 81(8): 1499-1509.
- Stroes-Gascoyne, S., Hamon, C.J., Maak, P., 2011. Limits to the use of highly compacted bentonite as a deterrent for microbiologically influenced corrosion in a nuclear fuel waste repository. Physics and Chemistry of the Earth, 36(17-18): 1630-1638.